UNIVERSITY OF OKLAHOMA

GRADUATE COLLEGE

INFLUENCE OF FACING ON THE CONSTRUCTION AND STRUCTURAL PERFORMANCE OF GRS BRIDGE ABUTMENTS

A DISSERTATION

SUBMITTED TO THE GRADUATE FACULTY

in partial fulfillment of the requirements for the

Degree of

DOCTOR OF PHILOSOPHY

By

RIDVAN DOGER
Norman, Oklahoma
2020

INFLUENCE OF FACING ON THE CONSTRUCTION AND STRUCTURAL PERFORMANCE OF GRS BRIDGE ABUTMENTS

A DISSERTATION APPROVED FOR THE
SCHOOL OF CIVIL ENGINEERING AND ENVIRONMENTAL SCIENCE

BY THE COMMITTEE CONSISTING OF

Dr. Kianoosh Hatami, Chair

Dr. Amy Cerato

Dr. Gerald Miller

Dr. Kanthasamy Muraleetharan

Dr. Peter J. Attar

Acknowledgments

Dedicated to my beloved late father, Ali Doger…

I would like to express my deepest appreciation to my advisor Dr. Kianoosh Hatami for giving the opportunity to work on this research project and support during the progress of my Doctor of Philosophy Degree. I am extremely grateful to my committee for their contributions throughout my research and academic courses. I want to mention that the funding for this project was provided by Oklahoma Department of Transportation (ODOT) through SP&R Item No. 2262-Phase II.

I am fortunate to have my wife, three daughters and other family members for the extraordinary support and patience during my Doctor of Philosophy Degree. I'd like to acknowledge the invaluable assistance from Mike Schmitz, the Fears Structural Laboratory Manager, and those of graduate students, Jerome Boutin and Matsuura Kazunori, and undergraduate research assistants Stephen Schnabel, Coleman Ross, Uzeir Hodzic, John King, Daniel Farley, Vuth Chea, Kirby Falcon and Jackie Pham during the construction and testing of the GRS abutment models with their tight schedules under different weather conditions.

Table of Contents

List of Tables

List of Figures

ABSTRACT

Geosynthetic Reinforced Soil-Integrated Bridge System (GRS-IBS) technology has been developed significantly over the last decade through extensive support and promotion by the Federal Highway Administration (FHWA). It is considered as a viable and cost-effective bridge construction alternative to the conventional, deep-foundation bridge abutment systems for local and county roads across the U.S. In this study, large concrete blocks (2 ft. high × 2 ft. deep × 4 ft. wide) were used as facing to construct full-scale (8 ft. high) model GRS bridge abutments to investigate their possible structural contribution to the load-bearing capacity and performance of the abutments, and their potential to further reduce the construction time and labor requirements for GRS-IBS, leading to further cost savings. Three instrumented model GRS abutment models were constructed in an outdoor test station to compare the construction speed and structural performance of models with larger blocks relative to those with standard CMU block facing. Numerical modeling was performed to compare with the results from the full-scale surcharge load testing of all three GRS abutment models. Results of the study showed that large concrete block facing GRS abutment models were constructed in shorter period of time and showed greater load-bearing capacity and smaller deformations relative to the nominally identical models with CMU facing alternative. Nevertheless, all GRS bridge abutment models showed significantly larger load-bearing capacity relative to the requirements stipulated in current design guidelines.

Keywords: geosynthetics, reinforced soil, GRS-IBS, bridge abutments, full-scale model tests, accelerated bridge construction

Chapter 1. Introduction

1.1. Background

Geosynthetic Reinforced Soil-Integrated Bridge System (GRS-IBS) technology has been developed primarily over the last decade through extensive support and promotion by the Federal Highway Administration (FHWA; Adams *et al.* 2012a,b) as a viable and cost-effective bridge construction alternative to the conventional, deep-foundation bridge abutment systems for local and county roads across the United States. GRS is also used extensively for retaining wall construction, but the focus of this research is on their application as bridge abutments.

Concrete Masonry Unit (CMU) block (e.g. 7.625-inch high × 7.625-inch deep × 15.625-inch wide) is the most commonly used material for the facing in GRS bridge abutments (Hatami *et al.* 2016). However, it this study, it was hypothesized that using the large concrete blocks (2 ft. high × 2 ft. deep × 4 ft. wide) in the facing of GRS bridge abutments would lead to better structural performance and faster construction speed, resulting in more reliable bridge abutments and further cost savings. These large concrete blocks are already available through local suppliers in the United States.

A set of three full-scale instrumented GRS abutment models was constructed at the test station on the OU South Campus to compare the load-bearing capacity and performances of large concrete block and CMU-block models at full-scale. These full-scale GRS abutment models also provided the opportunity to compare their construction speed with data that would be useful for field applications.

The GRS abutment models were built following the FHWA guidelines (Adams *et al.* 2012 a, b). However, they also satisfy the most recent FHWA guidelines (*Adams et al.* 2018). Recently updated guidelines include several updates based on continued research conducted at the Federal Highway Administration's Turner-Fairbank Highway Research Center. The user feedback resulting from the use of GRS in the construction of more than 300 bridges was also included with additional details on the design, construction, quality assurance, in-service inspection, maintenance, and repair of the GRS-IBS.

Numerical modeling was carried out using FLAC v.7.0 (Itasca 2011) software to compare the numerical modeling results with the full-scale surcharge load testing experimental data of all three GRS abutment models.

1.2. Need for the Study

While the economic advantage of GRS-IBS over the conventional bridge abutment systems has been repeatedly demonstrated in many projects in different states, it has been observed that the cost savings and reduced construction time could significantly decrease for larger GRS-IBS (Hatami 2016, 2017). This could explain why GRS-IBS has so far, not been considered as a mainstream construction technique for large interstate bridge abutments carrying high-volume traffic. A thorough study of large concrete block GRS abutments could help verify and quantify potential cost savings for the bridge construction industry to adopt GRS-IBS for a wider variety of projects (including on-system bridges) across the United States and globally.

1.3. Study Hypotheses, Objectives and Tasks

The hypotheses of this research are:

1) Using larger concrete blocks in the GRS abutment facing could help improve stability, control deformations, and reduce reinforcement costs as compared to more commonly used CMU blocks

2) Using larger concrete blocks in the GRS abutment could reduce construction time as compared to the CMU facing alternative

The main objective of this research is to study the performance of large concrete block GRS abutment models relative to that of a comparable CMU-facing model with respect to their load-bearing capacity and performance under strip-footing pressure simulating bridge abutment load. Widely used CMU and alternative large concrete block were selected as two different facing systems for GRS bridge abutments. Full-scale testing and numerical modeling was carried out on three different GRS abutment models to compare the structural performance, construction speed and costs of two facing alternatives.

Results of this research study can help practicing engineers develop safer and more cost-effective methods to construct bridge abutments when GRS bridge abutments are deemed appropriate for the project at hand, leading to cost savings and faster construction of bridge abutments.

1.4. Organization of Dissertation

This dissertation is comprised of ten chapters. Chapter 1 includes the background, need for the study, study objectives and the layout of the dissertation.

Chapter 2 provides an introduction and background on the GRS-IBS technology, including its design requirements, FHWA guidelines (Adams *et al.* 2018), advantages and limitations of using large concrete blocks. Selected case studies are also provided on the performance of GRS-IBS systems.

Detailed description of approach and methods are discussed in Chapters 3 through 6. Chapter 3 includes descriptions on the instrumentation and equipment used in the study and related laboratory tests. Chapter 4 provides details on the construction and load testing of full-scale CMU and large concrete block GRS abutment models, and Chapter 5 contains details on their deconstruction procedure including survey of their internal deformation. Chapter 6 includes details on numerical simulation of GRS abutment models.

The collection of test results in this study and corresponding discussions are included in Chapters 7 through 9. Results on construction performance and labor requirements of GRS Abutment Models #1-#3 are provided in Chapter 7. Chapter 8 includes the corresponding results and discussions for the surcharge load testing stage and the deformation readings during the deconstruction of the GRS Abutment models. Numerical modeling of the GRS abutments and corresponding results are discussed in Chapter 9.

Finally, Chapter 10 summarizes the findings and conclusions of the study and includes recommendations for future work along this study.

Chapter 2. Literature Review

2.1. Background

A survey of recent studies on GRS-IBS is provided in this chapter, which includes several studies on commonly used CMU facing GRS abutments. This survey of related literature indicates that to the best of the author's knowledge no comprehensive studies have been carried out to compare the construction speed and load-bearing performances of large concrete block and CMU-facing GRS bridge abutments, which is the focus of the present study.

Another unique point of this study is that the behavior under large surcharge loads (i.e. 10 or 40 ksf) has never been tested in any laboratory or field tests that performed with small or full-scale GRS abutment models before. The full-scale GRS abutment models tested in this study were built following recommendations in FHWA guidelines (Adams *et al.* 2012 a, b; 2018). The literature review is separated into four different categories, which include instrumented field studies, laboratory testing, performance survey and cost analysis, and analytical studies.

Instrumented field studies

In recent years, GRS walls have been increasingly used to support bridge abutments. Several recent field observations of GRS bridge abutments have also been reported, which have confirmed the advantages of GRS bridge abutments:

Ardah 2018 and Saghebfar *et al.* 2017 monitored newly constructed GRS-IBS abutments with CMU facing for one single-span bridge at Maree Michel bridge site in Louisiana. Bridge deformations, settlements, strains along the reinforcement, vertical and horizontal stresses within the abutment, and pore water pressures were measured by the instrumentation readings. It was observed that the magnitude and distribution of strains along the reinforcements vary with depth. Measured abutment deformations indicated that maximum total settlements across the width of a GRS bridge abutments were significantly less than the design value.

Boeckmann *et al.* 2017 monitored Rustic Road GRS-IBS that was constructed on a low-volume road in Boone County, Missouri. The monitoring system included, settlement plates and inclinometers to record displacement within the structure, earth pressure cells to measure total stresses and piezometers to pore pressures within the abutment backfill. After 19 months of monitoring, external and internal displacements were negligible and the backfill was typically dry and drained quickly after precipitation events.

Hatami *et al.* 2015 reviewed available GRS-IBS bridges with a reported performance monitoring program data that was collected by other researchers. Collected data showed that the magnitudes of the bridge settlement values were higher than lateral deformation at most of the monitored bridges.

Lawrence 2014 monitored the first GRS-IBS with 109 ft. long span in Hawaii. The GRS abutments were instrumented to measure vertical pressures, lateral pressures, bridge footing settlement and lateral displacement of the GRS facing. CMU block with 8-inch high, 12-inch deep, 16-inch length was used as facing element. A finite element analysis was performed to compare results with the measured data and the results gave similar results for footing settlement and facing lateral pressure.

Budge *et al.* 2014 monitored the first application of the GRS-IBS technology with CMU facing for a rural railroad crossing, BR 66564, located in southwestern Minnesota. The instruments consisted of 2-D deformation, pressure, 3-D position, temperature, and weather monitoring. The structure had a span length of 77.5 ft. and the maximum abutment height was 22.7 ft. Performance data suggested that the vertical deformation occurred rapidly and as the fill and structural elements were placed. The continuing horizontal and vertical deformations observed at site were small and difficult to measure even with state-of-the-art systems.

Vennapusa *et al.* 2012 presented an analysis from two field demonstration projects conducted to evaluate the feasibility and cost effectiveness of the use of GRS bridge abutments with CMU facing on low-volume roads in Buchanan County, Iowa. Test results indicated that shear strength parameters and permanent deformation behavior of granular fill material improved when reinforced with geosynthetic.

Laboratory testing

The potential benefits of a well-restrained structural facing have been demonstrated in previous studies (Bathurst *et al.* 2006, Hatami *et al.* 2008, Huang *et al.* 2010). Another research showed that a decrease in reinforcement vertical spacing (i.e., smaller than 1 ft.) resulted in a composite behavior of the Geosynthetic-Reinforced Soil structure (Wu *et al.* 2013).

Several recent large-scale Geosynthetic Reinforced Soil Structures with different heights and sizes have been tested with surcharge loading at test centers throughout the world and showed the advantages of using these structures. Some of the details and focus areas of these research studies are listed below:

Bourgeois *et al.* 2011 tested a full-scale model of a railway embankment with concrete panel facing that was built, instrumented, and tested near Rouen, France to understand the deformations induced by train loads. The distance between the vertical walls was 26.25 ft. The embankment was 54.13 ft. wide and 13.53 ft. high. It was built on a stiff subgrade layer. Numerical models showed that the soil-strip interface parameters have a major influence on the predicted behavior.

Ahmadi *et al.* 2012 focused on the experimental and analytical investigations of small-scale physical model tests. The results showed that the maximum tensile force on the reinforcement layers depends on any of the following factors; the location of the footing with respect to the wall, type of reinforcement, number of reinforcing layers, depth below the footing to the first layer of reinforcement, spacing between reinforcing layers and dimensions of the reinforcement compared with the dimensions of the wall.

Nicks *et al.* 2013 performed mini-pier performance tests that were used to investigate GRS material by FHWA. The typical performance test was 6.4 ft high with square inside dimensions of 3.2 ft. The parameters that varied among tests were reinforcement spacing, geotextile strength, soil type, and frictionally connected facing element (i.e. CMU and no facing). The results showed that the angularity of gravel fill impacted the strength of the backfill. The frictionally connected CMU facing had a direct positive impact on the performance of GRS with no facing element. Higher reinforcement strength (4,800 lb/ft) produced a stiffer and stronger response than the lower reinforcement strength (2,400 lb/ft) for open-graded backfill.

Nicks *et al.* 2016 performed thirteen GRS mini-pier performance tests that were conducted to study the effect of tensile strength, vertical reinforcement spacing, facing elements, and backfill properties with different surcharge loads. The square base area was 10.76 ft^2 and height of each

mini-pier was 6.56 ft. The data showed that the reinforcement spacing played a larger role than the reinforcement strength in terms of vertical and lateral deformations. The lateral movement of the wall unit was at the maximum in the top third region of the GRS. It was showed that with 4,178 psf surcharge, the estimated lateral deformation was less than 0.5% the height of the wall.

Xiao *et al.* 2016 performed reduced-scale model tests that were conducted to investigate the behavior of the GRS walls on rigid foundations subjected to static loading at different offset distances to the facing. The test box dimensions were 2.62 ft. high × 4.92 ft. deep × 1.31 ft. wide. A poorly-graded dry river sand and punched-drawn biaxial geogrid made of polypropylene material were used in the model tests. Solid concrete facing unit dimensions were 1.77-inch high × 1.97-inch deep × 1.97-inch wide. It was observed that the failure surfaces started from the edge of the footing. The slip surfaces under the footing loading had a good agreement with Spencer's two-part wedge method.

Ahmadi *et al.* 2018 constructed two full-scale mechanically stabilized earth (MSE) wall models. One test was conducted with a rigid and one with a flexible wall face. A strip-footing load was applied MSE walls with dimension of 13.12 ft. high × 9.84 ft. deep × 13.12 ft. wide. The stresses in the fill, strains in the reinforcement and the horizontal deflection of the wall were measured during testing. The backfill was constructed with poorly graded sand, and the reinforcement was a geogrid with a maximum tensile strength of 40 kN/m at the break strain of less than 6.6%. Rigid full height concrete panels were used for the tests. The results indicate that the tensile force on reinforcement layers for rigid facing was less than the flexible facing. The maximum strains in the reinforcement layers occurred in the upper layers right below the strip footing load.

Kakrasul *et al.* 2018 focused on the lateral displacements of the wall facing and the settlement of a loading plate on reduced-scale GRS wall models in the laboratory. The wall models were constructed with CMU and wrapped-around facing. The dimensions of each model test wall were 3.28 ft. high × 3.94 ft. deep × 1.18 ft. wide. The results showed that the wall with wrapped-around facing had larger settlement and lateral wall facing displacements than the wall with CMU facing.

Zheng *et al.* 2018 presented the dynamic response of a half-scale GRS bridge abutment system using a shaking table. 8.86 ft. high GRS bridge abutment was constructed using well-graded sand backfill, modular facing blocks, and uniaxial geogrid reinforcement. Results indicated the GRS bridge abutment experienced small deformations. For two earthquake motions, the maximum incremental residual facing displacement in model scale was 0.04-inch, and the vertical strain was 0.7%.

Nicks *et al.* 2019 constructed three large-scale GRS abutment models with each having different dimensions, ranging from square to rectangular. The height and width for each model were 6.23 ft. and 5.25 ft. respectively. The length along the face of GRS abutments A, B, C were 5.91 ft., 12.47 ft., and 18.7 ft., respectively. AASHTO No. 8 aggregate backfill, 70 kN/m biaxial woven polypropylene geotextile, and CMU facing were used for all models. The results indicated that under a dead load surcharge due to a bridge superstructure, ranging from 2.737 psf to 2,967 psf, the stress distributions appear to follow Boussinesq theory.

Xu *et al.* 2019 conducted four model tests to investigate the performance of the GRS abutment subjected to static footing load. Two influencing factors were considered, which were reinforcement spacing and types (biaxial geogrid and uniaxial geogrid). The test box had dimensions of 5.91 ft. high × 9.84 ft. deep × 3.28 ft. wide. The results showed that the

reinforcement spacing had significant effects on the performance of the GRS abutment, and compared to uniaxial geogrid, biaxial geogrid with similar tensile strength provided more lateral restraint to the backfill soil.

Performance Survey and Cost Analysis

FHWA guidelines (Adams *et al.* 2012 a, b; 2018) primarily recommend GRS-IBS for low-volume roads. However, they have also been built on higher volume roads (e.g. with AADT as large as nearly 40,000 in the case of 1122 Bridge in Yauco, Puerto Rico), and they were all performing well (Ngo 2016).

There are currently various facing unit choices on the market. Hallow version of CMU block (e.g. 7.625-inch high × 7.625-inch deep × 15.625-inch wide) is the most popular choice, which has been used in 80% of the cases surveyed, and this type of facing is more suitable for the projects that require a minimum compressive strength of 4,000 psi according to the FHWA guidelines (Adams *et al.* 2012).

Hatami *et al.* 2016, Ngo 2016 and Pena 2017 studied the performance of four (4) field GRS-IBS in Kay County in Northern Oklahoma using manual surveys, and found that they all showed satisfactory performance despite flooding periods and recorded seismic activity during the 2015 and 2016 period.

Geosynthetic reinforcement (Mirafi HP570) and CMU facing unit were used in Montana DOT 2018 research. This long-term performance study in Montana showed that GRS abutments can be a sustainable and economical solution to support bridges on local roads after monitoring the structure between July 2014 and May 2018 at the South Fork Dry Fork Marias River.

Reported accounts of GRS-IBS projects in the United States over the period between 2011 and 2017 have shown that using GRS-IBS technology can save 25% to 60% on construction costs (Hatami *et al.* 2016, Daniyarov *et al.* 2017). A technical note recently published by FHWA has also reported similar cost-saving advantages (Nicks 2019).

The abutment cost can increase relative to conventional deep-foundation alternatives in the case of larger GRS abutments where a significant quantity of fill material would have to be placed and compacted (Hatami *et al.* 2016, Pena 2017). In such cases, the use of large concrete block as the facing of GRS bridge abutments could also help with faster and less labor-intensive construction procedures, leading to further cost savings.

Analytical studies

Zheng *et al.* 2018 conducted a numerical investigation of deformation and failure behavior for GRS bridge abutments using finite-difference analysis. It was found to be that the reinforcement vertical spacing, reinforcement stiffness, backfill soil friction angle, and lower GRS wall height had the most significant effects on abutment deformations. Reinforcement and backfill soil properties had little effect on the geometry of the failure surface. The failure surface found to be as bilinear, starting at the heel of the bridge seat, moving downward to an intersection point at mid-height, and then diagonally to the toe of the lower GRS wall.

Xu *et al.* 2019 proposed a method in this study that stronger and more tightly-spaced reinforcement can help increase the sliding stability of reinforced soil retaining walls. Backfill friction angle had the greatest influence on factor of safety among all the parameters investigated. More accurate estimates of reinforced soil wall deformations can be obtained due to horizontal and vertical seismic loads as compared to conventional pseudo-static Mononobe-Okabe approach.

Xie *et al.* 2019 focused on a limit equilibrium approach to estimate the bearing capacity of strip footings placed on Geosynthetic Reinforced Soil Structures. The research shows that the log-spiral mechanism is more likely to occur when the footing is located closer to the facing or the GRSS is tall. The geometry of failure surface is described by the log-spiral equation (Eq. 1):

$$r = r_0 e^{(\theta - \theta_0)\tan\phi'} \quad [1]$$

where

r: radius of the spiral, r_0: starting radius at $\theta=0$

ϕ': angle of friction of soil, θ: angle between r and r_o

There are some classic methods to calculate the active earth force in absence of strip load. The classical solutions of lateral earth pressure are Coulomb's (1773) and Rankine's (1857) earth pressure theories. These fundamental solutions still form the basis of earth pressure calculations. Rankine's theory considers the state of stress in a soil mass when the condition of plastic equilibrium has been reached. The soil is assumed to be homogenous and isotropic. Current FHWA Guidelines (Adams *et al.* 2018) recommend using classical soil mechanics for active earth pressure with using Rankine's theory in Section 4.3.5.1. The magnitudes of active Rankine lateral earth pressure coefficient and the lateral earth pressure for cohesive-frictional (c-ϕ) soils are given as:

$$K_a = \frac{1-sin\phi}{1+sin\phi} \quad [2]$$

$$P_a = K_a \gamma z - 2c\sqrt{K_a} \quad [3]$$

When the horizontal stress becomes equal to the active pressure the soil is assumed in the active Rankine state.

Coulomb's theory considers the stability of a wedge of soil between a retaining wall and a trial failure plane. The friction between the wall and the soil is included in the analysis. The friction angle between the wall and backfill material is denoted by δ. The Coulomb lateral earth pressure coefficient and corresponding lateral earth force are determined using the following equations:

$$K_a = \left(\frac{\sqrt{\frac{\sin(\alpha-\phi)}{\sin\alpha}}}{\sqrt{\sin(\alpha+\delta)}+\sqrt{\frac{\sin(\phi+\delta)\sin(\phi-\beta)}{\sin(\alpha-\beta)}}} \right)^2 \quad [4]$$

$$P_a = \frac{1}{2} K_a \gamma H^2 \quad [5]$$

Adams *et al.* 2018 also give recommendations on how to evaluate lateral pressures at the location of interest for stress distribution through a soil mass for an area under a uniform surcharge to use the Boussinesq's Method in NAVFAC 1986 (Eq. 6):

$$\sigma_z = \frac{2.Q.z^3}{\pi.(r^2+z^2)^2} \quad [6]$$

2.2. A Brief Overview of the FHWA Design Recommendations

FHWA guidelines (Adams *et al.* 2012) was recently updated in 2018 with the current FHWA guidelines (Adams *et al.* 2018). GRS-IBS has three main components that are defined in current FHWA guidelines (**Figure 1**):

(1) integrated approach, which incorporates the approach section of the roadway with the bridge superstructure to generate a joint-less transition between the bridge and the roadway;

(2) bridge abutment, which is comprised by modular facing elements, compacted granular fill and a set of tightly-spaced geosynthetic reinforcement layers;

(3) reinforced soil foundation (RSF).

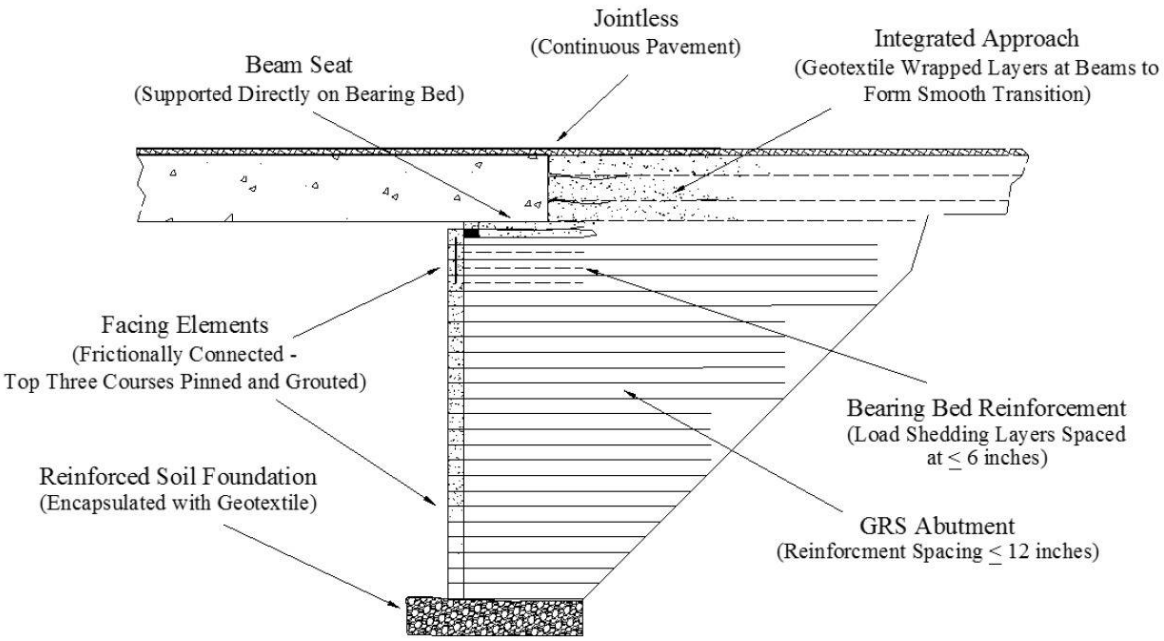

Source: FHWA.

Figure 1. Typical GRS-IBS cross-section

Bridge abutment is designed to support traffic load in which backfill carries most of the load during the service life of the bridge. Open or well-graded aggregate, or a combination of both can be used as bridge abutment's backfill material. Adams *et al.* 2018 recommend using angular aggregate, which provides greater shear strength, and its gradation should allow for optimum compaction, workability, and drainage. Backfill material should be compacted to achieve a minimum of 95%

of maximum dry unit weight based on the AASHTO T-99 (Standard Proctor) procedure. Open-graded type aggregate mix is preferred for the RSF and bridge abutment backfill.

The bridge abutment facing element provides a formwork for backfill compaction, and serves as a facade that protects the granular fill from outside weathering. The Concrete Masonry Unit (CMU), with actual dimensions of 7.625-inch high × 7.625-inch deep × 15.625-inch wide, is most commonly used as facing element for the GRS bridge abutment. Facing block alignment and compaction of the backfill are the critical processes for proper construction of the abutment. Adequate compaction without changing the alignment of the facing unit is also essential for a long service life. Adams *et al.* 2018 recommend the use of geosynthetics for the integrated approach and GRS bridge abutments.

2.3. Advantages of Using Large Concrete Blocks Compared to CMU

The larger size of these blocks in the construction of GRS bridge abutments can have the following important advantages over the more common CMU blocks:

- Construction can be faster by using readily available equipment (e.g. a track hoe)
- It is less challenging to level and align the blocks during the construction with having less block layers along the height of the bridge abutment facing. This could lead to time saving and a more structurally sound bridge abutment facing (Pena, 2017).
- Increasing the weight and thickness of the GRS concrete facing increases its structural capacity, which together with an adequately constrained toe condition could help reduce the deformations of the bridge abutment during its service life. The potential benefits of a

well-restrained structural facing have been demonstrated in previous studies (Bathurst *et al.* 2006, Huang *et al.* 2010).

- The larger and heavier facing blocks allow for better compaction of the GRS fill. Studies have demonstrated the importance of proper compaction of the backfill behind the facing in the stability and performance of GRS walls (Hatami *et al.* 2008).
- The use of recycled and/or leftover materials, as is the case for large concrete blocks used in this study, is beneficial in reducing waste and carbon footprint toward developing more sustainable solutions for the construction and repair of transportation-related infrastructure and facilities.
- Large concrete blocks are available in concrete plants through local suppliers. The blocks used in the present study were 2 ft. high × 2 ft. deep × 4 ft. wide in size and had longitudinal tongue-and-groove keys, which provides added stability when they need to be stacked up to significant heights.

2.4. FHWA Design Recommendations

The design recommendations given in FHWA (Adams *et al.* 2018) guidelines for GRS bridge abutments are summarized as:

- GRS bridge abutment generally supports a single-span with span length no longer than 140 ft.
- GRS bridge abutment and wingwalls should not exceed a height of 30 ft.
- High-quality granular backfill material used in GRS bridge abutment serves as the main component to support the traffic load. The friction angle of the backfill should be $\geq 38^{o}$,

and the backfill should achieve 95% or greater maximum dry unit weight based on the AASHTO T-99 Standard Proctor procedure.

- Open-graded aggregates provide better drainage for GRS bridge abutment backfills. Well-graded aggregates are preferred for reinforced soil foundations (RSF) and integrated approach backfills. Maximum aggregate size is recommended to be between 0.50-inch and 2-inch with fines content of less than 5%.
- 12-inch or less spaced layers of geosynthetic reinforcement should be used to reinforce the GRS bridge abutment with a minimum ultimate strength of 4,800 lb/ft.
- A common facing option is the Concrete Masonry Unit (CMU) (i.e. actual dimensions of 7.625-inch high × 7.625-inch deep × 15.625-inch wide) with a minimum compressive strength of 4,000 psi and water absorption limit of 5%.
- The facing system is not considered a structural element in design, because a GRS composite is not supported externally.
- External stability checks for GRS include direct sliding, bearing resistance of the foundation soil, and global stability.
- Internal stability checks include bearing resistance, deformations, and required reinforcement strength.
- Allowable bearing pressure on the GRS abutment is 4 ksf.
- Vertical settlement limit under maximum service load is 0.5% of the total facing height.
- Lateral deformation limit under maximum service load is 1% of the total facing height.
- Lateral deformation should be estimated from vertical deformation based on concept of zero-volume change.

- Utilities can be placed in the reinforced zone, passing either perpendicular or parallel through the GRS fill. All utilities that pass through the GRS abutment should follow local, State, and Federal utility codes.
- GRS walls and abutments have exhibited excellent performance under moderate to high level earthquakes.

2.5. Case Studies

There are several GRS bridge abutment projects throughout the United States that were designed and built using CMU blocks for their facing. For example, four GRS-IBS projects were built over Dry Creek in Kay County, Oklahoma over the period between April 2014 and February 2015. The abutments for two of the GRS bridges were built with CMU facing. The settlement performances of the bridges were monitored following their construction (Hatami *et al.* 2016). These GRS-IBS projects in Kay County are unique in the United States because they were built near two additional bridges that were supported on conventional pile abutments. These bridges are all approximately 7 ft. high at their beam seat and they are located within a two-mile segment of 44th Street. This set of GRS-IBS projects have allowed a side-by-side comparison of their performance with one another, and with two additional bridges with conventional bridge abutment designs that share essentially identical climatic, geotechnical, seismic and traffic loading conditions (Hatami *et al.* 2016). Results of the survey data on these GRS-IBS projects so far have demonstrated their satisfactory performance despite having been submerged after significant periods of precipitation in Spring 2015 and 2016, and frequent seismic activity in Northern Oklahoma (Hatami *et al.* 2016, Pena 2017). **Figure 2** shows one of the bridges in Kay County, OK before and after the construction of a GRS-IBS.

Figure 2. (Left) Condition of the old bridge; (Right) New GRS bridge abutment with CMU block facing in Kay County, OK, (Photographs Courtesy of Mr. Tom Simpson)

Another GRS-IBS project was built in Lincoln County with the GRS abutment height of 17 ft. at its beam seats. This bridge was more challenging to build because of its height and the steep back-slope. It is a significant GRS-IBS project in Oklahoma, which was completed successfully in only one month in July 2016 (Hatami *et al.* 2016) (**Figure 3**).

Figure 3. (Left) Condition of the old bridge; (Right) New GRS bridge abutment with CMU block facing in Lincoln County, OK, (Photograph courtesy of Mr. Tom Simpson)

The GRS-IBS projects in Kay County were found to cost between 51% and 58% of piled bridge abutment alternatives. However, this significant cost advantage could be diminished in the case of larger GRS-IBS projects, such as the project in Lincoln County stated earlier.

Among other example GRS-IBS projects in the U.S. are the Maree Michel bridge on Route LA 91 Vermilion Parish, LA, which was also monitored by measuring bridge settlements, pore water pressures, reinforcement strains, and stresses in selected locations within the bridge abutment. Three piezometers were installed at the bottom and at one-third and two-thirds of the height from the bottom of the abutment, respectively. A total of 55 strain gauges were installed along five geosynthetic layers in the abutment. Results indicated that the soil foundation settlement was increased with surcharge load, and more movements occurred near the center of the abutment than the corners. The measurements of bridge abutment deformations indicate that the maximum total settlements across the GRS bridge abutment were less than 0.47-inch, which was significantly less than the design value of 0.8-inch (Saghebfar *et al.* 2017).

Another example GRS-IBS project is located in Pondera County, MT, at the South Fork-Dry Fork Marias River Crossing, which was constructed in 2013. Five different detailed site inspections were done between July 2014 and May 2018. Bridge condition remains the same as reported in 2018. Slab to pavement approach is level with a smooth transition. Minimum level of cracks on the CMU blocks were observed after construction (Montana DOT 2018). This long-term performance study shows the GRS bridge abutment is a sustainable and economical solution.

Chapter 3. Study Approach

3.1. Overview

In this study, three full-scale instrumented GRS abutment models were constructed, and surcharge load tested to examine their load-bearing capacity and performance, as well as their construction speed as explained in more detail in the following sections. The three GRS abutment models in this study had two different facing systems: i.e. a widely used CMU block type, and an alternative using large concrete blocks from a local manufacturer. Results from these alternative bridge abutment systems were used to compare with numerical models for additional parametric studies to examine influences of selected design factors such as backfill and reinforcement properties on their predicted performance. Results of the study were used to develop a proposed cross-section for GRS abutments with large concrete block facing.

The performances of GRS abutment models were monitored using different sensors and manual readings as listed below:

- Reinforcement strains were calculated using readings from sixteen Wire Potentiometers (WP) during both the construction and surcharge load testing phases (**Figure 4**). WPs were also installed on the front and the top of the abutment models to measure their deformations during their surcharge load testing.
- Vertical pressures underneath facing blocks and at selected locations inside the GRS fill were measured using Earth Pressure Cells (EPCs) (**Figure 4**).

- Surcharge load was measured using Load Cells (LCs) (**Figure 5**).
- Geotextile reinforcement layers were also used to observe and measure internal settlements in the GRS fill through manual measurements during the deconstruction stage of the tests (**Figure 5**).
- Data Acquisition Systems were used for LC and WP readings (**Figure 6**).
- Data Loggers were used to collect the data from EPCs (**Figure 6**).
- Facing deformations were measured using manual readings before and after compaction of each GRS lift (**Figure 7**).

Figure 4. (Left) Wire Potentiometers; (Right) Earth Pressure Cells

Figure 5. (Left) Load cells during surcharge load testing; (Right) Deconstruction of the models


Figure 6. (Left) DAS for WP and LC readings; (Right) Data Loggers for EPC readings


Figure 7. (Left) Reference points on CMU blocks for manual reading of facing deformations; (Right) Large concrete blocks

The study approach is discussed in more detail in the chapters listed in **Table 1**.

Table 1. Approach and methods chapter list

Chapter #	Content
3	Overview, Instrumentation and Equipment, Laboratory Tests
4	Full-scale Testing of CMU and Large Concrete Block Facing GRS Abutment Models
5	Deconstruction of Full-Scale GRS Abutment Models
6	Numerical Simulation of GRS Abutment Models

3.2. Instrumentation and Equipment

Details of the instrumentation and equipment that were used during the construction of the bridge abutment models are as the following:

- Inside dimensions of the full-scale test box are 9 ft. high × 15.5 ft. deep × 8 ft. wide.
- Two 180-ton capacity hydraulic cylinders were used at the top for surcharge load testing of the models.
- Tractor was used to transport the gravel fill into and from the box.
- A Jumping-Jack (Chicago Pneumatic Gas Rammers MS780: 4 hp Honda GX120, 11-inch × 13-inch shoe size, Compaction Frequency: 12 Hz, Amplitude: 2.5-inch to 3.15-inch, Impact force: 18.6 kN/blow) compactor was used to compact the fill in 8-inch lifts in GRS Abutment Models #1 and #2 with one pass only on full throttle. In contrast, GRS Abutment Model #3 was compacted in 12-inch lifts with one pass only. These GRS abutment models are discussed in detail in Chapter 4.
- CMU blocks were carried without using a forklift. However, a small forklift was used to install the large concrete blocks up to the third row of the facing. A larger forklift was used both to place and remove the fourth row of large concrete blocks in Models #2 and #3.
- Gravel fill, CMU blocks and large concrete blocks were stored in a storage area near the test box during the construction and deconstruction process to reduce construction time.
- An 8 ft. × 10 ft. area shed adjacent to the test box was used to house and protect the data acquisition systems, computers and dataloggers against weather conditions.
- Wire potentiometers on the back of the test box were protected against weather conditions using tarp covers, and their wirelines inside the gravel fill were protected against compaction damage using protective layers of sand.

- Wire potentiometer specs: Measurement Specialties PT101-0010-111-1110
  92.010 mV/V/inch between 92.100 mV/V/inch
- One (1) 9-inch diameter Earth Pressure Cell at 82-inch (Model #1), 87-inch (Model #2) and 81-inch (Model #3) above the foundation slab: Geokon 4800 with 2 MPa
- One (1) 9-inch diameter Earth Pressure Cell at 47-inch above the foundation slab: Geokon 4810 with 2 MPa
- Three (3) 9-inch diameter Earth Pressure Cells underneath the blocks: Geokon 3500 with 2 MPa
- Datalogger 8021-1X + CR1000 (4-20mA gages) with Loggernet software
- Datalogger 8002-16-1 (16 channel) with Logview software

Figure 8 shows an elevation map of drilled holes on the back wall of the outdoor test box, which were used to run the wire potentiometers (extensometers) through to measure displacements of selected points on the geotextile reinforcement. Four layers of reinforcement were instrumented in each GRS abutment model. The size of all geotextile layers in the GRS abutment models in this study was kept the same (48-inch wide × 90-inch deep) to isolate and compare the influence of block size (i.e. Large concrete blocks vs. CMU blocks) on the GRS performance.

There is a set of 20 drilled holes at the back of the test station for WP connections, 16 of which were used to connect the WPs. Selected holes at 27-inch, 51-inch, and 75-inch above the foundation slab were used for all three GRS Abutment models. Holes at 91-inch level were used for only GRS Abutment Model #2, and 87-inch level were used for GRS Abutment Models #1 and

#3. The 108-inch tall walls of the test station were used as reference to measure GRS fill settlements during the deconstruction phase of the abutment models.

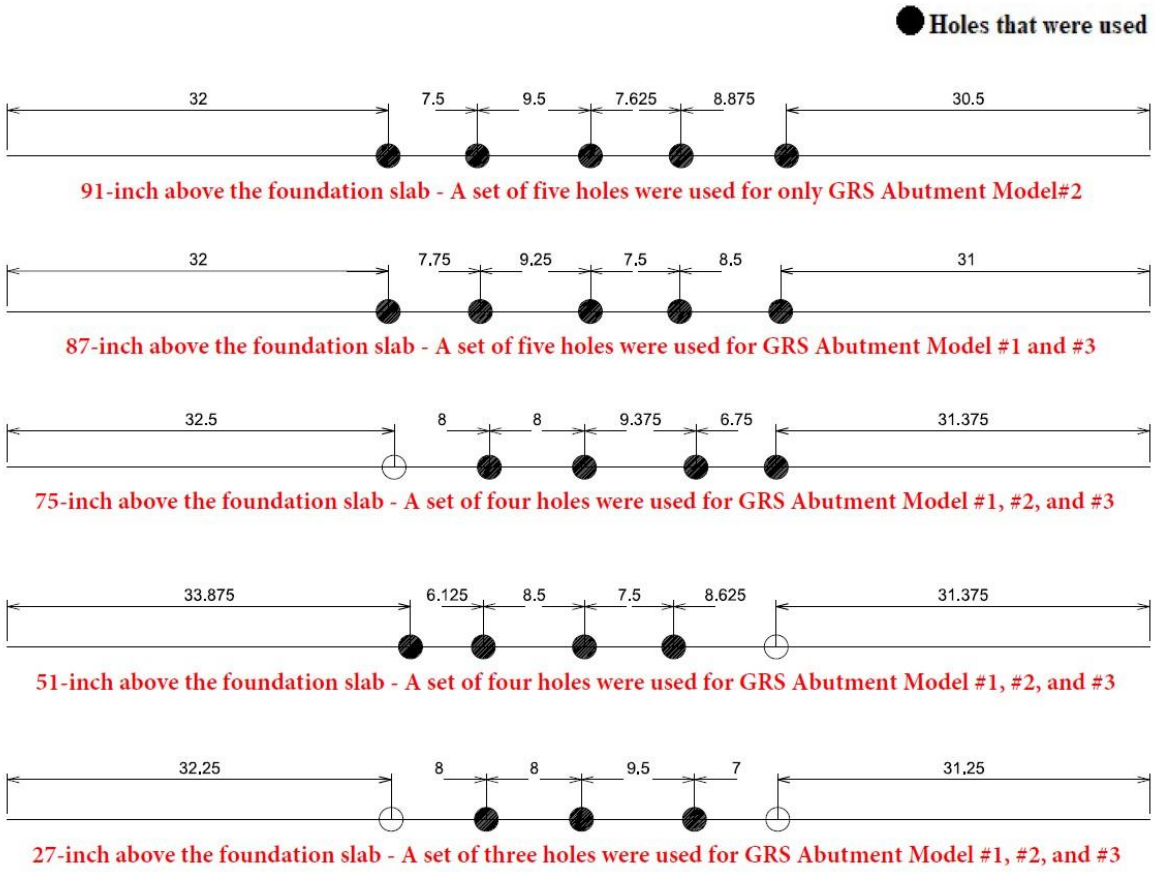

Figure 8. Drilled holes at the back of the test station that were used for WP connections

Location of each WP connections at different levels of GRS abutment models were selected to record the strain levels with highest accuracy during the surcharge load testing. Three different Earth Pressure Theories (i.e. Rankine, Coulomb and Log-Spiral) were considered as discussed in Section 2.1. The locations of each slip plane were calculated based on GRS abutment models and assumed material properties to locate the WP connections at four different levels for each GRS abutment model (i.e. 27-inch, 51-inch, 75-inch and 91-inch for GRS Abutment Model #2)

Designed WP connection plans at different reinforcement levels for this study are shown in **Figures 9 through 13**. A slight difference between a reinforcement elevation in GRS Abutment Model #1 relative to that in Models #2 and #3 (i.e. 91-inch elevation vs. 87-inch elevation) is due to height differences between the CMU blocks and large concrete blocks used in the respective models. CMU block facing is manufactured 0.375-inch less than its nominal dimensions for mortar placement (i.e. 7.625-inch high × 7.625-inch deep × 15.625-inch wide). In comparison, large concrete blocks used in this study are manufactured precisely in 2 ft. high × 2 ft. deep × 2 ft. wide or 2 ft. high × 2 ft. deep × 4 ft. wide dimensions.

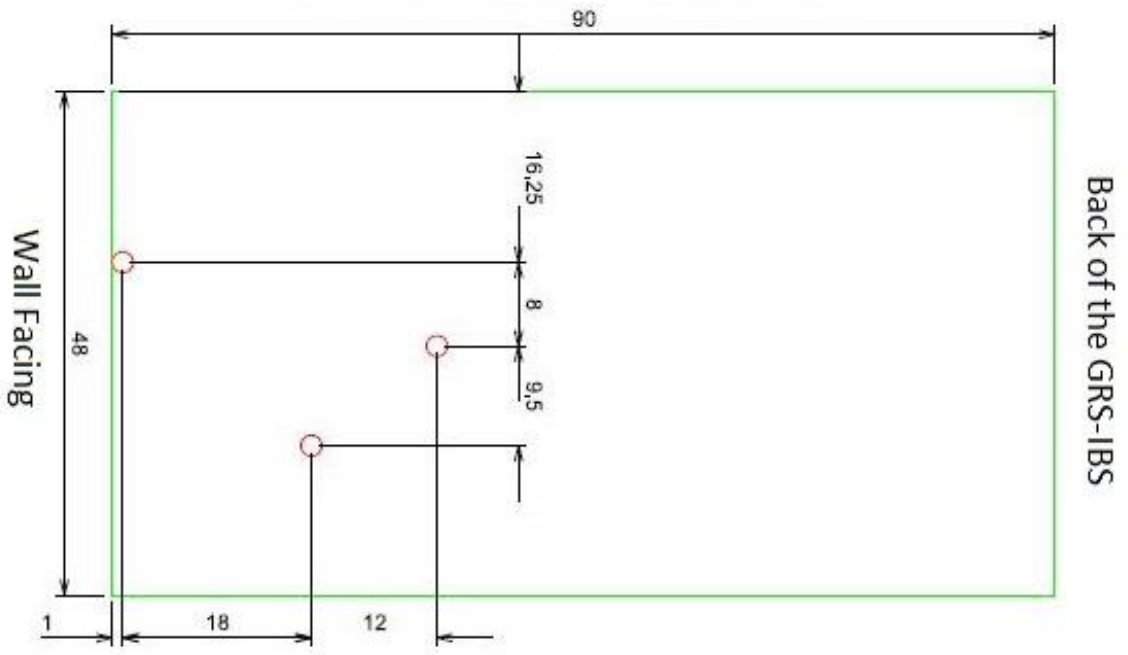

Figure 9. Plan view of WP connections to geotextile reinforcement at H = 27-inch above the foundation slab of GRS Abutment Models #1-#3 (dimensions are in inches)

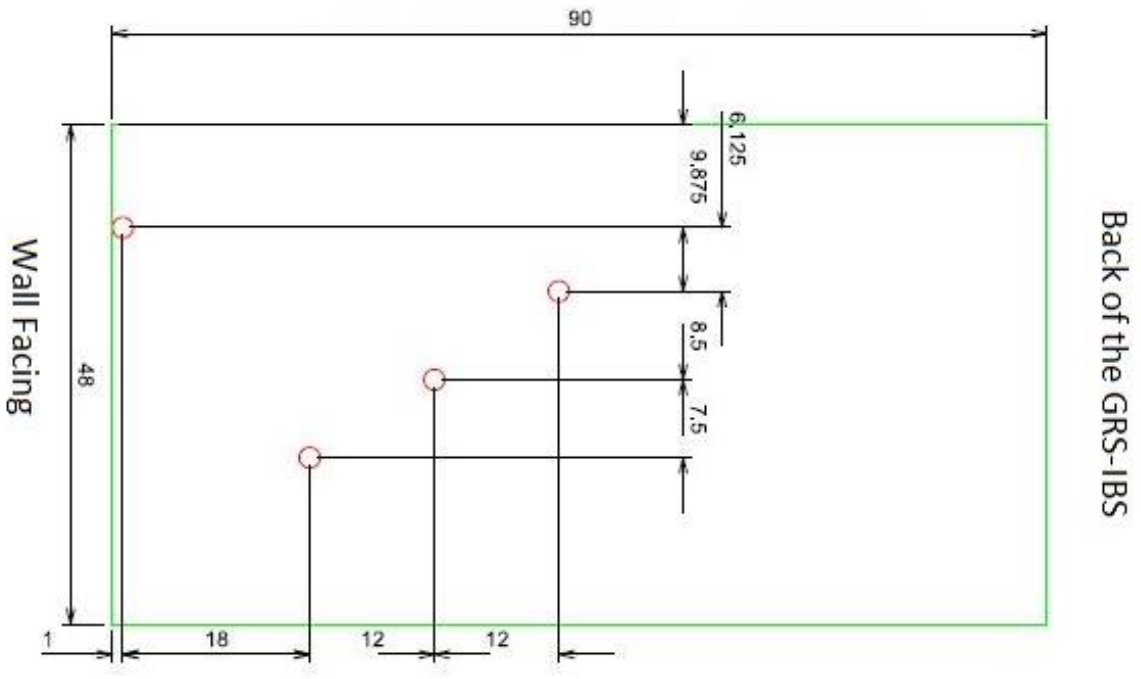

Figure 10. Plan view of WP connections to geotextile reinforcement at H = 51-inch above the foundation slab of GRS Abutment Models #1-#3 (dimensions are in inches)

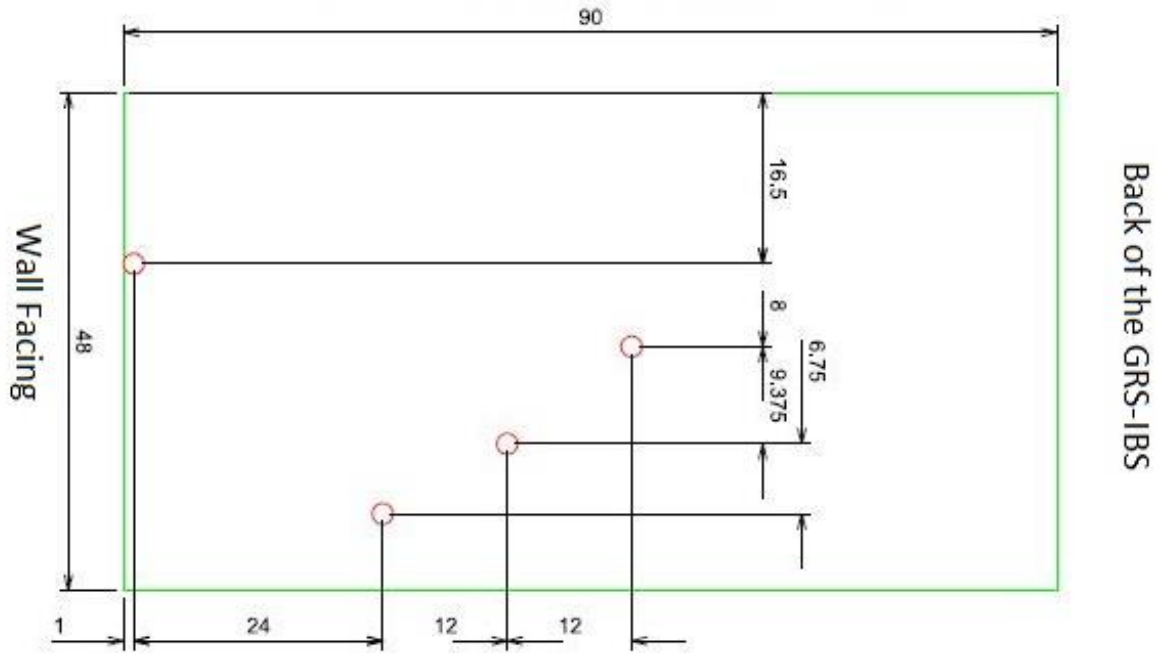

Figure 11. Plan view of WP connections to geotextile reinforcement at H = 75-inch above the foundation slab of GRS Abutment Models #1-#3 (dimensions are in inches)

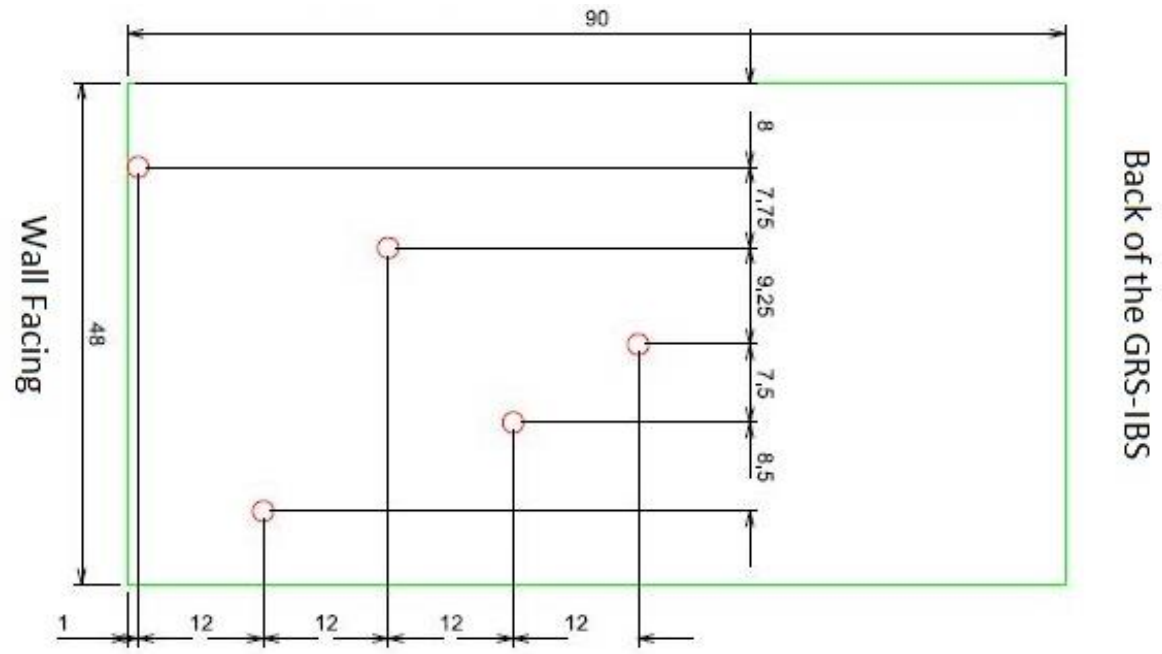

Figure 12. Plan view of WP connections to geotextile reinforcement at H = 87-inch above the foundation slab of GRS Abutment Models #1 and #3 (dimensions are in inches)

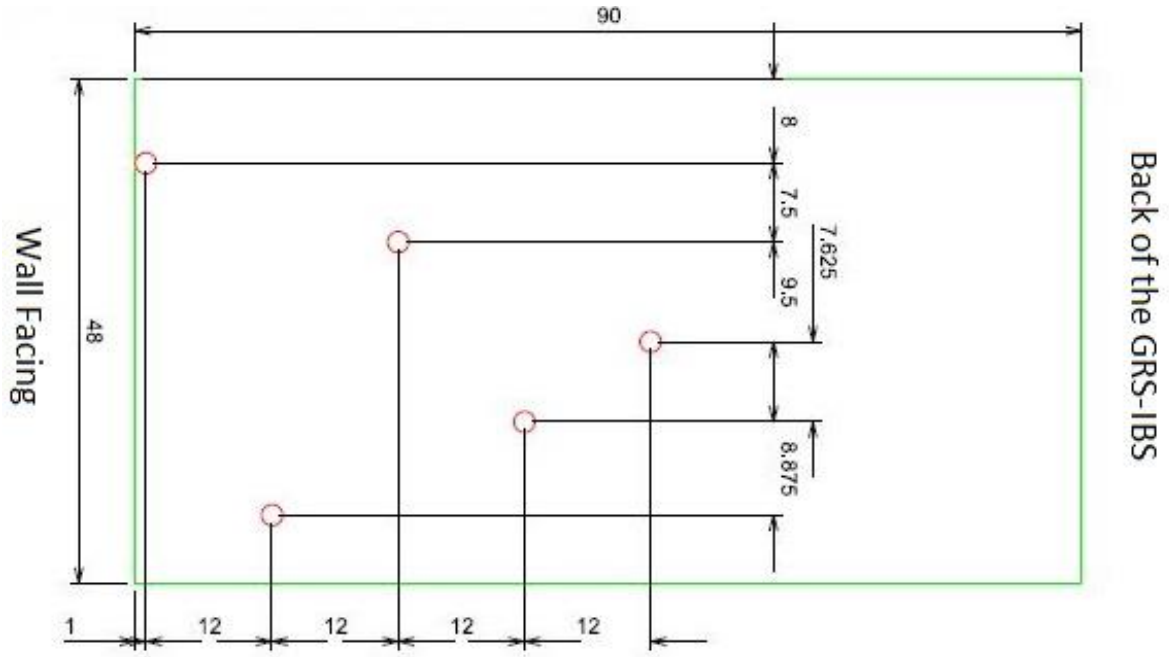

Figure 13. Plan view of WP connections to geotextile reinforcement at H = 91-inch above the foundation slab of GRS Abutment Model #2 (dimensions are in inches)

The reinforcement used in the models was Mirafi HP570, which is a polypropylene woven geotextile and satisfies the FHWA ultimate strength requirements of 4.8 k/ft. by 4.8 k/ft., and a minimum strength of 1.37 k/ft. at 2% strain in cross-machine direction (XD) as per the ASTM D4595 test protocol. The geotextile is produced in 5 yd by 100 yd roll dimensions. The geotextile should be unrolled perpendicular to the back of the facing to achieve the highest strength of the geosynthetic (i.e. XD). WP connections on the reinforcement were prepared using steel wires, plastic tubing, 2-inch by 2-inch geotextile patches, bolts, nuts, washers, clamps and plastic glue (**Figures 14 and 15**). The geotextile patch was used to help distribute the connection load evenly in the local area and reduce the movement of the bolted connection as much as possible. Nevertheless, the connections were all checked after surcharge load testing had been concluded, and it was observed that this method was successful in maintaining the integrity of the connections given the magnitude of surcharge loads that were applied on the models.

Figure 14. (Left) WP connections at 27-inch level reinforcement layer; (Right) WP connections at 51-inch level reinforcement layer

Figure 15. (Left) WP connections at 75-inch level reinforcement layer; (Right) WP connections on the geotextile reinforcement

Three EPCs were placed underneath the facing blocks in each model to measure vertical stress under the facing during construction and loading stages of the tests. EPC cables and EPCs were protected against rough surfaces of the blocks by placing them in the middle of a nominal 3-inch layer of sand and also to ensure a well distributed load on the EPC plates. **Figures 16 and 17** show EPC arrangements under large concrete blocks and CMU facing, respectively.

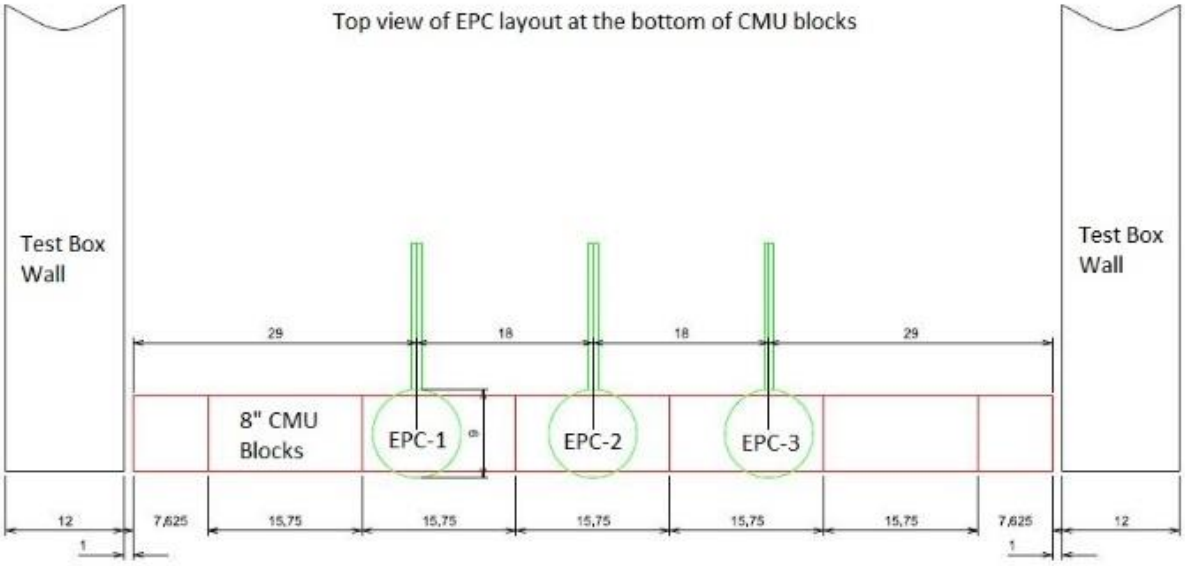

Figure 16. EPC layout under the facing of GRS Abutment Model #1 (plan view; dimensions are in inches)

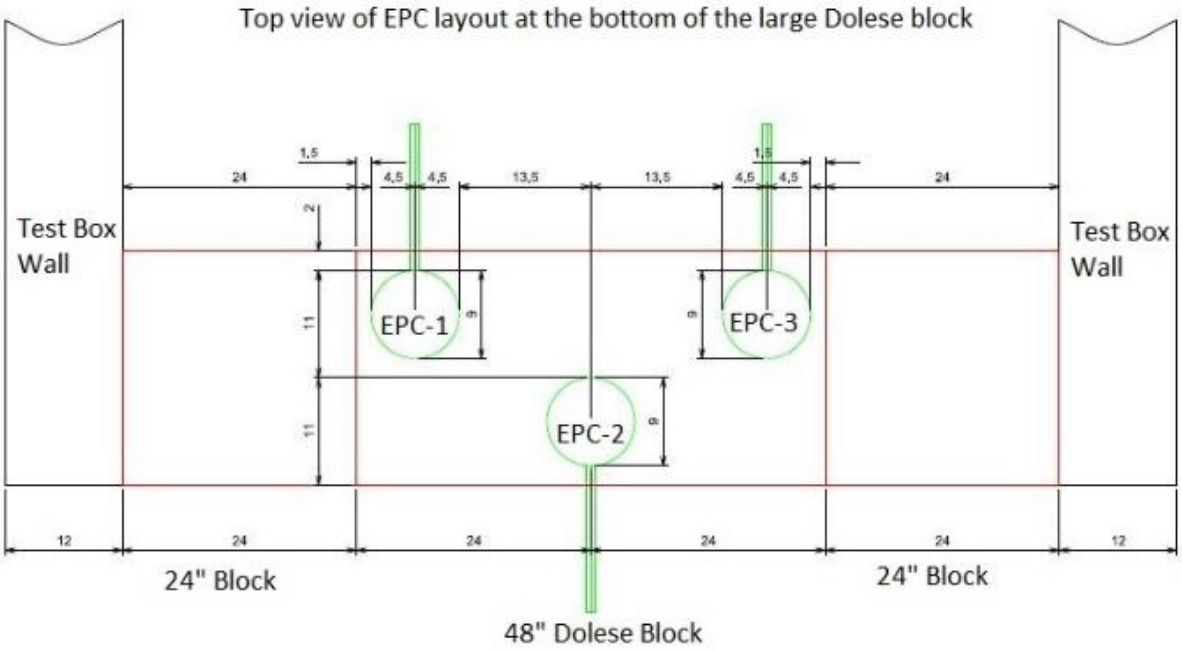

Figure 17. EPC layout under the facing of GRS Abutment Models #2 and #3 (plan view; dimensions are in inches)

CMU blocks used in Model #1 have some construction advantages in that, they are light (each block weighs approximately 36 pounds) and comparatively easy to handle and place without a need for forklifts or cranes. In comparison, large concrete blocks used in this study weigh approximately 2,400 pounds (half blocks weigh 1,200 pounds), which require the use of a forklift to be installed in the abutment facing. However, their larger dimensions make it possible to cover a much larger facing area, equivalent to that of nearly sixteen CMU blocks at a time (**Figure 18**).

Figure 18. (Left) Manual placement of CMU facing blocks; (Right) Placement of large concrete blocks using a forklift

The gravel backfill was transported to the test box using a front-loader tractor and was compacted using a Jumping-Jack with the same amount force applied to each backfill lift (**Figure 19**).

Figure 19. (Left) Compaction of GRS fill; (Right) Placement of the fill inside the test station

3.3. Laboratory Tests

A series of large-scale pullout tests was carried out on the geotextile reinforcement material under different overburden pressures (i.e. 12-inch and 18-inch of soil, and a third test with additional airbag surcharge on the top of the soil; **Figure 20**). These tests were carried out to ensure that the sensors and the data acquisition system (DAS) that were planned for use in the outdoor tests were in good operational conditions. In these tests, actuator, DAS and EPC data were simultaneously collected using separate computer stations and programs.

Figure 20. (Left) Pullout actuator and DAS; (Right) Geotextile reinforcement during pullout test

Two 400 kips (400,000 pounds) capacity load cells were used to measure the applied load on abutment models using 180-ton-hydraulic cylinders (**Figure 21**). The load cells were calibrated on a hydraulic testing machine with a devoted DAS. Five Earth Pressure Cells (EPC) were calibrated using Labview software, Geokon dataloggers and blocks of known weight (**Figure 22**).

Figure 21. (Left) 400 kip-capacity load cell; (Right) Calibration procedure for the load cell

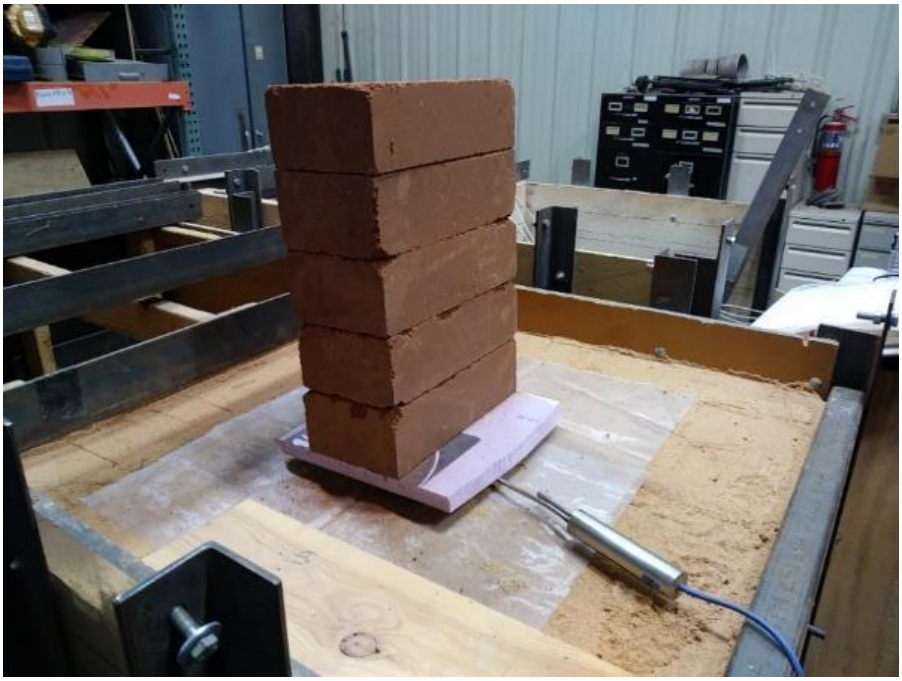

Figure 22. Earth pressure cell calibration

Locations of WP connections on geotextile reinforcement were selected based on predicted slip planes in the GRS fill under surcharge loading. The friction angle for the gravel fill for that analysis was determined from large-scale direct shear tests (8-inch high × 12-inch deep × 12-inch wide shear box) prior to the full-scale tests on the abutment models (**Figures 23 and 24**). Results indicated a value of 48^{o} friction angle for the fill aggregate at 40 psi Normal Stress and 45 psi Shear Stress (i.e. 3/8" #2 Cover supplied by Dolese Bros.), which is comparable to the range of values reported by Nicks *et al.* 2013 and 2014 for different open graded aggregates (values between 47^{o} and 48^{o} were reported for AASHTO #89 aggregate using the same scale direct shear tests).

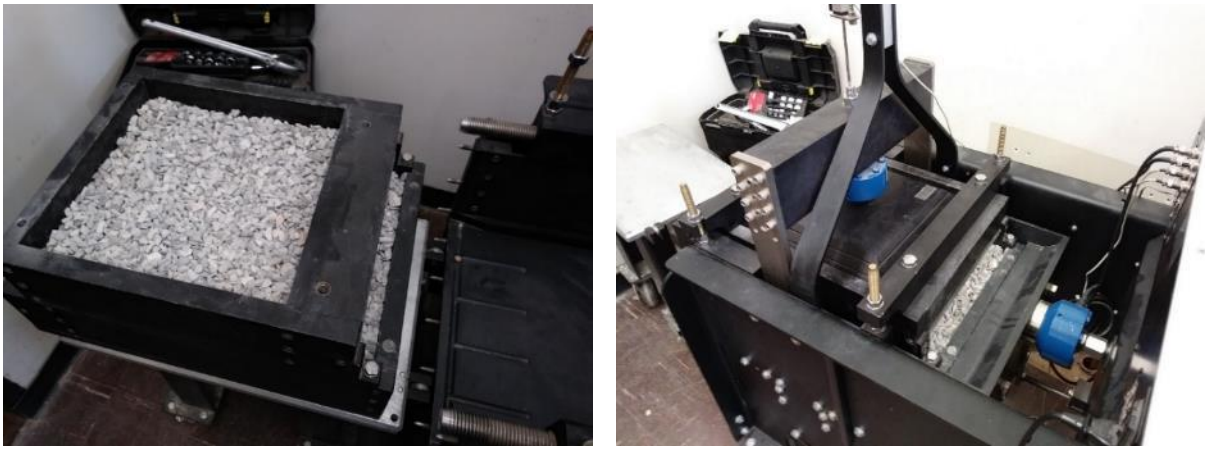

Figure 23. (Left) 3/8" #2 Cover fill material in the large-scale DST machine before testing; (Right) Test in progress

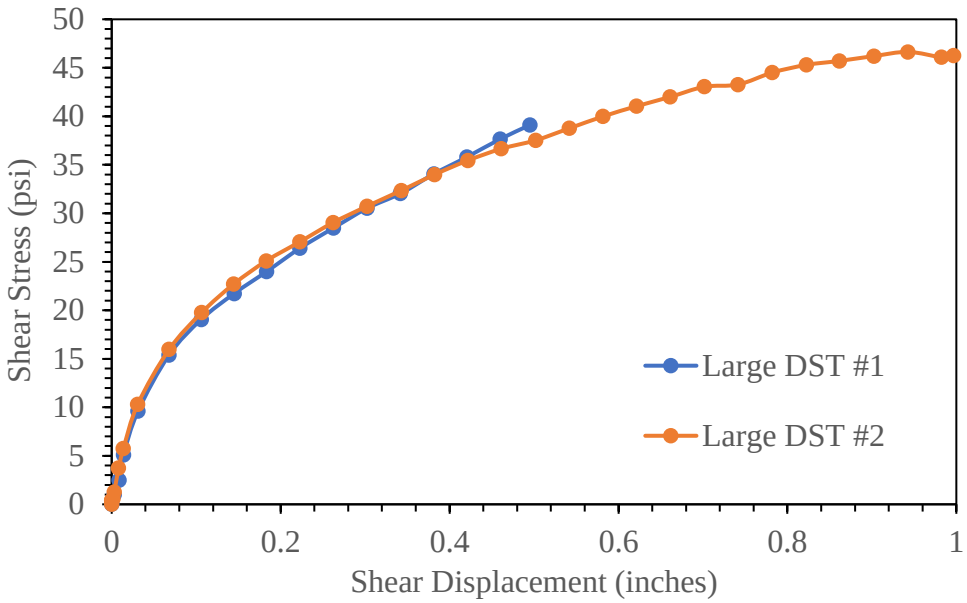

Figure 24. Shear Displacement vs. Shear Stress (Large DST)

The open-graded granular backfill material, 3/8" #2 Cover, was used for the full-scale GRS abutment models. FHWA recommends using well-graded VDOT-21A or open-graded AASHTO #89 granular fill material for GRS bridge abutments. The gradation of the 3/8" #2 Cover aggregate is similar to that of AASHTO #89 but with a lower fines content (**Table 2**). This makes 3/8" #2 Cover aggregate more drainable than AASHTO #89, which in turn is used as a drainable GRS fill. Additionally, the 3/8" #2 Cover aggregate is usually in stock at most Dolese plants, which makes it widely and easily available across Oklahoma.

Table 2. Comparison of AASHTO #89 and 3/8" #2 Cover aggregate gradations

Aggregate Sieve Size	Weight % passing amount	
	AASHTO #89	3/8" #2 Cover
0.50-inch	100	100
0.375-inch	90-100	90-100
No. 4	20-55	0-25
No. 8	0-15	0-5
No. 16	0-10	--
No. 50	0-5	--
No. 200	--	0-2

A series of sieve analysis tests (ASTM C136) was carried out to verify the gradation of the GRS backfill (**Figure 25**). The compaction requirement for GRS fills is a minimum of 95% maximum dry density, γ_{d_max}, as per AASHTO T-99 (Adams *et al.* 2018). ASTM D698 (standard effort) and ASTM D1557 (modified effort) Proctor test protocols are not suitable to find the γ_{d_max} values for the fill material that was used for GRS abutment models. An average unit weight of 95 pcf was determined for the compacted fill using a large-scale (i.e. 4 ft. × 4 ft. × 2/3 ft.) test bed as shown in **Figure 26**.

Figure 25. (Left) Sieve analysis of 3/8” #2 Cover aggregate at the lab; (Right) Taking samples of the gravel at site

Figure 26. Field evaluation of GRS fill unit weight

Standard (4-inch diameter mold) and modified (6-inch diameter mold) Proctor tests molds were used to determine the corresponding dry unit weight values. γ_d = 100 pcf for the 4-inch diameter

mold, and γ_d = 105 pcf for the 6-inch diameter mold values were found as the dry unit weight values.

Two different samples of 3/8" #2 Cover aggregate were tested to determine their particle size distributions and how they compare with AASHTO #89 aggregate, and the grain size distribution data provided by the supplier. The samples were oven dried first. The test results are shown in **Figures 27 and 28**, which confirm that the aggregate that was available for the GRS abutment models while comparable with AASHTO #89, is indeed more drainable due to smaller percentages of finer particles (**Figure 27a**; as had been anticipated), and shows a very good agreement with the more drainable (i.e. the lower) limit of the data provided by the supplier (**Figure 28a**).

The same aggregate sample was oven dried again and used in a follow-up sieve (2^{nd}) analysis to determine the increased amounts of finer particles as a result of Proctor compaction hammer, which is also anticipated in the field. Results are shown in **Figures 27b and 28b**, which indicate that while the aggregate sample contains slightly increased amounts of finer particles, (1) its overall gradation is otherwise practically unchanged, (2) maintains its drainable properties for the intended GRS fill application, and (3) its gradation still falls within the limits provided by the supplier (**Figure 28b**).

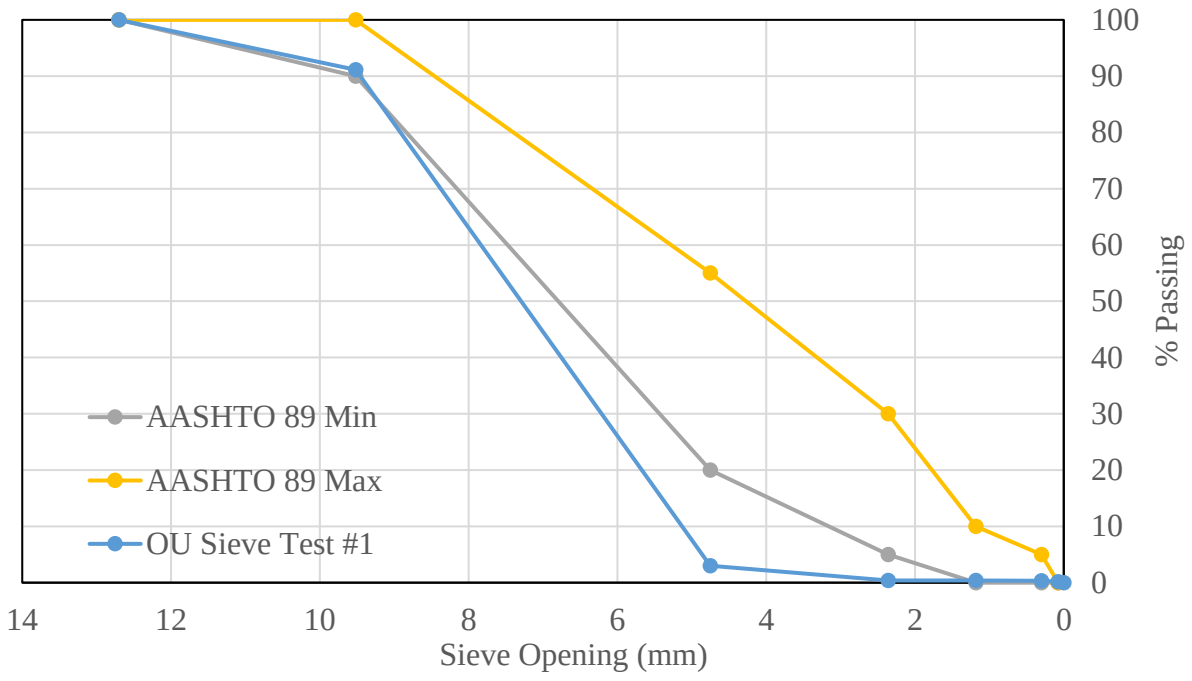

(a)

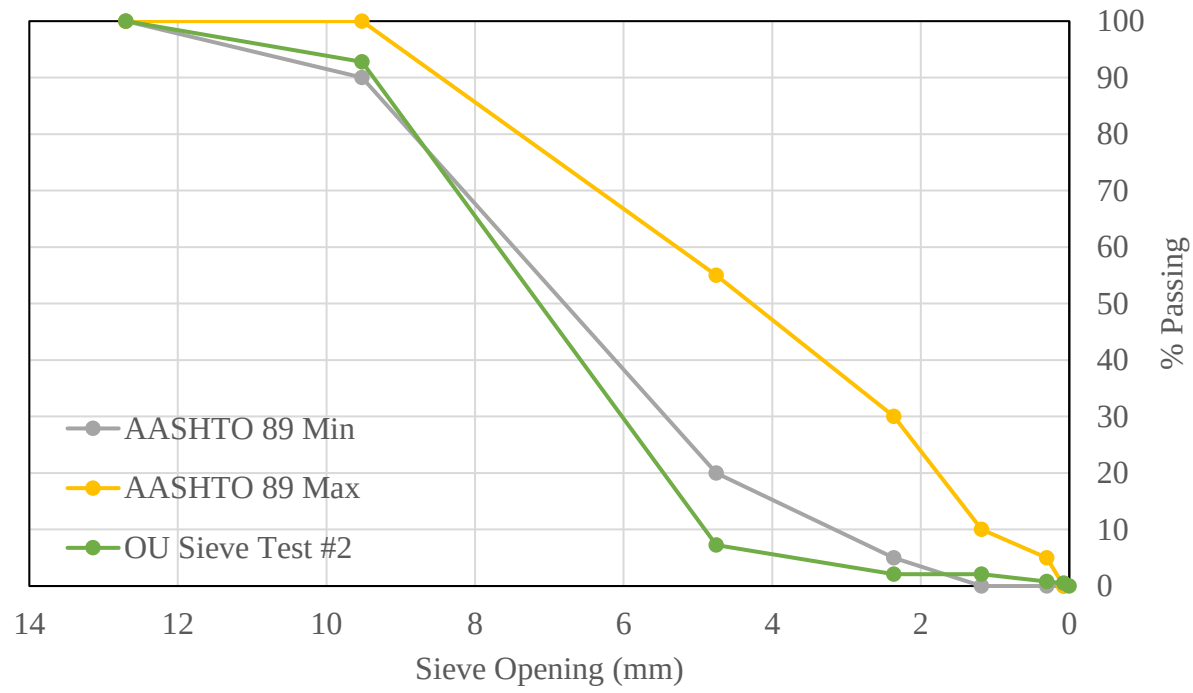

(b)

Figure 27. Comparison of sieve analysis results for 3/8" #2 Cover aggregate from this study with particle size distribution of AASHTO #89 aggregate gradation of sample before compaction test (a); After compaction with Proctor hammer (b)

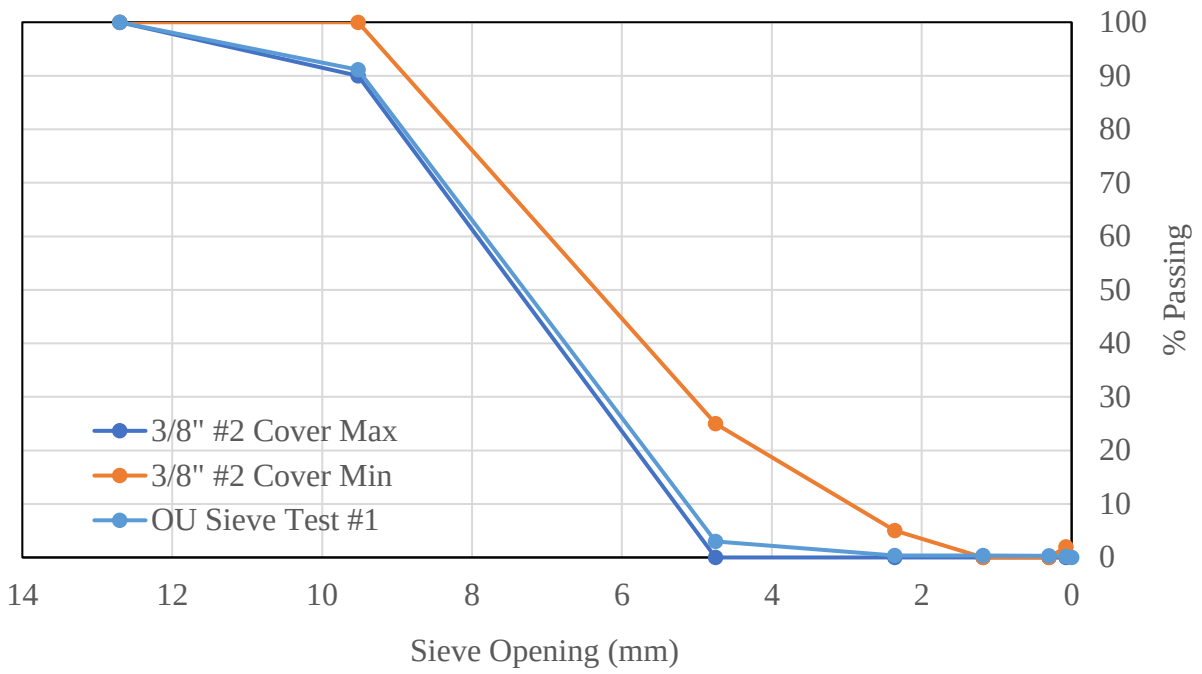

(a)

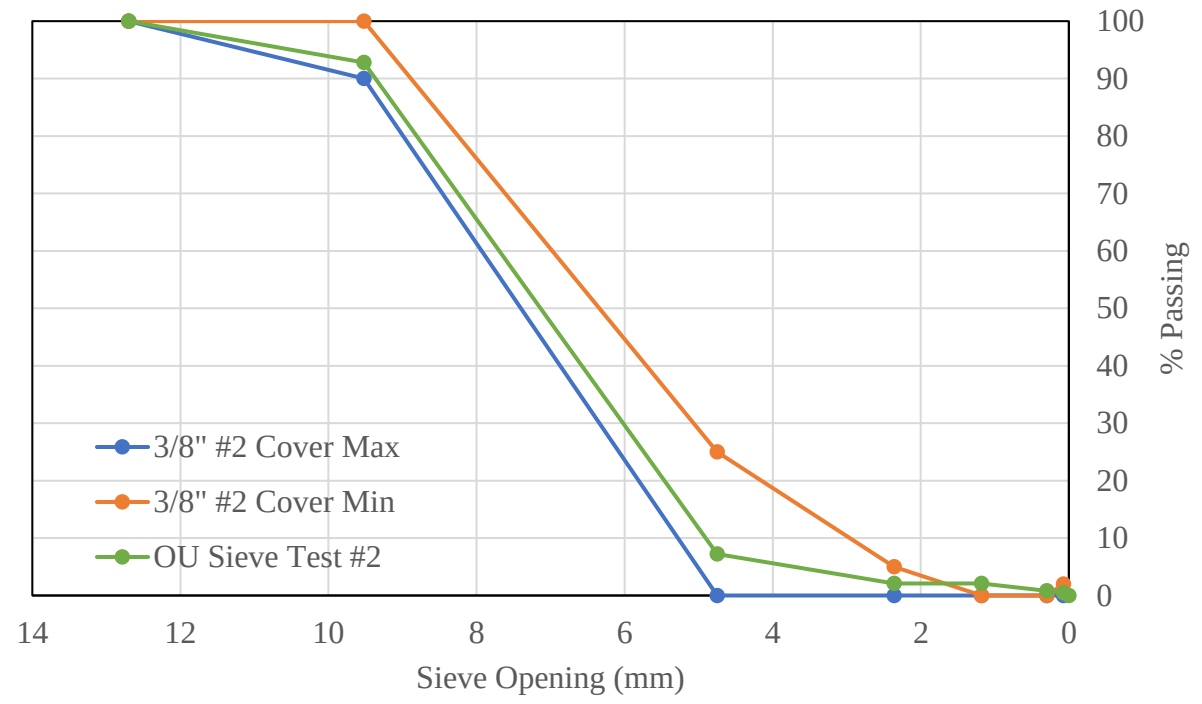

(b)

Figure 28. Comparison of sieve analysis results for 3/8" #2 Cover aggregate from this study with particle size distribution provided by the supplier gradation of sample before compaction test (a); After compaction with Proctor hammer (b)

Chapter 4. Full-scale Testing of CMU and Large Concrete Block Facing GRS Abutment Models

4.1. Overview

Full-scale testing was done in several stages. There were three different GRS abutment models planned and designed for performing this research study. The design and construction of these GRS abutment models are described in the following sections.

The service load pressure on the GRS bridge abutment is 4 ksf according to the FHWA guidelines (Adams *et al.* 2018). This translates to a line load of 20 kips that needed to be applied on the GRS abutment model using the 8 ft. by 0.625 ft. loading beam available at the test station. The loading frame, together with two 180-ton capacity hydraulic cylinders and 400 kips load cells possess an order of magnitude larger capacity to apply much larger loads on the abutment models.

In planning the instrumentation layout for the GRS abutment models in this study the simulated bridge load using the loading beam was placed 24-inch behind the facing column as a reasonable distance for the 8 ft. high GRS abutment models to instigate a global slip plane behind the facing (passing through the toe), given the value of the GRS fill friction angle was determined as 48^{o} (Section 3.3). The location of the loading beam and anticipated slip plane geometry happened to be also consistent with one of the earlier design examples on GRS abutment models (Wu *et al.* 2006), which was 8 ft. high similar to the models built and tested in this study. The location of the back of the abutment facing inside the test box was kept the same for both facing types (i.e. CMU

blocks and large concrete blocks) regardless of their size to keep the size of the abutment fill identical between the two facing models (**Figure 29**).

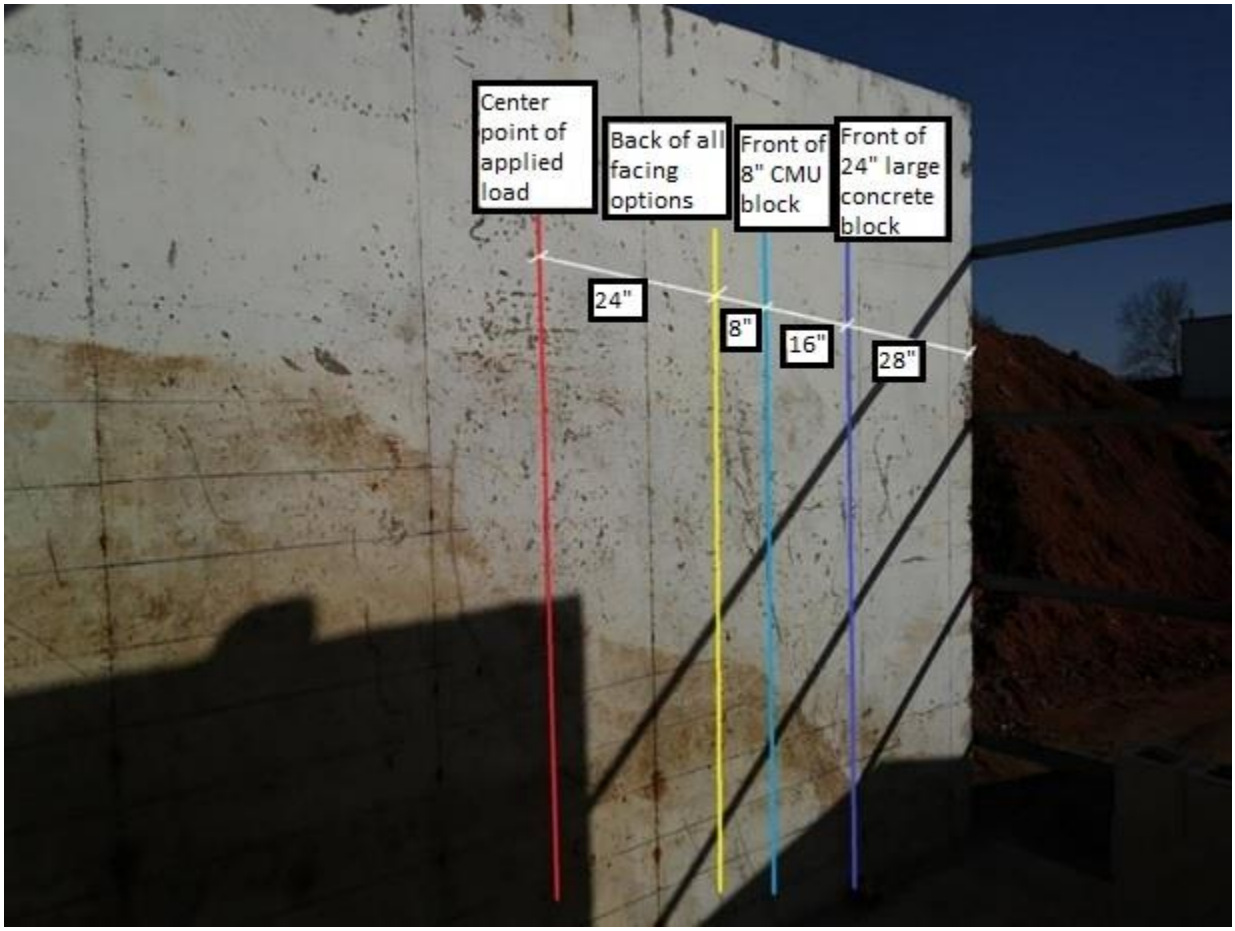

Figure 29. Locations of the loading beam and GRS facing as projected on the sidewalls of the test box

4.2. GRS Abutment Model #1: CMU Block Facing with 8-inch Geotextile Spacing

Construction and surcharge load testing of an instrumented CMU block facing (7.625-inch high × 7.625-inch deep × 15.625-inch wide) GRS abutment model with 7.675-inch geotextile spacing is named as GRS Abutment Model #1. This stage is considered as 'Control test' to compare with

GRS Abutment Model #2 and GRS Abutment Model #3. Control test setup was designed according to Adams *et al.* 2012. Full-scale test box inside dimensions are (9 ft. high × 15.5 ft. deep × 8 ft. wide). Two 180-ton capacity hydraulic cylinders were used for surcharge load at the top with the help of electric hydraulic pump. **Figure 30** shows the front view of OU Fears lab full-scale test box.

Figure 30. (Left) Front view of OU Fears lab empty full-scale test box; (Right) Front steel frames for WP connections

There were two full blocks in the middle and two half blocks on each side of the focus area of the facing. Focus area of mid-section width of the facing was 48-inch long. Eighty full and forty half-cut CMU block facing units were used including extra for accounting damages. There were eleven geotextile layers with 8-inch spacing inside the granular backfill. The results were compared by selecting four different geotextile layer levels. The wire potentiometers (WP) setup heights are shown in **Figure 31**. Points close to failure plane and load concentration have more wire potentiometers. Wire potentiometers were used to measure the displacement at a certain point.

Strain levels can also be calculated with the data collected at a certain level with different displacement readings.

There was a set of 16 WPs inside the granular backfill in the test box for GRS Abutment Model #1. Data from these WPs were used to calculate reinforcement global strains, ϵ_{ij}, according the following equation (Eq. 7):

$$\epsilon_{ij} = \frac{u_i - u_j}{\Delta l_{ij}} \quad [7]$$

where i and j denote contact points WPi and WPj on a given reinforcement layer, respectively, and Δl_{ij} is the distance between the contact points i and j.

There were five WP's in front of the facing to measure the displacements during loading. At least six points were selected at each block level to measure the displacements manually during the construction. Facing deformations were recorded before and after the compaction. These reference points were used to compare the deformation readings collected by the front WPs during the surcharge load test. Two WPs at the top of the loading steel frame were used see if there was a differential settlement during the surcharge load testing.

There was a set of three Earth Pressure Cells (EPC) at the bottom of the facing blocks and they were located within 3-inch sand layer. There was one EPC placed at a closer location to the loading and one EPC placed in the mid-section of the setup. Grand total of five EPCs were used in GRS Abutment Model #1 setup. **Figure 31** shows the cross-section view of GRS Abutment Model #1. The surcharge load distribution on EPCs were initially calculated with Boussinesq's Method in NAVFAC (1986) (Also see Eq. 6 earlier in Section 2.1). EPC at a closer location to the loading,

EPC placed in the mid-section and EPCs under the facing blocks should receive approximately 0.2%, 1.2%, and 0.6% of the surcharge load based on Boussinesq's Method.

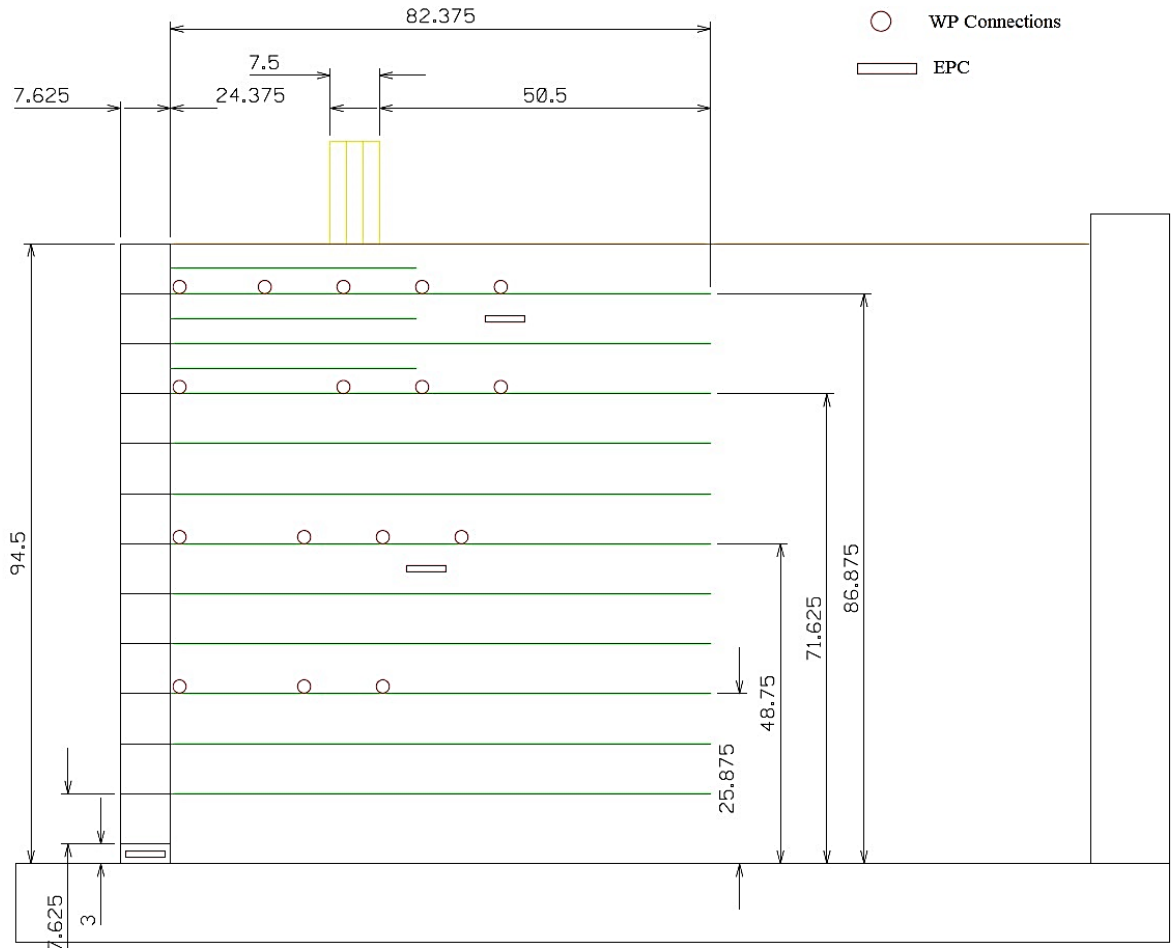

Figure 31. Schematic instrumentation layout for GRS Abutment Model #1 (CMU block facing with 8-inch reinforcement spacing; Dimensions are in inches)

CMU blocks has some construction advantages when they are used for facing. They are light, around 36 pounds, easy to handle and place. They do not require special tools like forklifts or cranes. However, large concrete block weighs around 2,400 pounds (2 ft. high × 2 ft. deep × 4 ft. wide). Smaller version of large concrete block (2 ft. high × 2 ft. deep × 2 ft. wide) weighs around 1,200 pounds. Both large concrete blocks require forklift or crane to install.

Labor requirements for the entire construction activity of all three abutment models were recorded in detail to compare the construction speed of the CMU block facing GRS abutment model relative to the large concrete block facing alternatives.

A 3-inch-thick sand layer was placed underneath the first-row of 8-inch CMU blocks to accommodate the earth pressure cell assemblies (**Figure 32**). As a result, an 11-inch-thick gravel layer at the bottom of the test box was needed and placed for the first lift of the GRS fill. A front-loader tractor is used to place higher lifts of the GRS fill through the earth ramp on the east side of the test box.

Figure 32. (Left) Installation of the first three EPCs under the CMU blocks before covering with sand; (Right) After covering with sand

Shortly after the start of construction, the 3-inch-thick sand layer that was placed under the blocks to protect the EPCs had slightly settled due to heavy rain and loss of some sand. Consequently, an extra fill material at the front (toe) of the facing blocks was placed to prevent further loss of sand in any future precipitation event. Since then, no further settlement of the facing blocks was observed as a result of this precaution (**Figure 33**).

Figure 33. (Left) Placement of the first-row of CMU blocks; (Right) Placement of backfill lift

Due to the compaction of the fill material, an outward movement of the CMU blocks was observed. Therefore, a setback distance of 0.50-inch for each row of the CMU blocks was started to use to counter this movement. The Jumping-Jack compactor was limited to a point farther away than 1.5 ft. from back of the facing, and a hand tamper was used instead to pack the gravel, which has shown to work well for the purpose (**Figure 34**). Placement of the second-row of CMU blocks and third-row can be seen in **Figure 35**.

Figure 34. (Left) Compaction of GRS fill using a Jumping-Jack equipment; (Right) Movement observation of CMU blocks after compaction

Figure 35. (Left) Placement of the second-row of CMU blocks; (Right) Third-row

During the installation of wire potentiometers (WP) on the reinforcement layers, sand was used to cover the WP cables and sleeves, followed by careful placement of a protective gravel layer (**Figure 36**). This is done to minimize any damage from the placement and compaction of the gravel fill using heavier equipment during the construction process. Afterwards, the GRS fill for each lift is dumped using a tractor bucket over the east sidewall of the test box and compacted, as described earlier.

Figure 36. (Left) Protection of WP cables and sleeves through careful placement of sand; (Right) Gravel layers after placement of sand

A tarp was used to cover the WPs at the back of the test box against moisture and weather elements (**Figure 37**). Additionally, all WPs were wrapped individually with paper towels and plastic bags, before mounting them on the wooden racks at the back of the test station. The temperature and weather conditions were also recorded to help with future analysis and interpretation of the test results.

Figure 37. (Left) WPs at the back of test box; (Right) WP protection measures

In order to measure facing displacements, six points were marked at every CMU block row and their outward movement were monitored and measured relative to their placement (initial) location before and after compaction (**Figure 38**). Compaction is done in one pass in the transverse direction relative to the GRS facing with the lowest energy setting of the Jumping-Jack. The energy imparted by the compactor was determined using any available data by the Jumping-Jack's manufacturer (i.e. Compaction Frequency: 12 Hz and Amplitude: 2.5-inch to 3.15-inch).

Figure 38. Numbered facing blocks for displacement measurements

WP and EPC readings were taken during the construction process. The readings of three EPCs and three WP readings were recorded initially. Four EPCs and seven WPs were recorded when the GRS height was at the eight-row. Two different data-loggers (Geokon 8002-16 and 8021) were used to record the EPC readings. WP readings were recorded at the same time using a separate (LabVIEW-based) Data Acquisition System (DAS) (**Figure 39**).

Figure 39. (Left) Installation of the fourth EPC; (Right) Readings from the WPs

Meanwhile, the cross beam of the loading frame was raised by approximately 24-inch to have sufficient space between the loading assembly (including load cells) and the top of the GRS fill. The loading frame was originally designed and fabricated for such a possibility and therefore, there were already bolt holes available at the top of the loading frame for this purpose. A large capacity forklift was rented for this operation.

FHWA guidelines recommend that additional reinforcement layers be installed underneath the bridge abutment load to form a shallow reinforced footing in the top portion of the GRS fill. Therefore, additional reinforcement layers (45-inch in length) were installed at mid-levels of the tenth through twelfth CMU block rows. Additionally, the top three CMU blocks were filled with ready-mix concrete, and they were connected using steel rebars to prevent the top rows from excessive lateral movement and cracking in the vicinity of the applied surcharge load (**Figure 40**).

Figure 40. (Left) Placement of the reinforcement layers for shallow footing under the loading beam; (Right) Connecting the top three CMU blocks using concrete and rebar as per the FHWA guidelines

The construction of GRS Abutment Model #1 was completed. Meanwhile, the total personnel hours for the entire construction activity was recorded to compare the construction speed of this

control CMU block facing GRS abutment model with the large concrete block facing alternatives (i.e. GRS Abutment Models #2 and #3). **Figure 41** depicts the construction progress of the placement of the final lifts of the GRS fill (i.e. #12 of the CMU blocks).

Figure 41. GRS Abutment Model #1 at the end of construction

All wire potentiometer (WP), load cell (LC) and earth pressure cell (EPC) cables were elevated from the ground level to protect them against any traffic and/or grounds-keeping activity in the vicinity of the test station. The cables were marked individually to ensure that all sensors were correctly connected to the data acquisition system located in the nearby shed. The WPs installed previously at the back of the test box were protected against weather conditions using tarp and individual plastic covers. Afterwards, the installation of the loading assembly was completed and ancillary instruments, which had load cells and WPs for measuring the settlement of the loading beam at the top of the GRS fill. The load cells and front WPs were protected with tarp until the surcharge load testing date (**Figure 42**).

Figure 42. (Left) View from West side of the test station of WPs and the connecting cables to DAS housed in the shed; (Right) Back view

During the installation of the loading assembly, the loading beam was placed on the top of the GRS fill using a forklift and was centered under the hydraulic pistons (**Figure 43**). The bottom dimensions of the loading beam are approximately 8 ft. wide by 0.625 ft. deep. The final instrumentation setup was done afterwards.

Figure 43. (Left) Front view of the installation of the loading beam under the hydraulic pistons; (Right) Back view

Figure 44. Installation of five WPs to measure facing deformation at different levels

The front WPs were installed on steel racks at 40-inch, 64-inch, and 88-inch above the foundation slab (**Figure 44**). The electric-hydraulic pump and its hose connections were tested for proper operation in preparation for the load test (**Figure 45**).

Figure 45. Attachment of the electric-hydraulic pump to the loading assembly

Finally, cylindrical loading extension blocks were placed between the hydraulic cylinders and the load cells to apply the load evenly during the test (**Figure 46**).

Figure 46. Placement of load cells and their extension blocks before the test

The load cells and hydraulic pistons were checked to examine their conditions after the load test (**Figure 47**). The load cells were needed to be sent out to the manufacturer for factory recalibration. Deconstruction procedure was performed after the surcharge load testing of GRS Abutment Model #1. The reference heights marked on each side of the test station were used to find the deformation profiles of each geotextile layers. Detailed measurements and photos were taken for analysis.

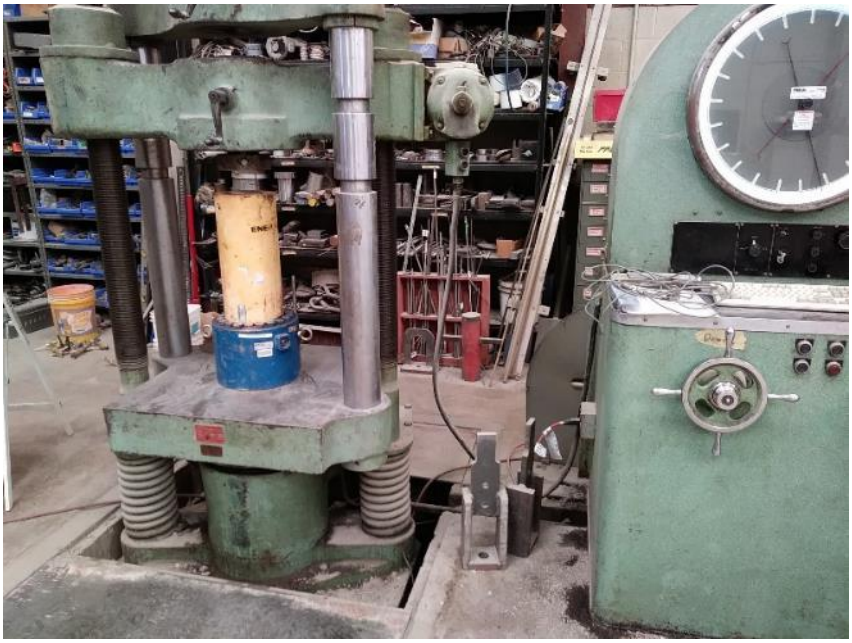

Figure 47. Testing of load cells and hydraulic pistons after the conclusion of GRS Abutment Model #1 surcharge load testing

4.3. GRS Abutment Model #2: Large Concrete Block Facing with 8-inch Geotextile Spacing

Construction and surcharge load testing of an instrumented large concrete block facing (24-inch high × 24-inch deep × 48-inch wide) GRS abutment model with 8-inch geotextile reinforcement spacing is named as GRS Abutment Model #2. There was a set of three large concrete blocks on each row of the GRS abutment model facing (one full block in the middle and two half blocks on each side). Focus area of mid-section width of the facing was 48-inch long. Five full and ten half-cut CMU block facing units were used including extra for accounting damages. Eleven layers of full-length geotextiles were used for GRS Abutment Model #2.

Twenty-two WPs (sixteen WPs inside, two WPs at the top and four WPs in front) and five EPCs were used for the test setup. At least six points were selected at each block level to measure the displacements manually during the construction like GRS Abutment Model #1. Deconstruction

procedure were performed after the surcharge load testing like GRS Abutment Model #1. **Figure 48** shows the cross-section view of GRS Abutment Model #2.

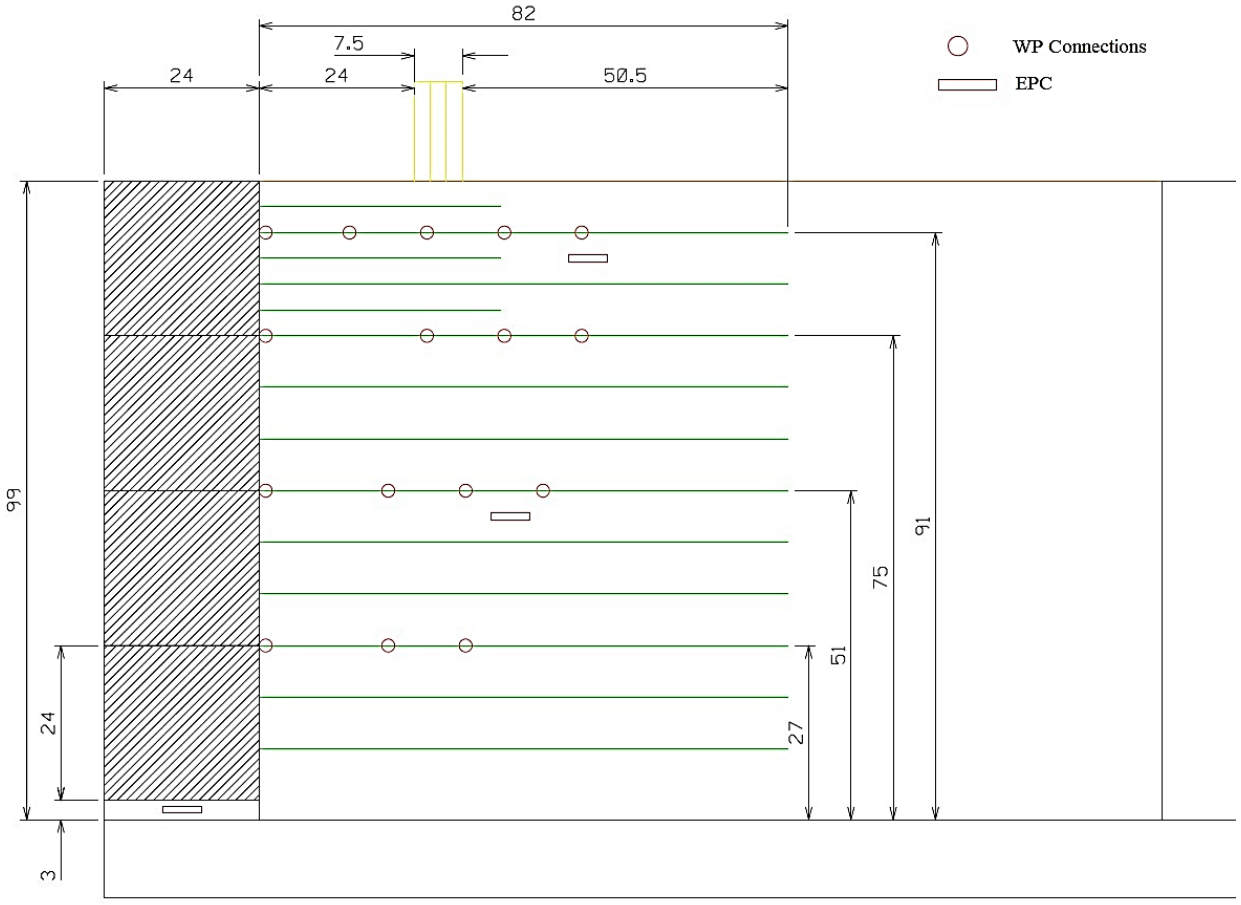

Figure 48. Schematic instrumentation layout for GRS Abutment Model #2 (Large concrete block facing with 8-inch reinforcement spacing; Dimensions are in inches)

Due to differences between the nominal and actual dimensions of the large concrete blocks, and existence of shear keys on their sides, their placement and fitting in the test box proved to be much more time-consuming than had been anticipated. It is understood that this additional effort does not reflect the construction time in the field, and hence it was noted accordingly when calculating

and comparing the total labor hours against those for the CMU block alternative. In the meantime, as a solution, additional 0.50 to 0.75-inch of concrete was shaved off from one side of one of the half-blocks (i.e. in addition to removing its side shear key) to expedite their installation within the confines of the test box.

Similar to GRS Abutment Model #1, the bridge abutment model facing was comprised of a 48-inch wide middle section (referred to as the instrumented/observation section), which is flanked by two 24-inch wide facing columns with separate reinforcement layers, and separated by full-height construction joints in the facing. However, in GRS Abutment Model #1, the observation section was comprised of three 16-inch long CMU blocks whereas in GRS Abutment Model #2, only one 48-inch long block was sufficient for each level to construct this section of the bridge abutment model. Two half-blocks (i.e. 24-inch wide) were placed on each side of the middle block to complete the length of the facing at each level. Also, as opposed to the first bridge abutment model where all three EPCs were installed in the same row under the 8-inch-thick CMU blocks, the EPCs in GRS Abutment Model #2 were staggered across the width of the large concrete block. All three EPCs were checked and calibrated before installation.

Similar to what was done in GRS Abutment Model #1, a 3-inch-thick sand layer was used to protect the EPCs and distribute the load on them evenly. The EPCs were placed at the middle of the sand layer, 1.5-inch above the bottom of the test box. All cables and WP wire extensions were also covered with sand to protect them during the construction and loading stages of the test.

The large concrete blocks have male and female shear keys on their sides. Therefore, one male shear key on one of the 24-inch wide half blocks had to be removed using a drill hammer so that all three large concrete blocks could be fitted side-by-side within the available width inside the test box. Some additional material also had to be removed from the side of the half-blocks (i.e.

approximately 0.50-inch of concrete from each block) to ensure that the blocks would be able to move outward with no interference from the sidewalls during the loading stage of the test (**Figure 49**).

Figure 49. Removal of shear key and a thin layer of material from the side of a large concrete half-block before its installation in the GRS abutment model

A forklift with chains was used to carry the large concrete blocks from the storage area to the test box (**Figure 50**). 24-inch and 48-inch wide large concrete blocks weigh approximately 1,200 pounds and 2,400 pounds respectively. A larger capacity forklift was needed to be able to build the final sections (upper rows of blocks) of the GRS Abutment Model #2. During the placement of the large concrete blocks, care was taken to ensure that their backside would line up exactly at the same location as the back of the CMU block facing in GRS Abutment Model #1 (**Figure 51**). Afterwards, the exposed sand layer and the EPC cables were covered with gravel at the toe of the facing blocks to protect them against erosion and any possible damages during construction.

Figure 50. (Left) Transporting the large concrete blocks in the test box; (Right) Placing them

Figure 51. (Left) Installing the second large concrete block of the first-row; (Right) Third large concrete block

The GRS fill was compacted using a Jumping-Jack in 8-inch lifts to maintain consistency with the procedure used in GRS Abutment Model #1. Much heavier large concrete blocks allowed for a hassle-free and significantly better compaction effort than the lighter CMU blocks, which showed a tendency to move outward if the compaction equipment would get too close to the facing. This helped with both the speed and the quality of the GRS compaction in the region immediately behind the facing (i.e. uniformity of the unit weight relative to the rest of the GRS fill), which incidentally, has significant influence on the facing deformation and the GRS performance as a

whole. Similar to GRS Abutment Model #1, a front loader tractor was used to transport and place the GRS fill inside the test box before spreading and compaction (**Figure 52**).

Figure 52. (Left) Compaction of the GRS bridge abutment fill behind the first-row of large concrete blocks; (Right) Installation of the first geotextile layer

In order to install the last row of large concrete blocks between the elevations 75-inch through 99-inch above the foundation slab on the GRS abutment model, a larger lift truck was needed than what OU Fears Lab had available. **Figure 53** shows the installation of the top row of large concrete block facing using a rental lift truck. Throughout the construction stage, deformations of the GRS facing column were surveyed at six points on each row of blocks to compare with those of GRS Abutment Model #1.

Figure 53. (Left) Installation of the top (forth) row of large concrete block facing; (Right) The subsequent elevation view of the GRS bridge abutment

Additional geotextile reinforcement layers (48-inch wide × 45-inch depth at the middle section, and 24-inch wide × 45-inch deep at each side) were installed at three different elevations (i.e. 79-inch, 87-inch and 95-inch) as part of the reinforced footing section underneath the bridge deck as per the FHWA guidelines. Wire potentiometers (WP) were used during the construction stage at selected elevations (i.e. 25-inch, 51-inch, 75-inch and 91-inch above the foundation slab) to measure movements of reinforcement layers during construction and the subsequent surcharge load testing stage. The GRS fill was compacted using a Jumping-Jack compactor in 8-inch lifts to maintain consistency with the procedure used in the construction of GRS Abutment Model #1 (**Figure 54**).

Figure 54. (Left) Installation of the top geotextile reinforcement layer at Elevation 91-inch above the foundation slab; (Right) Compaction of final aggregate lift using a Jumping-Jack compactor

Due to differences between the nominal and actual dimensions of the large concrete blocks, and existence of shear keys on their sides, their placement and fitting in the test box proved to be much more time-consuming than had been anticipated. It is understood that this additional effort did not reflect the construction time in the field, and hence it was noted accordingly when calculating and comparing the total labor hours against those for the CMU block alternative. Additional 0.50-inch to 0.75-inch of concrete had to be shaved off from one side of one of the half-blocks to expedite their installation within the confines of the test box.

The retrofitting of loading beam was completed, and carried on to install all the pieces and instruments necessary to set it up for a new surcharge load testing including the only available 400 kips load cell, steel spacers, front and top wire potentiometers (WP) and the hydraulic pump (**Figure 55**).

Only one 400 kips load cell was available for this test, because the other (older) load cell had been inspected by the manufacturer and was found to have become inaccurate and essentially inoperative after the GRS Abutment Model #1 surcharge load testing. Therefore, the total load was estimated on GRS Abutment Model #2 by multiplying the measured load from the available load

cell by a factor of two assuming that the load was applied uniformly on the bridge abutment model by the two hydraulic jacks. However, for GRS Abutment Model #3, a new load cell was purchased in time for its surcharge load testing.

Twenty-two WPs and five EPCs were installed, and all surcharge load testing data were recorded using two EPC data loggers and an additional data acquisition system. Furthermore, **Figure 55** shows safety precautions that were taken during the GRS Abutment Model #2 surcharge load testing. Steel spacers and the load cell were all secured against uncontrolled drop using steel chains and ties, in case significant movements would occur in the GRS abutment model during testing.

Figure 55. (Left) Front view of safety precautions for surcharge load testing of GRS Abutment Model #2; (Right) Back view

4.4. GRS Abutment Model #3: Large Concrete Block Facing with 12-inch Geotextile Spacing

Construction and surcharge load testing of an instrumented large concrete block facing (24-inch high × 24-inch deep × 48-inch wide) GRS abutment model with 12-inch geotextile reinforcement spacing is named as GRS Abutment Model #3. There was one full block in the middle and two half blocks on each side. Focus area of mid-section width of the facing is 48-inch long. Block setup

was same as GRS Abutment Model #2. Seven layers of full-length geotextile were used for GRS Abutment Model #3, instead of having eleven layers of full-length geotextile similar to the one in GRS Abutment Model #2.

Twenty-two WPs (sixteen WPs inside, two WPs at the top and four WPs at the front section) and five EPCs were used for the test setup. At least six points were selected at each block level to measure the displacements manually during the construction and deconstruction procedure that were performed after the surcharge load testing as similar to GRS Abutment Models #1 and #2. **Figure 56** shows the cross-section view of GRS Abutment Model #3.

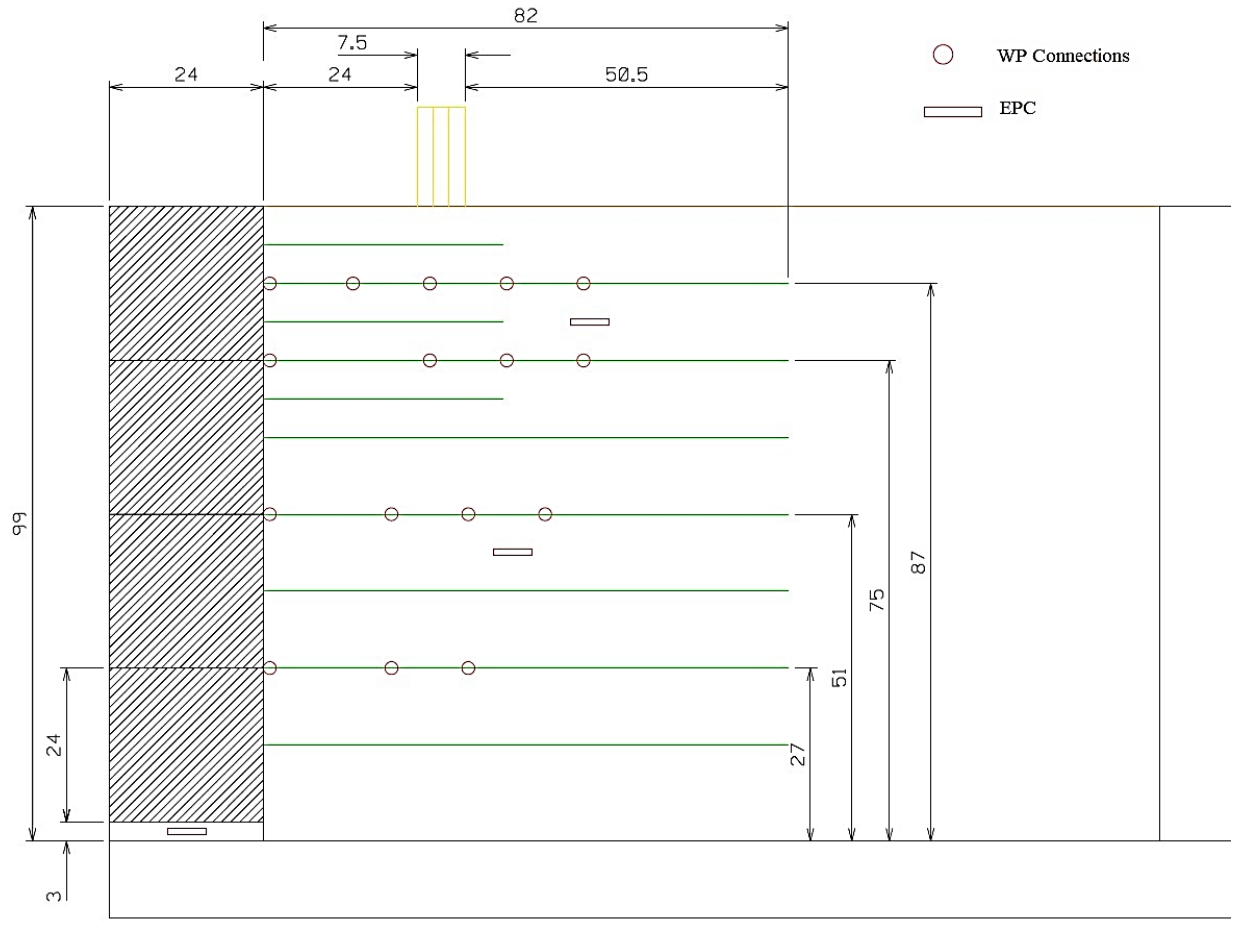

Figure 56. Schematic instrumentation layout for GRS Abutment Model #3 (Large concrete block facing with 12-inch reinforcement spacing; Dimensions are in inches)

The construction of GRS Abutment Model #3 was started by installing three of the EPCs underneath the first large concrete block in the central section of the GRS facing. Similar to the procedure for GRS Abutment Model #2, a 3-inch-thick sand layer was placed underneath the first-row of blocks to protect the EPCs (**Figure 57**).

Figure 57. (Left) Front view of the installation of the first-row of facing blocks in GRS Abutment Model #3; (Right) Side view

Then, the first lift of GRS gravel was placed and compacted (12-inch-thick standard lift plus an additional 3-inch to match the sand layer underneath the first-row of facing blocks), followed by the first geotextile layer at 15-inch above the foundation slab (**Figure 58**). Similar to the previous GRS abutment models, the compaction was done using one pass of a Jumping-Jack over the entire backfill area. However, in contrast to the previous GRS abutment models that the GRS fill was placed and compacted in 8-inch lifts, in GRS Abutment Model #3, the GRS fill was placed and compacted in 12-inch lifts, matching the spacing of reinforcement layers in this GRS abutment model with an anticipated, reduced construction time as a result.

Figure 58. (Left) Installation of the first reinforcement layer in GRS Abutment Model #3; (Right) Compaction of the GRS fill at every 12-inch lift

In GRS Abutment Model #3, full-length (90-inch) reinforcement layers were installed at elevations 15-inch, 27-inch, 39-inch, 51-inch, 63-inch, 75-inch and 87-inch above the foundation slab. Shorter reinforcement layers were placed (48-inch wide × 45-inch deep into the GRS fill) at three levels 69-inch, 81-inch and 93-inch above the foundation slab. The distance between the shorter and longer reinforcement was 6-inch because of having 12-inch reinforcement spacing. This distance was 4-inch in GRS Abutment Models #1 and #2.

The installation of EPC at the elevation of 81-inch above the foundation slab was completed, and the last round of GRS fill compaction at the top of the GRS Abutment Model #3 was carried out at the 99-inch level. Similar to what it was observed in GRS Abutment Model #2, the fill was compacted using the Jumping-Jack, essentially right up to the facing with no concerns about unwanted block movements during construction, which was a clear advantage over the commonly used CMU blocks, which were used in the control GRS Abutment Model #1. Fully constructed GRS Abutment Model #3 is shown in **Figure 59**.

Figure 59. (Left) Front view of fully constructed GRS Abutment Model #3 before the start of surcharge load testing; (Right) Controlling the electric hydraulic pump during surcharge load testing

Chapter 5. Deconstruction of Full-Scale GRS Abutment Models

There were tightly spaced geotextile reinforcement layers and instrumentation inside the GRS fill. Therefore, it was manually and carefully excavated one layer at a time, while instruments were removed and the deformed geometry (i.e. settlements) was surveyed at each level. All measurements recorded and geotextile reinforcement layers were stored for analysis. The excavated fill was transported back to a nearby stockpile area using a front loader tractor for use in subsequent GRS abutment models (**Figure 60**). In addition to its reinforcement function, each geotextile layer served as a medium to help survey the deformations of the GRS fill at the corresponding level.

Figure 60. (Left) Initial stages of the deconstruction of GRS Abutment Model #1; (Right) Front view of the test station during deconstruction

Different stages of GRS fill excavation were recorded through photographs, and measurements were taken for the analysis. Settlements of reinforcement layers were profiled and measured along their length relative to markings on both sidewalls of the test box, which were used to determine the corresponding mean values for each elevation (**Figure 61**). Additional measurements were taken to determine maximum settlements in the GRS fill on a vertical plane at mid-point perpendicular to the facing (**Figure 62**). Each geotextile layer was carefully rolled, labeled and stored in the laboratory for observation and testing, as necessary.

Figure 61. (Left) Layer by layer manual excavation of GRS Abutment Model #1 backfill; (Right) Observed geotextile deformation

Inspection of the exhumed instrumented geotextile layers revealed that wire potentiometer (WP) connections at all elevations (i.e. 25-inch, 48-inch, 71-inch and 86-inch above the foundation slab) survived the entire construction and surcharge loading stages of the test (**Figure 62**). This observation has beneficial field implications in that, proper instrumentation practices such as the WP-geotextile connections used in this study could provide long-term data on field GRS bridge abutments with little loss of data as a result of installation damage or service loads. However, some

unintentional movements of wireline plastic sleeves in the GRS fill during construction could influence the measured movements, as was observed for some of the WPs at the 25-inch and 48-inch elevations in this GRS abutment model.

Figure 62. (Left) An exhumed instrumented geotextile reinforcement layer after the load test; (Right) Measuring settlements at each reinforcement layer

The top three CMU blocks, which had been filled with concrete and reinforced with steel rebars were demolished carefully so that their removal would not disturb the GRS abutment model (**Figure 63**). The geotextile layers were cut before the demolition process. The deconstruction of the GRS abutment model was much faster during the removal of the bottom layers, as they did not include infilled blocks, tightly spaced secondary reinforcement layers or dense instrumentation.

Figure 63. (Left) Demolition of the top three rows of CMU blocks; (Right) Final stages of GRS fill excavation from the test box

Inspection of the earth pressure cells (EPC) indicated that all five of them were in good condition, and recorded data throughout the construction and surcharge loading phases of the test. They were recalibrated for use in the second GRS abutment model. The facing column of the GRS bridge abutment was placed on a 3-inch-thick sand layer across its running length to embed the EPCs for their protection and promote uniform distribution of vertical pressure on the instruments. Upon excavation, it was found that the sand layer had undergone 1.5-inch of settlement. A major portion of this settlement was attributed to the hollow-core geometry of the overlying row of CMU block, which allowed the intrusion of sand inside the facing units (**Figure 64**). However, despite periods of significant precipitation during the construction of GRS Abutment Model #1 no noticeable sand erosion was found, due to the placement of some extra gravel at the foot of the facing column during construction. The compressible sand layer underneath the facing column provided a more natural boundary condition resembling a reinforced soil foundation (RSF) in the field, as compared to the otherwise rigid reinforced concrete floor of the test box. Nevertheless, the magnitude of facing settlement in any future CMU block facing GRS abutment models can be reduced by preventing the intrusion of sand in the first-row of blocks, using one of the following solutions:

(1) infilling the first-row of CMU block with concrete, (2) placing a timber layer between the sand and the first CMU block row, (3) using a geotextile separator on the top of the sand layer. However, this type of sand intrusion-related settlement is not expected in the subsequent bridge abutment models using the large concrete blocks because of their solid (i.e. impervious) construct.

Figure 64 also shows the imprint of GRS fill on the east sidewall after the test indicating the area of peak stress concentration and settlement underneath the loading beam.

Figure 64. (Left) Settlement of sand layer underneath CMU blocks; (Right) Scratch marks on the painting of the east sidewall indicating the pressure bulb

Similar to their placement during the construction period in GRS Abutment Models #2 and #3, removing and transporting the top rows of the large concrete blocks required the use of a high-capacity forklift, which was accomplished using a large rental forklift. The blocks were moved to a near-site storage area. The bridge abutment aggregate was excavated layer-by-layer carefully and was removed and deposited near the test station using a tractor (**Figure 65**). During the excavation process, the conditions of different embedded sensors were also inspected before their removal.

Figure 65. (Left) Removal of the large concrete blocks using a large forklift; (Right) Excavation and removal of bridge abutment gravel using shovels and a tractor

Careful excavation and surveying of GRS Abutment Models #2 and #3 at first-row level (Row #1), the wire potentiometer (WP) connections at the elevation of 27-inch above the foundation slab, and Earth Pressure Cells (EPC) located under the first-row of large concrete blocks can be seen in **Figure 66**.

Figure 66. (Left) Instrumented reinforcement at the elevation of 27-inch above the foundation slab; (Right) EPCs located under the first-row of large concrete blocks in GRS Abutment Models #2 and #3

The test station was cleaned up and prepared. The gravel and large concrete blocks were again relocated closer to the test station (**Figure 67**).

Figure 67. (Left) Test box after excavation and removal of GRS Abutment Model #2; (Right) Fill gravel and large concrete block storage area for the construction of GRS Abutment Model #3

Chapter 6. Numerical Simulation of GRS Abutment Models

External stability checks (i.e. direct sliding, bearing resistance of the foundation soil, and global stability) and internal stability checks (i.e. bearing resistance, deformations, and required reinforcement strength) must be done to design a GRS bridge abutment based on FHWA guidelines (Adams *et al.* 2018).

Preliminary stability analyses were performed on the GRS abutment models using different computer programs to determine suitable locations to measure reinforcement deflections within the GRS mass during the tests using WPs. **Figures 68 and 69** show screenshots of TenCate MiraSlope® and TensarSoil® analysis programs, respectively, which are two available computer programs from the industry. It is understood that in-house geotechnical software programs developed by specific geosynthetic manufacturers are designed for use with their own specific geosynthetic and/or facing block products. Therefore, more generic analysis programs such as FLAC v.7.0 (Itasca 2011) was used for the same purpose as an alternative, and their comparison with in-house industry software could be beneficial for verification purposes.

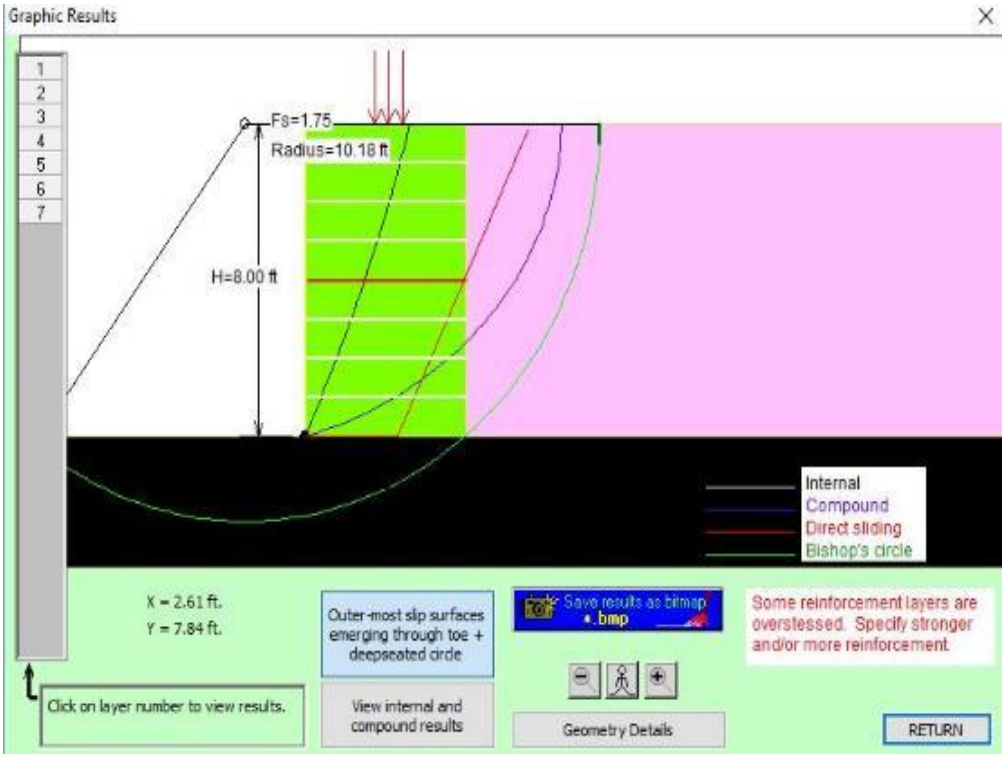

Figure 68. Screenshot of TenCate MiraSlope® Software for the analysis of GRS abutment models

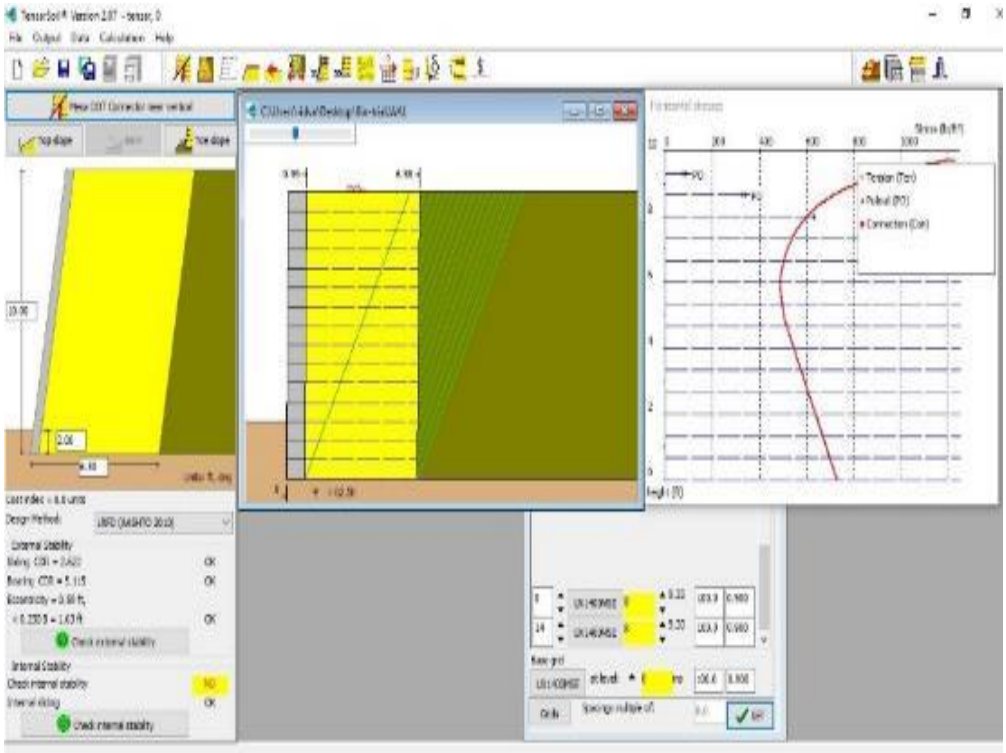

Figure 69. Screenshot of TensarSoil® Software for the analysis of GRS abutment models

In addition to the commercial programs noted earlier, three GRS abutment models in this study were analyzed using FLAC v.7.0 (Itasca 2011) software. FLAC v.7.0 is numerical modeling software for advanced geotechnical analysis of soil, rock, groundwater, and ground support in two dimensions. It is designed for geotechnical engineering projects that would require continuum analysis. FLAC v.7.0 utilizes an explicit finite difference formulation that can model complex behaviors, such as problems that consist of several stages, large displacements and strains, non-linear material behavior, or unstable systems (Itasca 2011).

Pena 2017 analyzed GRS abutment models with CMU and large concrete block facing options using FLAC v.7.0. CMU facing option was modeled as 84-inch high GRS abutment. Two types of large concrete blocks were used 16-inch high by 16-inch deep each (64-inch high GRS abutment), and 24-inch high by 24-inch deep each (72-inch high GRS abutment), respectively. The geotextile length was 90-inch for all three models. These FLAC v.7.0. model files were updated according to the full-scale GRS Abutment Models #1-#3 properties in this study.

Simulated data, such as all the dimensions of the model, geotextile spacing, and material properties are similar to the full-scale GRS Abutment Models #1-#3. Length (meter), density (kg/m^3), Force (Newton), Stress (Pa) and Gravity (m/sec^2) were used as SI system units for FLAC v.7.0 Numerical Modeling. The analysis also includes the construction stages (i.e. excavation of the reinforced foundation and construction of each lift by installing facing block, geosynthetic and gravel fill).

The summary of material properties that were used for FLAC v.7.0 Numerical Modeling can be seen in **Table 3**.

Table 3. Summary of assumed material and strength properties used in Numerical Modeling

Description	Material / Strength Properties
CMU	Model elastic Density=1,200 kg/m^3 Bulk modulus (K) =11×10^9 Pa Shear modulus (G) =8.3×10^9 Pa
Large concrete block	Model elastic Density=2,400 kg/m^3 Bulk modulus (K)=11×10^9 Pa Shear modulus (G) =8.3×10^9 Pa
3/8” #2 Cover backfill	Model Mohr-Coulomb Density=1,522 kg/m^3 Bulk modulus (K) =152.38×10^6 Pa (by assuming Poisson ratio ν=0.15 and Young modulus (E)=320×10^6 Pa) Shear modulus (G) =139.13×10^6 Pa Cohesion=0, Internal friction=48°, Dilation angle=14°
Geosynthetic reinforcement	Thickness=0.0008 m Young modulus (E)=2×10^9 Pa Yield strength at 5% strain=44×10^3 N/m Geotextile-backfill interface (kbond)= 500×10^3 N/m/m Geotextile-backfill interface (sbond)= 220×10^3 N/m/m Skin friction=48°
Backfill soil-facing block interface properties	Density=1,522 kg/m^3 Bulk modulus (K) =152.38×10^6 Pa Shear modulus (G) =139.13×10^6 Pa Cohesion=0, Interface friction=48°
3/8” #2 Cover backfill soil - native soil interface properties at the end of abutment	Density=1,937 kg/m^3 Bulk modulus (K) =11.1×10^9 Pa Shear modulus (G) =6.3×10^9 Pa Cohesion=13×10^3 Pa, Interface friction=48°

Young's Molulus (E) and poisson ratio (v) of 3/8" #2 Cover backfill (dense gravel) were assumed as 320×10^6 Pa (Obrzud and Truty 2012) and 0.15 (Zhu 2016), respectively to model gravel backfill as stiff as possible. Kbond (stiffness) and sbond (shear strength) values can be measured directly in laboratory pullout tests. These values were assumed based on recommended empirical calculation methods by FLAC v.7.0 user manual (Itasca 2011) for this study.

Assumed value of sbond was calculated by; Ultimate tensile strength of Mirafi HP570 woven geotextile is 70,000 N/m (4,800 lbs/ft). Cross-sectional area of geotextile is 0.0008 m^2 (length=1 m, and thickness=0.0008 m). Calculated maximum shear strength is 87.5×10^6 Pa. Assumed sbond equals π (0.0008 m)$\times(87.5\times10^6$ Pa) = 220,000 N/m/m. Initial Numerical Modeling trials showed that any change in kbond value has more direct effect than sbond value on structure's vertical and horizontal displacement characteristics during the application of surcharge load. After a calibration procedure, kbond value was selected as 500×10^3 N/m/m by using sbond value of 220,000 N/m/m.

Load-Strain curve for Mirafi HP570 woven geotextile in the cross-machine direction (XD) at 0.03%/minute strain rate (Cuelho and Ganeshan 2004) can be seen in **Figure 70**. SI (kN/m) units were converted to US (lbs/ft) units. Lowest strain rate graph was selected based on the small strain levels (i.e. maximum 0.0167%) recorded during the surcharge load testing as discussed in Section 8.4 in this study. As an example, it took 40 minutes from starting the surcharge load testing of GRS Model #2 until reaching the maximum load level of 236 kips (i.e. load rate was 5.9 kips/min). GRS Abutment Models #1-#3 sections modeled in FLAC v.7.0 are shown in **Figures 71 through 73**, respectively.

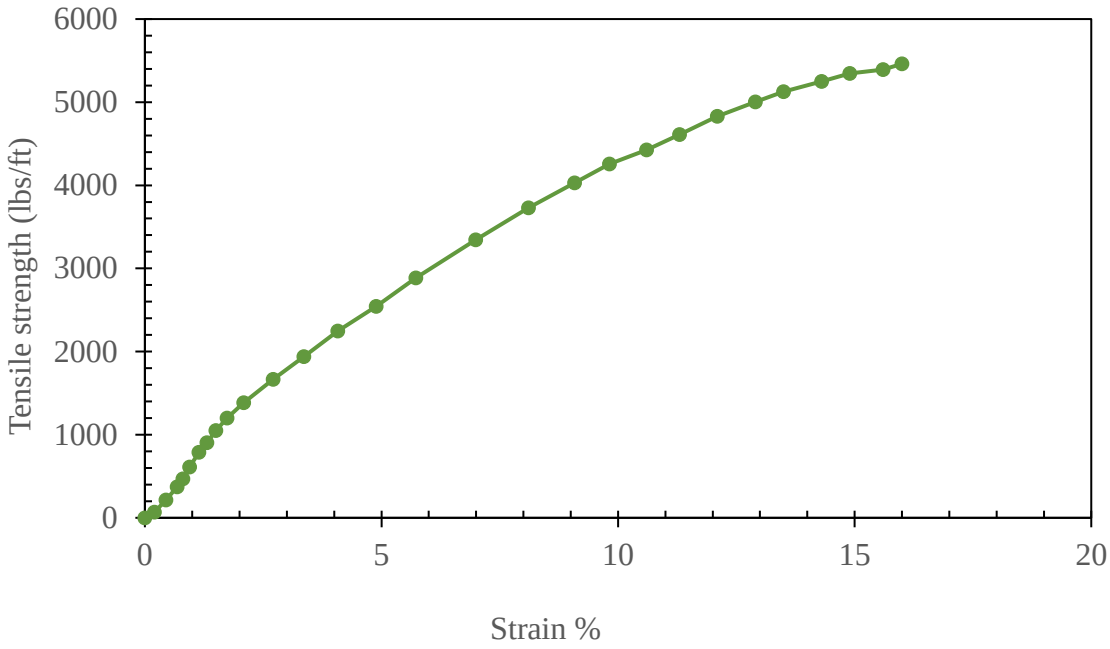

Figure 70. Load-Strain curve for Mirafi HP570 woven geotextile in the cross-machine direction (XD) at 0.03%/minute strain rate (Cuelho and Ganeshan 2004)

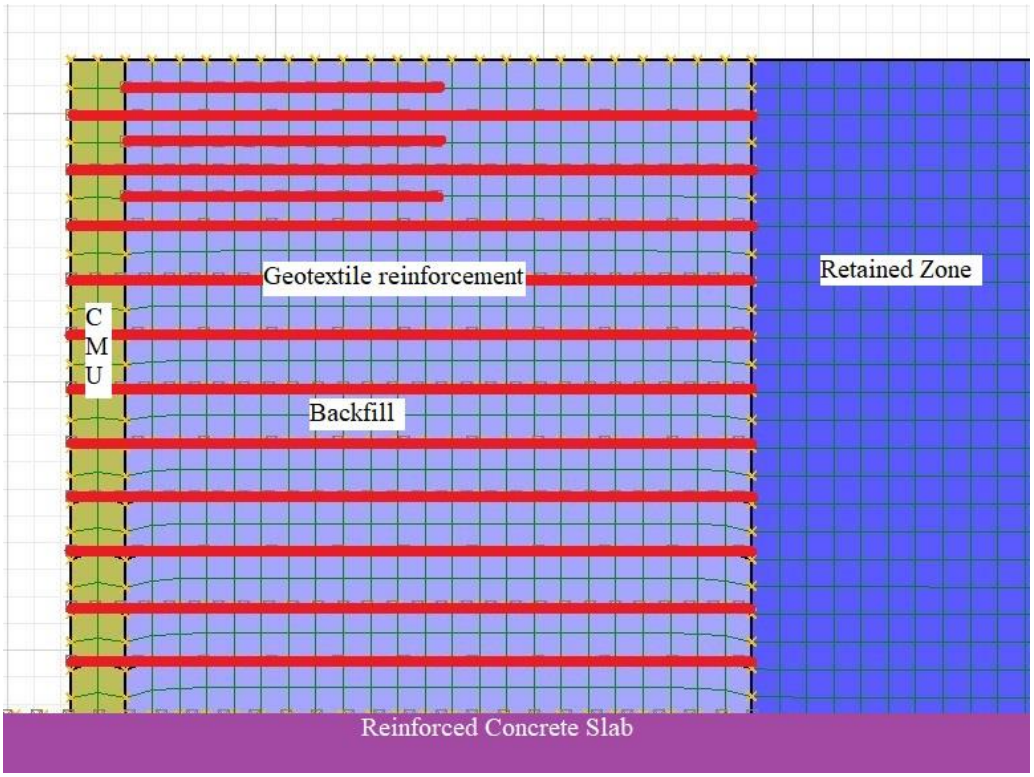

Figure 71. GRS Abutment Model #1 modeled in FLAC v.7.0

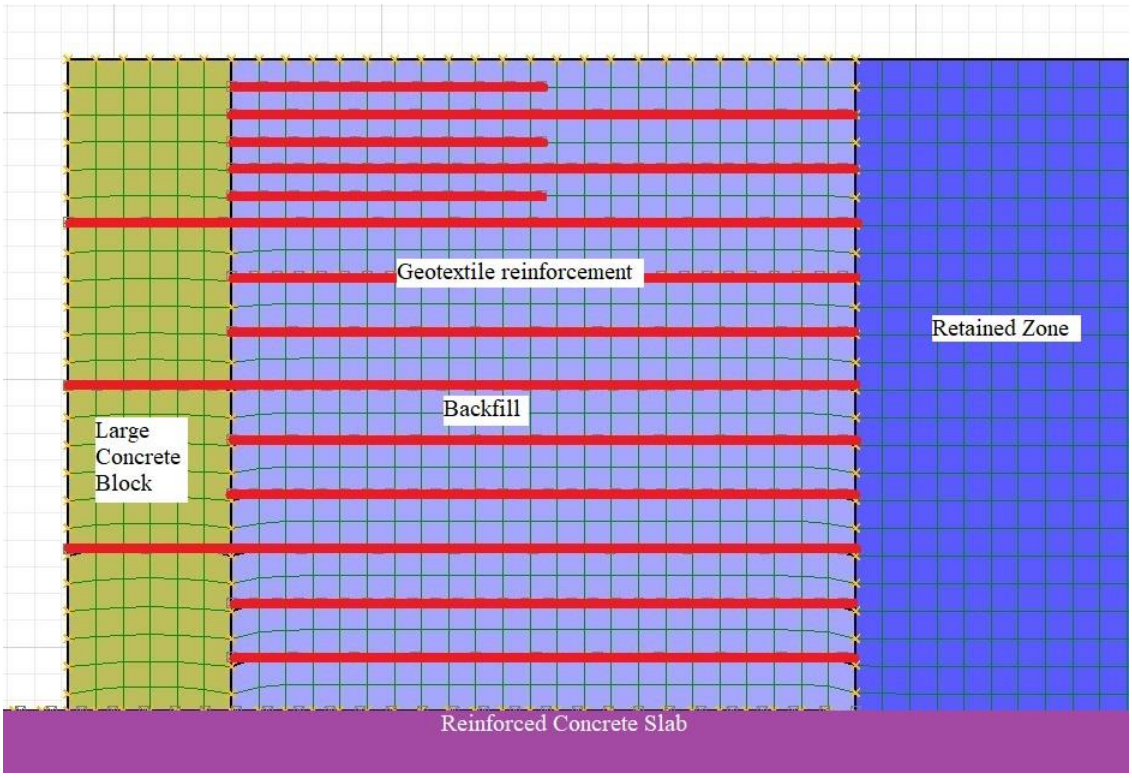

Figure 72. GRS Abutment Model #2 modeled in FLAC v.7.0

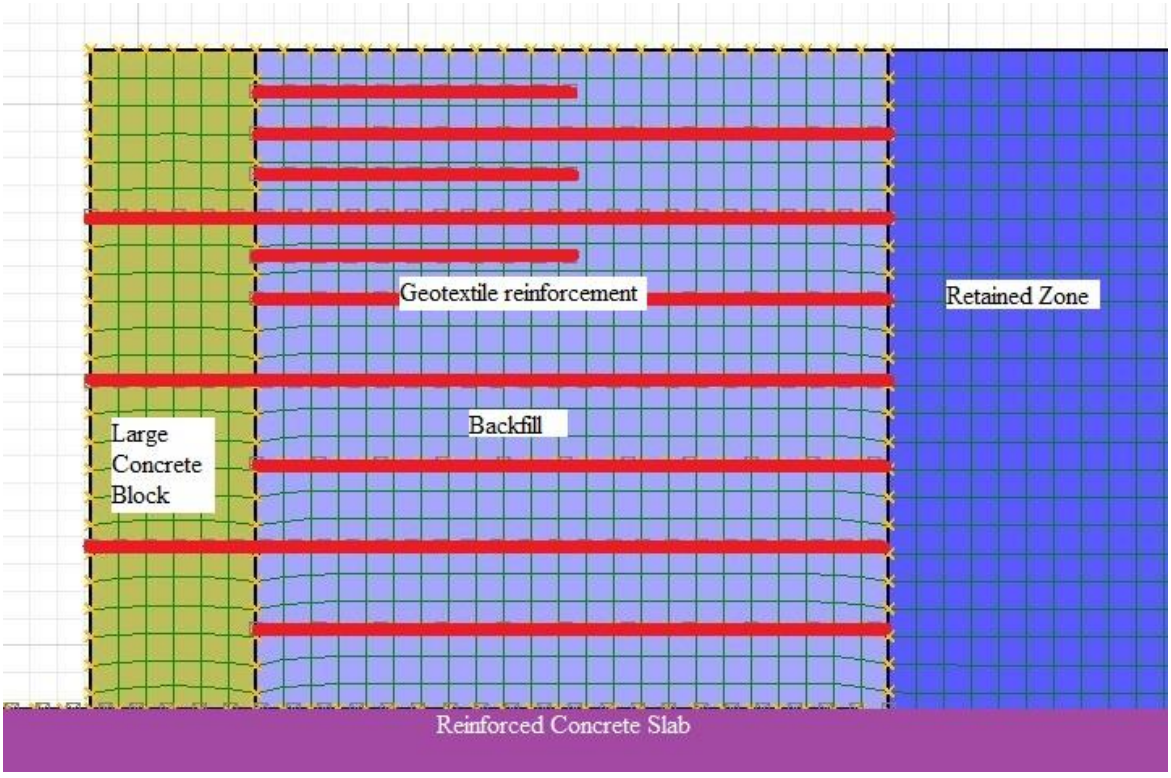

Figure 73. GRS Abutment Model #3 modeled in FLAC v.7.0

After calibrating the Numerical Modeling by FLAC v.7.0 software by using the full-scale surcharge load testing data as close as possible, several FLAC v.7.0 simulations as part of a parametric study were performed to investigate the influences of different parameters of the backfill material and different reinforcement strength values to predict the load-bearing and facing performance of GRS abutment models. Summary of parametric studies that were performed can be found in **Table 4**.

Table 4. Summary of parametric studies to predict the load-bearing and facing performance

Numerical modeling cases[1]	Backfill material strength properties	Backfill material elastic properties[2,3]	Reinforcement strength properties
Case #1	Friction angle =48° Cohesion =0	Bulk modulus (K) =152.38×10^6 Pa, Shear modulus (G) =139.13×10^6 Pa	4.8 k/ft
Case #2	Friction angle =45° Cohesion =0	Bulk modulus (K) =152.38×10^6 Pa, Shear modulus (G) =139.13×10^6 Pa	4.8 k/ft
Case #3	Friction angle =35° Cohesion =0	Bulk modulus (K) =152.38×10^6 Pa, Shear modulus (G) =139.13×10^6 Pa	4.8 k/ft
Case #4	Friction angle =48° Cohesion =0	Bulk modulus (K) =104×10^6 Pa, Shear modulus (G) =60×10^6 Pa	4.8 k/ft
Case #5	Friction angle =48° Cohesion =0	Bulk modulus (K) =152.38×10^6 Pa, Shear modulus (G) =139.13×10^6 Pa	2.4 k/ft
Case #6	Friction angle =48° Cohesion =0	Bulk modulus (K) =152.38×10^6 Pa, Shear modulus (G) =139.13×10^6 Pa	9.6 k/ft

Notes: [1] Cases #1 through 6 were repeated for GRS Abutment Models #1-#3 at 4 ksf, 10 ksf and 40 ksf surcharge load levels.

[2] Bulk modulus (K) =152.38×106 Pa and Shear modulus (G) =139.13×106 Pa were calculated by assuming Poisson ratio v=0.15 and Young modulus (E) =320×10^6 Pa.

[3] Bulk modulus (K) =104×106 Pa and Shear modulus (G) =60×106 Pa were calculated by assuming Poisson ratio v=0.26 and Young modulus (E) =151×10^6 Pa.

Chapter 7. Construction Results

7.1. Overview

Results in this dissertation are presented in separate sections relative to construction labor requirements for the full-scale GRS abutment models, surcharge load testing results, measurements during their deconstruction stage, and numerical modeling of their predicted response. These results are presented in the following chapters as listed in **Table 5**.

Table 5. Chapter list to present the results

Chapter #	Chapter Content
7	Overview, Labor Requirement Results, and Facing Deformation at the end of the Construction
8	Surcharge Load Testing and Deconstruction of GRS Abutment Models #1-#3 Results
9	Numerical Modeling Results

7.2. Labor Requirement Results

Labor requirements for the construction and instrumentation of the full-scale GRS abutment models in this study were recorded separately in person-hours on a daily basis. The construction activity was carried out by a team of graduate and undergraduate research assistants, which required time management around their individual weekly schedules.

Cumulative person-hours for GRS Abutment Model #1 that was constructed with CMU facing included an additional task of infilling the top three courses of the facing with ready-mix concrete and steel rebars to increase the strength of the facing blocks against cracking under heavy bridge loads as per the Section 3.5 in FHWA guidelines (Adams *et al.* 2018).

Figure 74 shows a comparison of cumulative construction times in person hours for all three GRS abutment models investigated in this study.

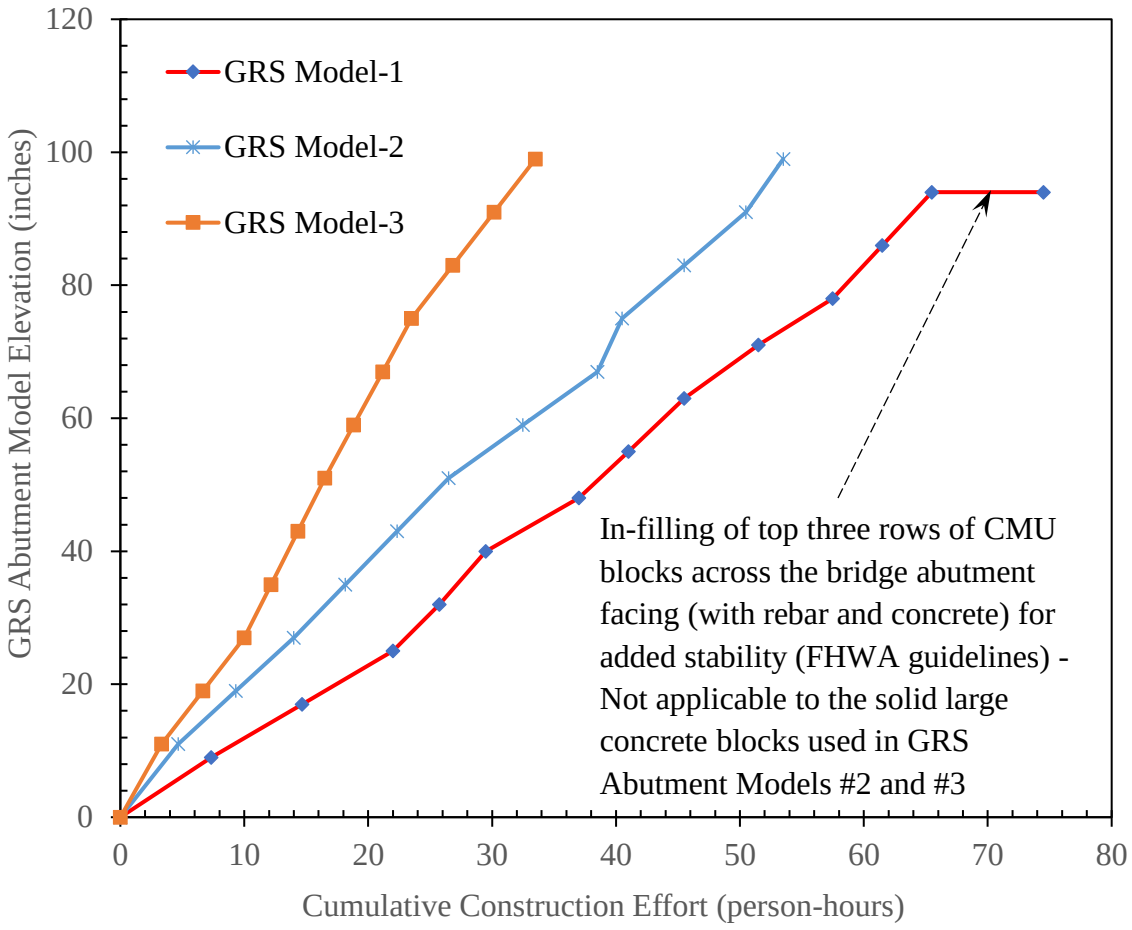

Figure 74. Comparison of cumulative construction effort vs. built elevation for the three GRS abutment models in this study

Results in **Figure 74** show that the construction of GRS Abutment Model #3 with large concrete block facing and 12-inch reinforcement spacing was significantly faster than that of GRS Abutment Model #1 (CMU block facing with 8-inch geotextile spacing). The cumulative construction time for GRS Abutment Model #3 was approximately 55% shorter than that for GRS Abutment Model #1, and 37% shorter than for GRS Abutment Model #2 (large concrete block facing with 8-inch geotextile spacing). These results indicate that the use of large facing blocks could indeed result in significant increases in the construction speed of GRS abutments, leading to cost savings and reduced traffic disruption.

The cost advantage of using large concrete blocks should be investigated in detail based on several factors that changes project to project (i.e. size and location of the project, local material and labor costs). The additional cost of using forklift or crane for installing the large concrete block should also be considered. It should be noted that, the cost of backfill gravel and the geosynthetics were same for GRS Abutment Models #1 and #2. Therefore, the facing block, labor and equipment (i.e. 5,000 lbs capacity forklift) cost are the key factors for comparing the total construction cost per ft^2 of facing.

For an example cost calculation, the cost of CMU block/ft^2 was assumed as \$6 (*estimated from lowes.com*) with including shipping. The total labor cost with CMU is \$4,500 (75 hours × \$60/man hour). \$60/man hour was estimated from *markupandprofit.com*. So, the total labor cost of CMU can be assumed as \$70/ft^2 of facing (\$4,500 divided by 64 ft^2 facing area). Total cost including facing and labor was estimated as approximately \$76/ft^2 for CMU facing option.

Based on the observations during the construction of GRS Abutment Models #2 and #3, a forklift could install approximately 50 ft^2 block/day. Daily rental rate of 5,000 lbs capacity forklift was assumed as \$200 including the fuel cost (*estimated from forkliftrentalusa.com*). Forklift cost was

calculated as $4/ft^2 of facing. The material cost of large concrete block (2 ft. high × 2 ft. deep × 4 ft. wide) was assumed as $100 based on ready-mix concrete prices (*estimated from concretenetwork.com*) per block including shipping with covering 8 ft^2. Block cost was calculated as approximately $12.50/$ft^2$. The total labor cost with using large concrete block was 45% (55% shorter than CMU facing option) of $4,500. Labor cost was calculated as $31.50/$ft^2$ of facing. Total cost including facing, forklift and labor was estimated approximately $48 for large concrete block facing option.

The aforementioned cost comparison indicates that using large concrete blocks as facing can still provide a more economical solution than the CMU alternative, even after including the additional equipment costs. The cost savings in the above example amount to 37% (i.e. $48/$ft^2$ vs. $76/$ft^2$), which include cost differences in facing block, labor and equipment expenditures as per the calculations presented above.

7.3. Facing Deformation at the end of Construction

Figures 75 through 80 show contour maps of deformation readings from manual survey at end of construction of the abutment models. Each abutment model has two different graphs to show the block movements since placement of the corresponding row at each level and the cumulative movement relative to a target vertical plane. The readings were taken relative to fixed reference points that were marked on sidewalls of the test station along its height.

The CMU blocks in Model #1 were 8-inch thick. It is worth noting that each row of CMU blocks was placed with a 0.50-inch setback and backfill compaction was limited to 1.5 ft. away from the back of the facing - as recommended in FHWA (2018) guidelines - to minimize anticipated block movement during compaction of the GRS fill. Instead, a 10-inch by 10-inch steel hand tamper was

used to compact the material at closer locations to the back of the facing to minimize the block movement. Also, deformation measurements and setback application started with the fifth row of blocks (i.e. 40 inches above the foundation slab) for GRS Abutment Model #1. Results in **Figures 75 and 76** indicate that maximum local facing movements recorded at the end of construction was 0.50 inches (block movements since their placement at the corresponding elevation) and 5 inches (cumulative movement relative to a target vertical plane), respectively.

In contrast to the CMU blocks, the large concrete blocks in GRS Abutment Models #2 and #3 were 24-inch-thick. The maximum facing movement measured using manual survey at the end of the construction of GRS Abutment Model #2 was 0.4-inch. Also, in contrast to GRS Abutment Model #1, the GRS fill in Models #2 and #3 was compacted evenly right up to the back of the facing. Furthermore, facing blocks in each row were placed on the top of the previous row with no setbacks. Comparison of results in **Figures 75 through 80** shows that in spite of greater compaction effort at the back of the large concrete blocks, the large concrete block facing abutment Models #2 and #3 incurred smaller facing movements than Model #1. Meanwhile, comparison of deformation results in **Figures 78 and 80** shows slightly larger displacements in GRS Abutment Model #3 relative to GRS Abutment Model #2, which is to be expected due to larger reinforcement spacing that was used in GRS Abutment Model #3.

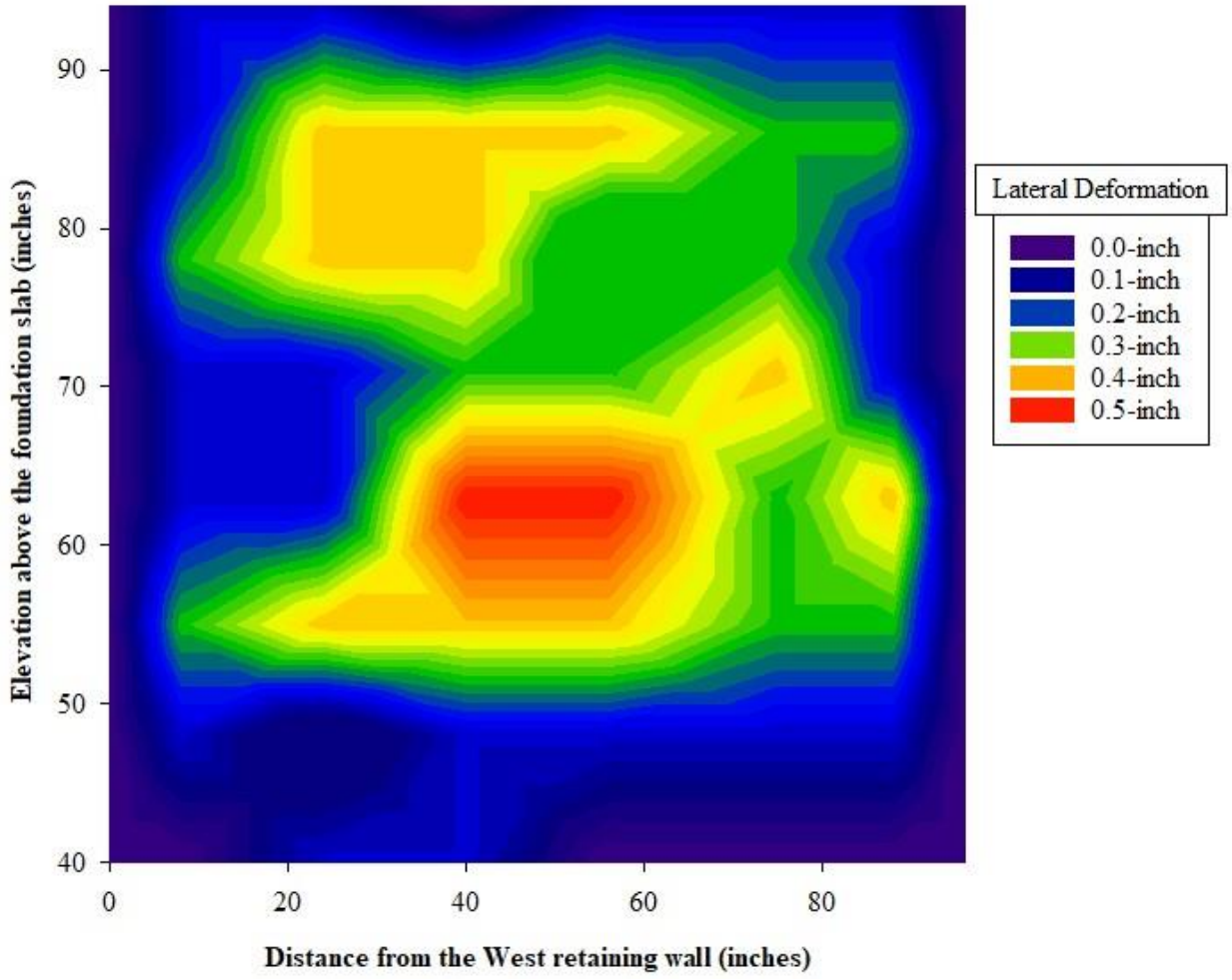

Figure 75. Contour maps of facing deformation for GRS Abutment Model #1 at end of construction: Block movements since placement of the corresponding row at each level. (Notes: (1) CMU blocks were placed with a 0.50-inch setback at each level; (2) The x-axis indicates measurements at six points across the facing from the West sidewall (i.e. 8-inch, 24-inch, 40-inch, 56-inch, 72-inch, and 88-inch))

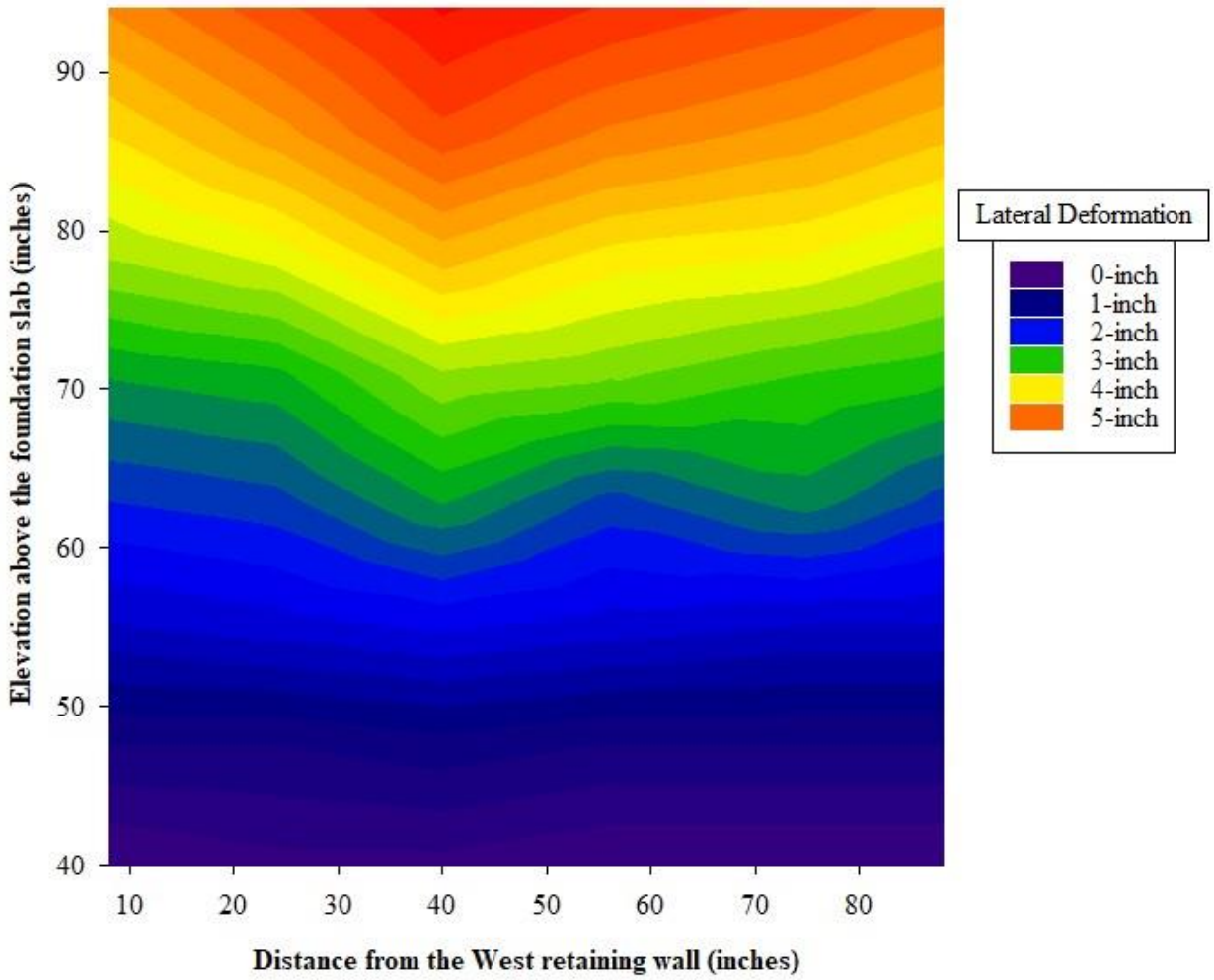

Figure 76. Contour maps of facing deformation for GRS Abutment Model #1 at end of construction: Cumulative movement relative to a target vertical plane. (Notes: (1) CMU blocks were placed with a 0.50-inch setback at each level; (2) The x-axis indicates measurements at six points across the facing from the West sidewall (i.e. 8-inch, 24-inch, 40-inch, 56-inch, 72-inch, and 88-inch))

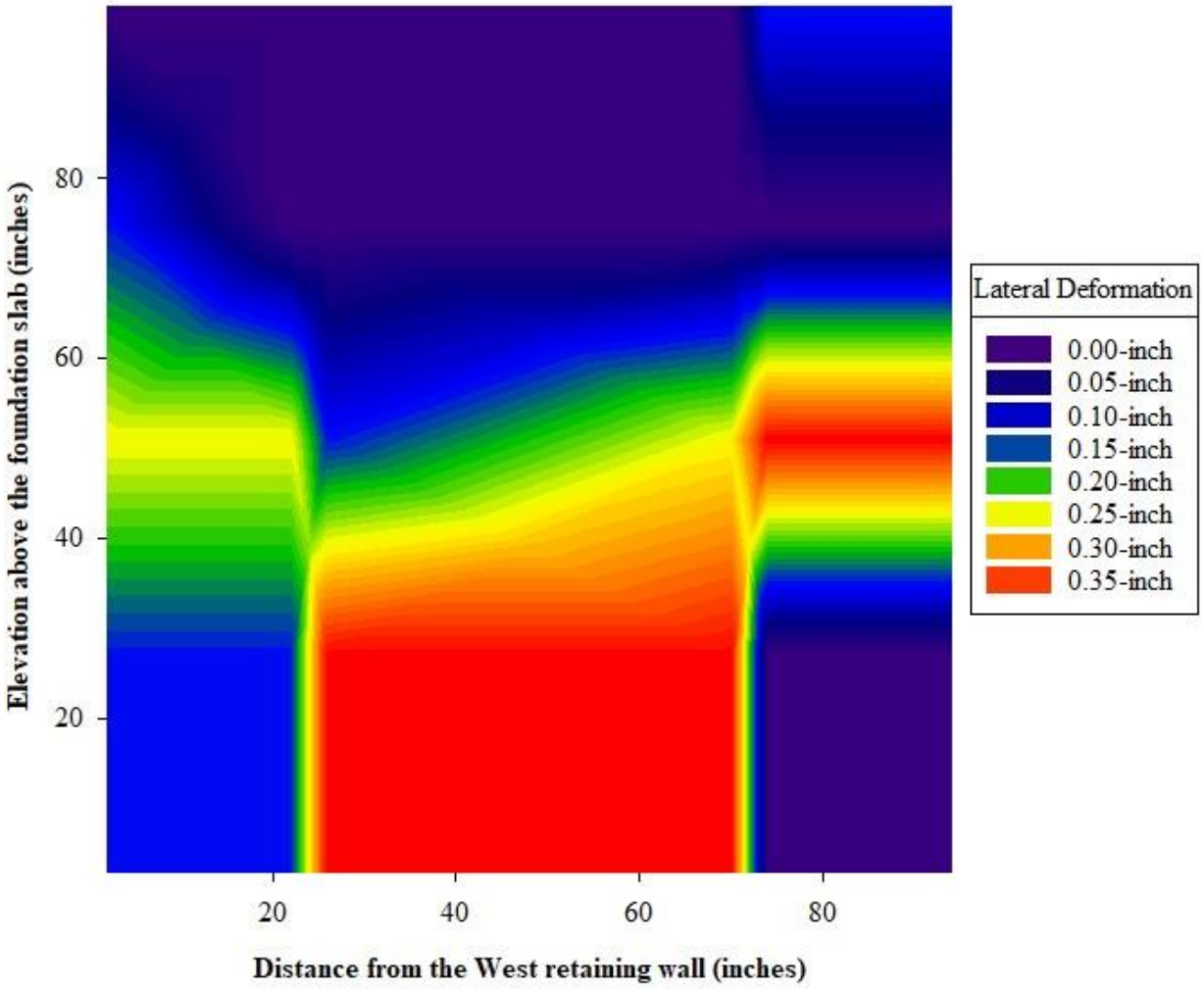

Figure 77. Contour maps of facing deformation for GRS Abutment Model #2 at end of construction: Block movements since placement of the corresponding row at each level. (Notes: The x-axis indicates measurement at six points across the facing (i.e. 2-inch, 22-inch, 26-inch, 70-inch, 74-inch, and 94-inch))

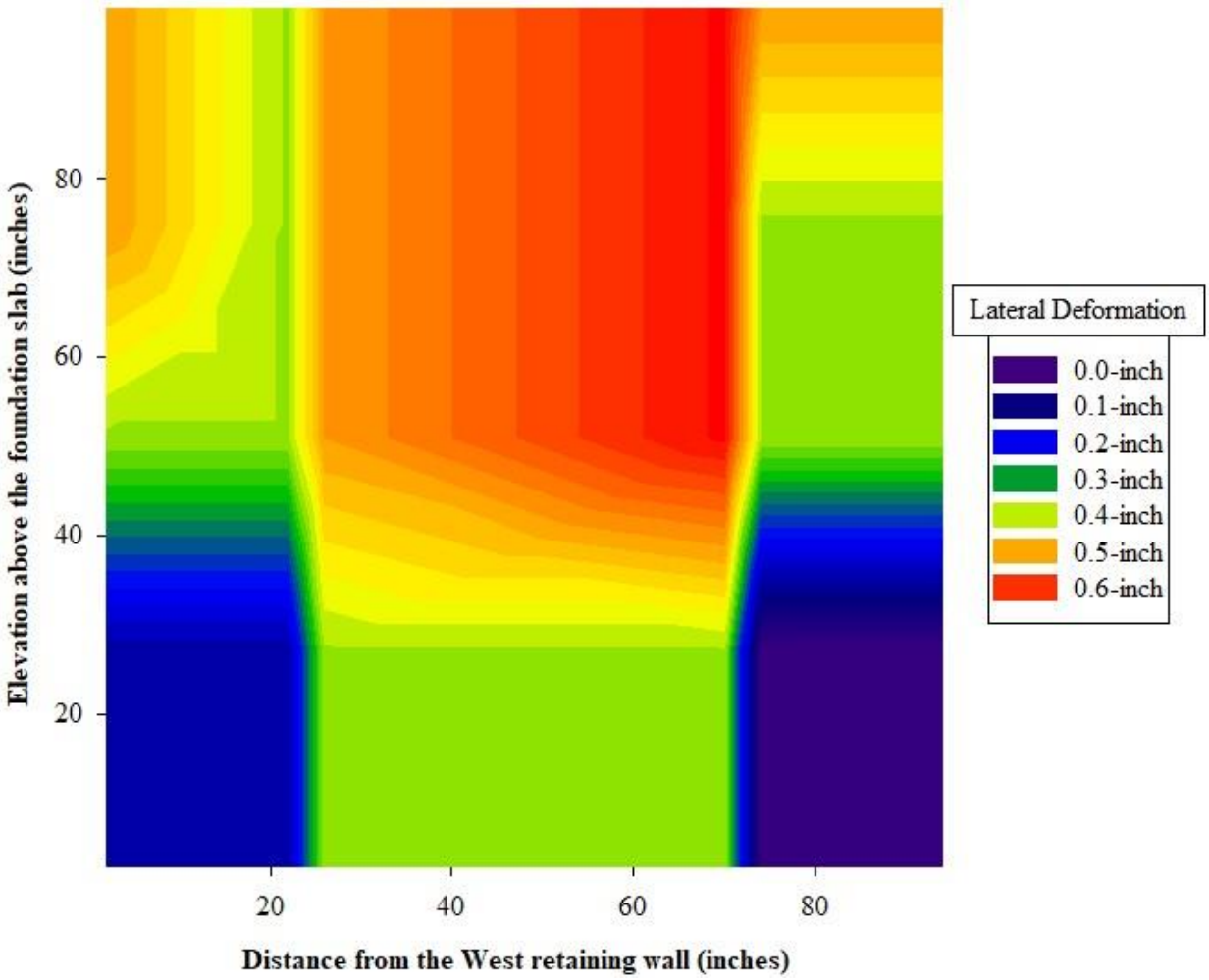

Figure 78. Contour maps of facing deformation for GRS Abutment Model #2 at end of construction: Cumulative movement relative to a target vertical plane. (Notes: The x-axis indicates measurement at six points across the facing (i.e. 2-inch, 22-inch, 26-inch, 70-inch, 74-inch, and 94-inch))

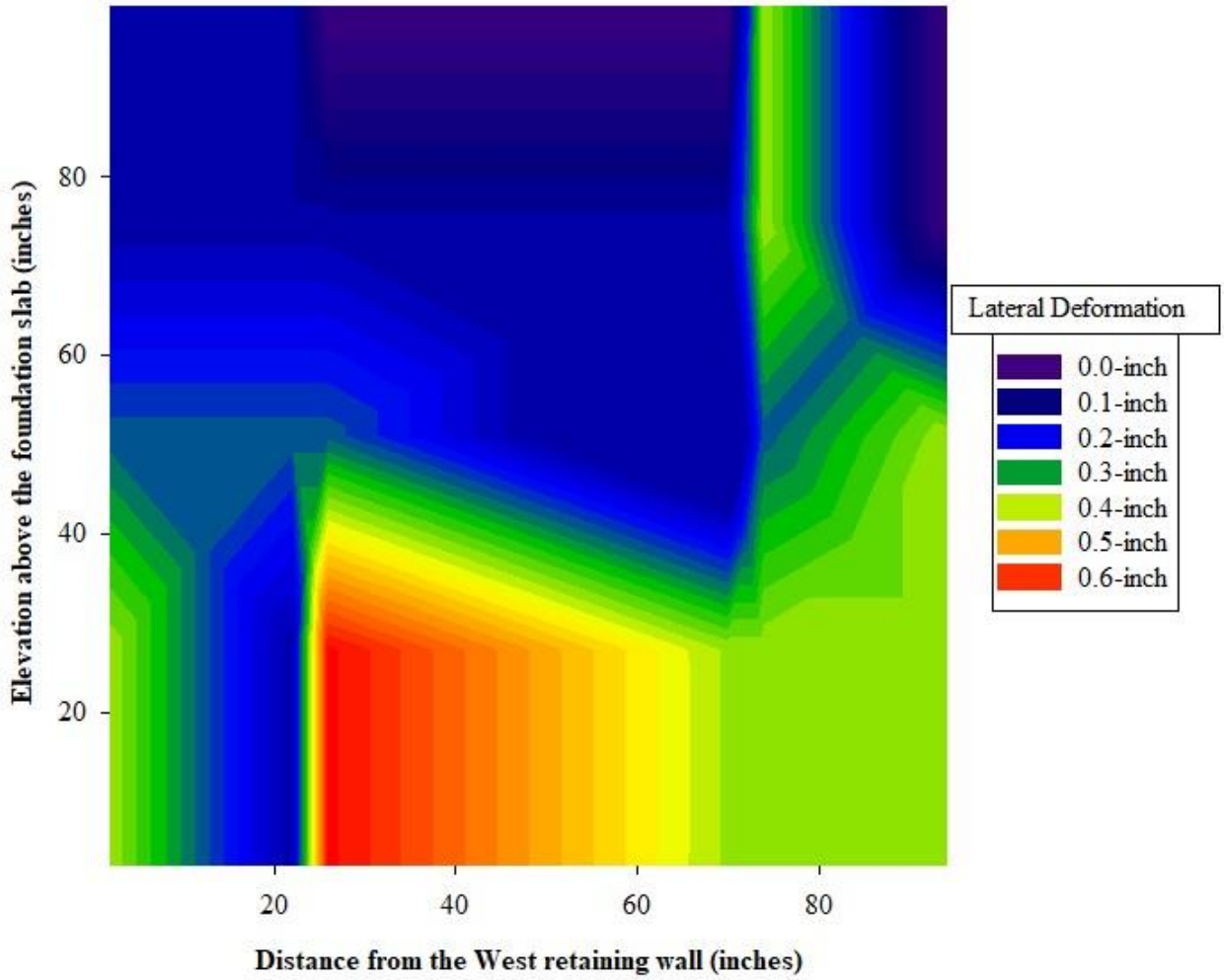

Figure 79. Contour maps of facing deformation for GRS Abutment Model #3 at end of construction: Block movements since the placement of corresponding row at each level. (Notes: The x-axis indicates measurement at six points across the facing (i.e. 2-inch, 22-inch, 26-inch, 70-inch, 74-inch, and 94-inch))

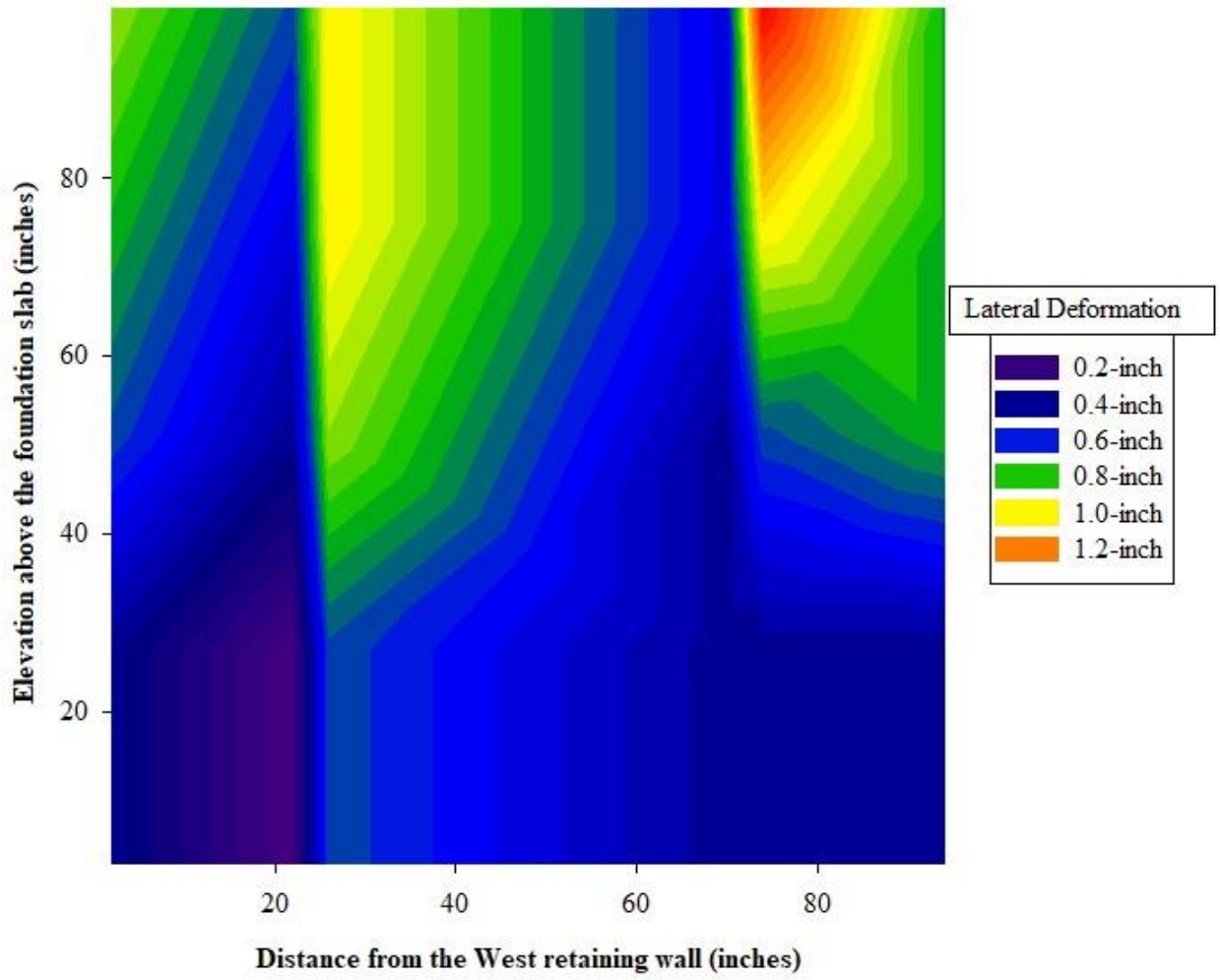

Figure 80. Contour maps of facing deformation for GRS Abutment Model #3 at end of construction: Cumulative movement relative to a target vertical plane. (Notes: The x-axis indicates measurement at six points across the facing (i.e. 2-inch, 22-inch, 26-inch, 70-inch, 74-inch, and 94-inch))

Figures 81 and 82 show the facing deformation comparison during the construction of three GRS abutment models based on the 3rd reading point and 4th reading point, respectively. It should be mentioned that both 3rd and 4th reading points are inside the focus area of the facing at each GRS abutment model (i.e. center 48-inch long section). It should be mentioned that the large concrete blocks were placed first, then backfill was compacted at every 8-inch and 12-inch for GRS Abutment Models #2 and #3, respectively. The large concrete block facing movement readings

were taken at every 24-inch lift (i.e. a total of three compaction cycles for GRS Abutment Model #2 and two compaction cycles for GRS Abutment Model #3).

The starting elevation above the foundation slab was taken as 3 inches because of the protective sand layer for the earth pressure cells underneath the facing blocks. **Figures 81 and 82** show that the large concrete block facing abutment Models #2 and #3 incurred smaller facing movements than GRS Abutment Model #1.

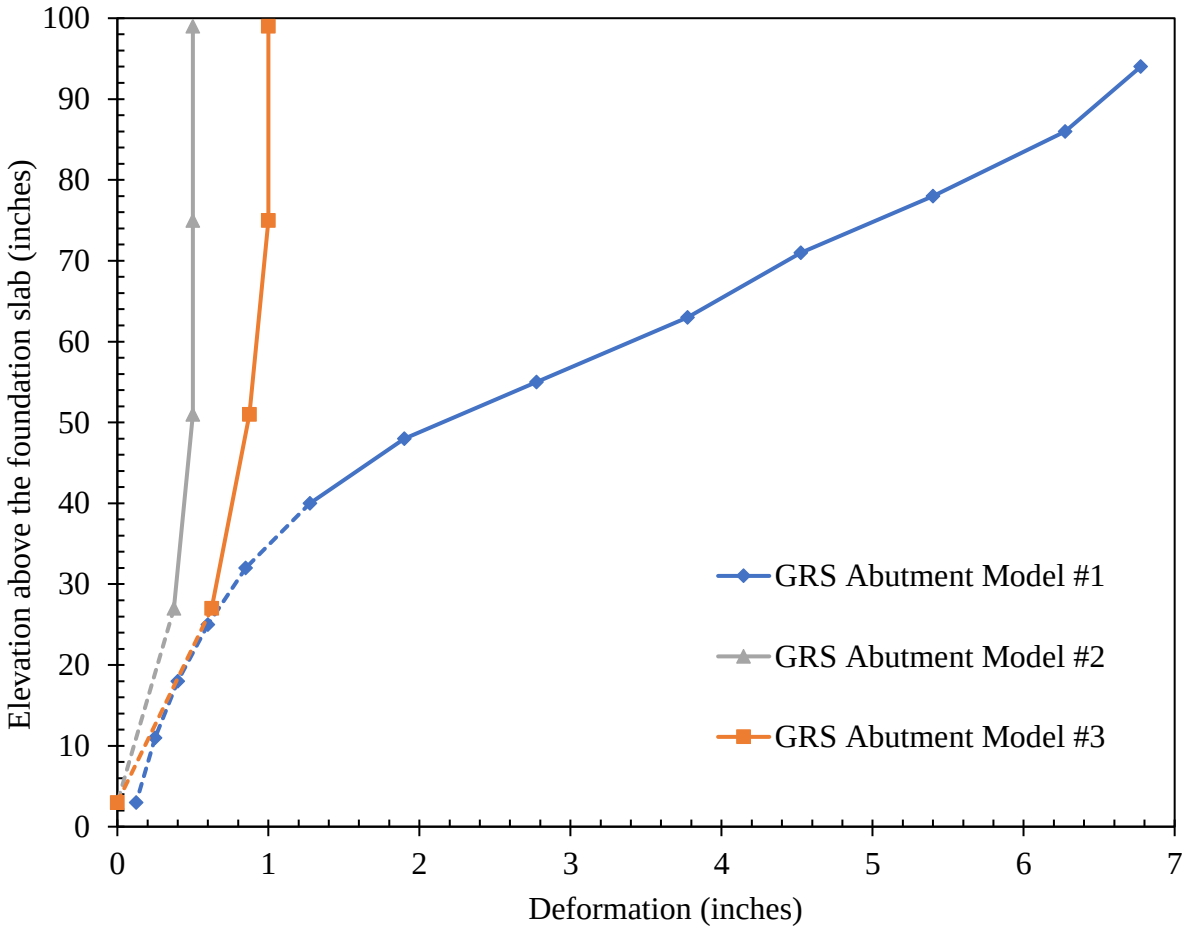

Figure 81. Facing deformation at 3rd reading location for GRS Abutment Models #1-#3 at end of construction: Cumulative movement relative to a target vertical plane

The dashed lines in **Figures 81 and 82** represent the extrapolated data of GRS Abutment Models #1-#3. As mentioned previously, the deformation measurements and setback placement of CMU started with the fifth row of blocks (i.e. 40 inches above the foundation slab) in GRS Abutment Model #1. In the case of large concrete blocks (i.e. GRS Abutment Models #2 and #3), facing movements were recorded only at the top of each block as the movement at the bottom of the first large block was found to be negligible.

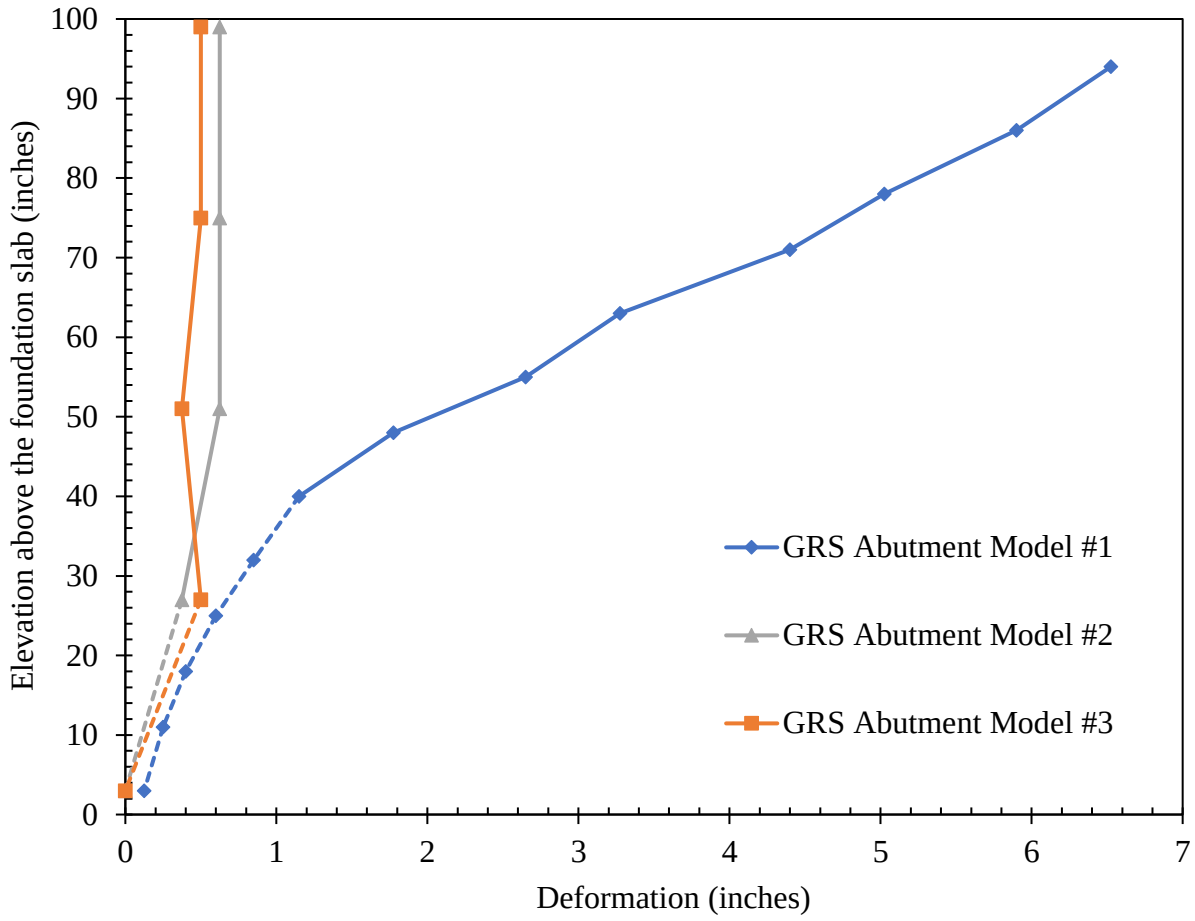

Figure 82. Facing deformation at 4th reading location for GRS Abutment Models #1-#3 at end of construction: Cumulative movement relative to a target vertical plane

Chapter 8. Surcharge Load Testing and Deconstruction Results

8.1. Visual Observations

Figures 83 and 84 show the lateral deformation and loading beam settlements observed after surcharge load testing of GRS Abutment Model #1, respectively. Nearly 6.5-inch of settlement was observed for the loading beam after the model abutment was subjected to 353 kips of simulated static bridge abutment load at the end of the test.

Figure 83. Facing deformation of GRS Abutment Model #1 at the end of surcharge load testing

Figure 84. Settlement of the loading beam on the top of the GRS fill at the end of surcharge load testing of GRS Abutment Model #1

Having the benefit of test data on GRS Abutment Model #1, the surcharge load testing on GRS Abutment Model #2 was aborted at a total magnitude of 236 kips, which allowed the research team to collect sufficient test data while limiting the loading magnitude on the model within a safe limit. **Figure 85** shows the frontal and top views of Model #2, and **Figure 86** shows the condition of the model abutment at its top surface after the conclusion of the test.

Figure 85. (Top) Front; (Bottom) top views of GRS Abutment Model #2 after the conclusion of its surcharge load testing

Figure 86. (Left) Top view of the settlement of the loading beam after the test of GRS Abutment Model #2; (Right) Closer view of the loading beam after the test

Figure 87 shows top views of the GRS Abutment Model #3 fill and the facing after the surcharge load testing was concluded. Some settlement (albeit considerably less than in GRS Abutment Model #1 with CMU blocks) can be observed under the loading beam. However, no lateral movement was detected for the facing blocks through plain observation. The surcharge load testing was aborted when the settlement of the loading beam reached approximately 2-inch (corresponding to approximately 200 kips of surcharge load) for safety purposes.

Figure 87. (Left) Back view of the loading beam after GRS Abutment Model #3 surcharge load testing; (Right) The top view of facing after the end of surcharge load testing

8.2. Load-Settlement Performance

Figure 88 shows measured load-settlement results for GRS Abutment Model #1. Design values of service load (4 ksf) and bridge abutment settlement (i.e. 0.50% of the height = 0.50% × 94-inch = 0.47-inch) are also marked in the figure for comparison purposes. Results show that GRS Abutment Model #1, effectively provided a minimum factor of safety of FoS = 353 kips/20 kips = 17.65 against instability, as the loading system was incapable of producing larger deformations than what is shown in **Figure 88** for safety reasons. FHWA guidelines recommend limiting the vertical settlement as maximum 0.47-inch. The surcharge load value was 40 kips at 0.47-inch vertical settlement, so the minimum factor of safety of FoS = 40 kips/20 kips = 2.0 based on the recommended vertical settlement limit in the FHWA guidelines. This attests to significant built-in factors of safety in GRS abutment systems, which requires further investigation through performance tests such as those done in this study as called for in the FHWA guidelines.

Results in **Figure 88** also indicate a very stable and linear performance on the part of the GRS abutment model all the way through the maximum surcharge load that could have been applied during the test. The magnitude of measured settlement at design load was found to be comparable to (and in fact, smaller than) the limiting value specified in the FHWA guidelines.

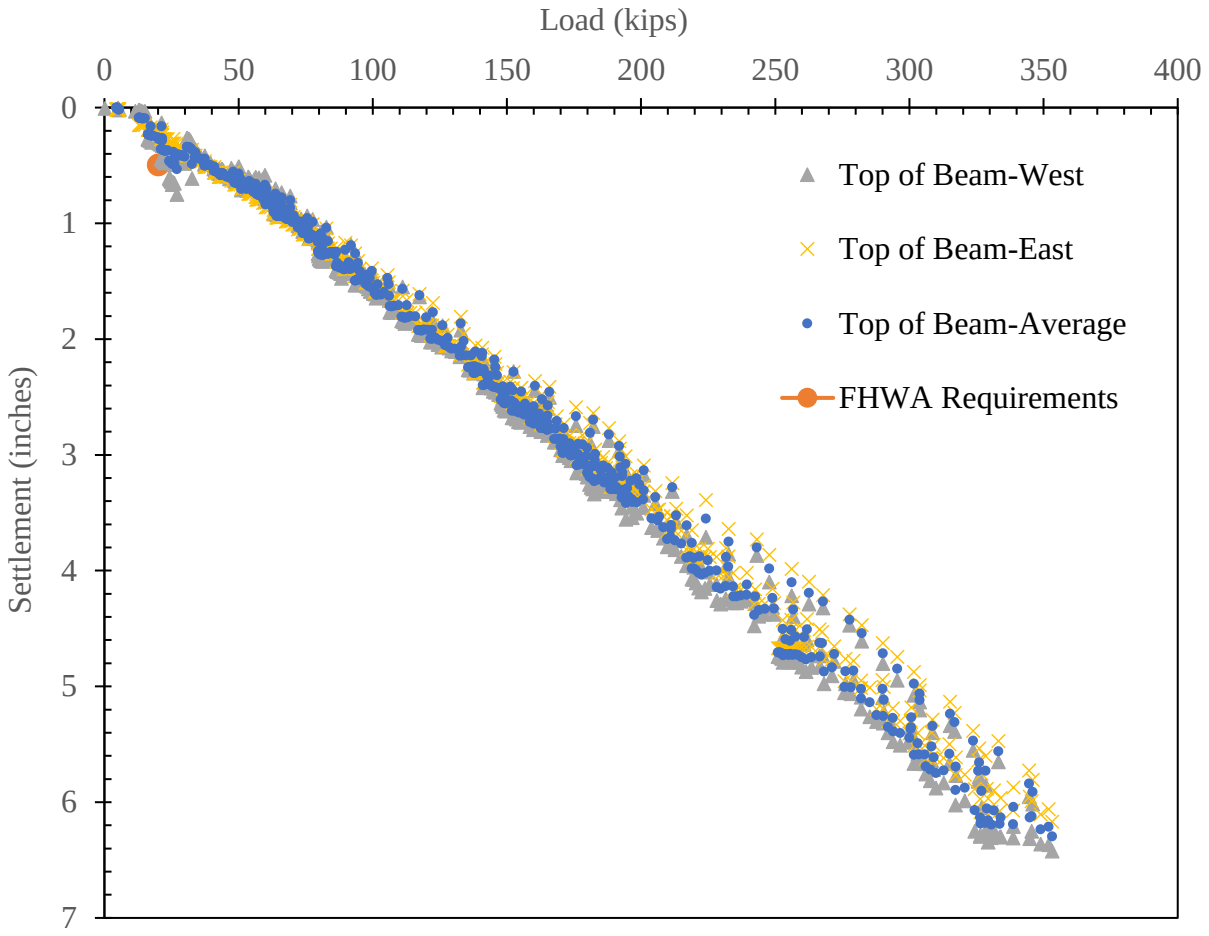

Figure 88. Measured load-settlement results for GRS Abutment Model #1

Figure 89 shows measured load-settlement results for GRS Abutment Model #2. Design values of bearing capacity (4 ksf) and bridge abutment settlement (0.50% of the height = 0.50% × 99-inch = 0.495-inch) are also marked in the figure for comparison purposes. Results show that the two WPs show consistent readings throughout the test up to approximately 236 kips of total load when the test was aborted for safety reasons. Readings from one load cell was used throughout the test, which multiplied by two to obtain the total surcharge load plotted in **Figure 89**. The surcharge load was removed gradually after reaching its maximum target value to produce unloading data on the model abutment performance as well. Data in **Figure 89** indicate that the abutment model

experienced 1.8-inch of permanent settlement at the top, and an additional 0.50-inch of elastic rebound after the removal of the surcharge load for a total of 2.3-inch of settlement at the maximum surcharge load level. The surcharge load value was 70 kips at 0.495-inch vertical settlement, so the minimum factor of safety of FS = 70 kips/20 kips = 3.50 based on the recommended vertical settlement limit in the FHWA guidelines.

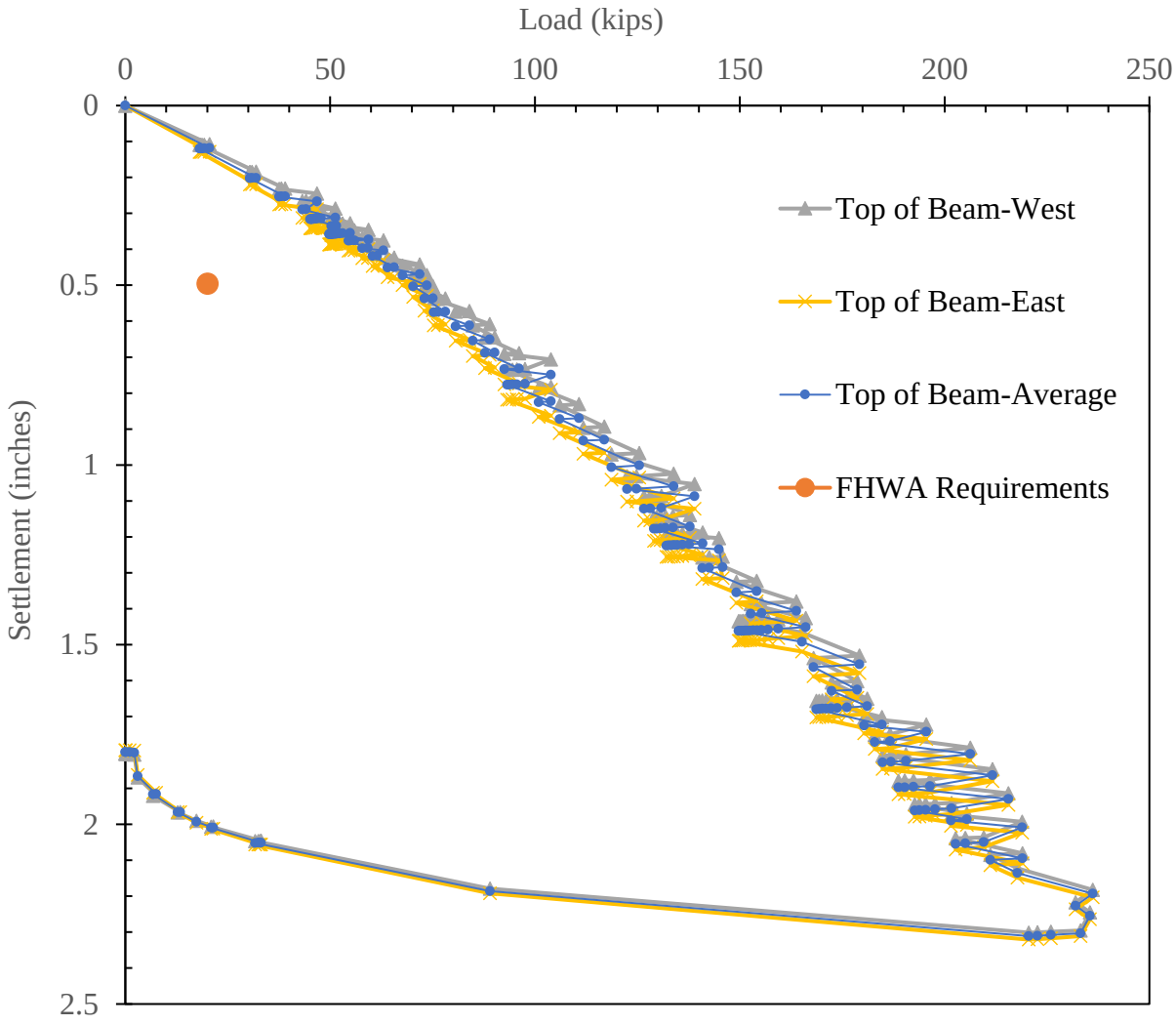

Figure 89. Measured load-settlement results for GRS Abutment Model #2

Figure 90 shows measured load-settlement results for GRS Abutment Model #3. Design values of bearing capacity (4 ksf) and bridge abutment settlement (0.50% of the height = 0.50% × 99-inch = 0.495-inch) are also marked in the figure for comparison purposes. Results show that the loading beam underwent several millimeters of seating adjustment across its span at the beginning of the test. However, afterwards, the two WPs show consistent readings throughout the test up to approximately 200 kips of total load when the test was aborted for safety reasons. Readings from two load cells were also similar throughout the test, which were added together to obtain the total surcharge load plotted in **Figure 90**, the surcharge load was removed gradually after reaching its maximum target value to produce unloading data on GRS fill performance for the analysis. Data in **Figure 90** indicate that the GRS abutment model underwent just over 1.67-inch of permanent deformation (i.e. settlement) at the top, followed by 0.375-inch of elastic rebound when the surcharge load was removed. The surcharge load value was 58 kips at 0.495-inch vertical settlement, so the minimum factor of safety of FS = 58 kips/20 kips = 2.9 based on the recommended vertical settlement limit in the FHWA guidelines.

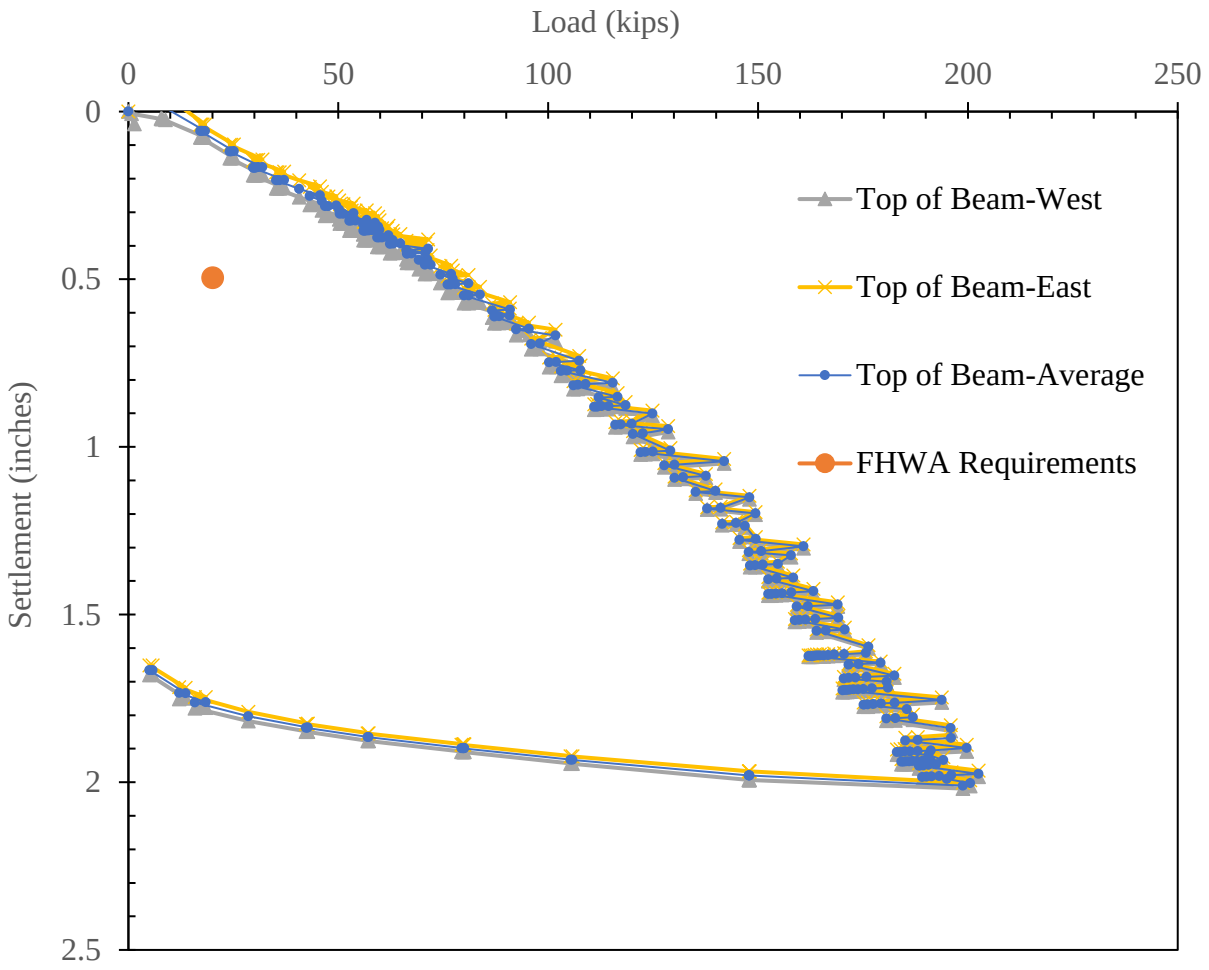

Figure 90. Measured load-settlement results for GRS Abutment Model #3

Figure 91 shows measured load-settlement responses of the beam representing bridge abutment for all three GRS abutment models tested in this study. The magnitudes of maximum load applied during these tests were different, as explained earlier in the corresponding sections.

In the first test (GRS Abutment Model #1), a significant amount of load was applied to determine if the GRS abutment would exhibit significant deformations and signs of internal slip planes within the GRS fill, in order to experimentally determine its ultimate load bearing capacity. However, it was observed that the abutment model remained stable even when the load applied approached the

limiting capacity of the loading frame. Having the advantage of observations and data from the first test, the research team decided to limit the applied load within safer magnitudes in the following tests, while adequate amounts of load were still applied to be able to compare the performances of all three GRS abutment models far beyond the serviceability limit recommended by the FHWA (i.e. 0.495-inch settlement at 20 kips of surcharge load based on 99-inch high structure). Data in **Figure 91** show that all three GRS abutment models were subjected to a minimum of 200 kips surcharge load.

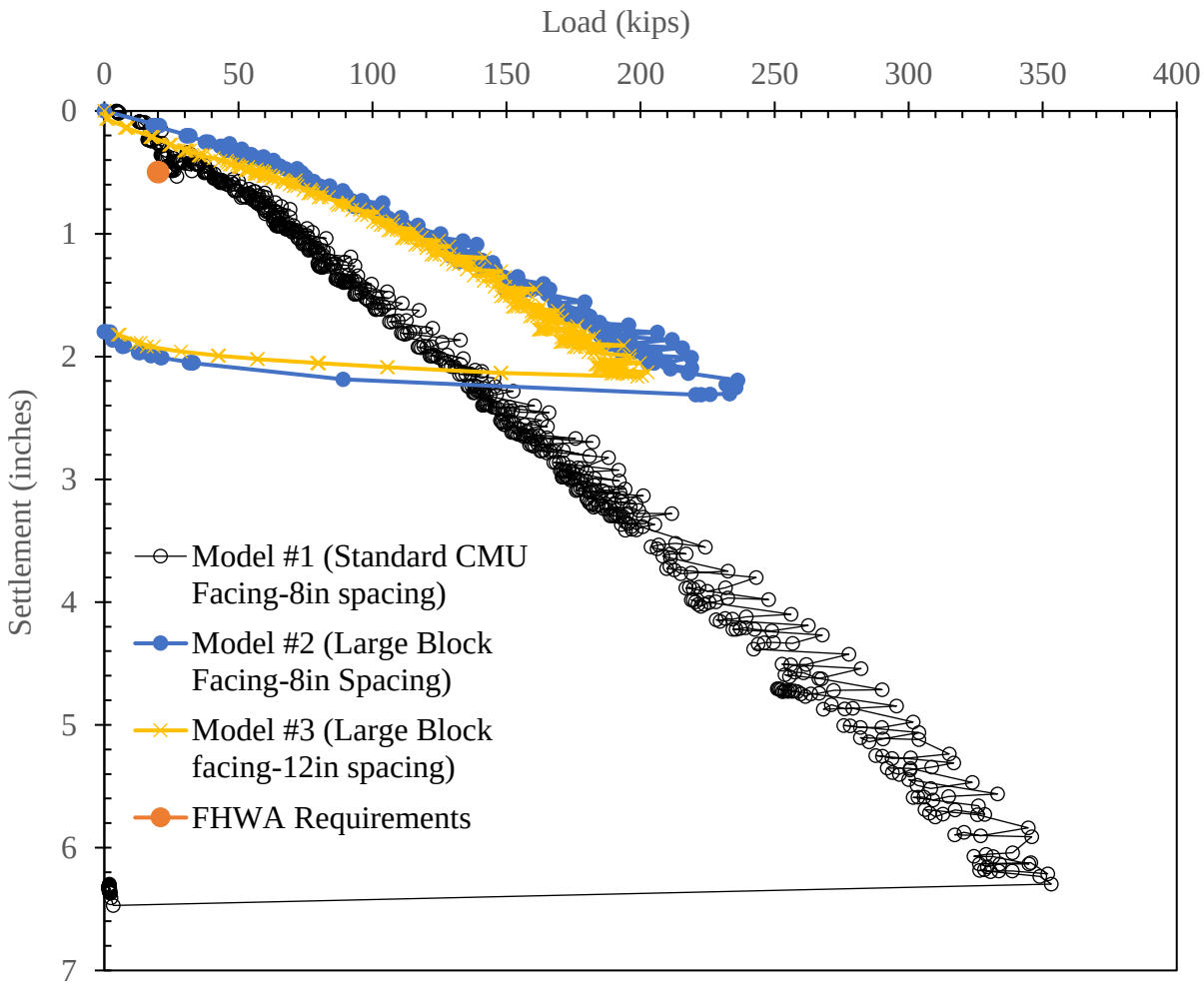

Figure 91. Measured load-settlement responses from wire potentiometers at the top of the loading beam on GRS Abutment Models #1-#3

Figure 92 shows a close-up scope of the measured load-settlement results within 200 kips for better comparison of the three GRS abutment models over a practical range of surcharge loads. Results indicate that for instance, at a mid-range load of 100 kips, Abutment Model #1 (i.e. CMU block facing with 8-inch geotextile spacing) showed the largest amount of settlement (i.e. 1.6-inch), whereas Abutment Model #2 (i.e. large concrete block facing with 8-inch geotextile spacing) exhibited the lowest amount of settlement (i.e. 0.7-inch). Abutment Model #3 (i.e. large concrete block facing with 12-inch geotextile spacing) showed only slightly larger settlement relative to Abutment Model #2 (i.e. 0.8-inch) and significantly smaller amount of settlement than Abutment Model #1, indicating that using large concrete block facing with increased reinforcement spacing could lead to an optimal design relative to both the performance and cost of GRS bridge abutments. Measured settlements at 200 kips of surcharge load are 3.3-inch, 2.05-inch and 2.1-inch, for Models #1-#3, respectively.

Results shown in **Figures 91 and 92** demonstrate that large concrete block facing (as was used in GRS Abutment Models #2 and #3) can indeed enhance the structural integrity and performance of GRS bridge abutments relative to the industry standard, which is the use of CMU blocks. These data show that the measured settlement of the control GRS Abutment Model #1 at 20 kips design load level was comparable to the limiting value per the FHWA requirements. In comparison, measured settlements for GRS Abutment Models #2 and #3 at the same load level were significantly lower (i.e. 0.1 and 0.2-inch, respectively), and both models consistently maintain their superior load-deformation performance throughout the test relative to that of GRS Abutment Model #1. At the maximum applied load level of 236 kips, the settlement in GRS Abutment Model #2 was only 2.3-inch as compared to 4.3-inch in GRS Abutment Model #1 (i.e. reduced settlements in GRS Abutment Model #2 relative to Model #1 by a factor of 2).

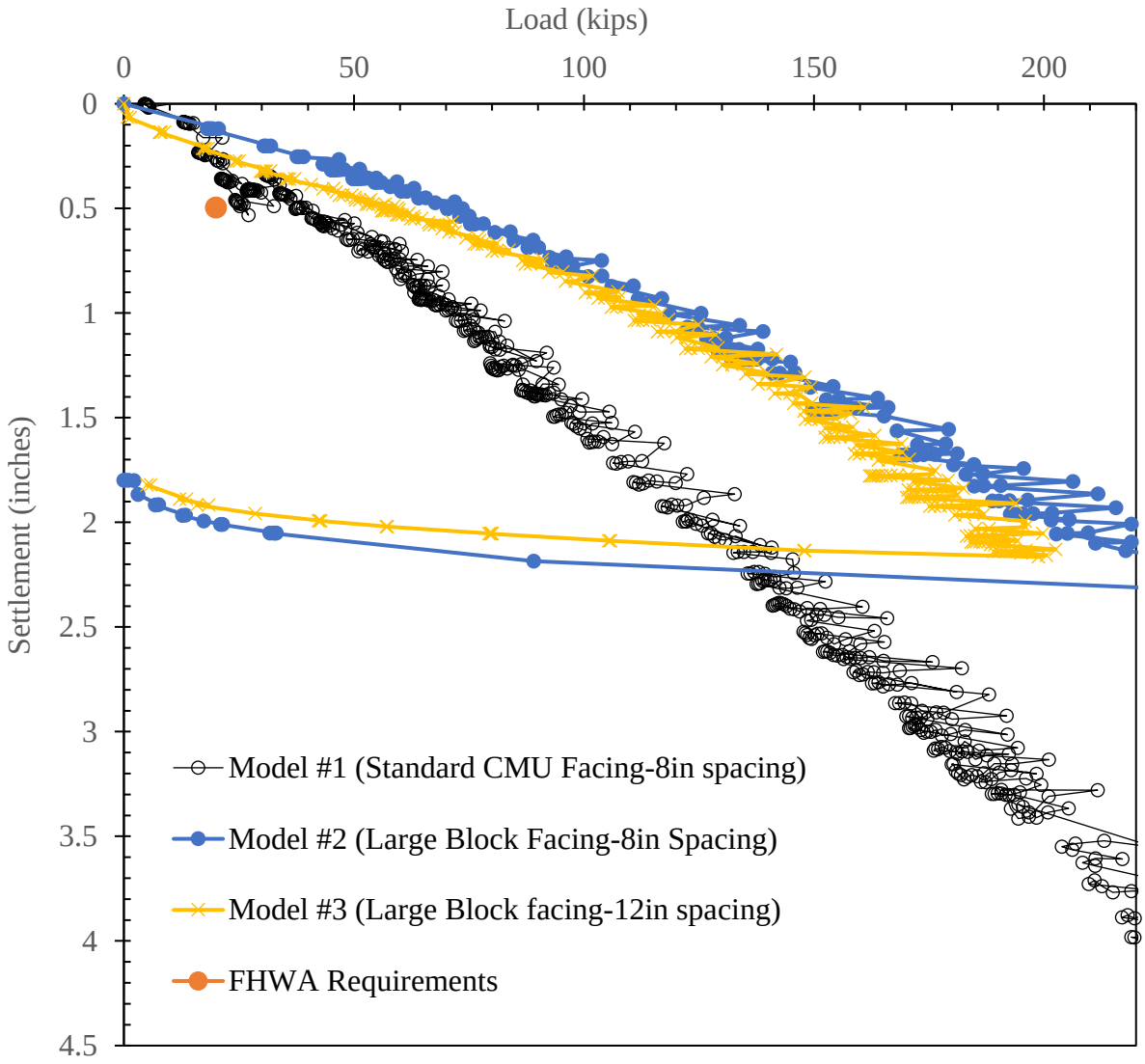

Figure 92. Measured load-settlement responses from wire potentiometers at the top of loading beam GRS Abutment Models #1-#3.(Note: Blown-up scope within 200 kips of surcharge load is provided for better comparison of performances.)

The considerable amount of reduced abutment settlement discussed above together with the reduced construction time observed in the case of large concrete block GRS abutment models, constitute significant outcomes of the study. In GRS Abutment Model #3, the possibility of additional cost savings was explored by reducing the number of reinforcement layers in the model abutment within the FHWA recommendations.

8.3. Facing Deformations

Figure 93 shows measured facing deformation results for GRS Abutment Model #1 during surcharge load testing from WP readings that were attached to facing blocks. Readings from the two WPs at the top (i.e. Row #12 of the facing blocks) show excellent agreement with each other, which indicates that the instrumented/observation section of GRS abutment model in the middle performed uniformly in plane-strain condition. Only one WP was attached to each of the lower blocks (i.e. Rows #5 and #8) because they were expected to undergo smaller deformations and show a similar level of agreement as well. Data in **Figure 93** indicate a maximum deformation of Δ = 1.6-inch, or Δ/H = 1.70% for a 94-inch high facing (as opposed to the nominal 99-inch, due to actual dimensions of CMU blocks) of the GRS abutment model.

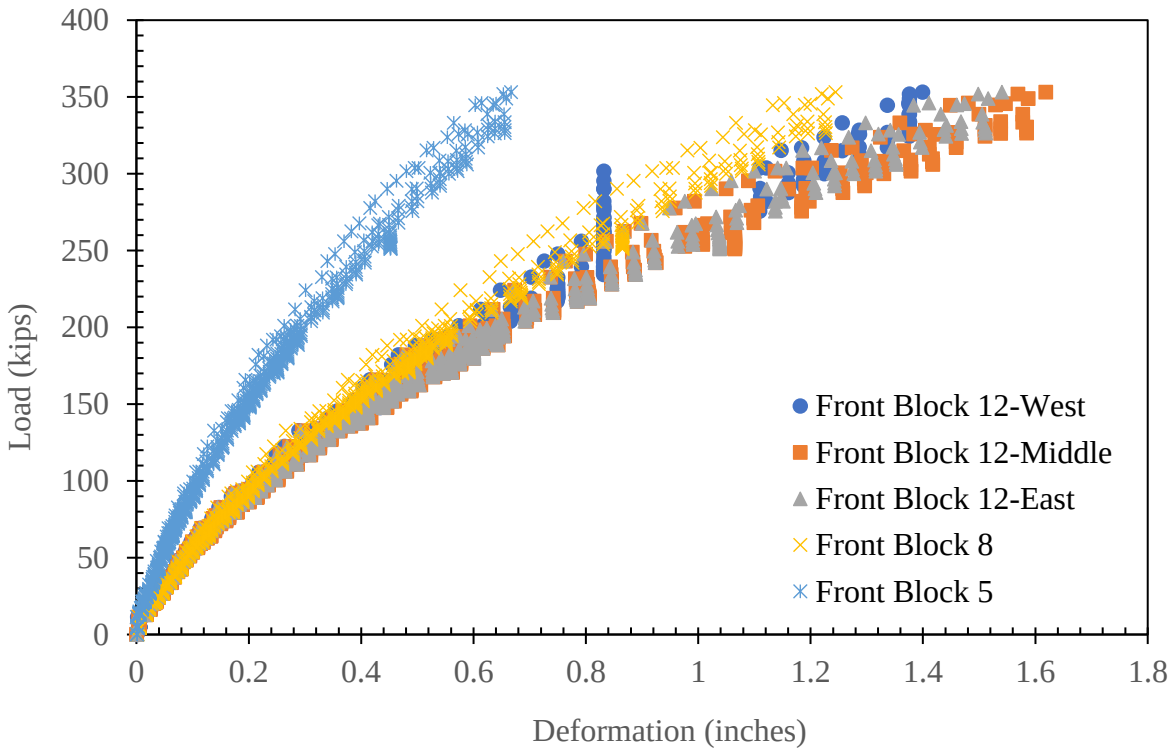

Figure 93. Measured facing deformation results from WPs during surcharge load testing of GRS Abutment Model #1. (Note: WP Row #4 = Block Level 12, Row #3 = Block Level 8, Row #2 = Block Level 5)

Progression of measured facing profile outward at three different elevations (Average of three WPs at Block 12 level, WP at Block 8 level and WP at Block 5 level) for selected load magnitudes (20, 50, 100, 150, and 200 kips) are shown in **Figure 94**.

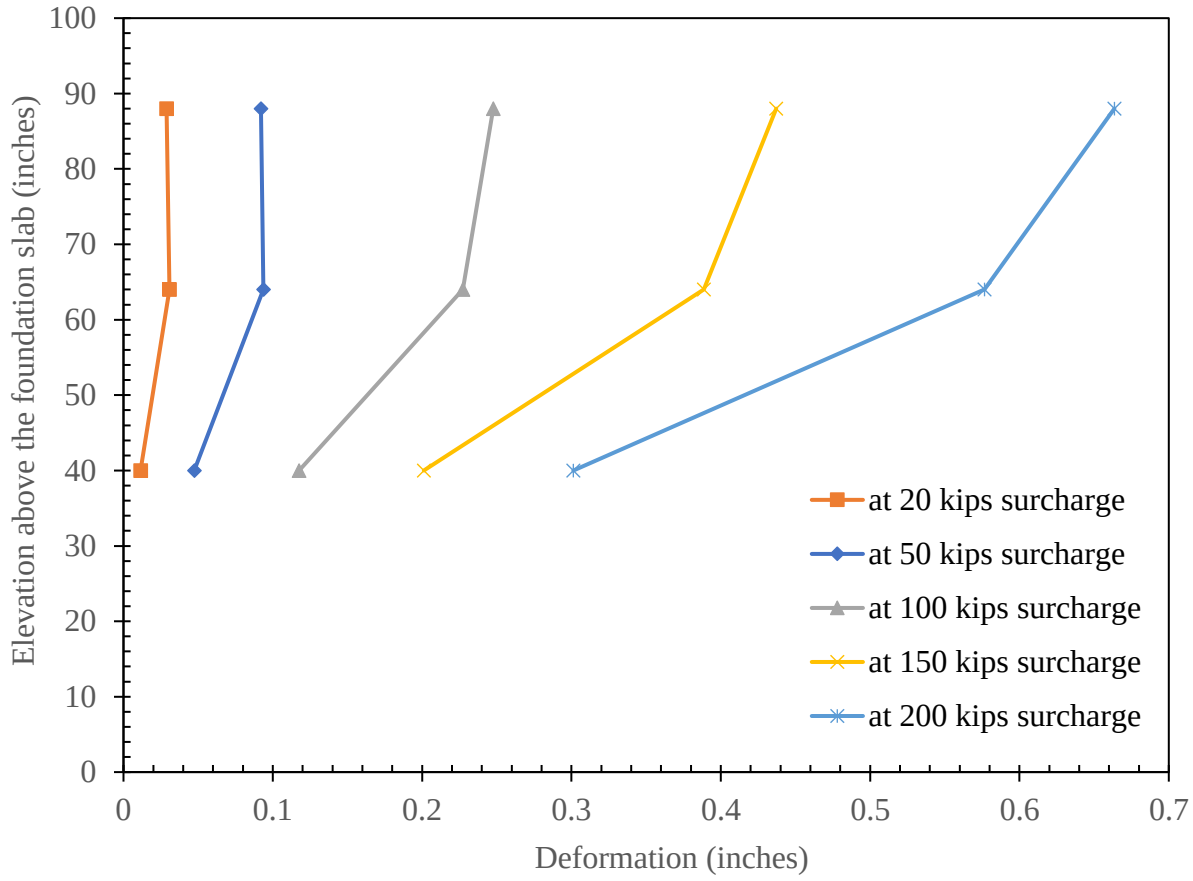

Figure 94. Progression of measured facing deformation profile from the front WPs at different elevations during surcharge load testing of GRS Abutment Model #1

Figure 95 shows measured facing deformation results for the GRS Abutment Model #2 during surcharge load testing from WP readings that were attached to facing blocks. Readings from the two WPs at the top (i.e. Row #4 of the facing blocks) show excellent agreement with each other,

which indicates that the instrumented/observation section of GRS abutment model in the middle performed uniformly in plane-strain condition. Only one WP was attached to each of the lower blocks (i.e. Rows #2 and #3) because they were expected to undergo smaller deformations and show a similar level of agreement as well. Data in **Figure 95** indicate a maximum deformation of $\Delta = 0.47$-inch, or $\Delta/H = 0.47\%$ (H: abutment height) for the 99-inch high facing of GRS abutment model.

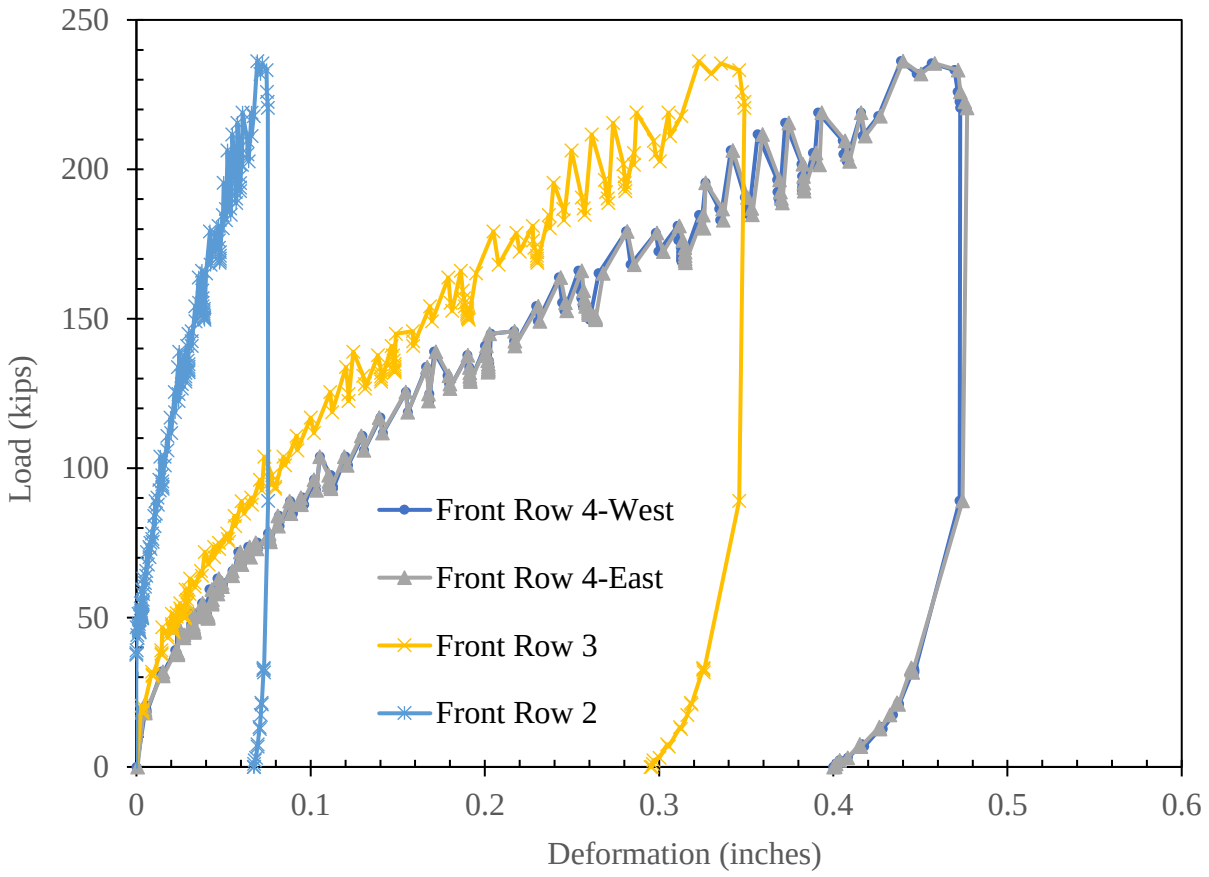

Figure 95. Measured facing deformation results from WPs during surcharge load testing of GRS Abutment Model #2 (Row #4 = Top large concrete block)

Progression of measured facing profile outward at three different elevations (Average of two WPs at Row #4 level, WP at Row #3 level and WP at Row #2 level) for selected load magnitudes (20, 50, 100, 150, 200 kips) are shown in **Figure 96**.

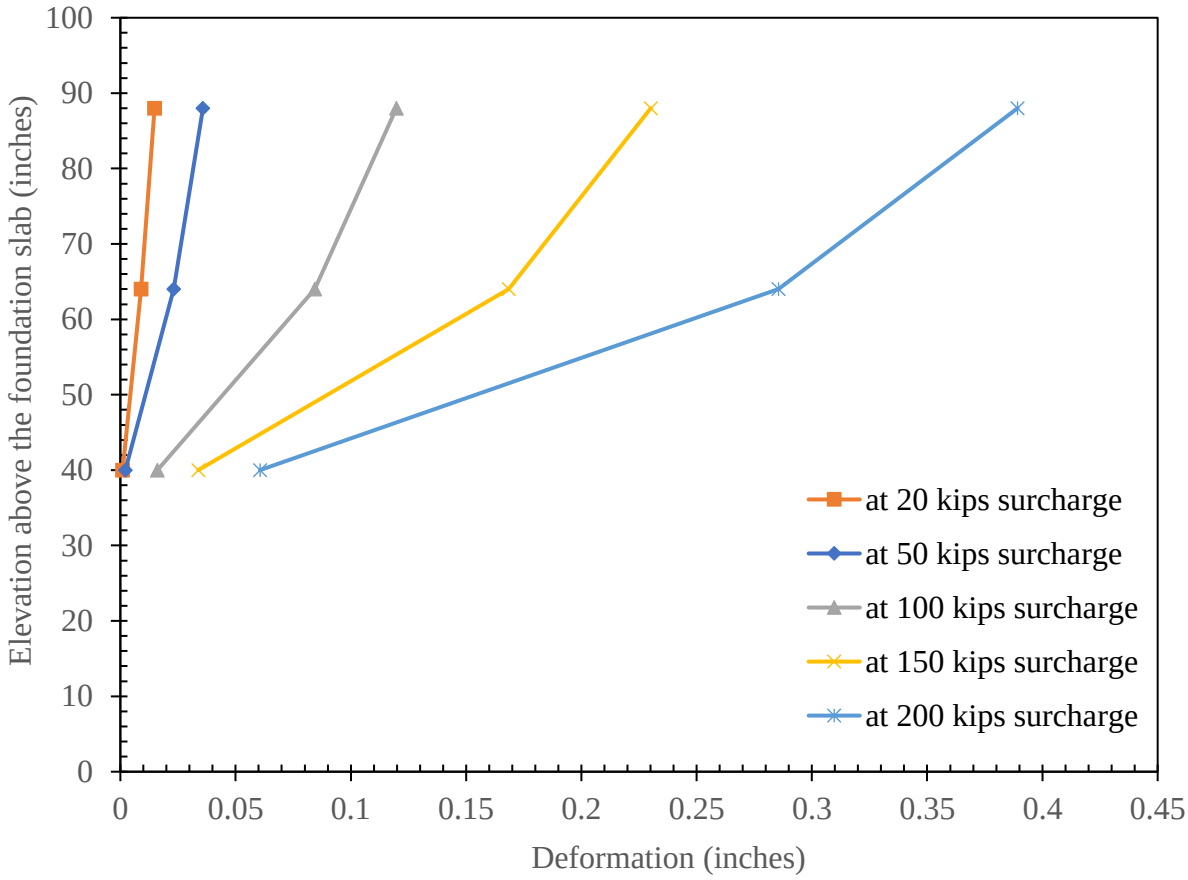

Figure 96. Progression of measured facing deformation profile from the front WPs at different elevations during surcharge load testing of GRS Abutment Model #2

Figure 97 shows measured facing deformation results for GRS Abutment Model #3 during surcharge load testing from WP readings that were attached to facing blocks. Readings from the two WPs at the top (i.e. Row #4 of the facing blocks) show excellent agreement with each other,

which indicates that the instrumented/observation section of GRS abutment model in the middle performed uniformly in plane-strain condition. Only one WP was attached to each of the lower blocks (i.e. Rows #2 and #3) because they were expected to undergo smaller deformations and show a similar level of agreement as well. Data in **Figure 97** indicate a maximum deformation of $\Delta = 0.33$-inch, or $\Delta/H = 0.333\%$ for the 99-inch high facing of GRS abutment model.

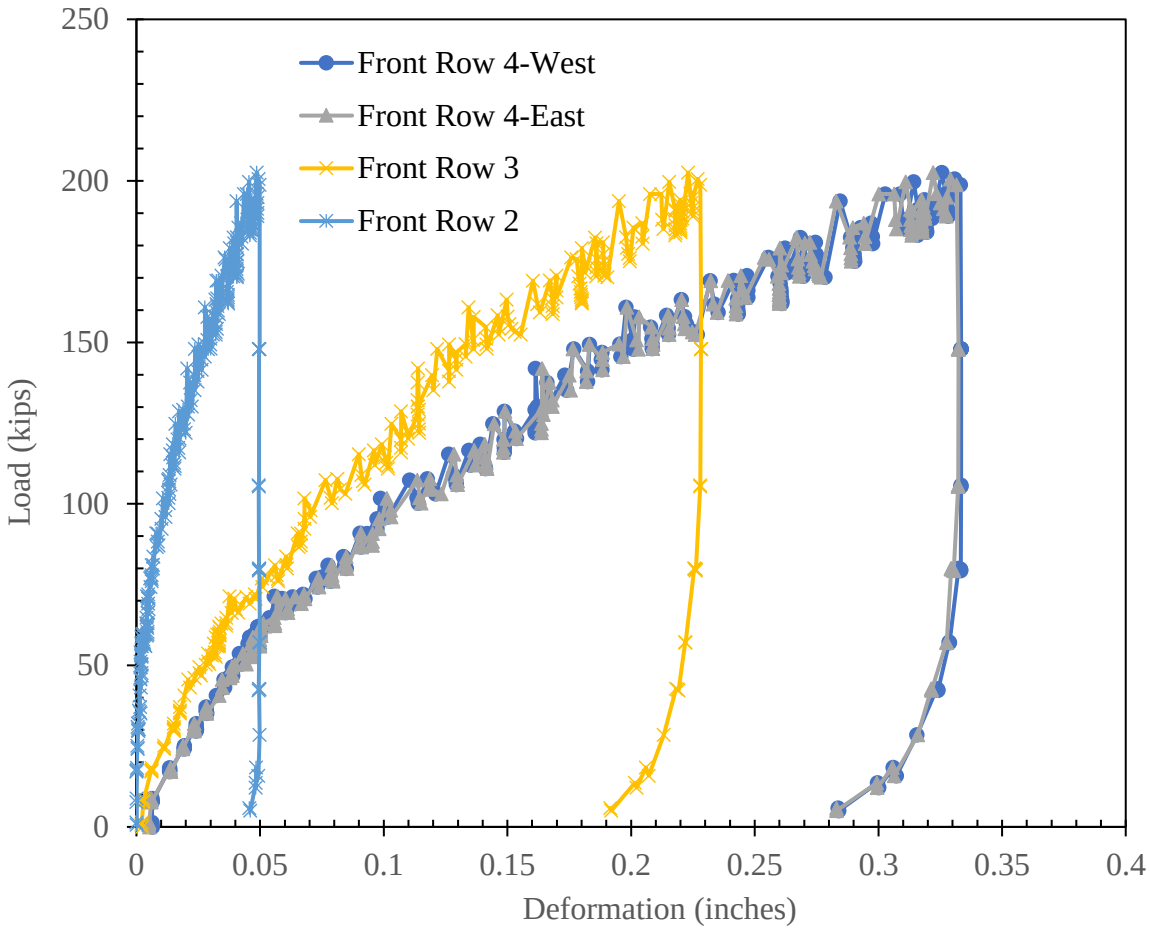

Figure 97. Measured facing deformation results from WPs during surcharge load testing of GRS Abutment Model #3 (Row #4 = Top large concrete block)

Progression of measured facing profile outward at three different elevations (Average of two WPs at Row #4 level, WP at Row #3 level and WP at Row #2 level) for selected load magnitudes (20, 50, 100, 150, 200 kips) are shown in **Figure 98**.

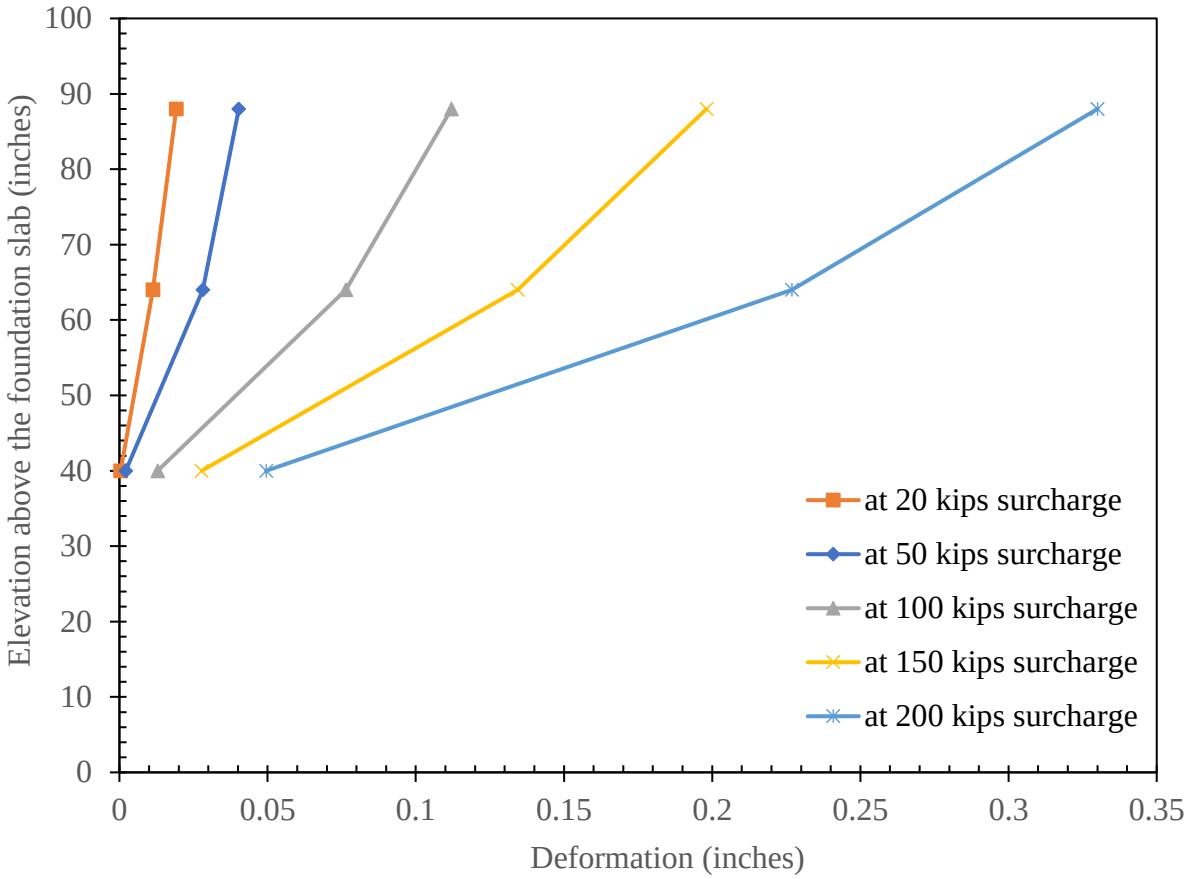

Figure 98. Progression of measured facing deformation profile from the front WPs at different elevations during surcharge load testing of GRS Abutment Model #3

Figures 99 through 101 show comparisons of measured facing deformations at different WP elevations during surcharge loading of the three model abutments in this study. Results show that all GRS abutment models by far exceeded the FHWA stiffness requirement of maximum

normalized facing deformation of 1% (relative to the bridge abutment height) for a 4 ksf surcharge load (equivalent to 20 kips in this study). As an example, results in **Figure 99** show a maximum deformation of Δ = 0.38-inch, or Δ /H = 0.38% at Row #4 level for 200 kips of surcharge load in the case of the 99-inch high GRS Abutment Model #2.

It should be noted that facing deformation readings for the CMU block facing bridge abutment model (i.e. GRS Abutment Model #1) were taken at the same elevations as those on GRS Abutment Models #2 and #3 for accurate comparison.

Finally, results in **Figures 99 through 101** show that load-deformation performance of GRS Abutment Model #3, i.e. large concrete block facing with increased (12-inch) reinforcement spacing was essentially the same as that of GRS Abutment Model #2 with 8-inch reinforcement spacing, and significantly better than that of the standard CMU block facing model for all elevations examined. This indicates that the use of large concrete block could lead to a more economical design (through wider reinforcement spacing) while maintaining the same performance level. This could help make the GRS bridge abutment alternative even more economically attractive for local road projects in different states across the U.S. This is a significant outcome of the study that awaits further verification through longer-term field studies in continuation of this project.

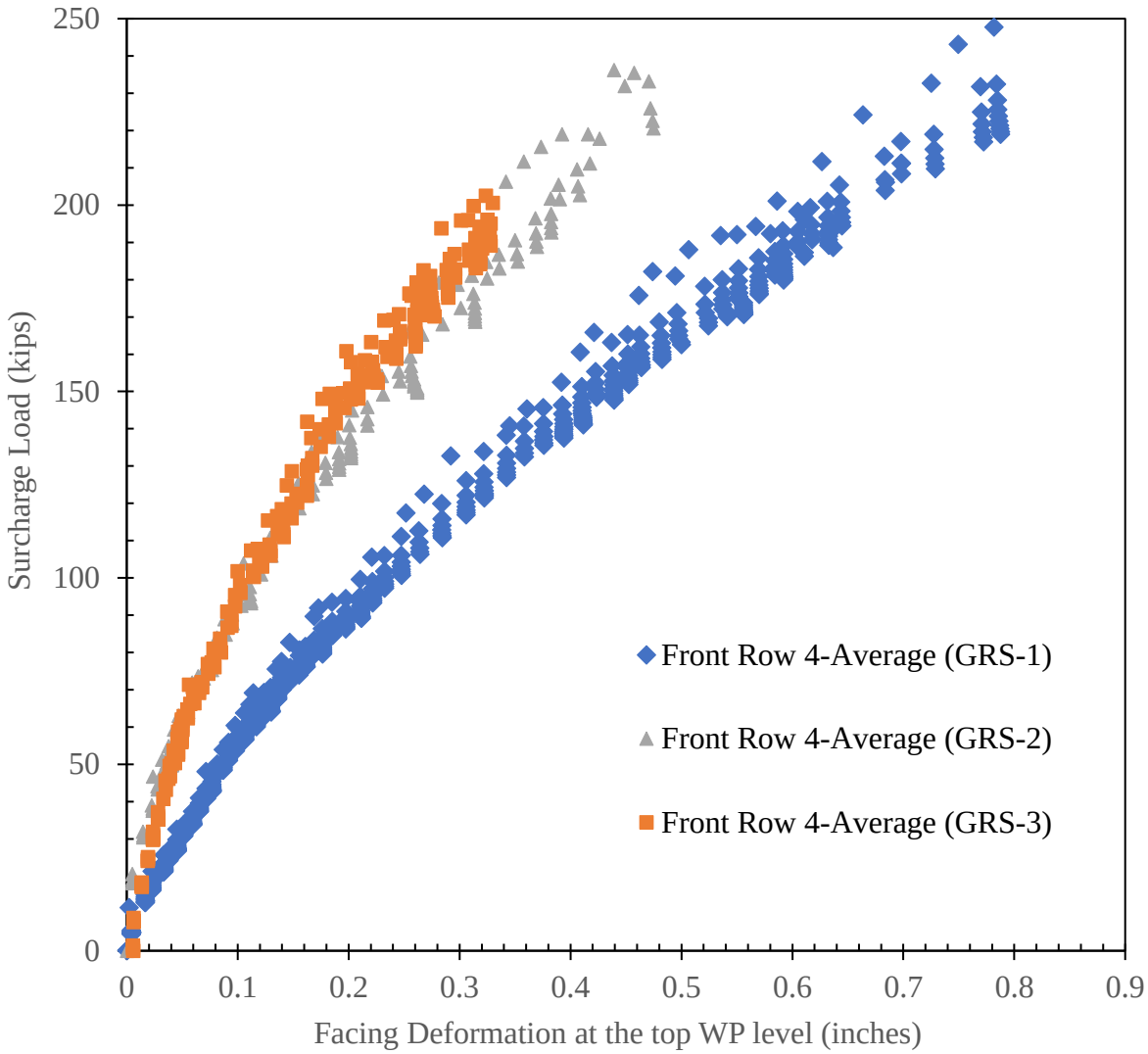

Figure 99. Measured facing deformation results at the top WP level (Row #4) during surcharge load testing of GRS Abutment Models #1-#3. (Note: Deformation values shown are mean values from three WPs for GRS Abutment Model #1, and two WPs for GRS Abutment Models #2 and #3 at the same elevation.)

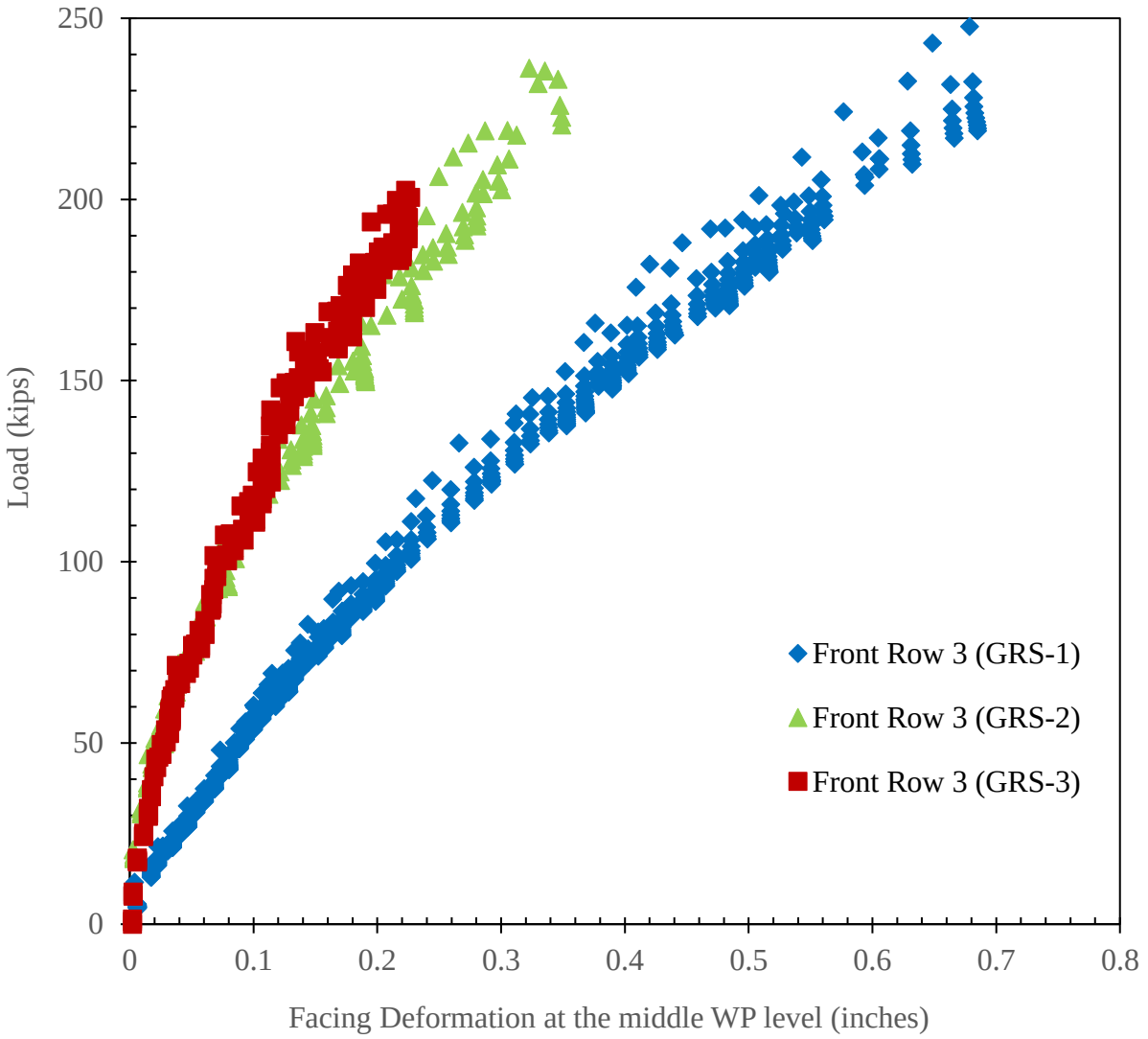

Figure 100. Measured facing deformation results at the WP level (Row #3) during surcharge load testing of GRS Abutment Models #1-#3

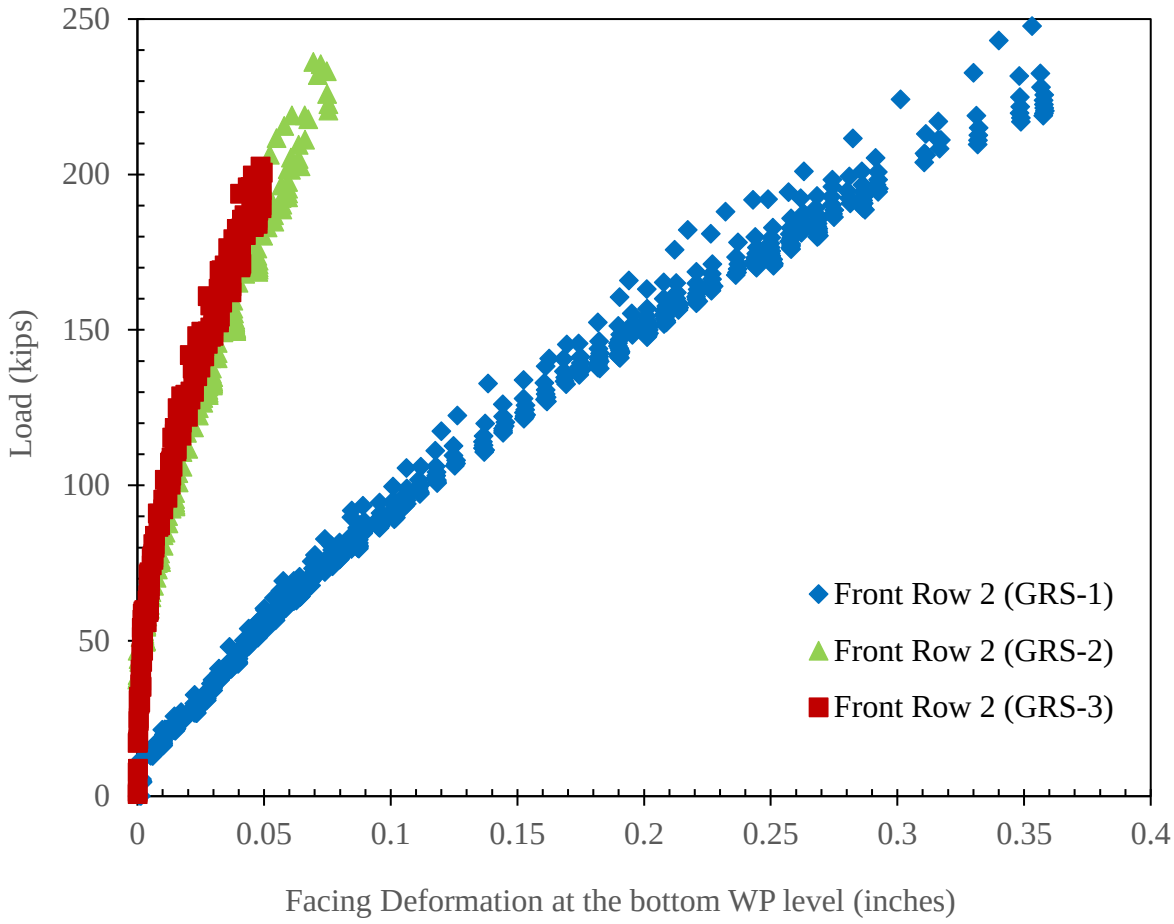

Figure 101. Measured facing deformation results at the bottom WP level (Row #2) during surcharge load testing of GRS Abutment Models #1-#3

Figures 102 through 104 show contour maps of facing deformation for GRS Abutment Models #1-#3 at end of surcharge loading, respectively. Measurements shown in these figures were taken manually at end of surcharge loading to compare against the wire potentiometer (WP) data that were obtained using a data acquisition system during the surcharge load tests. The comparison of outward facing deformation of GRS Abutment Models #1-#3 at the end of surcharge load testing (DAS and Manual Readings) are listed in **Tables 6 through Table 8**, respectively. Results in **Figures 102 through 104** are in satisfactory agreements with the recorded wire potentiometer data.

Table 6. Comparison of outward facing deformation of GRS Abutment Model #1 at the end of surcharge load testing (DAS and Manual Readings)

Location	DAS deformation WP readings (inches)	Manual deformation reading averages (inches)	Difference between DAS and manual readings (inches)
Block Row#12-West	1.3988	1.1875	0.2113
Block Row#12-Middle	1.6184	1.4375	0.1809
Block Row#12-East	1.5401	1.5	0.0401
Block Row#8-Middle	1.2444	0.875	0.3694
Block Row#5-Middle	0.6665	0.625	0.0415

Table 7. Comparison of outward facing deformation of GRS Abutment Model #2 at the end of surcharge load testing (DAS and Manual Readings)

Location	DAS deformation WP readings (inches)	Manual deformation reading averages (inches)	Difference between DAS and manual readings (inches)
Block Row#4-West	0.4565	0.25	0.2065
Block Row#4-East	0.4582	0.625	0.1668
Block Row#3-Middle	0.3355	0.3125	0.023
Block Row#2-Middle	0.0724	0.1875	0.1151

Table 8. Comparison of outward facing deformation of GRS Abutment Model #3 at the end of surcharge load testing (DAS and Manual Readings)

Location	DAS deformation WP readings (inches)	Manual deformation reading averages (inches)	Difference between DAS and manual readings (inches)
Block Row#4-West	0.3309	0.5	0.1691
Block Row#4-East	0.3292	0.375	0.0458
Block Row#3-Middle	0.2269	0.3125	0.0856
Block Row#2-Middle	0.0495	0.1875	0.138

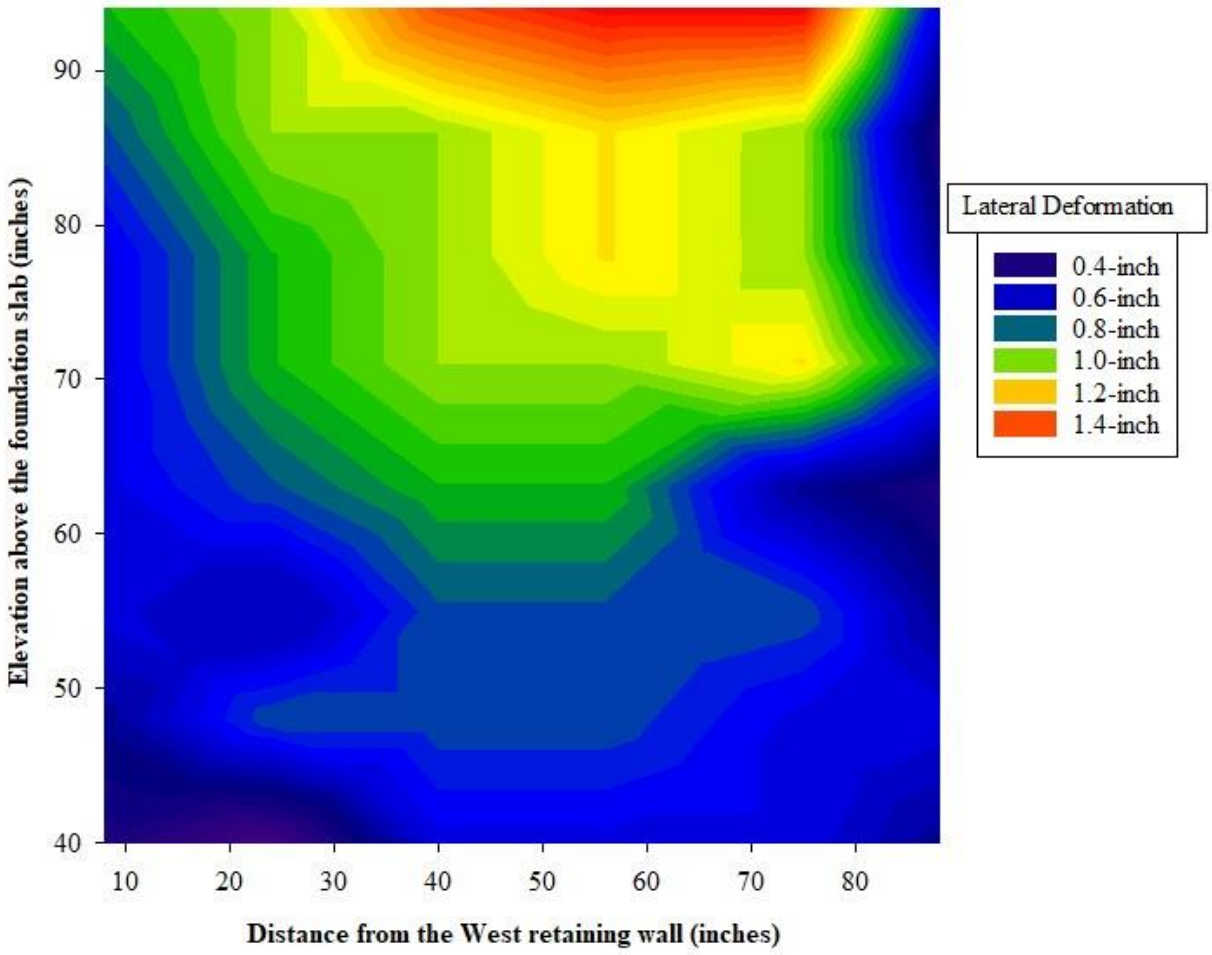

Figure 102. Outward facing deformation from manual survey of GRS Abutment Model #1 at the end of surcharge load testing. Maximum normal stress applied = 70.6 ksf (Note: The x-axis indicates measurement at six points across the facing (i.e. 8-inch, 24-inch, 40-inch, 56-inch, 72-inch, and 88-inch. Maximum surcharge load was 353 kips.)

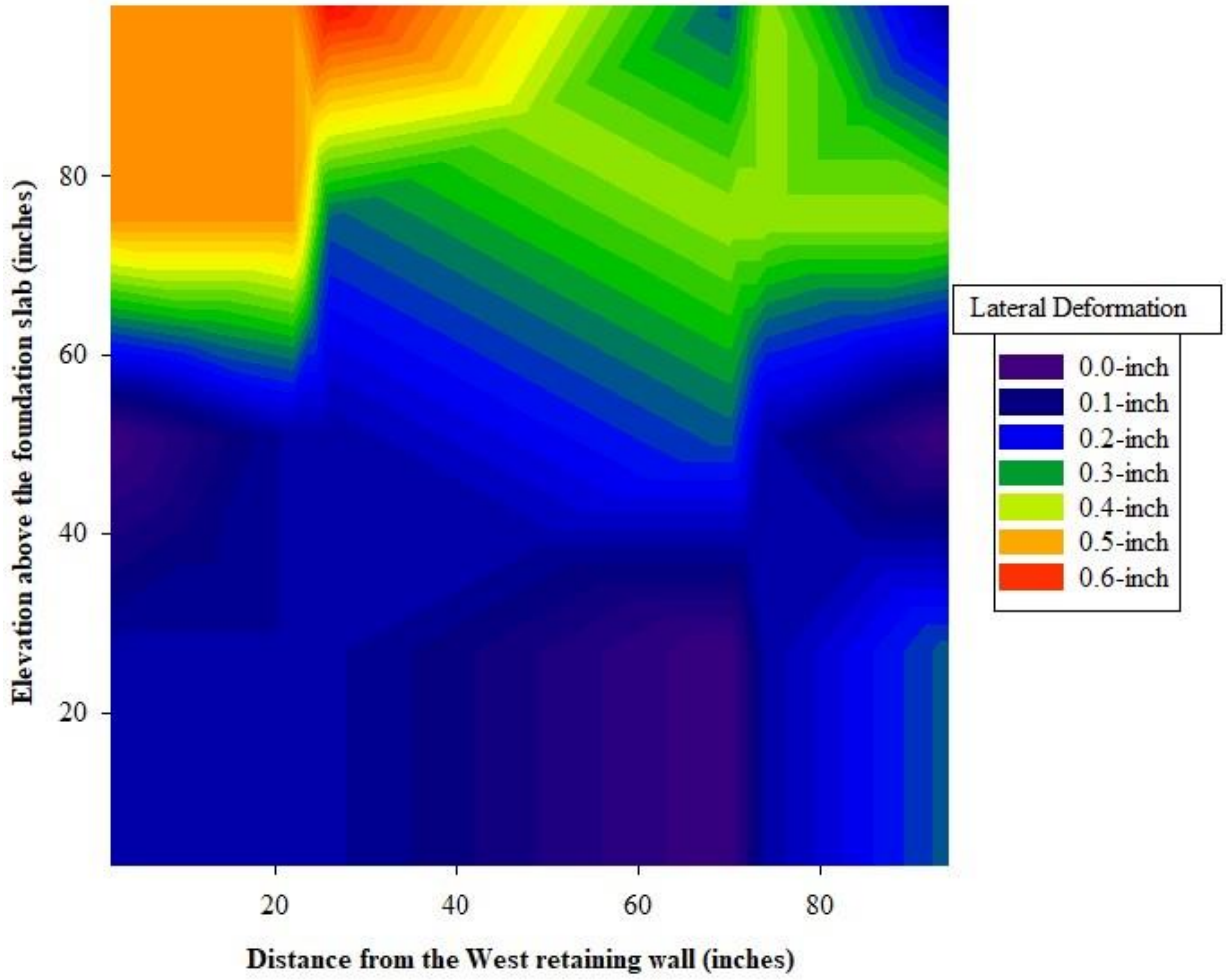

Figure 103. Outward facing deformation from manual survey of GRS Abutment Model #2 at the end of surcharge load testing. Maximum normal stress applied = 47.2 ksf (Note: The x-axis indicates measurement at six points across the facing (i.e. 2-inch, 22-inch, 26-inch, 70-inch, 74-inch, and 94-inch. Maximum surcharge load was 236 kips.)

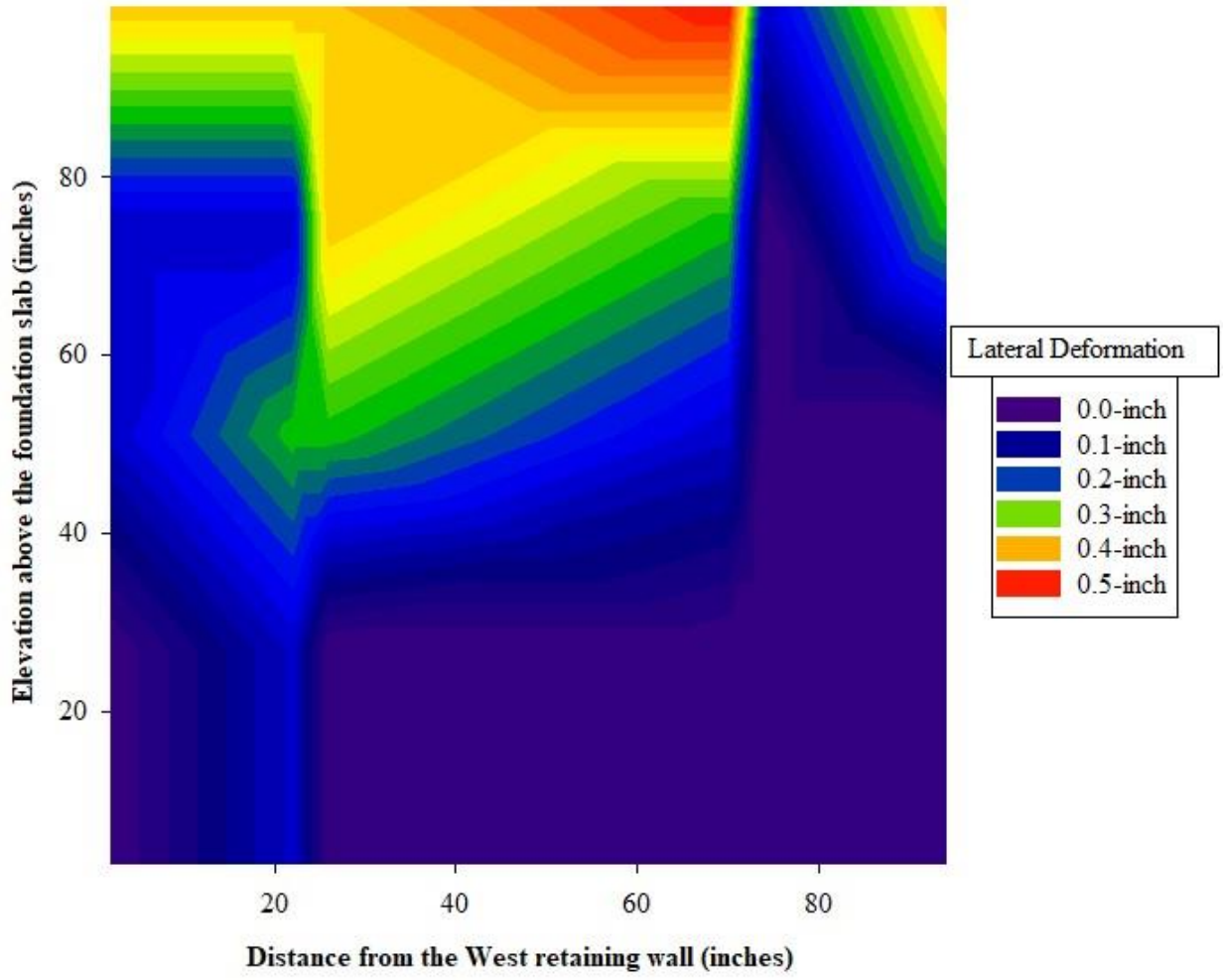

Figure 104. Outward facing deformation from manual survey of GRS Abutment Model #3 at the end of surcharge load testing. Maximum normal stress applied = 40 ksf (Note: The x-axis indicates measurement at six points across the facing (i.e. 2-inch, 22-inch, 26-inch, 70-inch, 74-inch, and 94-inch. Maximum surcharge load was 200 kips.)

8.4. Reinforcement Strains

Figure 105 shows measured lateral movements from WP readings of the top reinforcement layer (located at 86-inch above the foundation slab) during surcharge load testing of GRS Abutment Model #1. WP connection points on the reinforcement layers were numbered from the facing backwards (e.g. "86 inches-1" is the closest connection point behind the facing). Results in **Figure 105** show that the largest amount of extension in this reinforcement layer was underneath the

loading beam between WPs #2 & #3. Data shown in **Figure 105** and those obtained for the lower reinforcement layers (i.e. at elevations 25-inch, 48-inch and 71-inch above the foundation slab) were used to determine axial strain distributions in the reinforcement.

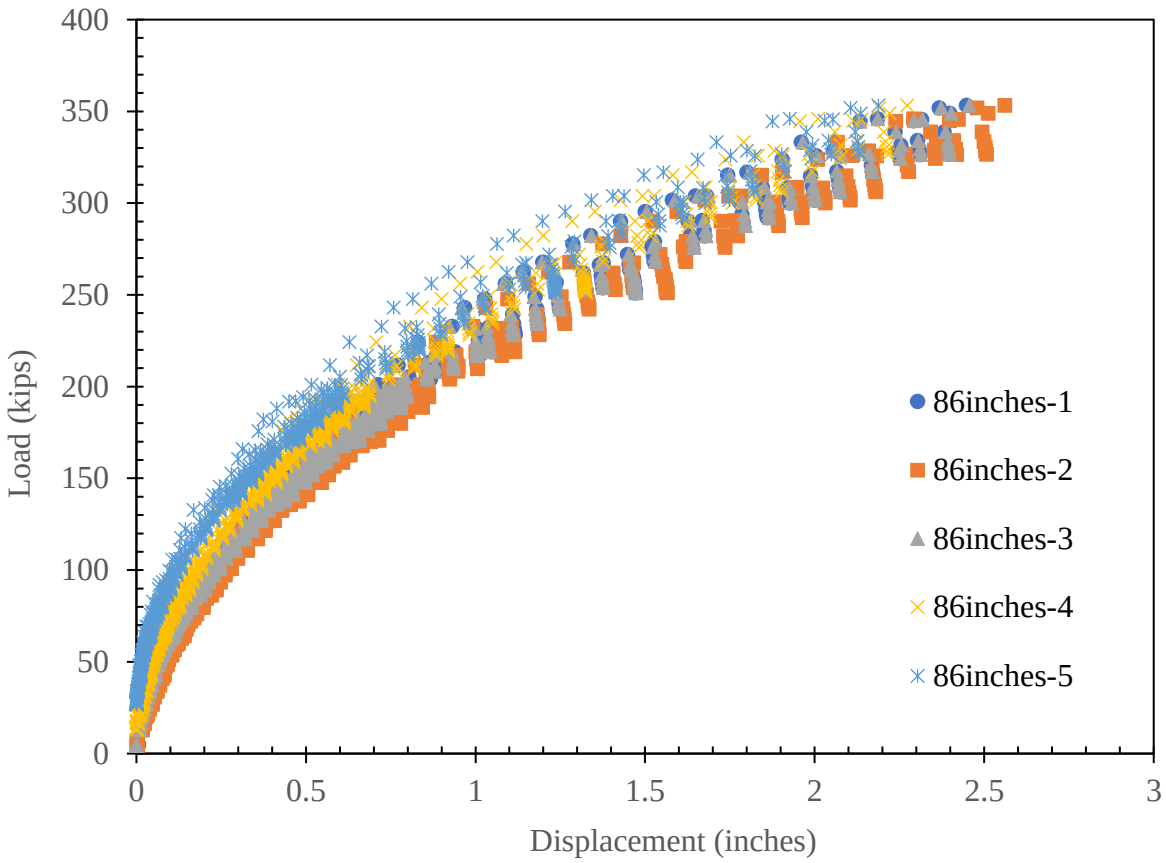

Figure 105. Wire potentiometer readings at the top reinforcement layer in GRS Abutment Model #1 (Elevation of 86-inch above the foundation slab) due to surcharge load. (Note: WPs were numbered sequentially from the facing toward the tail end of the reinforcement layer.)

Strain magnitude distributions between WP connection points at 86-inch, 71-inch, 48-inch, and 25-inch above the foundation slab during surcharge load testing of GRS Abutment Model #1 were shown in **Figures 106 a, b, c, and d**, respectively. Maximum strain level was recorded at 71-inch above the foundation slab under 40 ksf surcharge load as 0.015 %.

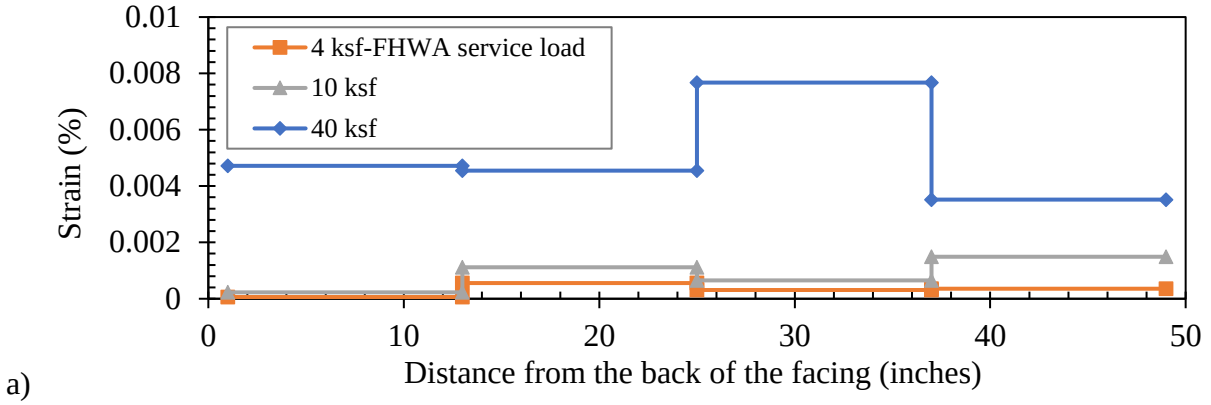

a)

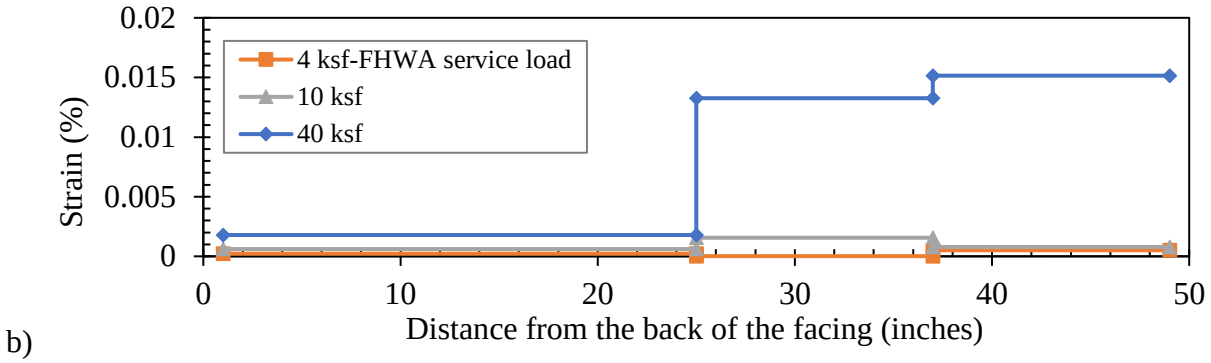

b)

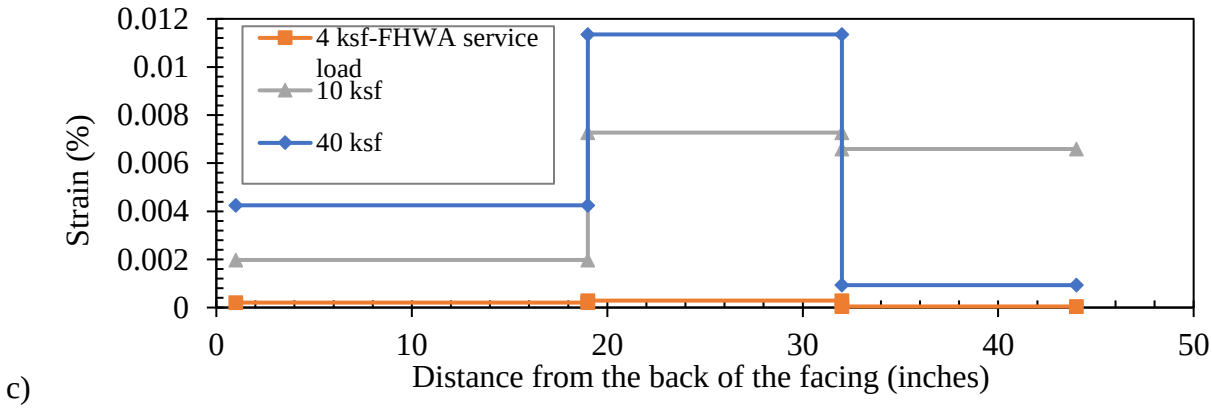

c)

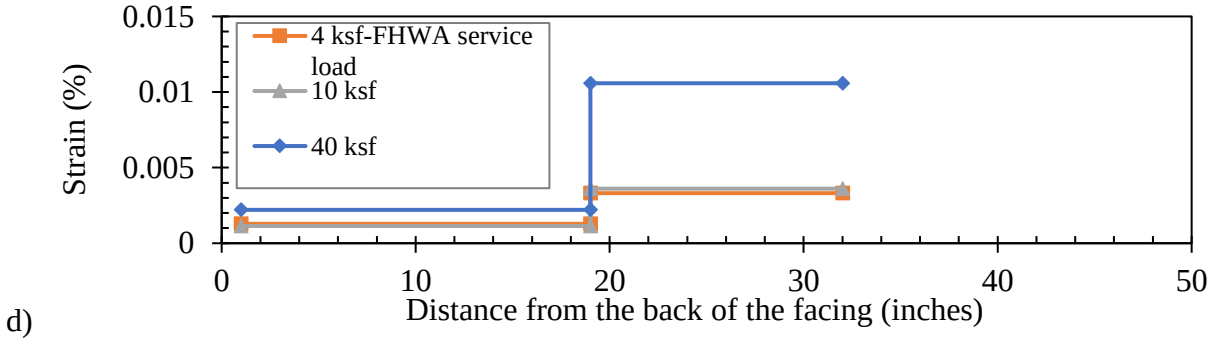

d)

Figure 106. Distributions of global strains between WP connection points at: a) 86-inch, b) 71-inch, c) 48-inch, and d) 25-inch levels above the foundation slab at: 4 ksf (FHWA service load), 10 ksf, and 40 ksf surcharge load levels (GRS Abutment Model #1)

Figures 106 a, b, c, and d show that the strain magnitudes were greater for higher surcharge load levels than lower ones. On the other hand, Figure **106 c** shows a higher strain value at 10 ksf than 40 ksf at the far edge. This might happen due to puncture by backfill material to one of the WP cables, or an unexpected cable movement during surcharge test loading.

Figure 107 shows lateral movements from WP readings of the top reinforcement layer (located at 91-inch above the foundation slab) during surcharge load testing of GRS Abutment Model #2. WP connection points on the reinforcement layers were numbered from the facing backwards (e.g. "91inches-1" is the closest connection point behind the facing). Results in **Figure 107** clearly show that the largest amount of extension in this reinforcement layer was underneath the loading beam between WPs #1 & #2. Data shown in **Figure 107** and those obtained for the lower reinforcement layers (i.e. at elevations 27-inch, 51-inch, and 75-inch above the foundation slab) were used to determine axial strain distributions in the reinforcement.

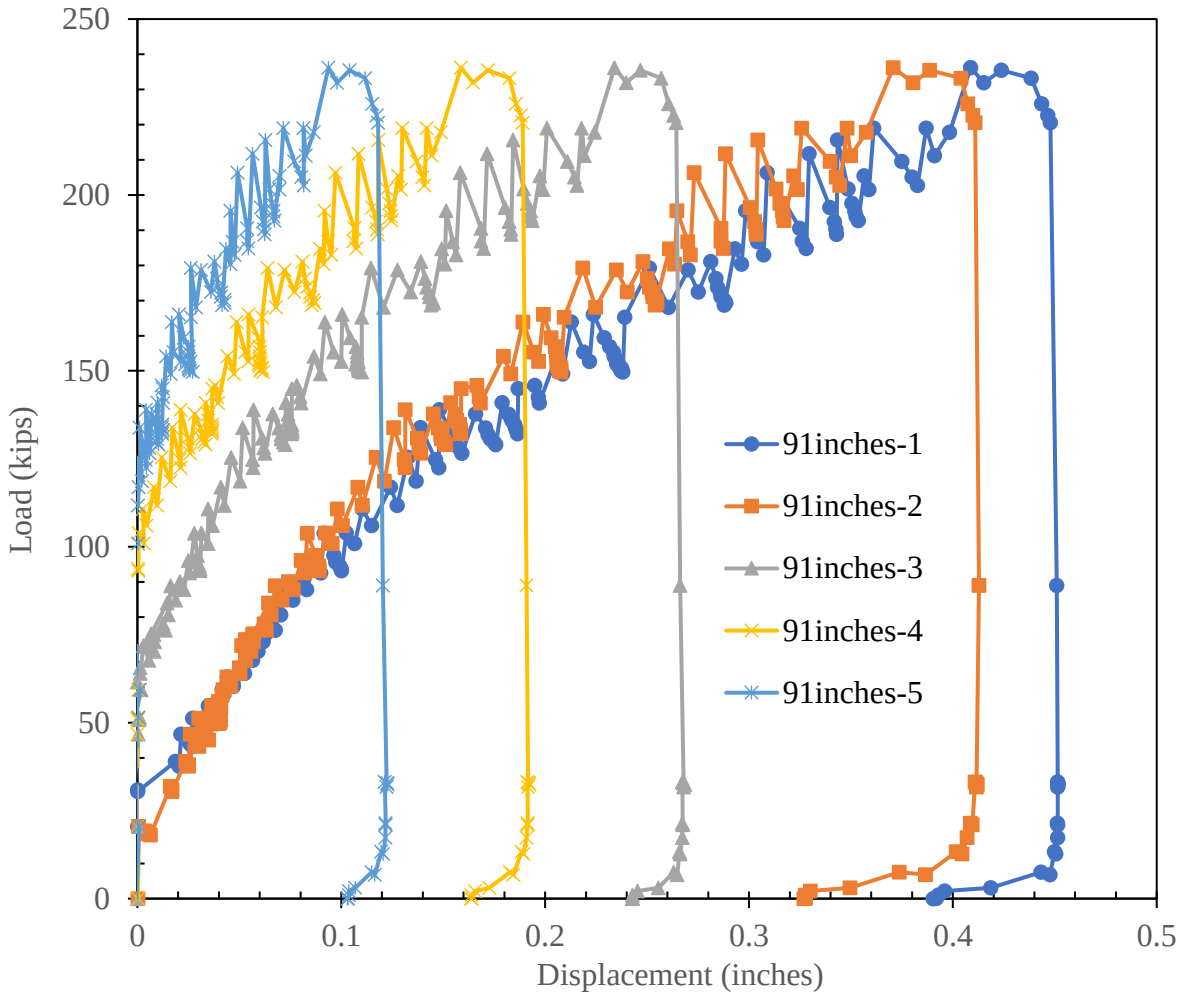

Figure 107. Wire potentiometer readings at the top reinforcement layer in GRS Abutment Model #2 (Elevation of 91-inch above the foundation slab) due to surcharge load.(Note: WPs were numbered sequentially from the facing toward the tail-end of the reinforcement layer.)

Strain magnitude distributions between WP connection points at 91-inch, 75-inch, 51-inch, and 27-inch above the foundation slab during surcharge load testing of GRS Abutment Model #2 were shown in **Figures 108 a, b, c, and d**, respectively. Maximum strain level was recorded at 75-inch above the foundation slab under 40 ksf surcharge load as 0.0167 %.

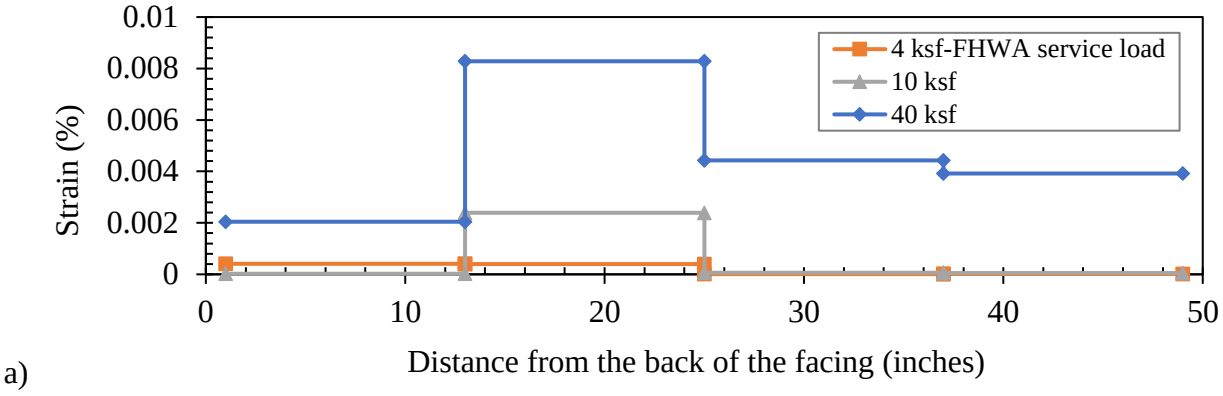

a)

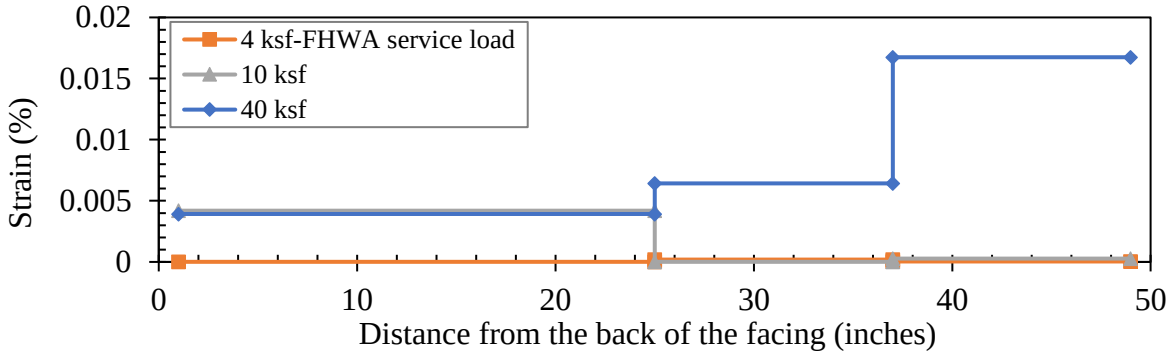

b)

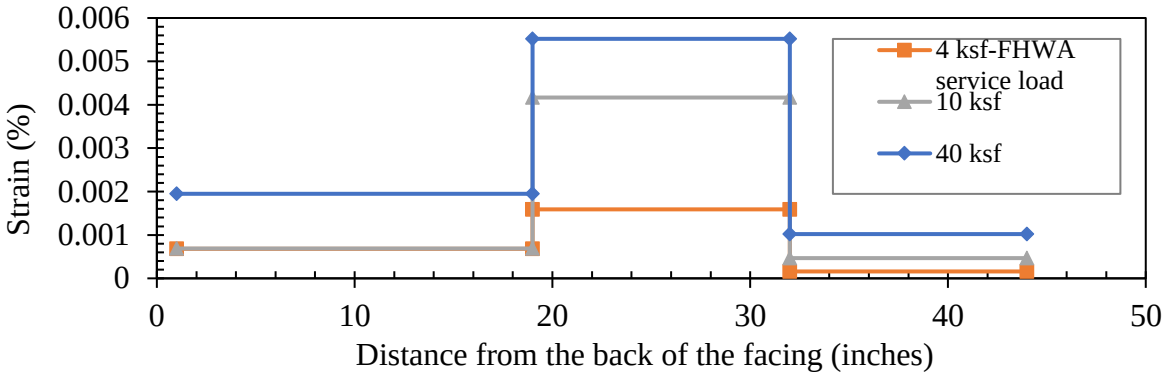

c)

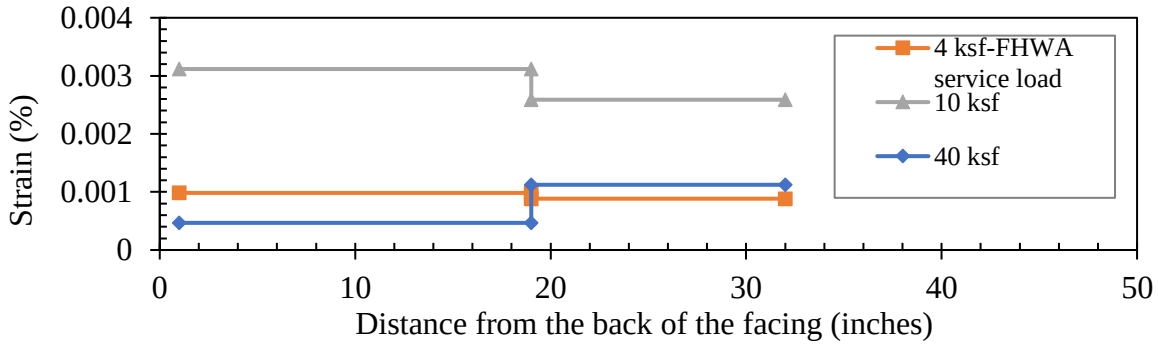

d)

Figure 108. Strain magnitude distributions between WP connection points at: a) 91-inch, b) 75-inch, c) 51-inch, and d) 27-inch above the foundation at: 4 ksf (FHWA service load), 10 ksf, and 40 ksf surcharge load levels (GRS Abutment Model #2)

Figures 108 a, b, c, and d show that the measured strain magnitudes were greater for higher surcharge load levels than lower ones. On the other hand, **Figure 108 d** shows higher strain values at 4 ksf and 10 ksf than 40 ksf kips. This might happen due to low level of accuracy at lower WP levels (i.e. 27-inch above the foundation slab), puncture by backfill material to one of the WP cables, or an unexpected cable movement during surcharge test loading.

Figure 109 shows lateral movements from WP readings of the top reinforcement layer (located at 87-inch above the foundation slab) during surcharge load testing of GRS Abutment Model #3. WP connection points on the reinforcement layers were numbered from the facing backwards (e.g. "87inches-1" is the closest connection point behind the facing). Results in **Figure 109** show that the largest amount of extension in this reinforcement layer was underneath the loading beam between WPs #2 & #3. Data shown in **Figure 109** and those obtained for the lower reinforcement layers (i.e. at elevations 27-inch, 51-inch and 75-inch above the foundation slab) were used to determine axial strain distributions in the reinforcement.

Strain magnitude distributions between WP connection points at 87-inch, 75-inch, 51-inch, and 27-inch above the foundation slab during surcharge load testing of GRS Abutment Model #3 were shown in **Figures 110 a, b, c, and d**, respectively. Maximum strain level was recorded at 87-inch above the foundation slab under 40 ksf surcharge load as 0.015 %.

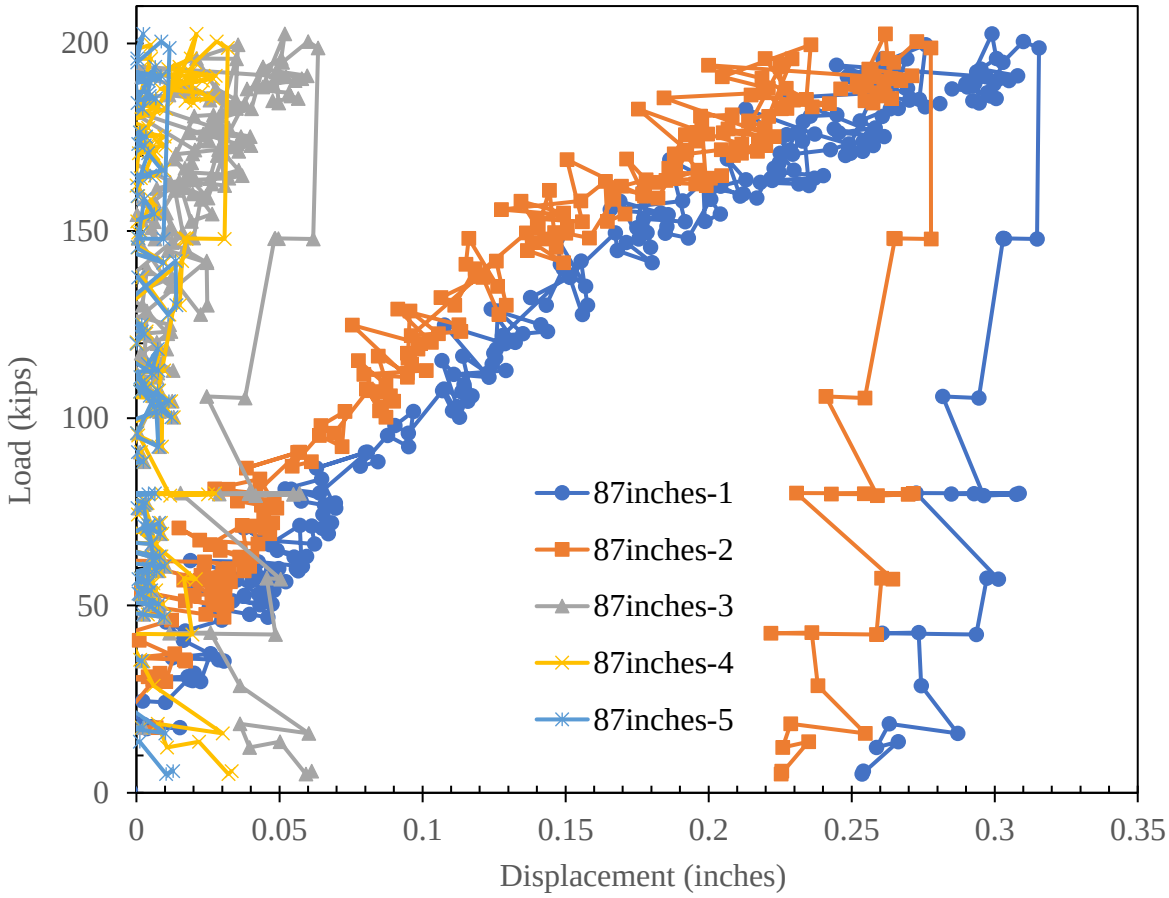

Figure 109. Wire potentiometer readings at the top reinforcement layer in GRS Abutment Model #3 (Elevation of 87-inch above the foundation slab) due to surcharge load. (Note: WPs were numbered sequentially from the facing toward the tail-end of the reinforcement layer.)

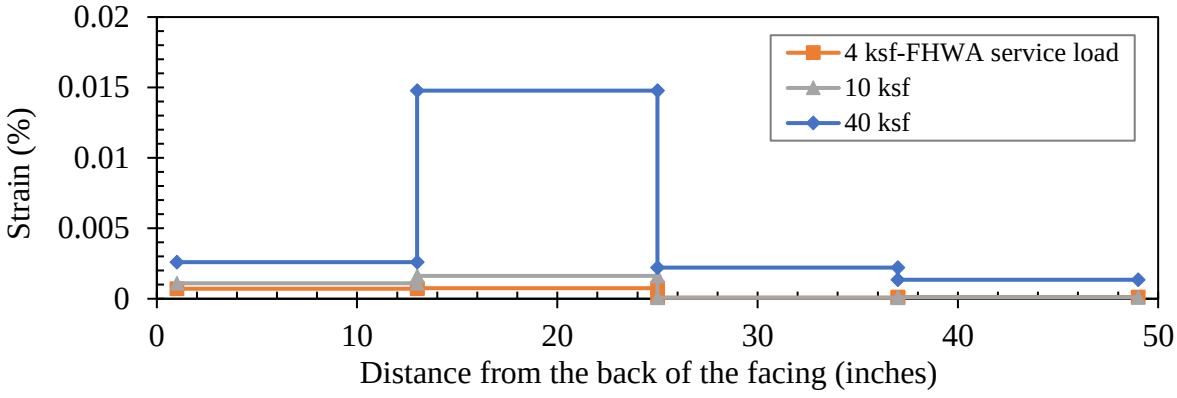

a)

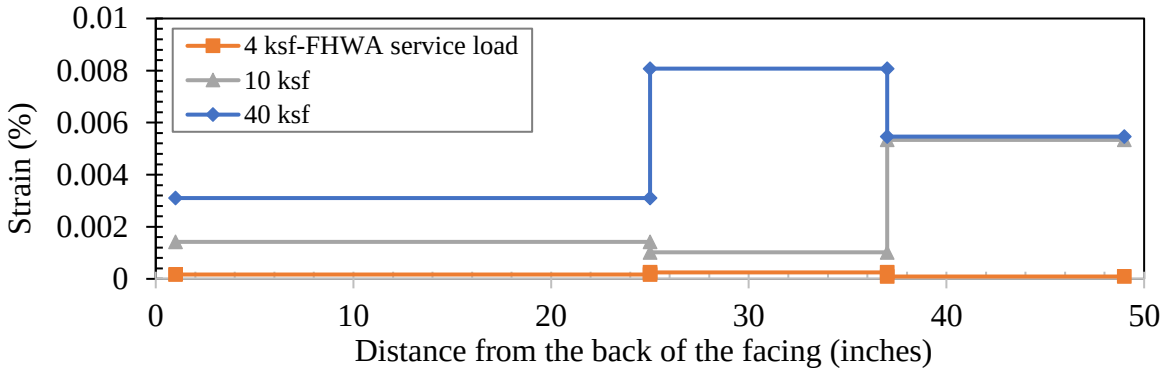

b)

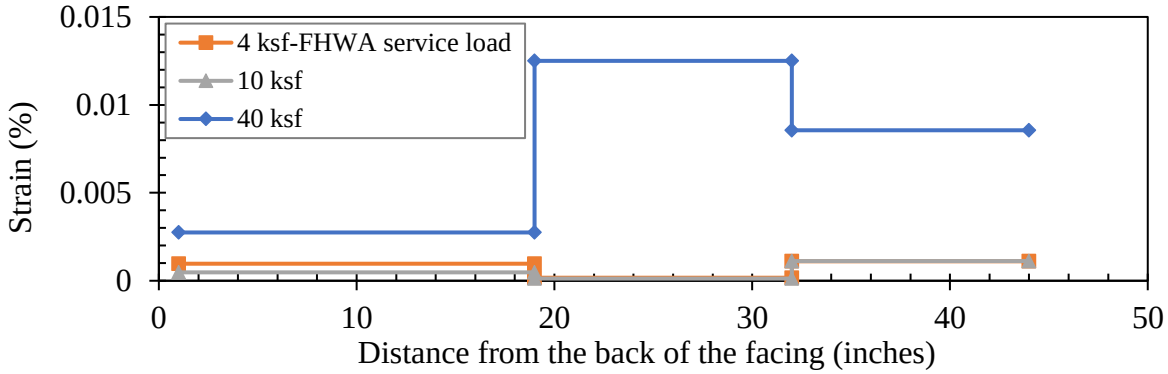

c)

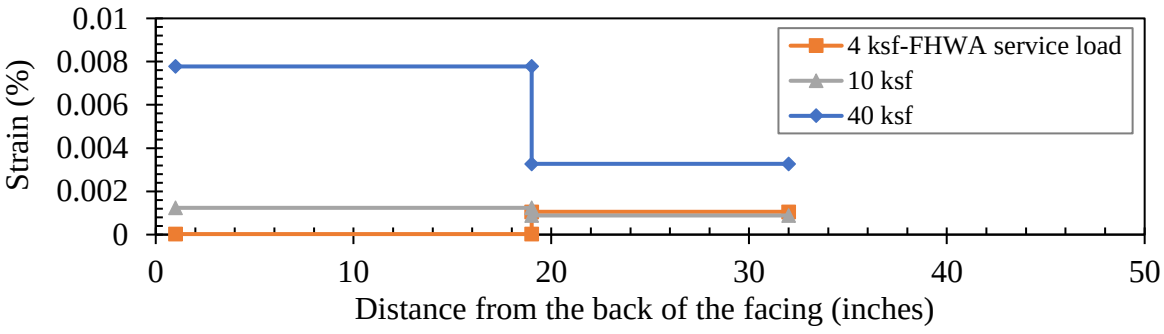

d)

Figure 110. Strain magnitude distributions between WP connection points at: a) 87-inch, b) 75-inch, c) 51-inch, and d) 27-inch above the foundation slab at: 4 ksf (FHWA service load), 10 ksf, and 40 ksf surcharge load levels (GRS Abutment Model #3)

Figures 110 a, b, c, and d show that the measured strain magnitudes were greater for higher surcharge load levels than lower ones. On the other hand, **Figure 109 c** shows a higher strain value at 4 ksf than 10 ksf. This might happen due to low level of accuracy at lower WP levels (i.e. 51-inch above the foundation slab), puncture by backfill material to one of the WP cables, or an unexpected cable movement during surcharge test loading.

Figure 111 shows measured data for WPs that were closest to, and farthest away from the facing, respectively (e.g. 86-1 and 86-5 in GRS-1). Results show similar deformation trends for individual WP contact points across different GRS abutment models examined. However, GRS Abutment Model #1 with CMU block facing show significantly larger reinforcement deformations from all WP contact points monitored in this study. Meanwhile, GRS Abutment Models #2 and #3 with large concrete facing blocks, but different reinforcement spacing, show comparable deformation readings, which are significantly smaller than those in GRS Abutment Model #1.

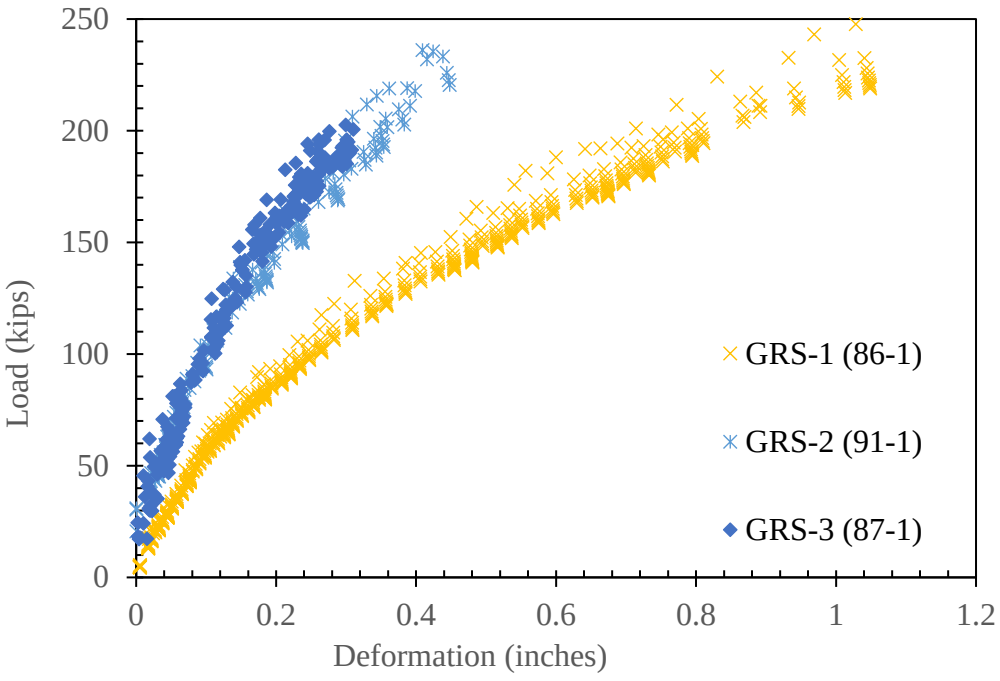

(a)

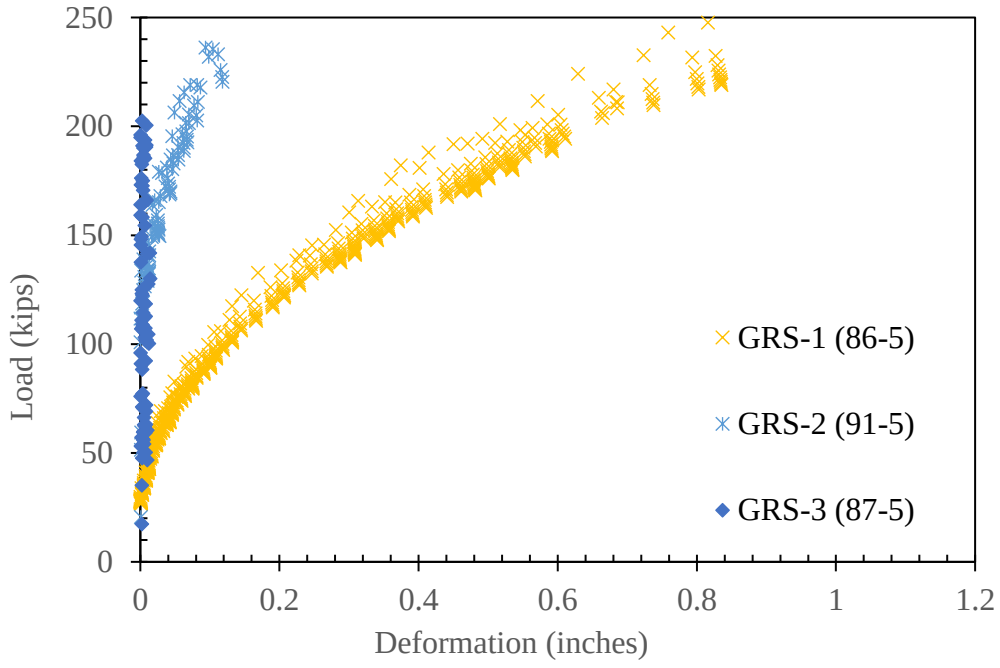

(b)

Figure 111. Load-deformation performances of the GRS abutment models within the backfill as measured using wire potentiometers (WPs) that were located: (a) closest to facing, and (b) farthest away from the facing. (Note: Numbers in parentheses indicate the elevations of the WPs above the foundation slab.)

Figures 112 through 117 show the locations of maximum calculated global strains from wire potentiometers (WP) in three abutment models at different surcharge load levels (i.e. 4 ksf, 10 ksf and 40 ksf). Maximum strain location between two WPs were assumed to be occurring at mid-point to simplify the visualization of overall strain measurement results. **Figures 113, 115 and 117** were prepared to show the mid-point of the maximum strain locations at each instrumented geotextile level and overall inclination based on different Earth Pressure Theories (i.e. Log-Spiral (Eq. 1), Rankine (Eq. 2 and Eq. 3), Coulomb (Eq. 4 and Eq. 5) Earth Pressure Theories as discussed in Section 2.1). For example, at 48-inch above the foundation slab in GRS Abutment Model #1, the maximum strain was measured between 19-inch and 31-inch away from the back of the facing. Thus, mid-point was taken as 25-inch.

Results show that the locations of maximum reinforcement strains in all three GRS abutment models that subjected to different surcharge load levels are more consistent with the overall inclination of Log-Spiral slip plane at the bottom and the location of the surcharge load at the top of each GRS abutment model. The surcharge beam was located close to the facing (i.e. 24-inch away from the back of the facing). Similar Log-Spiral mechanism was also observed in Xie *et al.* 2019's study when the footing is located closer to the facing as discussed in Section 2.1.

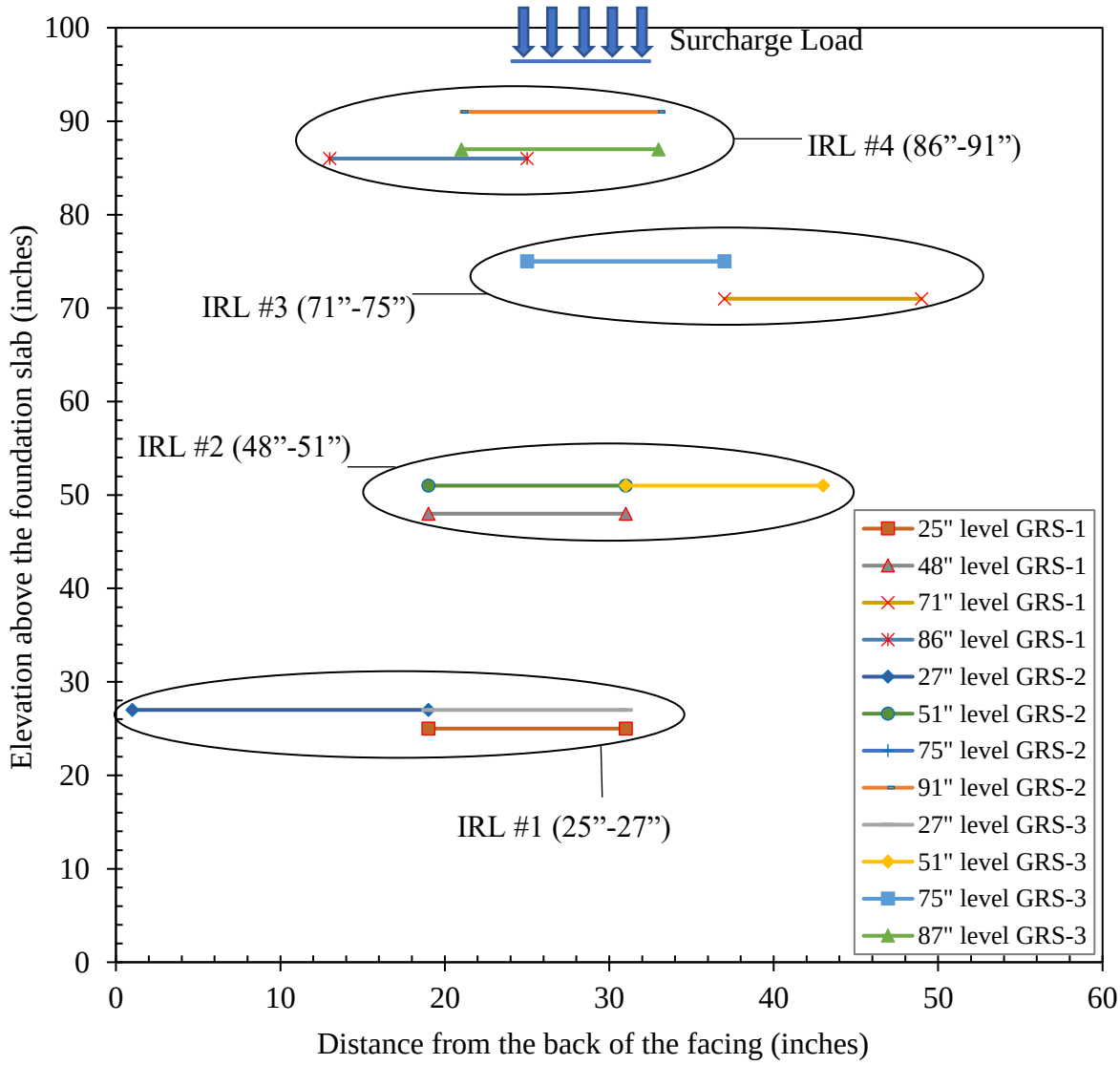

Figure 112. Locations of measured maximum reinforcement strains in GRS Abutment Models #1-#3 at 4 ksf surcharge load level. (Note: IRL is the Instrumented Reinforcement Layer; elevations in parentheses refer to IRL levels applicable in each GRS abutment model.)

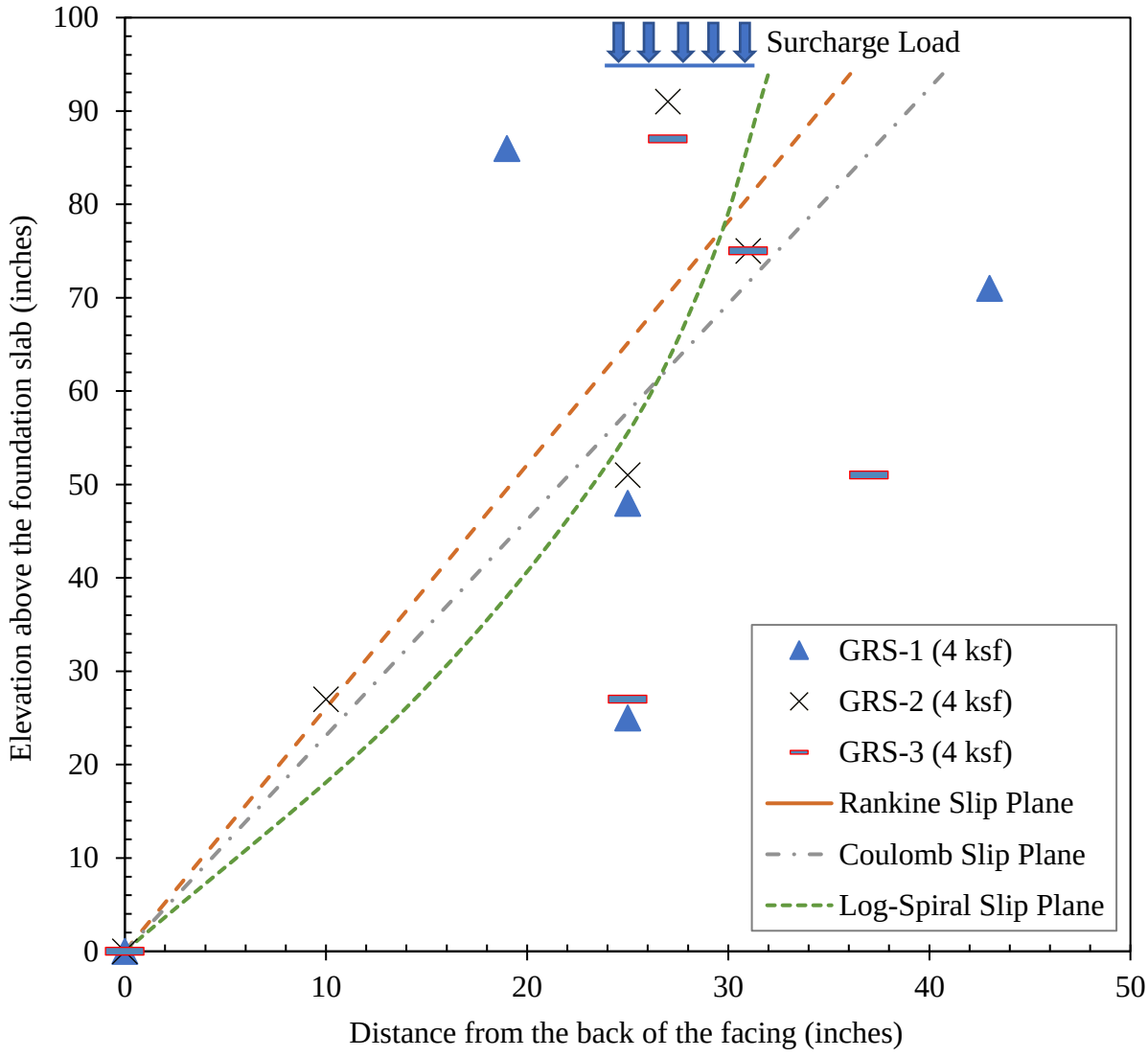

Figure 113. Mid-point locations of measured maximum reinforcement strains with estimated Rankine, Coulomb and Log-Spiral slip plane in GRS Abutment Models #1-#3 at 4 ksf surcharge load level

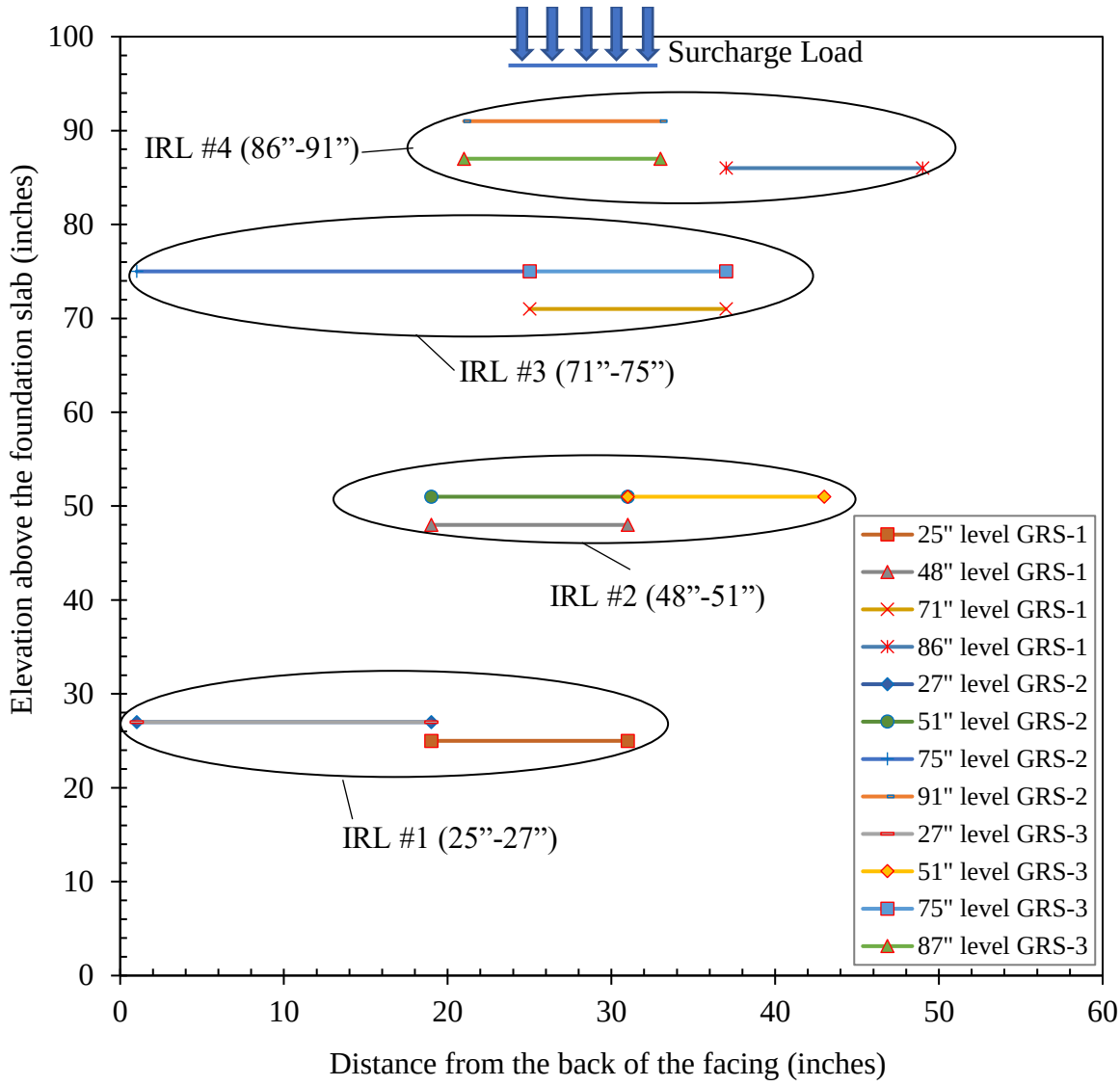

Figure 114. Locations of measured maximum reinforcement strains in GRS Abutment Models #1-#3 at 10 ksf surcharge load level. (Note: IRL is the Instrumented Reinforcement Layer; elevations in parentheses refer to IRL levels applicable in each GRS abutment model.)

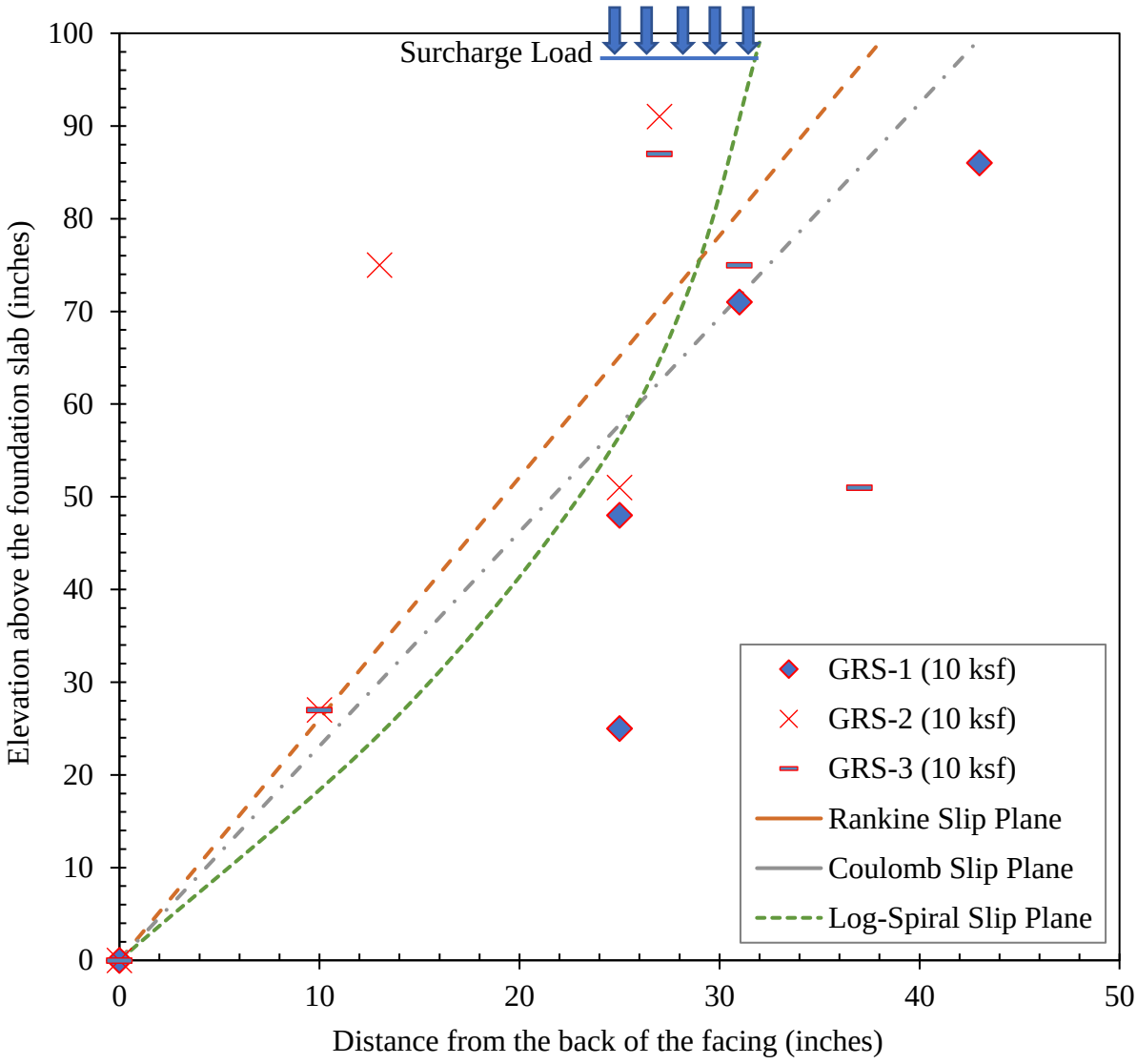

Figure 115. Mid-point locations of measured maximum reinforcement strains with estimated Rankine, Coulomb and Log-Spiral slip plane in GRS Abutment Models #1-#3 at 10 ksf surcharge load level

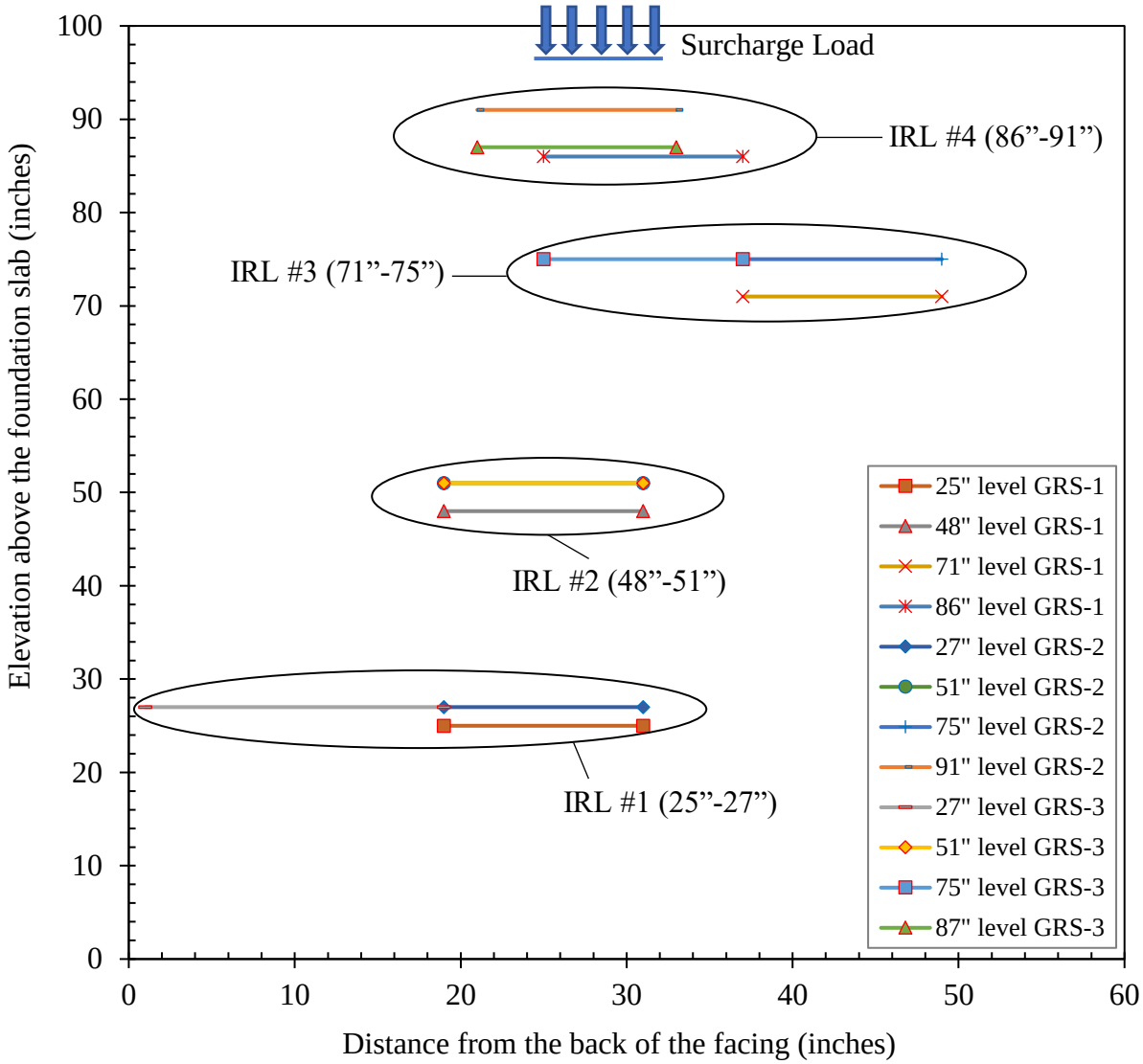

Figure 116. Locations of measured maximum reinforcement strains in GRS Abutment Models #1-#3 at 40 ksf surcharge load level. (Note: IRL is the Instrumented Reinforcement Layer; elevations in parentheses refer to IRL levels applicable in each GRS abutment model.)

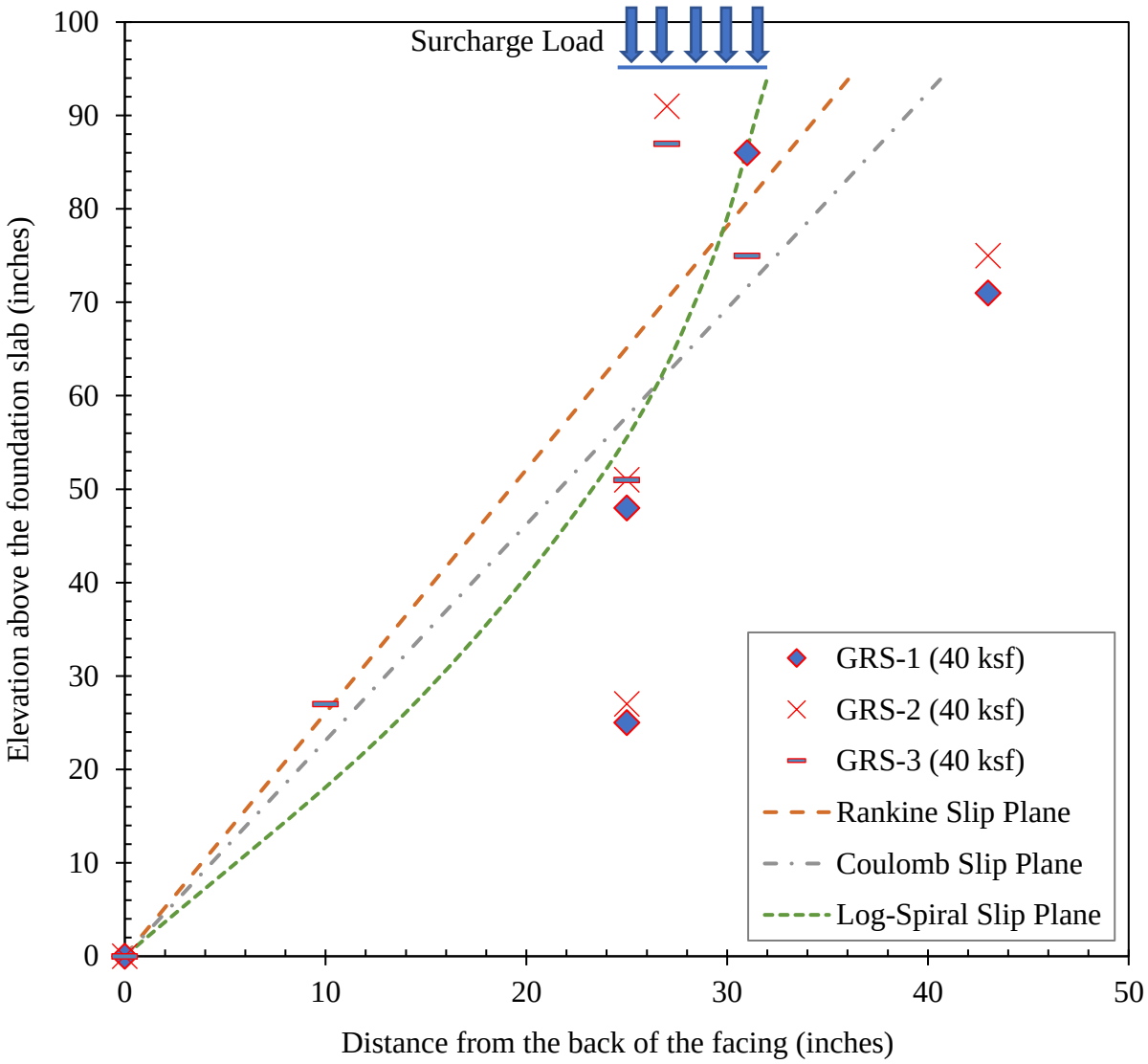

Figure 117. Mid-point locations of measured maximum reinforcement strains with estimated Rankine, Coulomb and Log-Spiral slip plane in GRS Abutment Models #1-#3 at 40 ksf surcharge load level

8.5. Vertical Pressures

Figure 118 shows the measured EPC-4 results (at mid-height of the GRS fill, **Figures 31, 48 and 56**) for all three GRS abutment models tested in this study. The data show that the pressure in the GRS fill increased linearly and steadily with the applied load in all GRS three bridge abutment

models until each test was aborted. The results for GRS Abutment Models #2 and #3 with large concrete blocks are in excellent agreement with each other, but they are nearly 25-30% less at higher surcharge loads than those for GRS Abutment Model #1 that was built with standard CMU blocks. A plausible reason could be the better compaction of the GRS fill that was possible in GRS Abutment Models #2 and #3 due to the presence of heavier facing blocks, resulting in a stiffer fill that was able to bridge over the EPC and transfer the simulated bridge load from above over a wider area within the GRS fill. This would result in lower magnitudes of pressure deeper inside the GRS fill including that measured by EPC-4 as shown in the figure.

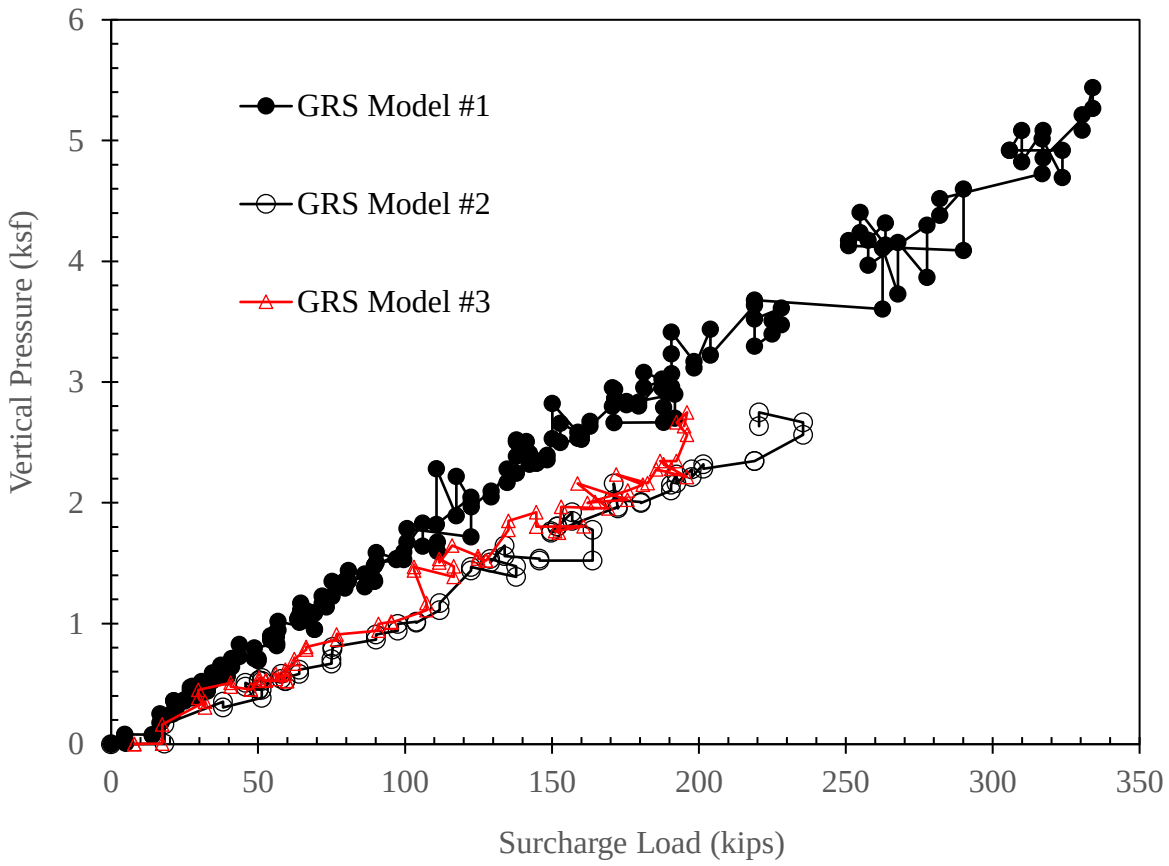

Figure 118. Measured vertical pressure by EPC at 47-inch above the foundation slab inside the fill material as a function of applied load for GRS Abutment Models #1-#3

The results in **Figure 118** are also similar to calculated surcharge distributions by Boussinesq's Method in NAVFAC 1986 (Eq. 6) in Section 2.1 of this study. EPC-4 placed in the mid-section should receive 1.2% of the surcharge load based on Boussinesq's Method. For example, EPC-4 readings at 100 kips for GRS Abutment Models #1-#3 are 1.5%, 1%, and 1%, respectively.

8.6. Summary of Surcharge Load Testing Results

Table 9 provides a summary data on full-scale GRS abutment models tested in this study to show the direct effect of facing type on the performance of the structure. The maximum applied load was different for all three GRS abutment models due to safety reasons. First method of calculating the factor of safety is to take the highest load at the end of the surcharge load testing. Second method is to use the surcharge load value at recommended vertical settlement limit (i.e. 0.5% of abutment height), and this method is more objective to show the advantages of using different facing options in GRS bridge abutments.

For example, GRS Abutment Models #1-#3's factor of safety based on vertical settlement limit was calculated as 2.0, 3.5 and 2.9, respectively. Similar comparison method can be applied to maximum lateral facing deformation values each GRS abutment models. Another comparison example, GRS Abutment Models #1-#3's lateral facing deformation at 200 kips were recorded as 0.65-inch, 0.34-inch and 0.33-inch, respectively. Results show that all GRS abutment models by far exceeded the FHWA stiffness requirement of maximum normalized facing deformation of 1% (relative to the bridge abutment height) for a 4 ksf surcharge load (equivalent to 20 kips in this study).

The constrained deformation modulus is an important parameter for the assessment of settlement of the backfill material. GRS Abutment Models #1-#3's constrained deformation modulus was

calculated as 1,127 ksf, 2,032 ksf, and 1,818 ksf, respectively. This outcome also has similar trend as the factor of safety calculated based on vertical settlement limit set by FHWA guidelines as shown in **Table 9**.

The cumulative construction time for GRS Abutment Model #3 was approximately 55% shorter than that for GRS Abutment Model #1 as discussed in Section 7.2. It has also better structural performance than GRS Abutment Model #1 as summarized in **Table 9**.

Table 9. Summary data on full-scale GRS abutment models tested in this study

GRS Abutment Model No.	Facing Type[1]	Lift Thickness/ Reinforcement spacing (in.)	Max. load applied (kips)	Max. vertical stress on the GRS fill (ksf)	FoS[2]	FoS based on Vertical Settlement limit[3]	Max. settlement at the top of GRS fill (in.)	Constrained deformation modulus[4], M (ksf)	Max. lateral facing deformation (in.)	Max. lateral facing deformation at 200 kips (in.)	Total construction effort (person-hours)	Net construction effort (person-hours)[5]
1	CMU	8	353	70.6	17.7	2.0	6.2	1,127	0.79	0.65	123.5	74.5
2	LB	8	236	47.2	11.8	3.5	2.3	2,032	0.47	0.34	102.5	53.5
3	LB	12	202	40.4	10.1	2.9	2.2	1,818	0.33	0.33	82.5	33.5

Notes:

[1]CMU: Concrete Masonry Units; LB: Large Blocks (Solid Concrete)

[2] Nominal value relative to design service load of 4 ksf without considering FHWA vertical settlement recommended value of 0.5% of abutment height (Adams et al. 2012a, b, 2018)

[3] Nominal value relative to design service load of 4 ksf with considering FHWA vertical settlement recommended value of 0.5% of abutment height (Adams et al. 2012a, b, 2018)

[4] Vertical stress / (Settlement ÷ Abutment height); calculated at maximum load as a lower bound value

[5] Less the amount of time (effort) spent on model instrumentation (i.e. construction only)

8.7. Results from Deconstruction

Figures 119 through 121 show settlements inside the GRS bridge abutment fill of GRS Abutment Model #1 due to surcharge load testing at selected reinforcement locations as sample results. The measurements were taken using manual survey during deconstruction of GRS abutment models as described in Chapter 5. Results shown correspond to elevations 94-inch, 90-inch and 86-inch level above the foundation slab. The 94-inch level is the top of the GRS abutment model, the 90-inch level corresponds to one of the shorter reinforcement layers of the shallow footing underneath the loading beam, and the 86-inch level represents a primary (i.e. full-length) reinforcement layer. Results in these figures show that maximum depressions and settlements consistently occurred underneath the loading beam (representing bridge abutment load) with larger values occurring closer to the GRS surface.

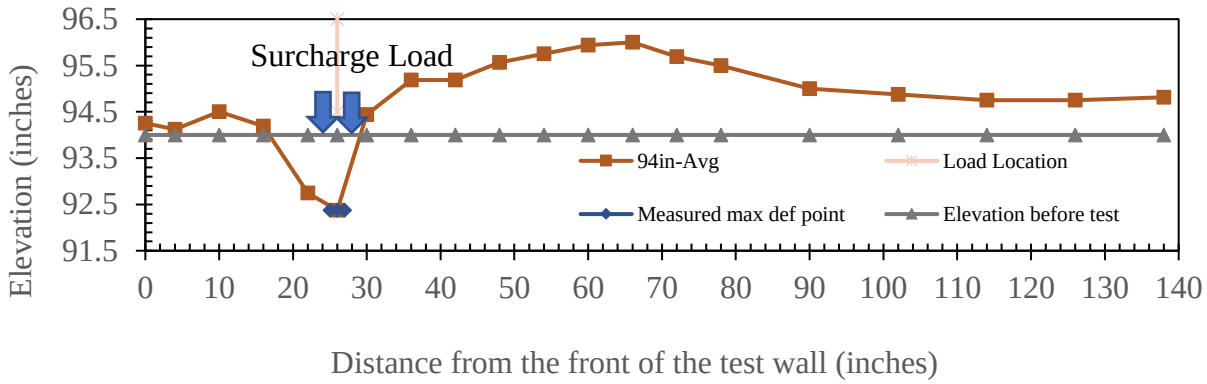

Figure 119. GRS Abutment Model #1 – Settlement profile after the surcharge load testing at maximum load of 353 kips at 94-inch level

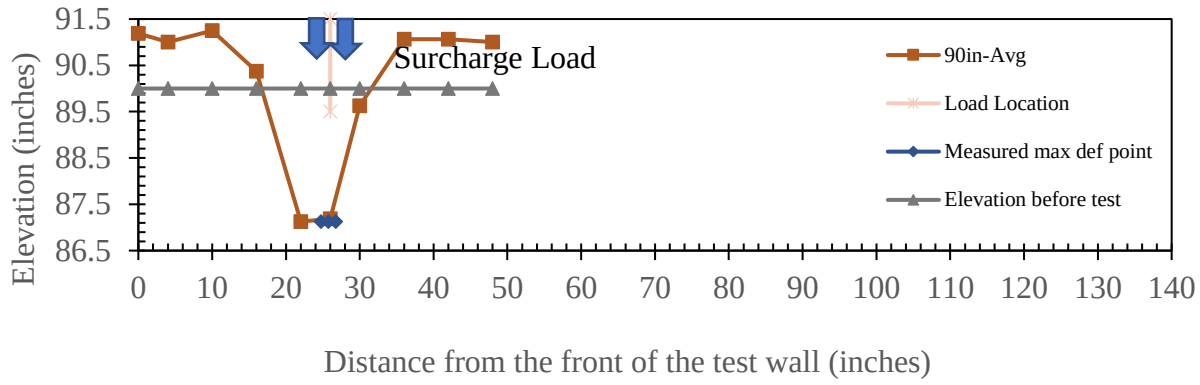

Figure 120. GRS Abutment Model #1 - Settlement profile after the surcharge load testing at maximum load of 353 kips at 90-inch level

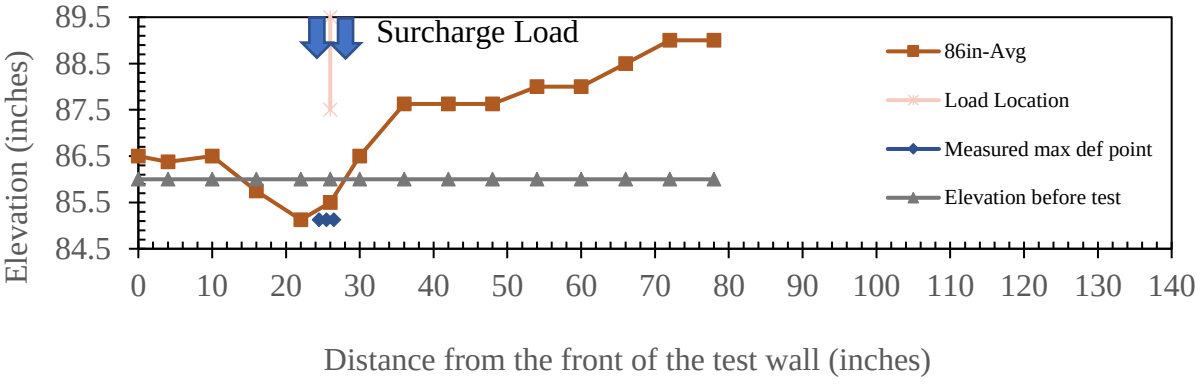

Figure 121. GRS Abutment Model #1 - Settlement profile after the surcharge load testing at maximum load of 353 kips at 86-inch level

Figures 122 through 124 show a complete set of survey data for all reinforcement levels in GRS Abutment Models #1-#3, respectively. Results shown are mean values of manual measurements that were taken against the East and West side walls of the test box at each reinforcement layer. The theoretical Rankine slip plane, Coulomb slip plane and Log-Spiral slip plane (i.e. Log-Spiral (Eq. 1), Rankine (Eq. 2 and Eq. 3), Coulomb (Eq. 4 and Eq. 5) Earth Pressure Theories as discussed in Section 2.1) for the granular fill are also shown in the figures. Survey data in **Figure 122 through 124** show that the locations of maximum deformations at reinforcement layers in all three GRS abutment models that subjected to different surcharge load levels are more consistent with

the overall inclination of Log-Spiral slip plane at the bottom and the location of the surcharge load at the top of each GRS abutment model.

Results in **Figures 122 through 124** also indicate that GRS settlements at locations outside the pressure bulb of the loading beam are negligible. For instance, settlements taper off beyond 31-inch below the top of the GRS fill (i.e. deeper than elevation 63-inch above the foundation slab). Apart from significant factors of safety obtained for all three GRS abutment models examined as given in **Table 9** (Section 8.6), the corresponding negligible amounts of GRS deformation observed in these tests serve as another indication that GRS bridge abutments can provide reliable supporting structures for roadway bridges without exhibiting noticeable settlements at intended service loads.

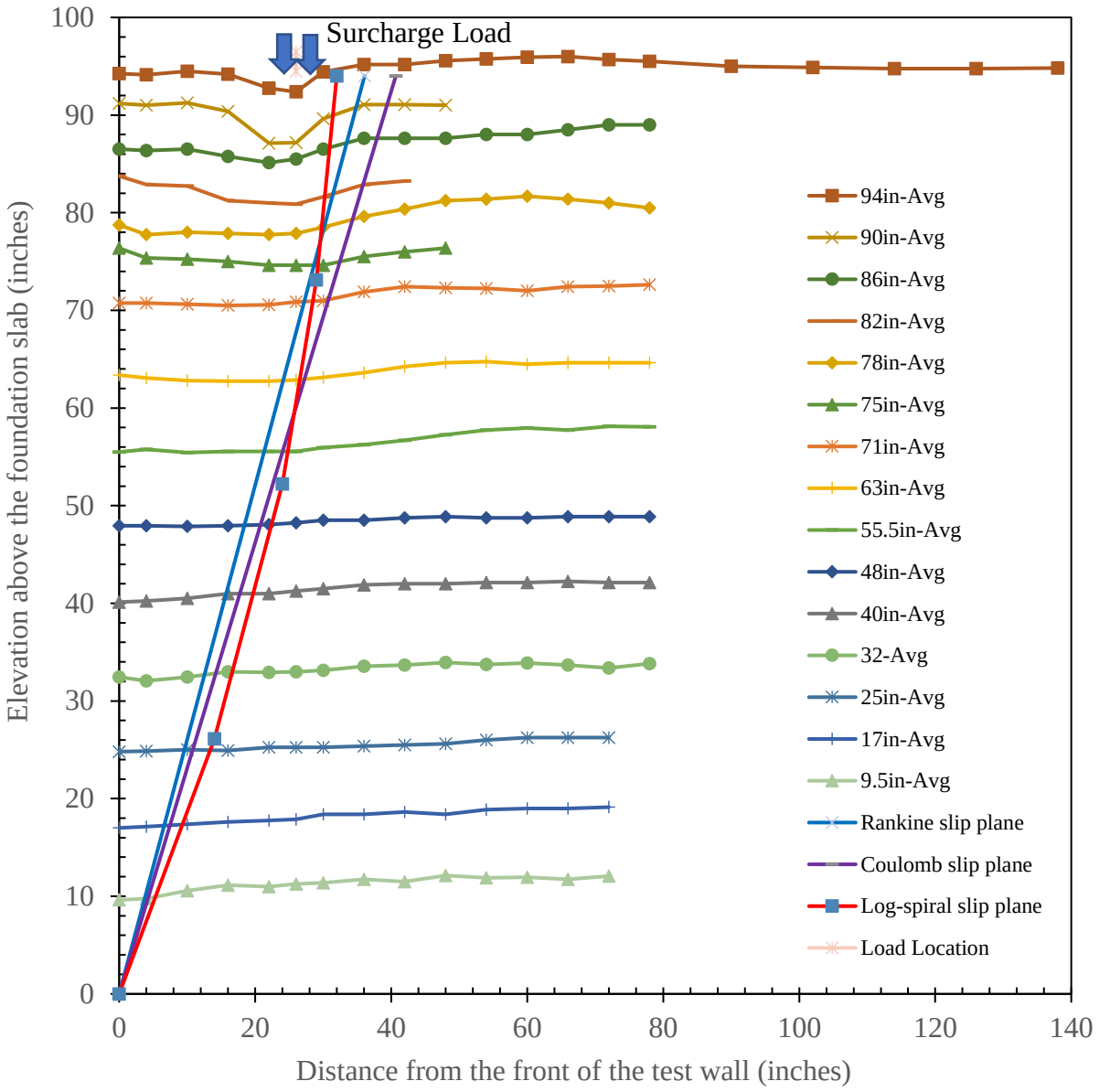

Figure 122. GRS Abutment Model #1 - Top of the gravel and geotextile average elevations after the surcharge load testing at maximum load of 353 kips

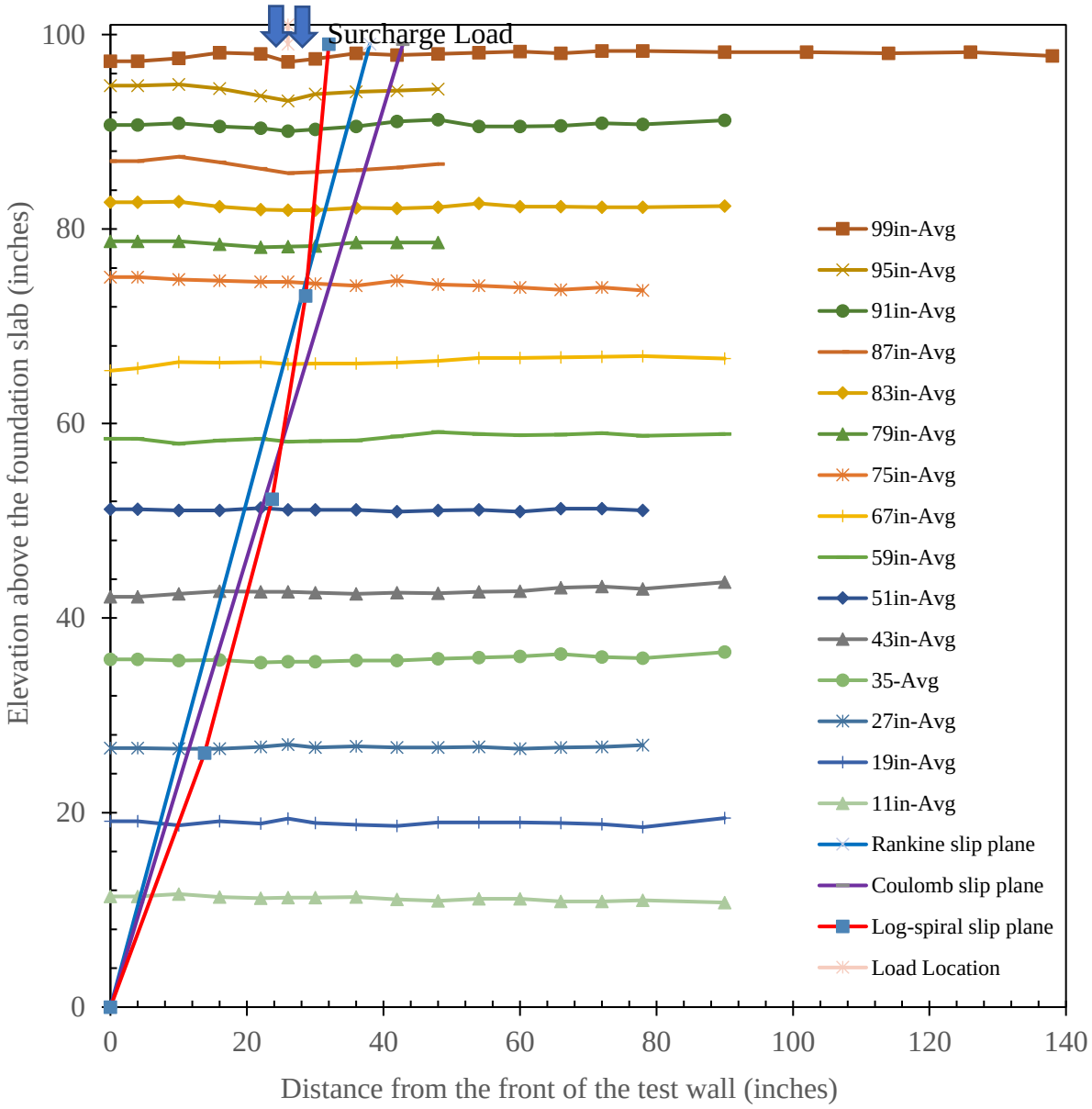

Figure 123. GRS Abutment Model #2 - Top of the gravel and geotextile average elevations after the surcharge load testing at maximum load of 236 kips

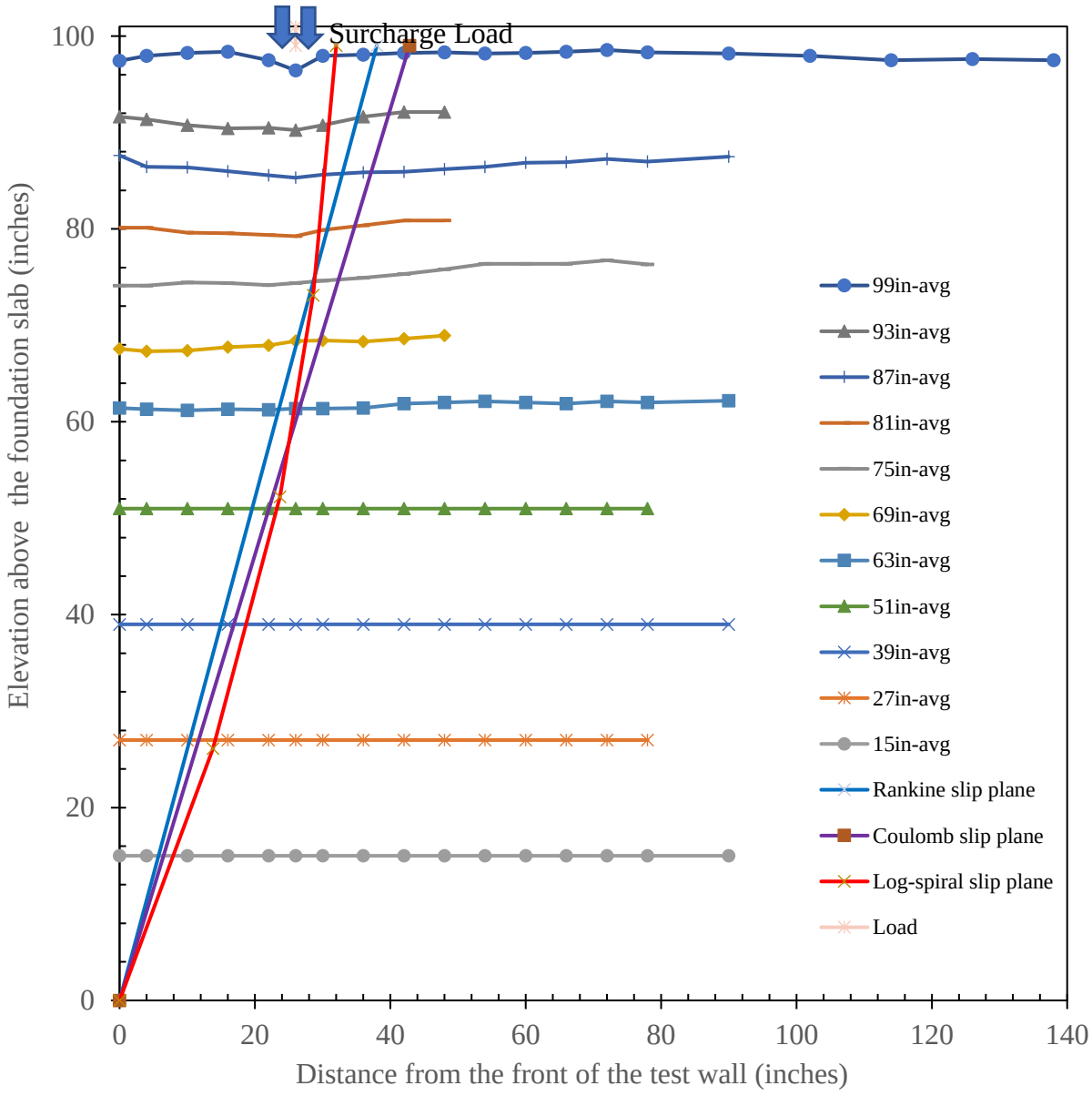

Figure 124. GRS Abutment Model #3 - Top of the gravel and geotextile average elevations after the surcharge load testing at maximum load of 200 kips

Figure 125 shows the amount of measured deformation at all geotextile reinforcement layers inside the fill of GRS Abutment Models #1-#3 after the surcharge load testing. The elevation readings were taken above the foundation slab. The measurements were taken using manual survey

and compared with before and after elevations. There is no significant settlement observed after 48-inch, 59-inch, and 51-inch for GRS Abutment Models #1-#3, respectively.

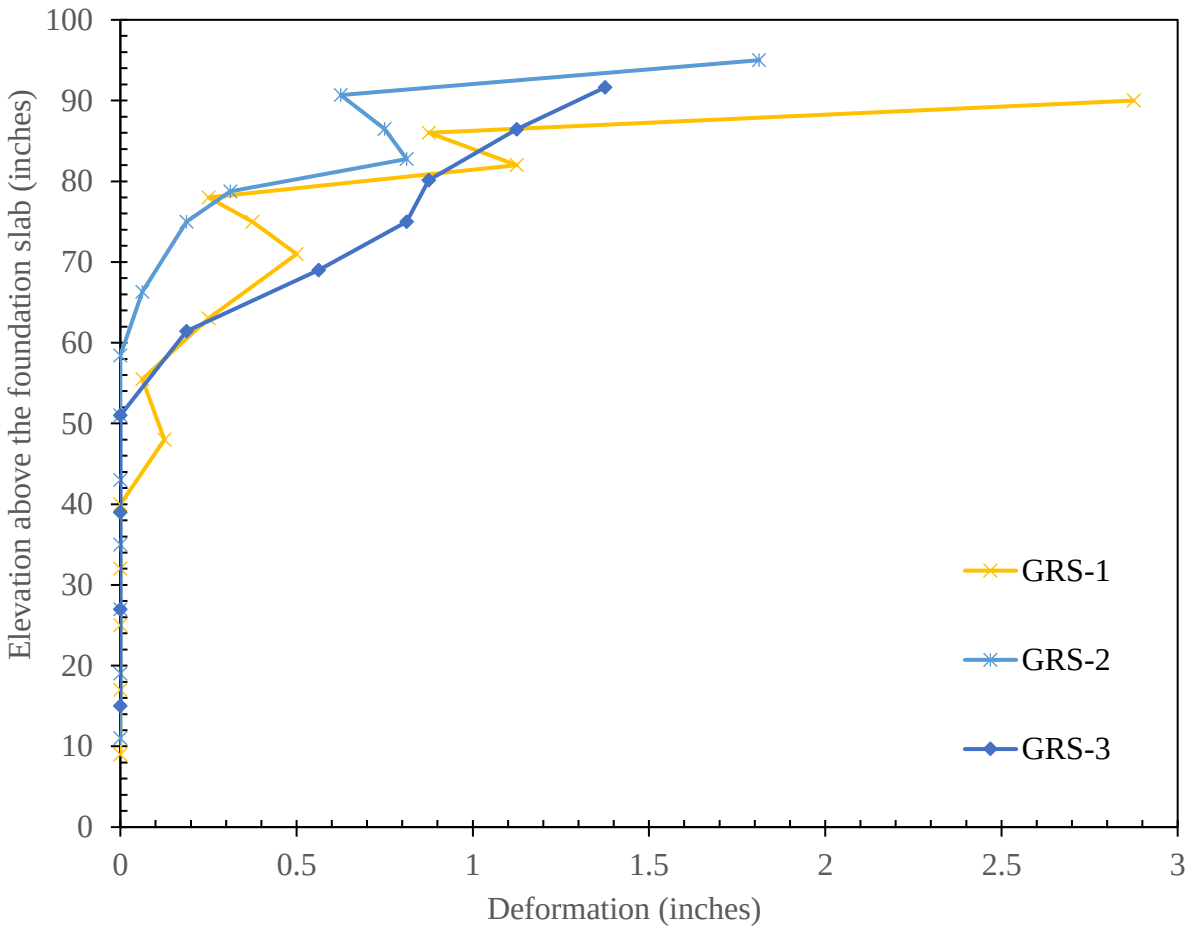

Figure 125. GRS Abutment Models #1-#3 – Geotextile deformation readings by manual survey after surcharge load testing

Chapter 9. Numerical Modeling Results

9.1. Load-Settlement Performance

The material properties that were used in the Numerical Modeling were reported in **Table 3** in Chapter 6. The comparison of load-settlement performance at the top of GRS Abutment Models #1-#3 were done by using FLAC v.7.0 analysis and full-scale surcharge load testing results at 4 ksf (FHWA-Service load), 10 ksf, and 40 ksf. The comparison of these results for GRS Abutment Models #1-#3 can be seen in **Figures 126 through 128**, respectively.

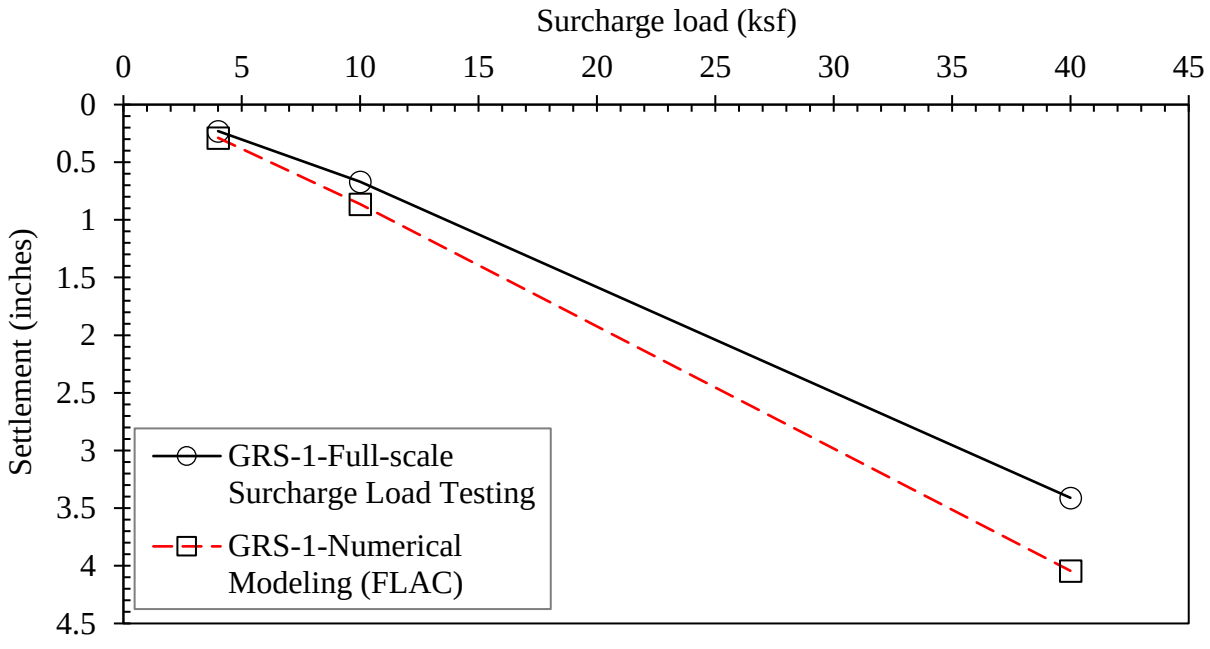

Figure 126. GRS Abutment Model #1- Load-Settlement comparison between full-scale surcharge load testing and Numerical Modeling (FLAC)

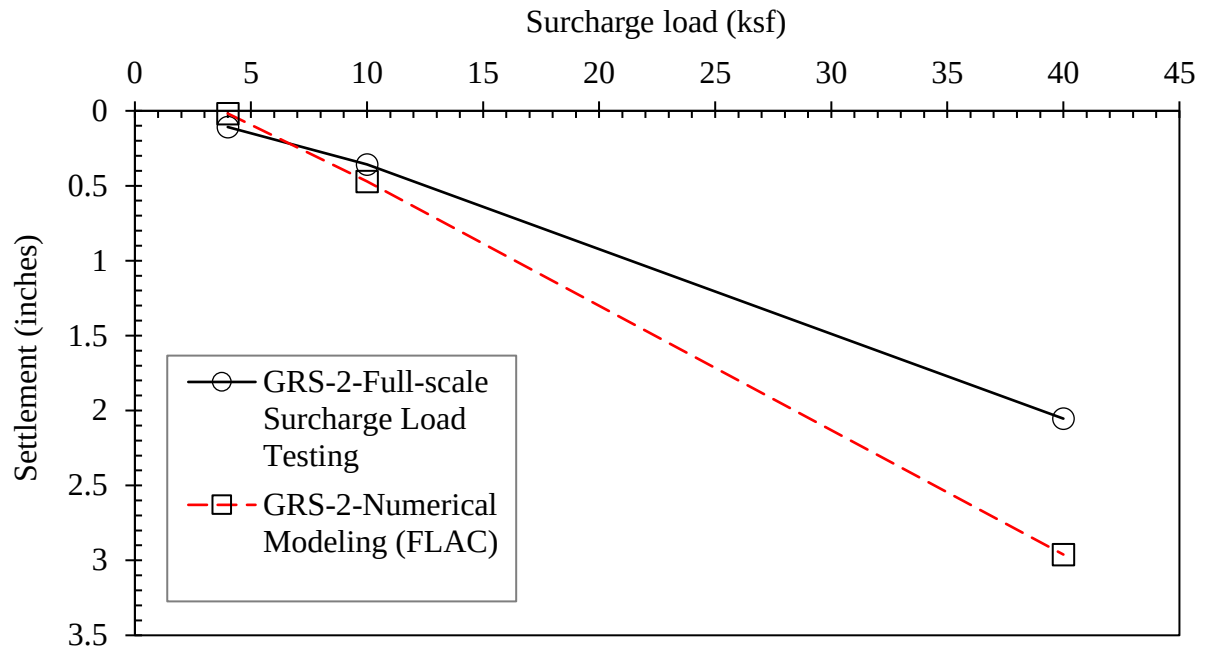

Figure 127. GRS Abutment Model #2- Load-Settlement comparison between full-scale surcharge load testing and Numerical Modeling (FLAC)

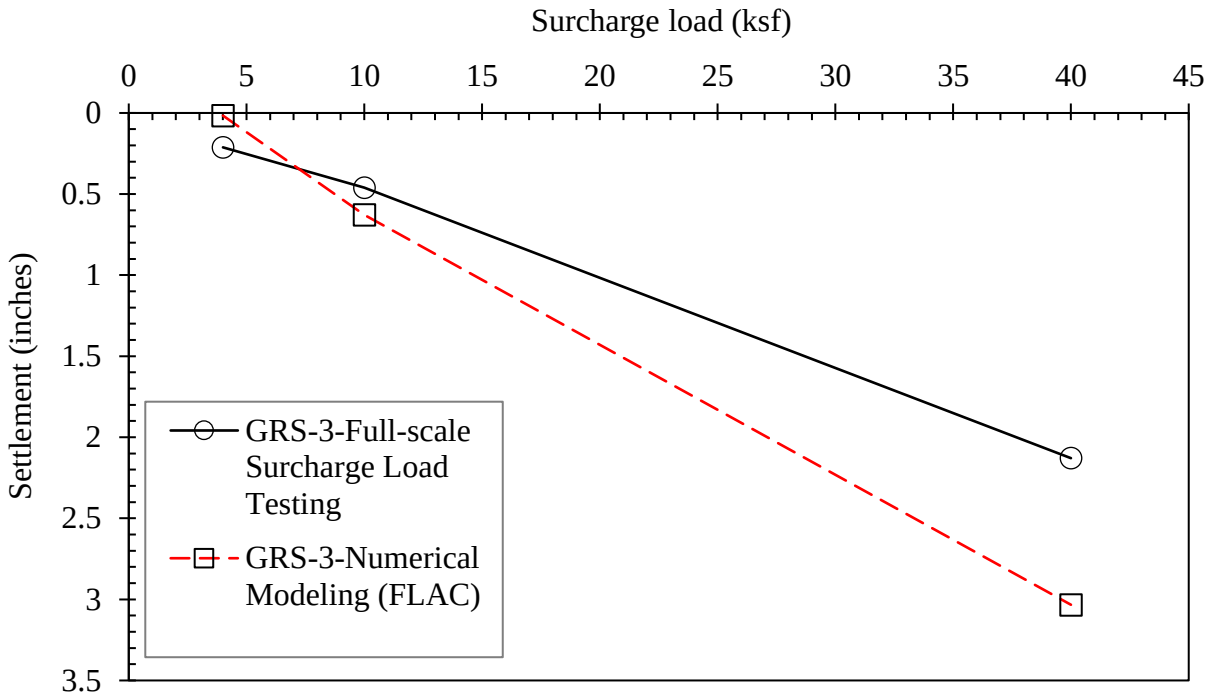

Figure 128. GRS Abutment Model #3- Load-Settlement comparison between full-scale surcharge load testing and Numerical Modeling (FLAC)

Similar results were observed between the FLAC v.7.0 analysis and full-scale surcharge load testing load-settlement performance. However, the difference between Numerical Modeling and full-scale surcharge load testing results gets larger at high surcharge load levels (i.e. 40 ksf). This may be due to the effect of side wall friction at full-scale surcharge load testing. Numerical Modeling does not take this side wall friction into account during the analysis. As it can be observed from the results in **Figures 126 through 128** the magnitude of all results is very small for both FLAC v.7.0 analysis and full-scale surcharge load testing (i.e. vertical settlement at 4 ksf: 0.28-inch and 0.23-inch for GRS Abutment Model #1, respectively)

The positive effect of large concrete block facing unit can easily been observed on structure's load-settlement performance by comparing the settlement values at the same surcharge load levels in Numerical Modeling (i.e. the settlement at 10 ksf of GRS Abutment Models #1 and #2 are 0.86-inch and 0.47-inch, respectively). Same observation can also be found at the full-scale load testing results (i.e. the settlement at 10 ksf of GRS Abutment Models #1 and #2 are 0.67-inch and 0.36-inch, respectively). Based in these examples, the reduction in the settlement is approximately 45% and 43% for Numerical Modeling and full-scale surcharge load testing, respectively. The results of GRS Abutment Model #3 with 12-inch reinforcement spacing show that the load-settlement performance is better than GRS Abutment Model #1, but worse than GRS Abutment Model #2.

9.2. Facing Deformations

Facing deformations at 4 ksf, 10 ksf, and 40 ksf surcharge load levels were analyzed with using top facing block lateral displacement data predicted by FLAC v.7.0 software. The comparison of facing deformations of GRS Abutment Models #1-#3 were done by using FLAC v.7.0 analysis and full-scale surcharge load testing results at 4 ksf (FHWA-Service load), 10 ksf, and 40 ksf.

Comparisons of these results for GRS Abutment Models #1-#3 are provided in **Figures 129 through 131**, respectively.

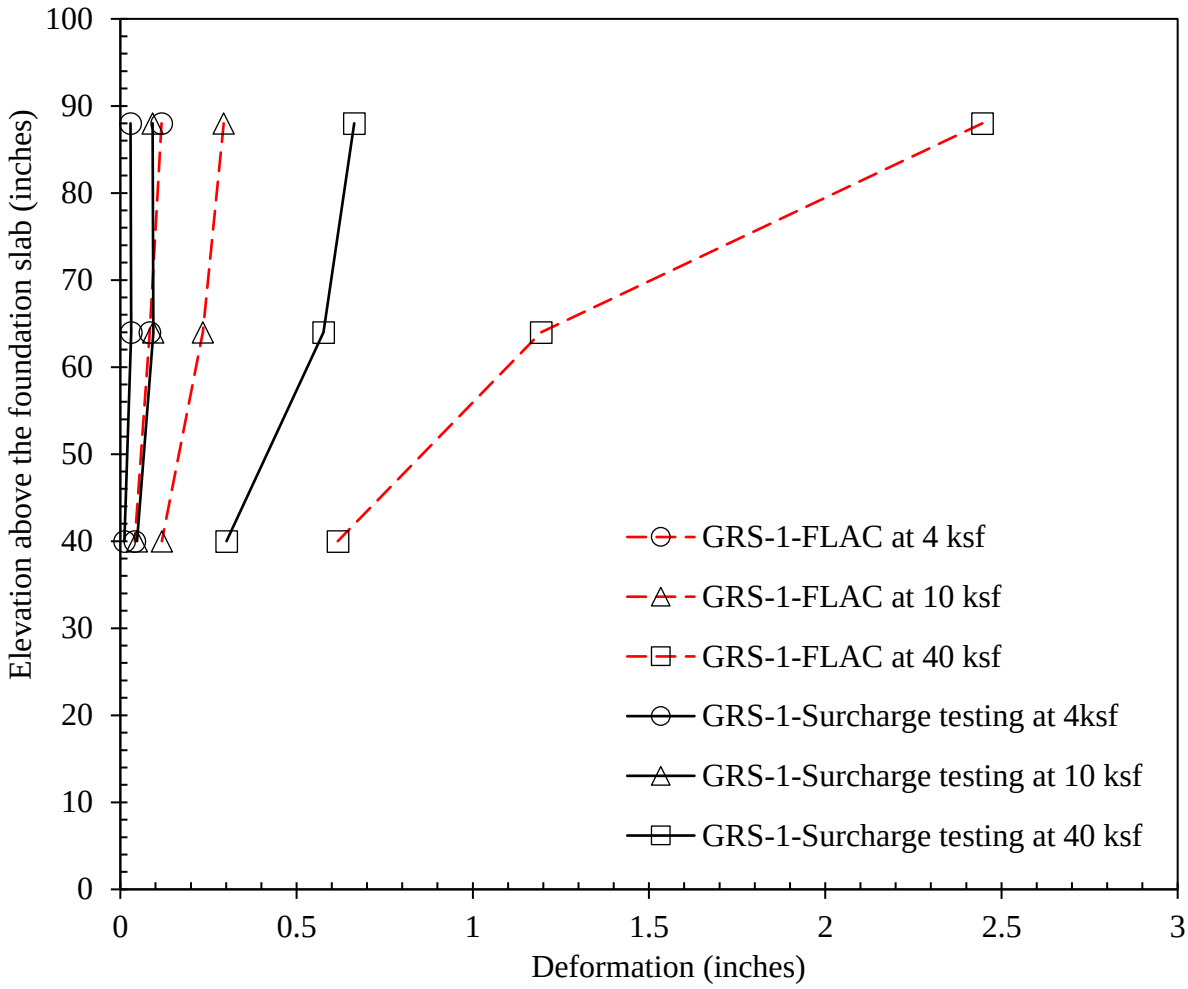

Figure 129. GRS Abutment Model #1- Facing deformation comparison between full-scale surcharge load testing and Numerical Modeling (FLAC)

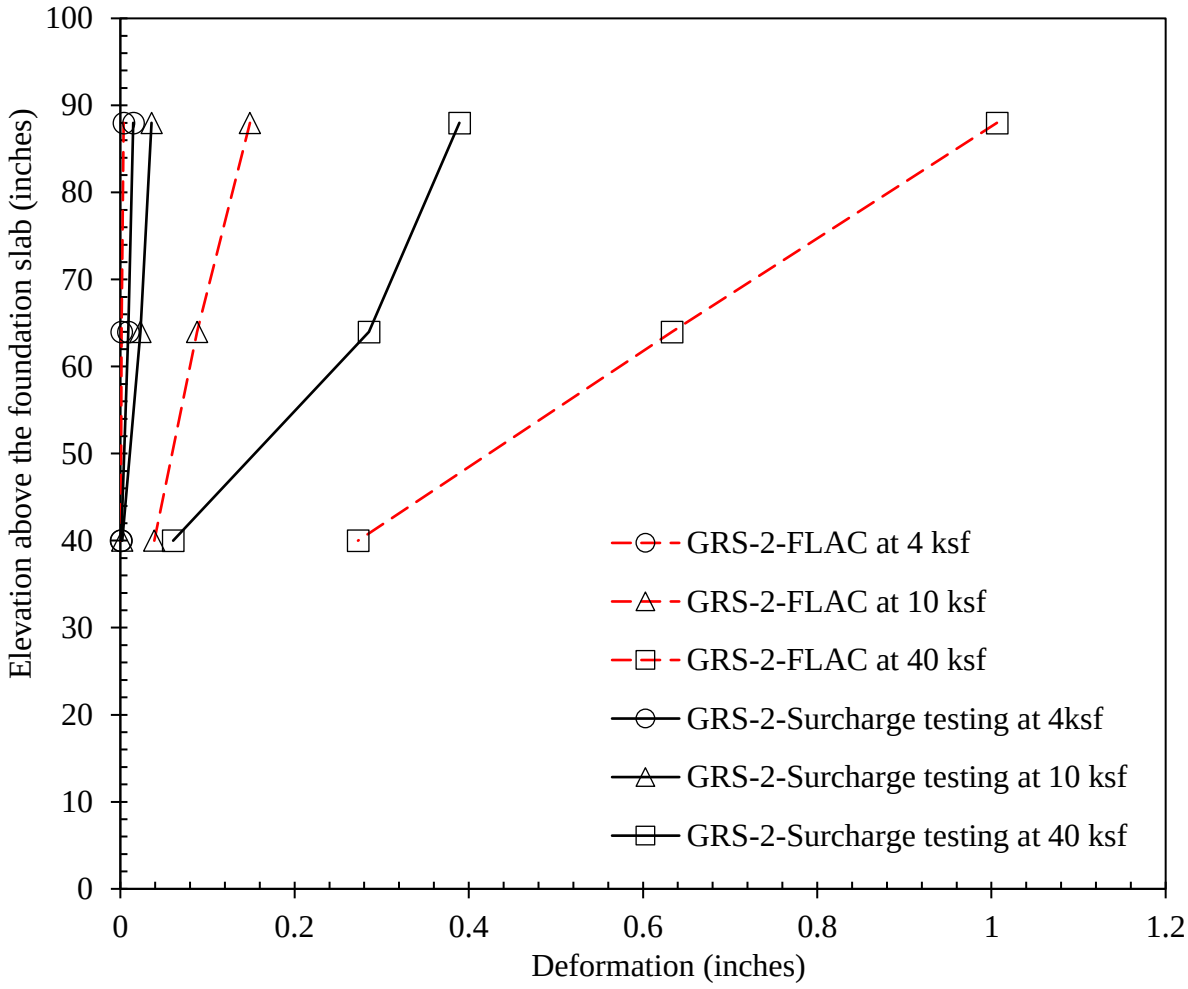

Figure 130. GRS Abutment Model #2- Facing deformation comparison between full-scale surcharge load testing and Numerical Modeling (FLAC)

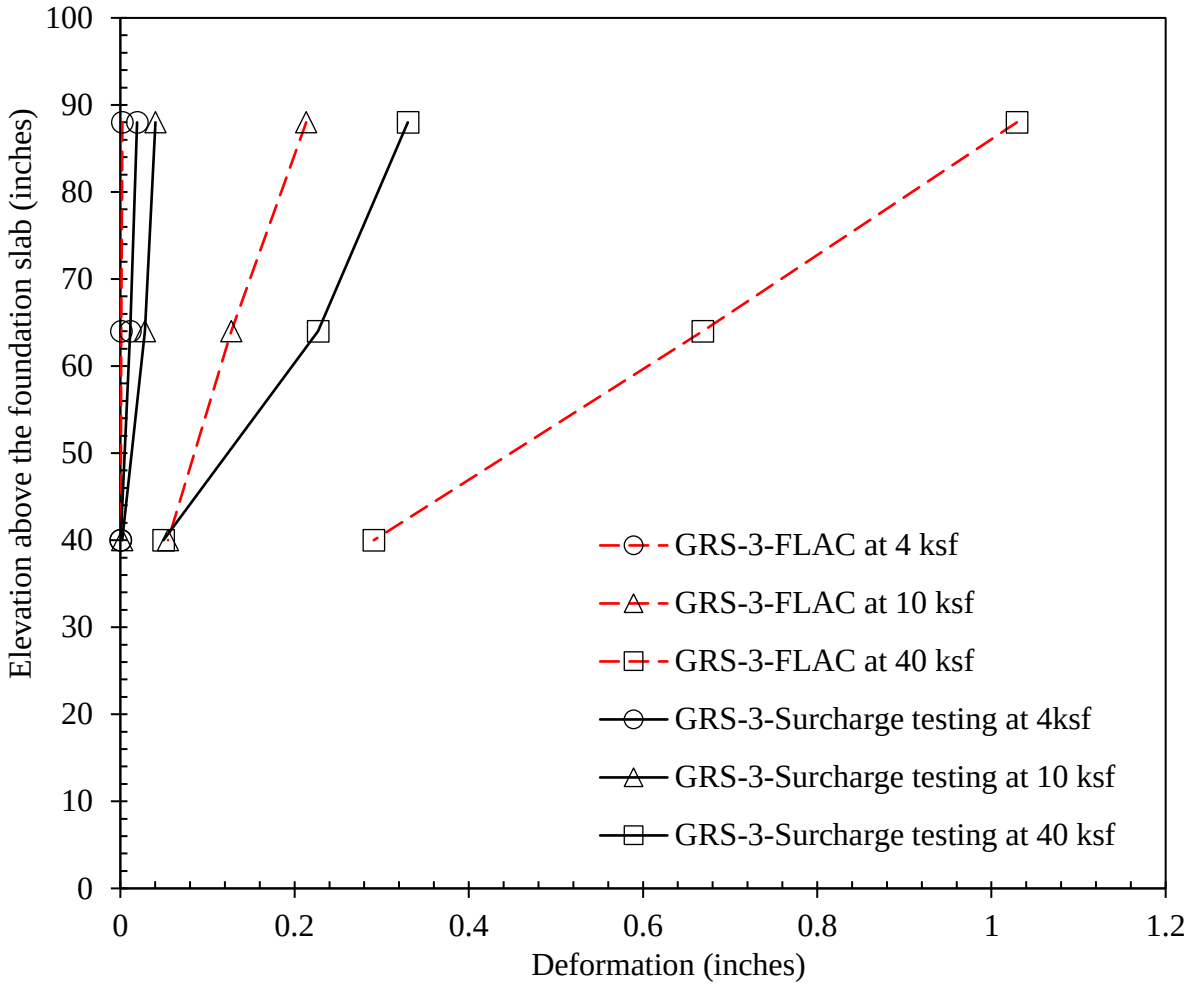

Figure 131. GRS Abutment Model #3- Facing deformation comparison between full-scale surcharge load testing and Numerical Modeling (FLAC)

The difference between Numerical Modeling predicted values and full-scale surcharge load testing results gets larger at high surcharge load levels (i.e. 40 ksf). This may be due to the effect of side wall friction at full-scale surcharge load testing. There is also friction between side by side facing blocks. Numerical Modeling does not take into account of these two types of acting friction during the analysis.

The facing deformation service limit that is recommended by FHWA is 1% of the height if the GRS abutment (i.e. approximately 1-inch for GRS models in this study). As it can be observed from the results in **Figures 129 through 131**, the magnitude of all results is still less than the recommended facing deformation service limit for both FLAC v.7.0 analysis and full-scale surcharge load testing, except for loads more than 20 ksf at GRS Abutment Model #1 only.

The positive effect of large concrete block facing unit can easily been observed on structure's facing deformation performance by comparing the predicted deformation values at the same surcharge load levels in Numerical Modeling (i.e. the facing deformation at 10 ksf of GRS Abutment Models #1 and #2 are 0.29-inch and 0.15-inch, respectively). Same observation can also be found at the full-scale load testing results (i.e. the facing deformation at 10 ksf of GRS Abutment Models #1 and #2 are 0.09-inch and 0.04-inch, respectively). The results of GRS Abutment Model #3 with 12-inch reinforcement spacing show that the facing deformation performance is better than GRS Abutment Model #1, but worse than GRS Abutment Model #2.

9.3. Reinforcement Strains

Maximum reinforcement strains at the instrumented levels shown in Chapter 4, and at 4 ksf, 10 ksf, and 40 ksf surcharge load levels were used to determine the corresponding peak tensile strength values, T_{max}, mobilized in each layer. This was done for both the numerical modeling and experimental test results using the mechanical response of the reinforcement shown in **Figure 70** (Chapter 6). Results shown in **Figures 132 through 134** indicate that the magnitude of T_{max} values are very small (i.e. all values are lower than 6 lbs/ft for all GRS models). The accuracy of the Numerical of Modeling is much greater. Thus, more precise measurements can be made at each geotextile layer, and the results follow a similar pattern as the surcharge load increases. On the

other hand, the strain measurements during surcharge load testing were made by using WPs, and the accuracy of the readings are limited due to very small movements in the geotextile. Unexpected movements in WP connections caused some data errors, especially at points far away from the surcharge loading. Geotextile layers that were closer to the surcharge load have high reinforcement strain values. Although, calculated T_{max} results from surcharge load testing for different elevations follow similar pattern with the Numerical Modeling results.

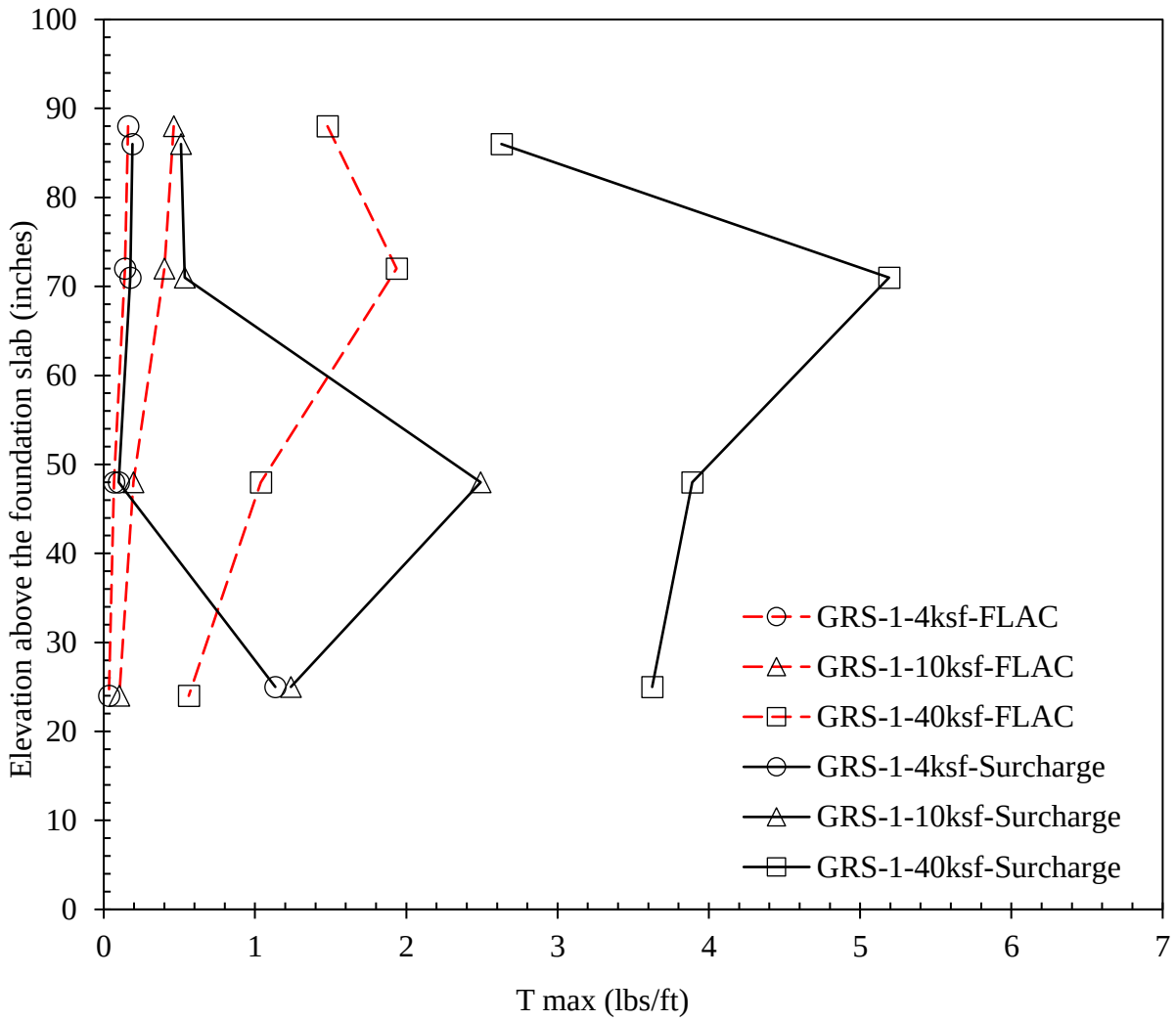

Figure 132. GRS Abutment Model #1- Maximum Tensile strength (T_{max}) comparison between full-scale surcharge load testing and Numerical Modeling (FLAC)

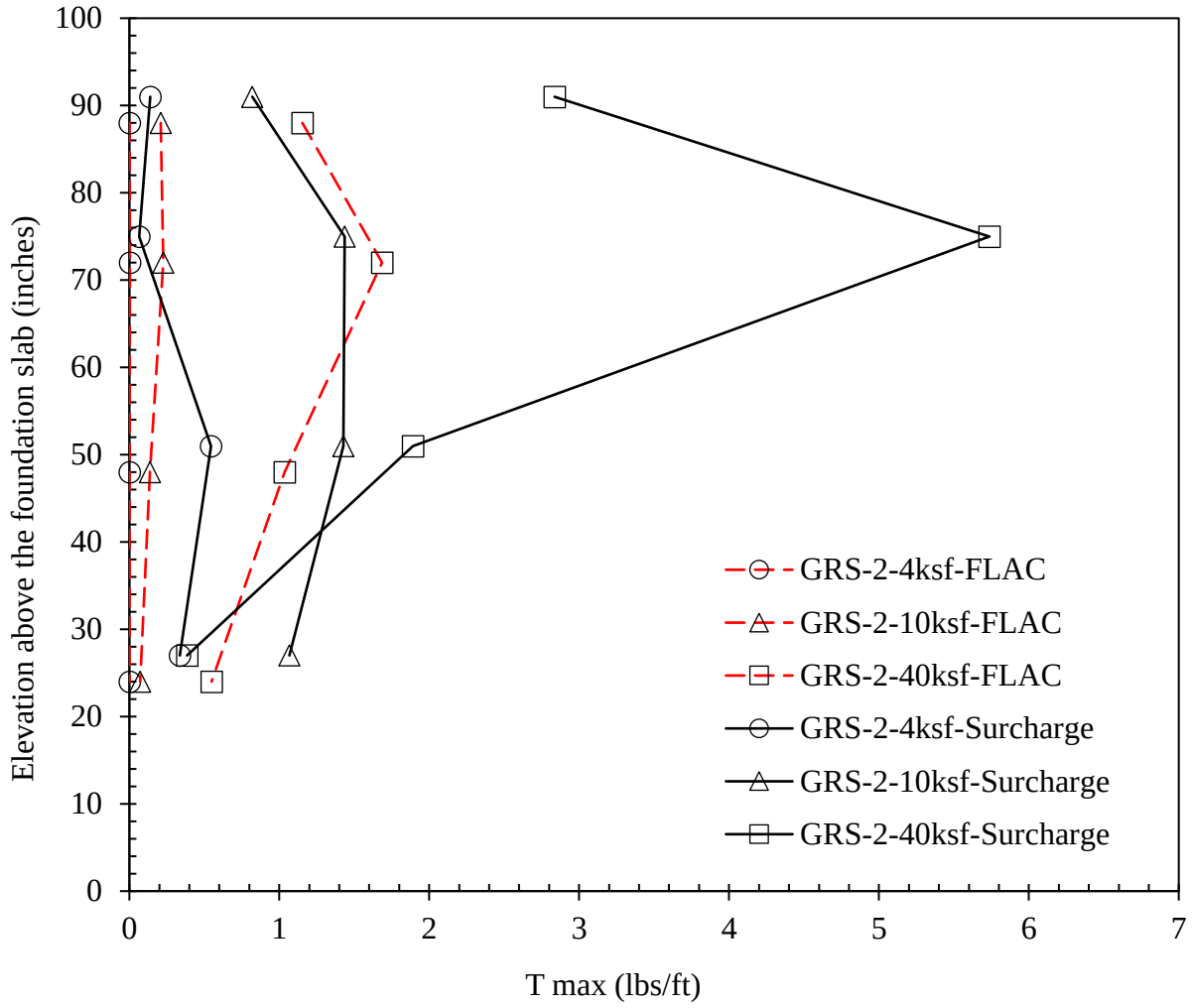

Figure 133. GRS Abutment Model #2- Maximum Tensile strength (T_{max}) comparison between full-scale surcharge load testing and Numerical Modeling (FLAC)

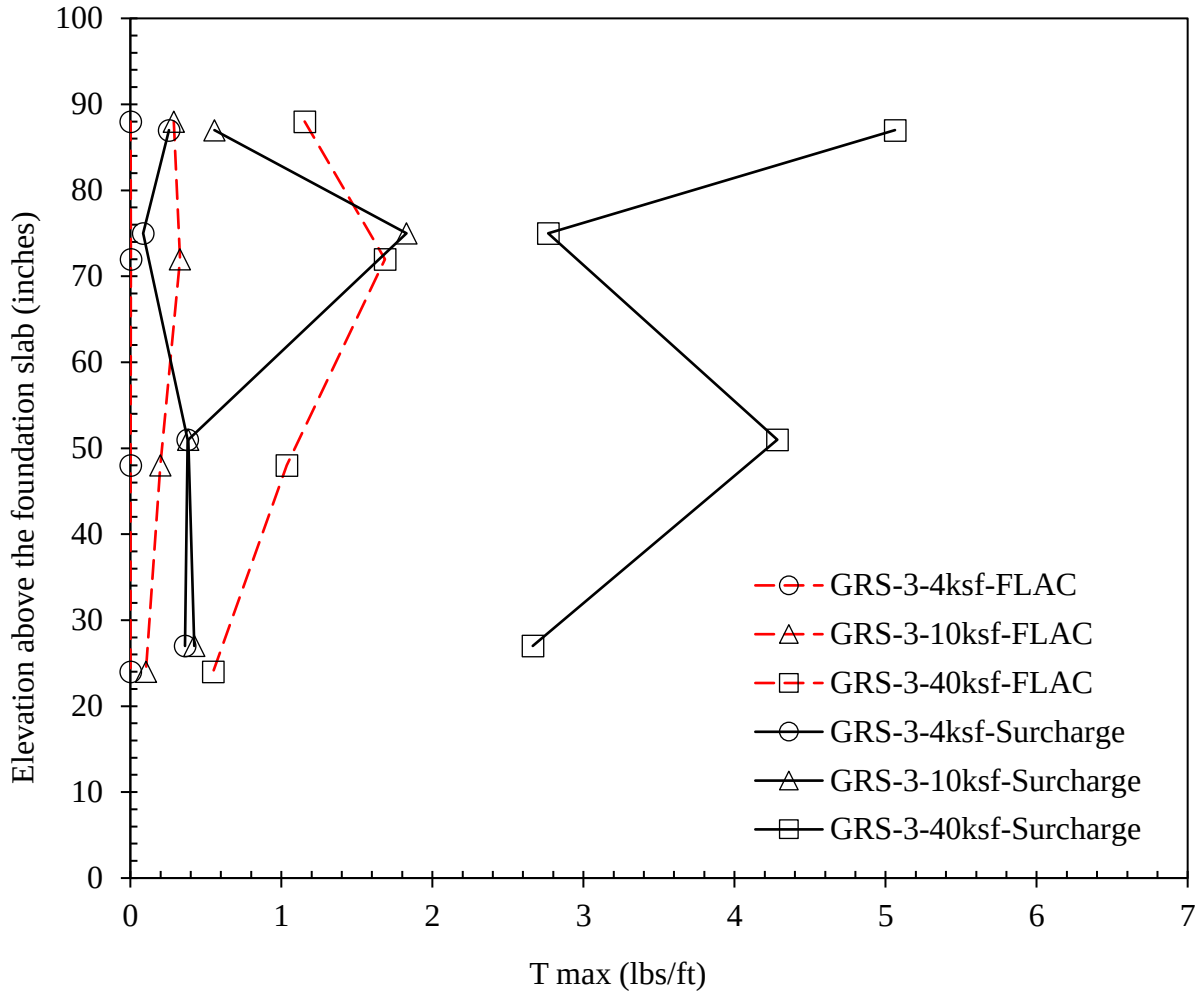

Figure 134. GRS Abutment Model #3- Maximum Tensile strength (T_{max}) comparison between full-scale surcharge load testing and Numerical Modeling (FLAC)

9.4. Deformations of GRS Fills at Selected Reinforcement Layers

Deformations of GRS fills at selected reinforcement layers were measured and recorded as described in Section 8.7. The maximum surcharge loading for the GRS Abutment Models #1 and #2 were 70.6 ksf (353 kips load) and 47.2 ksf (236 kips load), respectively. The only full-scale test stopped at 40 ksf (200 kips load) surcharge load level was GRS Model #3. The deformations GRS fills at selected reinforcement layers at 40 ksf surcharge load level were analyzed FLAC v.7.0

software with using y-displacement of geotextile layers at 90-inch, 84-inch, 78-inch, and 72-inch above the foundation level of GRS Abutment Model #3. These numerical model predicted values were compared with the full-scale surcharge load testing results from deconstruction manual survey readings at top four geosynthetic reinforcement layers of GRS Abutment Model #3 numbered as #11, #10, #9, and #8 from top to bottom (i.e. a set of two half reinforcement and a set of two full-reinforcement layers). Comparison of deformations of GRS fills at selected reinforcement layers between full-scale surcharge load testing and Numerical Modeling (FLAC) at 90-inch, 84-inch, 78-inch, and 72-inch above (i.e. at 93-inch, 87-inch, 81-inch, and 75-inch for full-scale load testing) the foundation slab during surcharge load testing of GRS Abutment Model #3 were shown in **Figures 135 a, b, c, and d**, respectively. The starting elevations at the back of the facing were matched for comparison purposes.

Results in these figures show that maximum depressions and settlements consistently occurred underneath the loading beam (representing bridge abutment load) with larger values occurring closer to the GRS surface. Both full-scale load testing measured results and Numerical Modeling predicted results show similar deformation pattern for each geotextile layer. Higher vertical deformation values were recorded from the Numerical Modeling due to reasons discussed in Section 9.1.

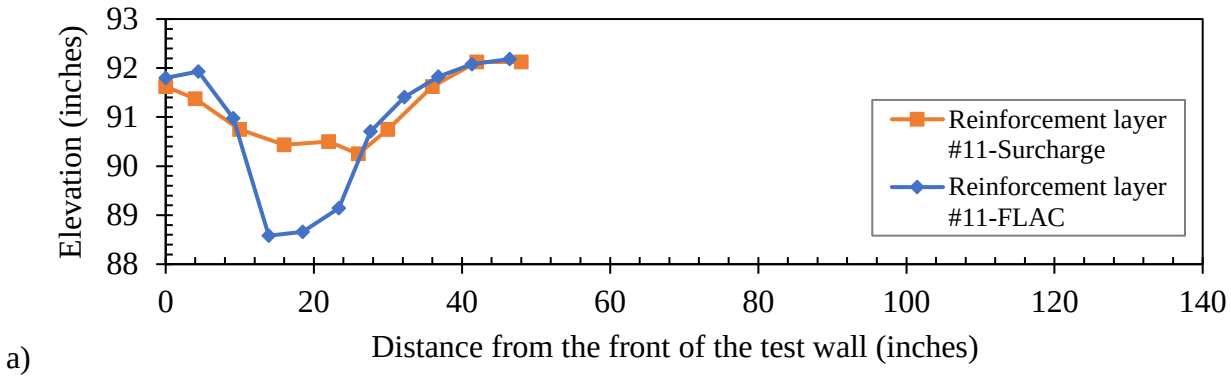

a)

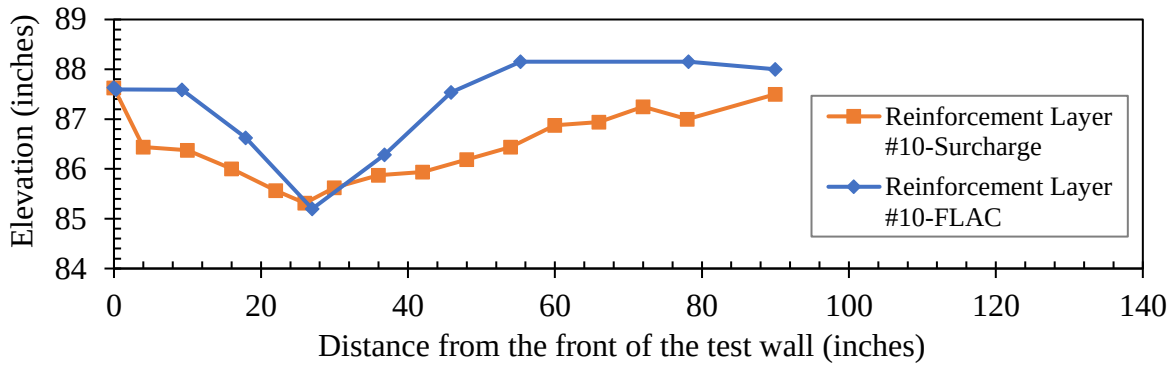

b)

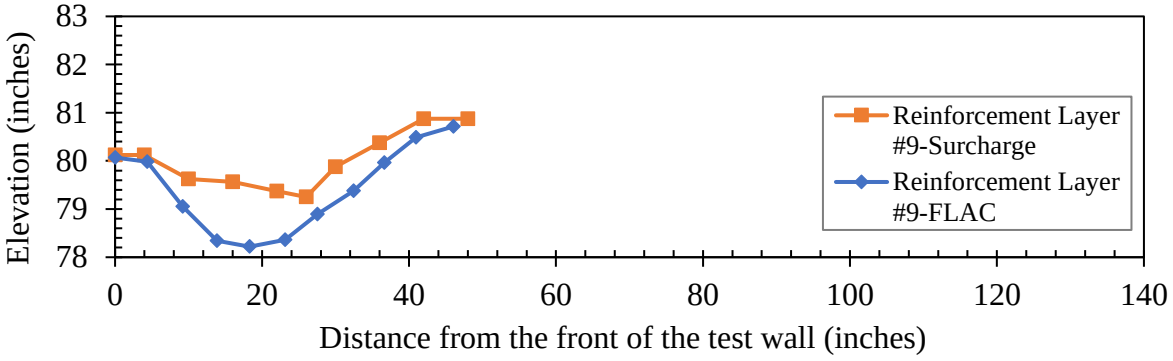

c)

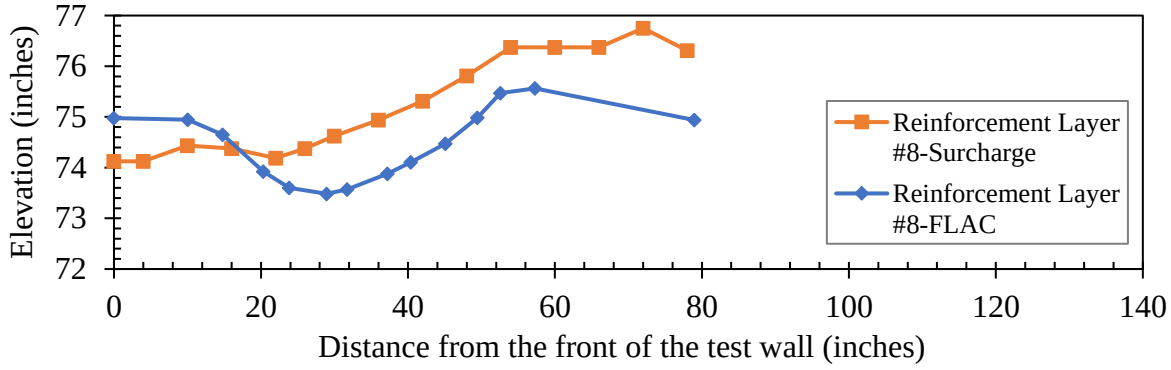

d)

Figure 135. GRS Abutment Model #3- Comparison of deformations of GRS fills at selected reinforcement layers between full-scale surcharge load testing and Numerical Modeling (FLAC)

9.5. Parametric Study (Load-Settlement Performance)

Several FLAC simulations as part of a parametric study were performed to investigate the influences of different parameters of the backfill material like lower friction angles (i.e. 35° and 45°), shear and bulk modulus values (i.e. $G=60\times10^6$ Pa and $K=104\times10^6$ Pa) after the calibration procedure. The influences of different reinforcement strength values (i.e. 2.4 k/ft and 9.6 k/ft) were also investigated to predict the load-bearing and facing performance of GRS Abutment Models #1-#3. A summary of the parametric study can be found in **Table 4** (Chapter 6).

The comparison of load-settlement performance at the top of GRS Abutment Models #1-#3 by Numerical Modeling (FLAC v.7.0) using different friction angles (35°, 45° and 48°) at 4 ksf, 10 ksf, and 40 ksf surcharge levels were given in **Figures 136 a, b and c**, respectively.

The results in **Figures 136** show that if the backfill material friction angle (i.e. 35°) gets lower than calibrated value (i.e. 48°), the vertical settlement increases dramatically. All GRS abutment models have similar load-settlement trends. It can be seen from the figures that the Numerical Modeling could not even be performed due the excessive deformations for loads higher than 10 ksf for GRS Abutment Models #1-#3 for friction angle of 35°. For this low friction angle scenario, the predicted load settlement values were 2.13 inches, 1.76 inches and 2.32 inches for GRS Abutment Models #1-#3, respectively. GRS Abutment Model #3 showed the highest amount of settlement because its uppermost short reinforcement layer was deeper (i.e. 6 inches from the top of the backfill) than that in Models #1 and #2 (i.e. 4-inch deep).

GRS Abutment Model #2 has the best load-settlement performance for all backfill friction angles that were used in Numerical Modeling based on the maximum vertical settlement values at each surcharge load levels. On the other hand, GRS Abutment Model #3 has slightly better load-settlement performance than GRS Abutment Model #1.

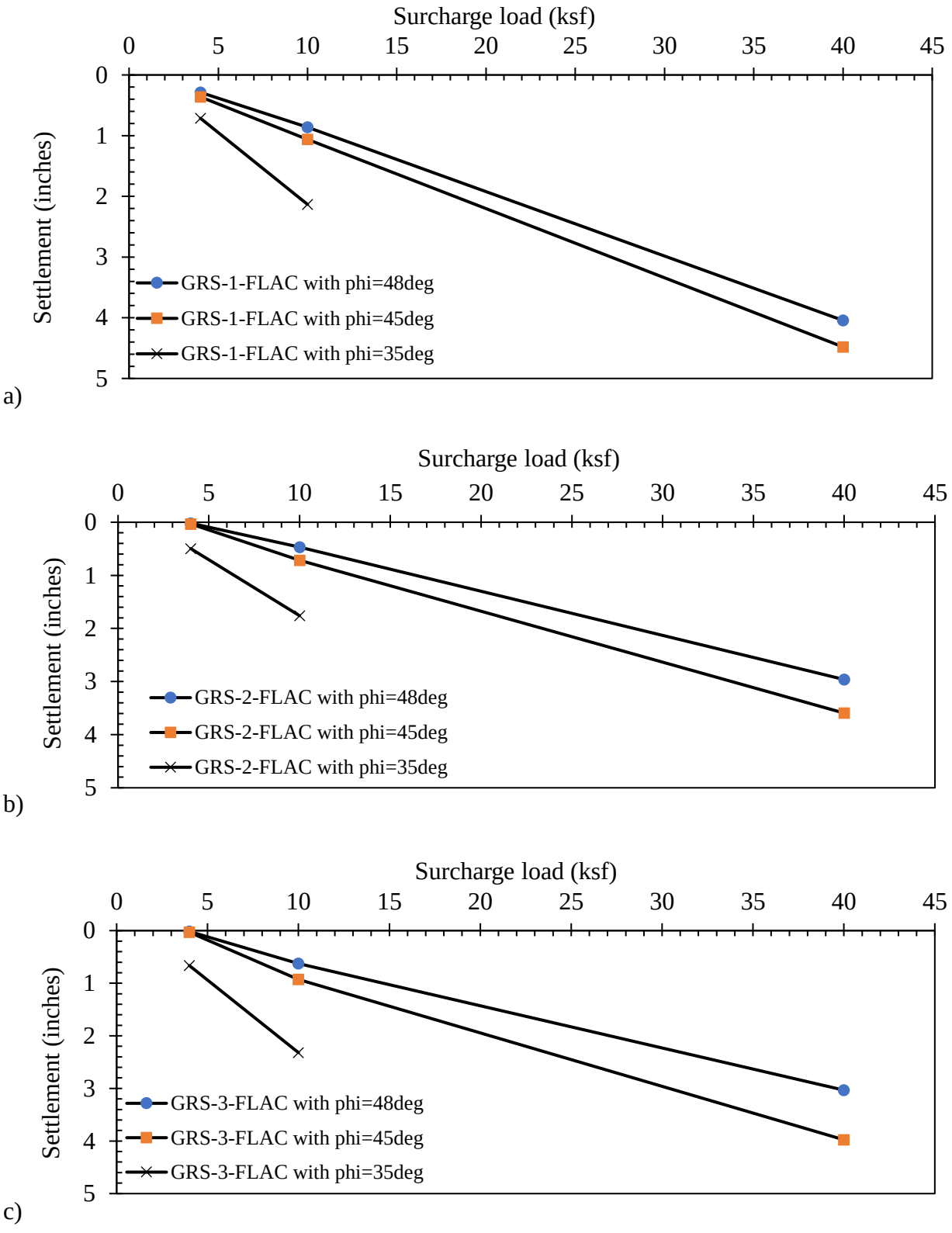

Figure 136. FLAC predictions of GRS Abutments' load-settlement performance for different backfill friction angle values at 4 ksf, 10 ksf and 40 ksf surcharge load levels: a) GRS Abutment Model #1, b) GRS Abutment Model #2, c) GRS Abutment Model #3

The comparison of load-settlement performance at the top of GRS Abutment Models #1-#3 from FLAC are given in **Figures 137 a, b and c**, respectively using different backfill elastic properties (K =153×10^6 Pa, G=139×10^6 Pa and K=104×10^6 Pa, G=60×10^6 Pa) at 4, 10 and 40 ksf surcharge levels.

Results in **Figure 137** show that if the backfill elastic properties (i.e. K=104×10^6 Pa, G=60×10^6 Pa) get lower than calibrated value (i.e. K =153×10^6 Pa, G=139×10^6 Pa that values were rounded for practicality), the vertical settlement increases. All GRS abutment models have similar load-settlement trends. Numerical modeling was able to be performed for GRS Abutment Models #1-#3 up to 40 ksf surcharge load level.

GRS Abutment Model #2 shows the best load-settlement performance for all backfill elastic properties that were used in Numerical modeling based on the predicted maximum vertical settlement values at each surcharge load level. On the other hand, GRS Abutment Model #3 has better load-settlement performance than GRS Abutment Model #1.

When the results in **Figure 137** were compared to the results in **Figure 136**, the effect of the backfill friction angle on the load-settlement performance is much more critical than the effect of the backfill elastic properties. The results in **Figure 137** were very close to each other even with using 32% lower K and 57% lower G value than the calibrated K and G values. At higher surcharge load levels like 40 ksf, the difference gets higher at GRS Abutment Model #3 (i.e. reinforcement spacing was 12-inch). This may be due to having higher reinforcement spacing than GRS Abutment Models #1 and #2.

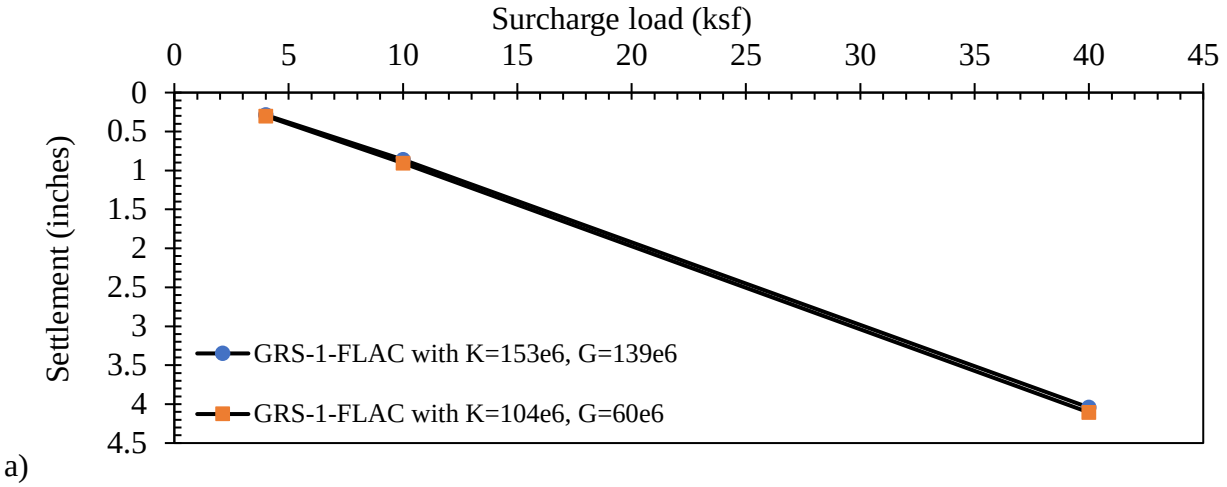

a)

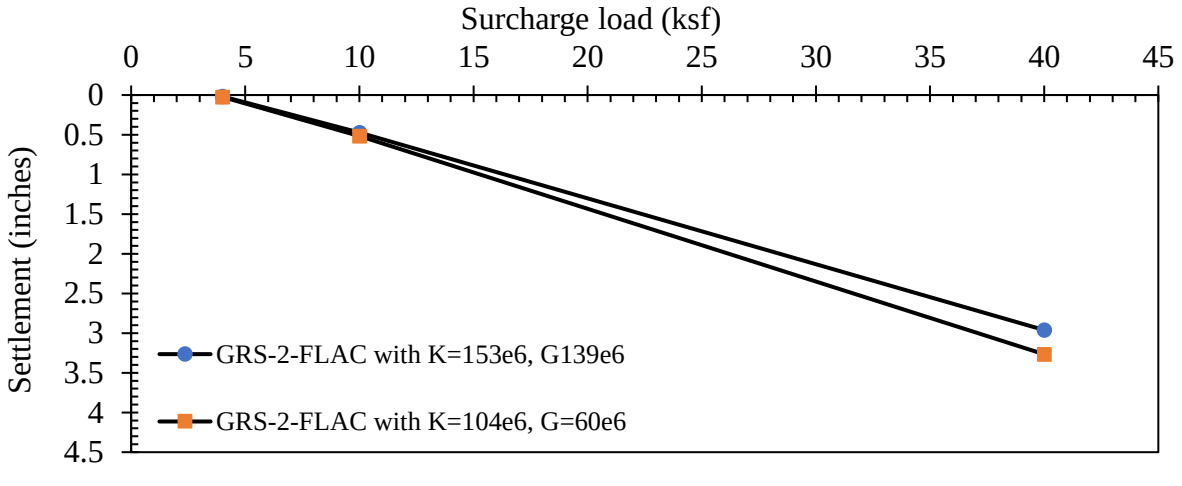

b)

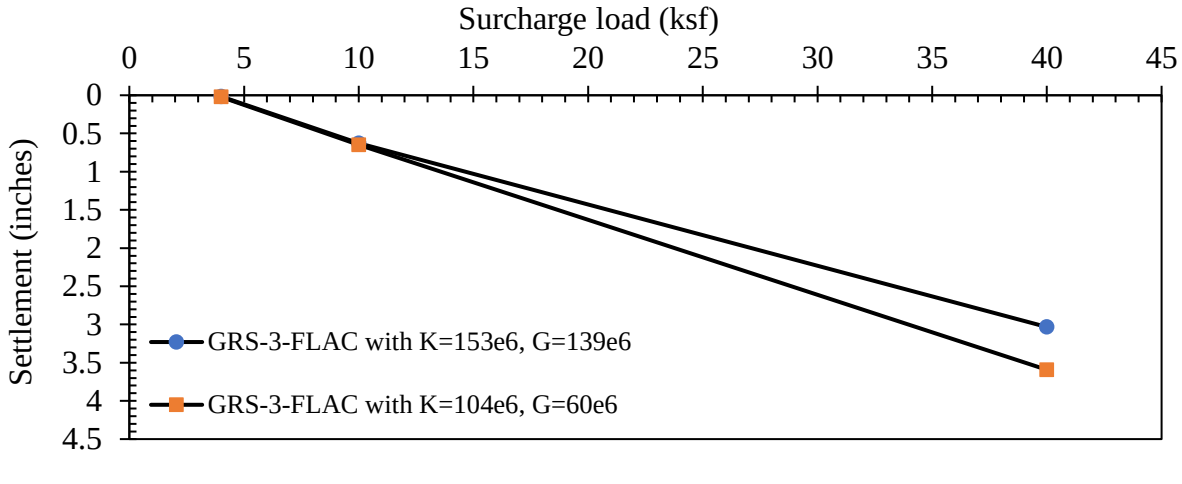

c)

Figure 137. Load-Settlement comparison by using FLAC v.7.0 with different backfill elastic properties at 4 ksf, 10 ksf and 40 ksf surcharge levels of a) GRS Abutment Model #1, b) GRS Abutment Model #2, c) GRS Abutment Model #3

The comparison of load-settlement performance at the top of GRS Abutment Models #1-#3 by Numerical Modeling (FLAC v.7.0) using different reinforcement strength values (2.4 k/ft, 4.8 k/ft and 9.6 k/ft) at 4 ksf, 10 ksf, and 40 ksf surcharge levels were given in **Figures 138 a, b and c**, respectively. Numerical Modeling was able to be performed for GRS Abutment Models #1-#3 up to 40 ksf surcharge load level.

Predicted results in **Figure 138** show that if the reinforcement strength value (i.e. 2.4 k/ft) gets lower than calibrated value (i.e. 4.8 k/ft), the vertical settlement increases. All GRS abutment models have similar load-settlement trends. On the other hand, if the reinforcement strength values (i.e. 9.6 k/ft) gets higher than calibrated value, the positive effect on the load-settlement performance is minimal. This indicates that, selecting an optimum geotextile reinforcement value is important to build economical GRS bridge abutments.

GRS Abutment Model #2 has the best load-settlement performance for all reinforcement strength values that were used in Numerical Modeling based on the maximum vertical settlement values at each surcharge load levels. On the other hand, GRS Abutment Model #3 has better load-settlement performance than GRS Abutment Model #1.

When the results in **Figures 136 through 138** were compared altogether, overall picture shows that the effect of the backfill friction angle on the load-settlement performance is much more critical than the effect of the backfill elastic properties and reinforcement strength parameters.

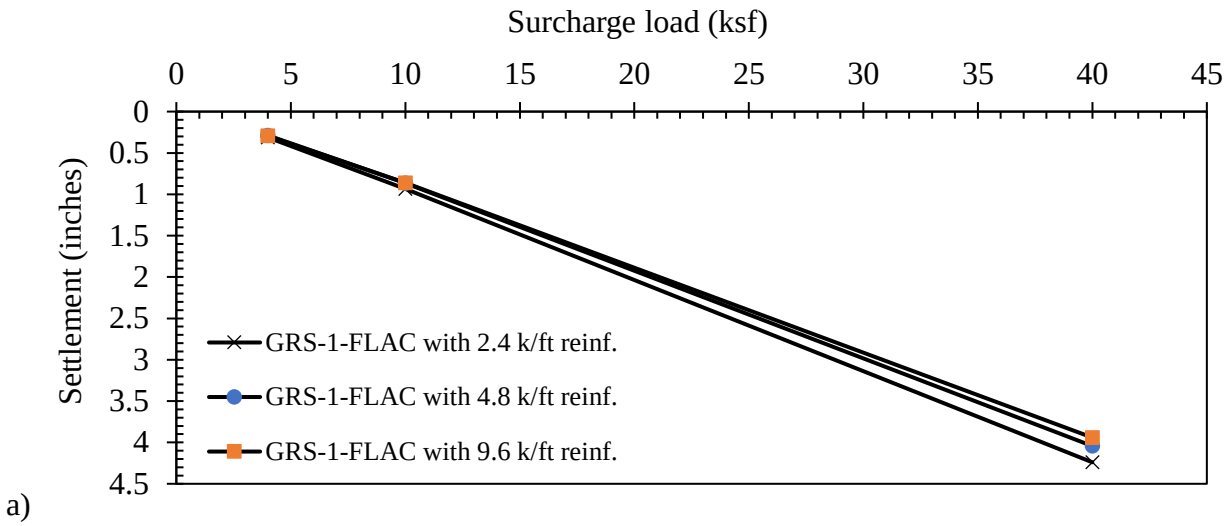

a)

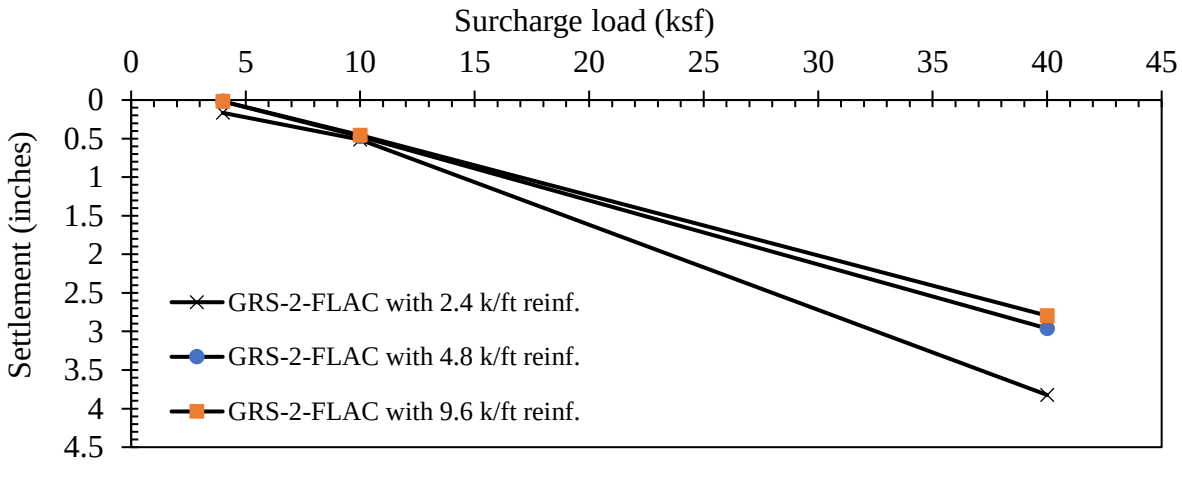

b)

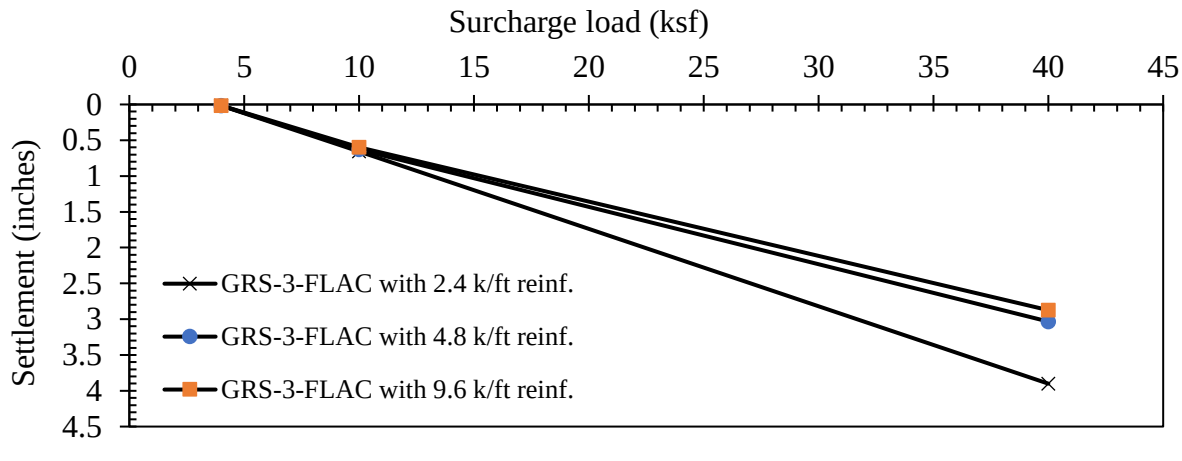

c)

Figure 138. Load-Settlement comparison by using FLAC v.7.0 with different reinforcement strength values at 4 ksf, 10 ksf and 40 ksf surcharge levels of a) GRS Abutment Model #1, b) GRS Abutment Model #2, c) GRS Abutment Model #3

9.6. Parametric Study (Facing Deformations)

After performing the parametric study on load-settlement performance, another parametric study was performed focusing on facing deformations to better understand the behavior of GRS abutment models. The comparison of facing deformations of GRS Abutment Models #1-#3 by using Numerical Modeling (FLAC v.7.0) with different friction angles (35°, 45° and 48°) were performed at 4, 10 and 40 ksf surcharge load levels (**Figures 139 through 141**, respectively).

Predicted results in **Figures 139 through 141** show that if the backfill material friction angle (i.e. 35°) gets lower than calibrated value (i.e. 48°), the facing deformations increase dramatically. All GRS abutment models have similar facing deformation trends.

Positive effect of large concrete block on facing deformations can easily be identified in 4 ksf service load level recommended by FHWA in **Figure 139**. It can be seen from the figures that the Numerical Modeling could not even be performed due the excessive facing deformations for loads higher than 10 ksf for GRS Abutment Models #1-#3 for friction angle of 35° (**Figure 141**).

GRS Abutment Model #2 has the best facing deformation performance for all backfill friction angles that were used in Numerical Modeling based on the maximum facing deformation values at each surcharge load levels. On the other hand, GRS Abutment Model #3 has better facing deformation performance than GRS Abutment Model #1.

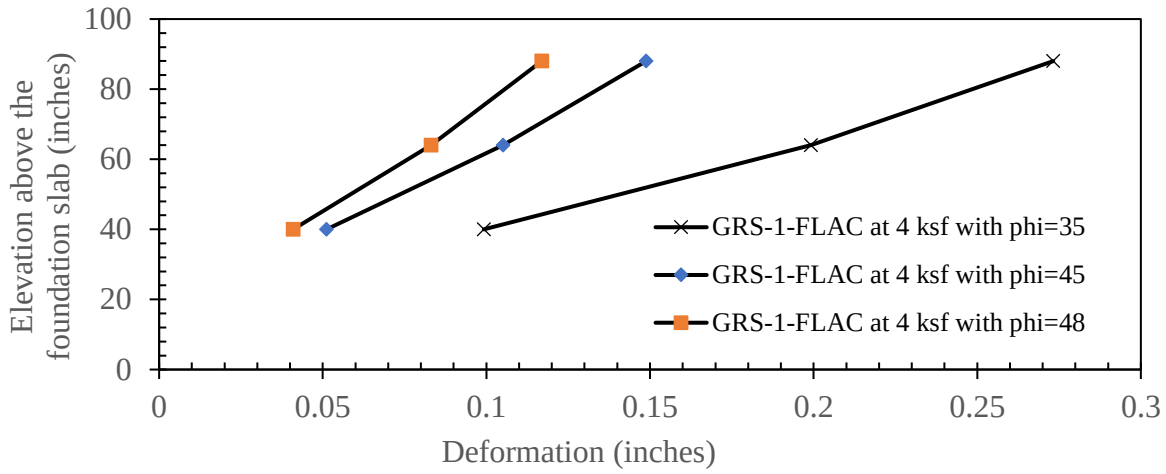

a)

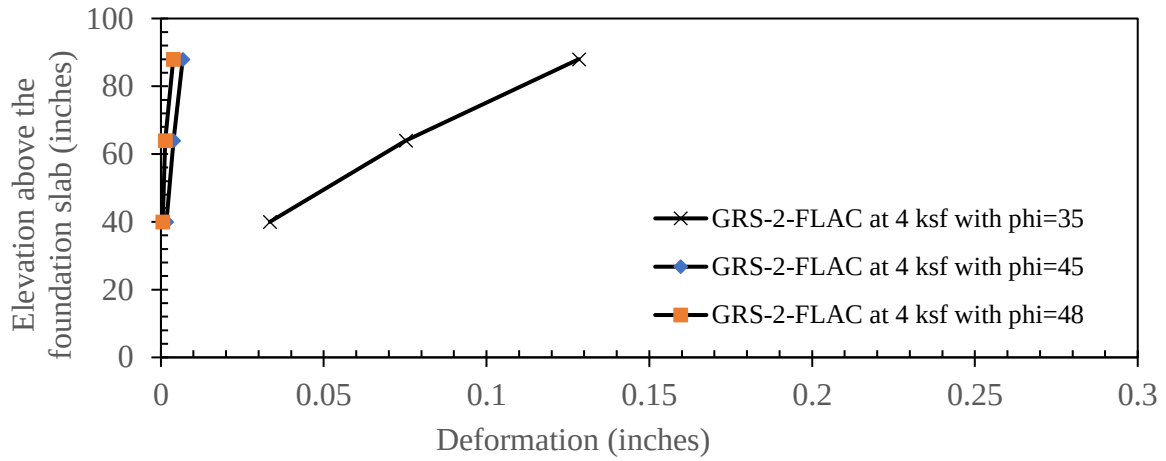

b)

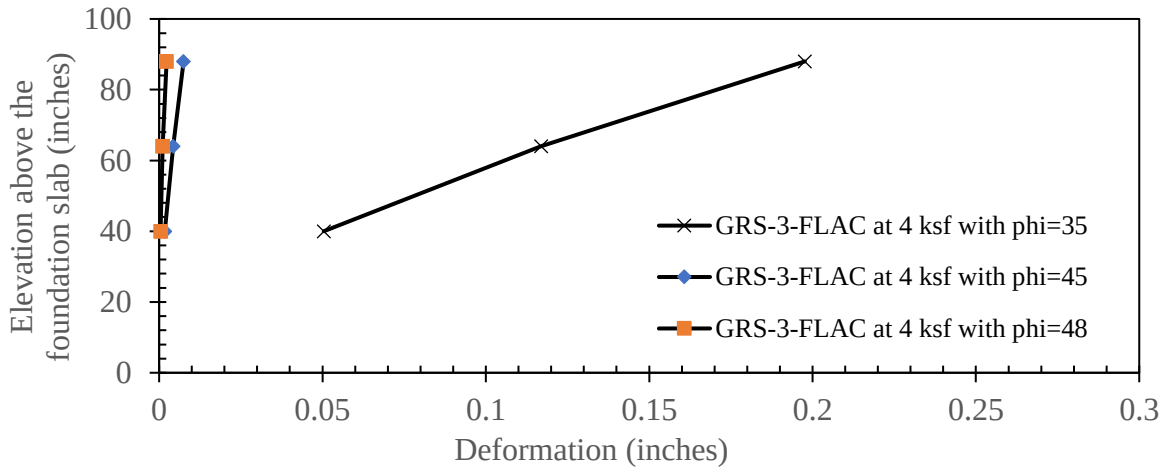

c)

Figure 139. Facing deformation comparison by using FLAC v.7.0 with different friction angles at 4 ksf surcharge level of a) GRS Abutment Model #1, b) GRS Abutment Model #2, c) GRS Abutment Model #3

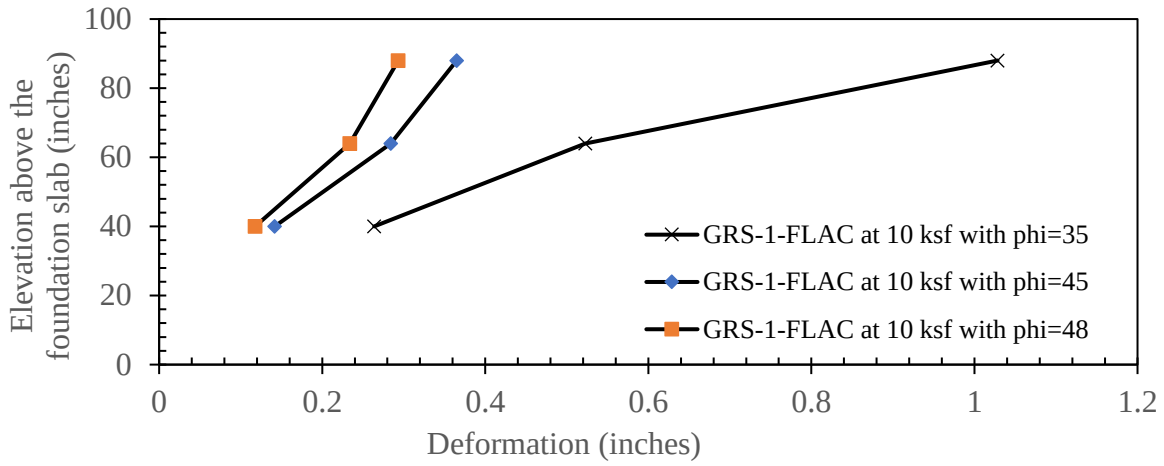

a)

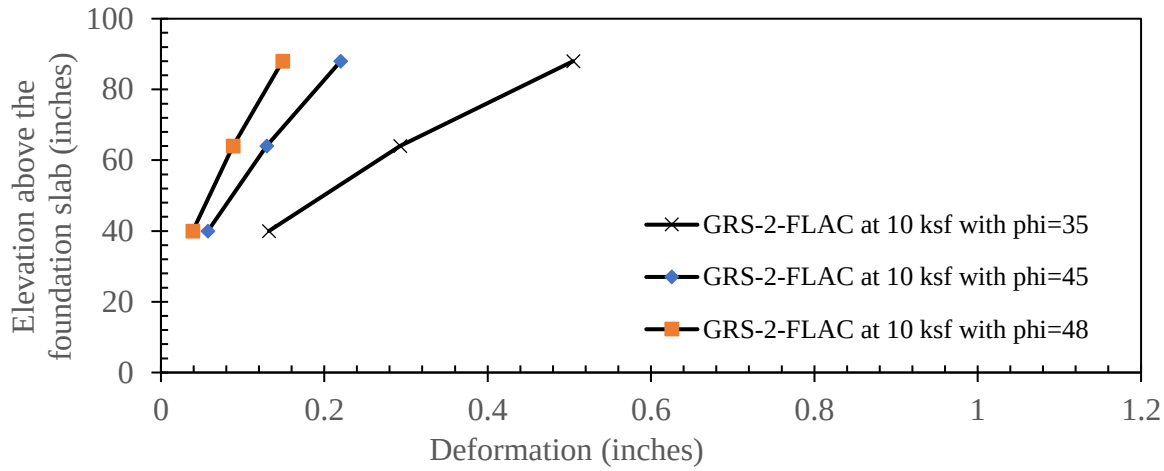

b)

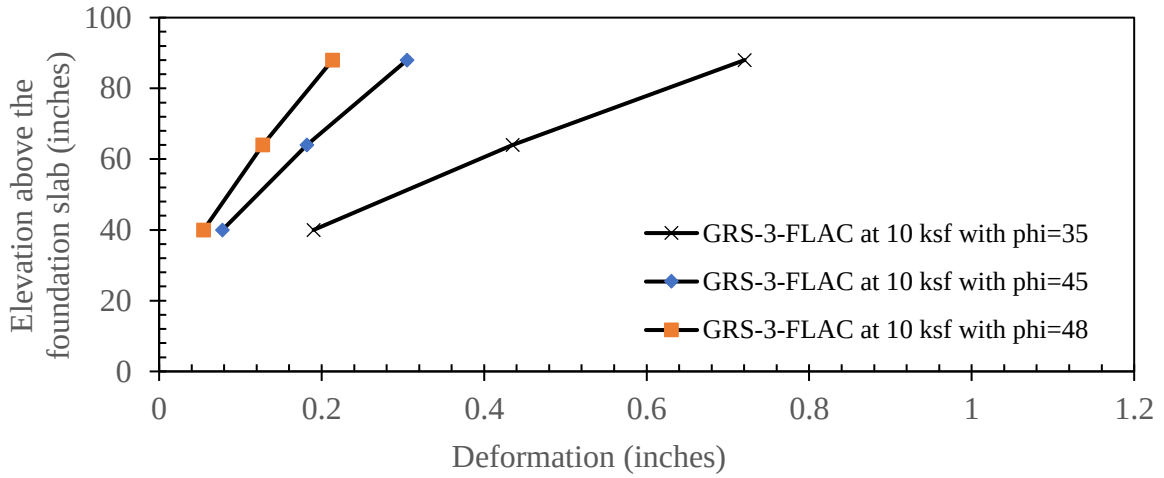

c)

Figure 140. Facing deformation comparison by using FLAC v.7.0 with different friction angles at 10 ksf surcharge level of a) GRS Abutment Model #1, b) GRS Abutment Model #2, c) GRS Abutment Model #3

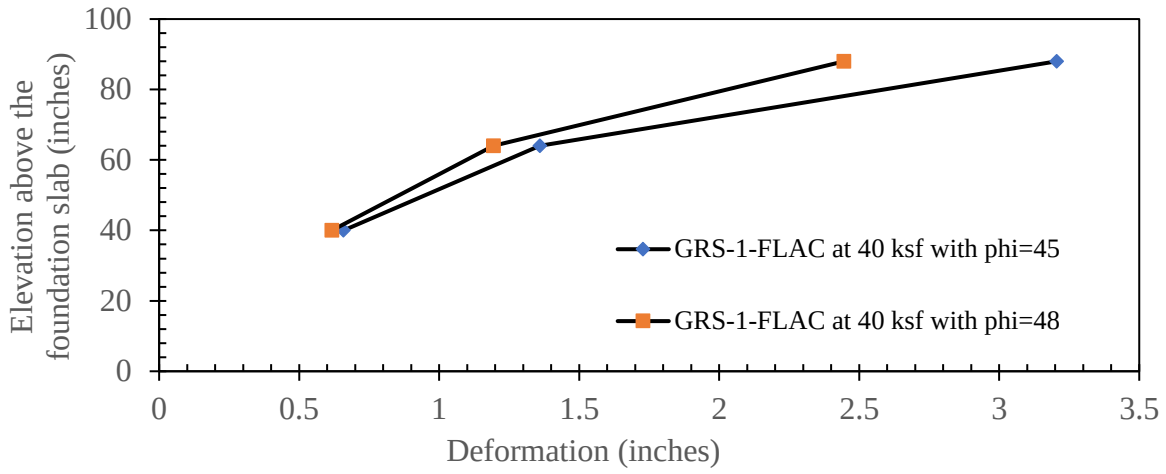

a)

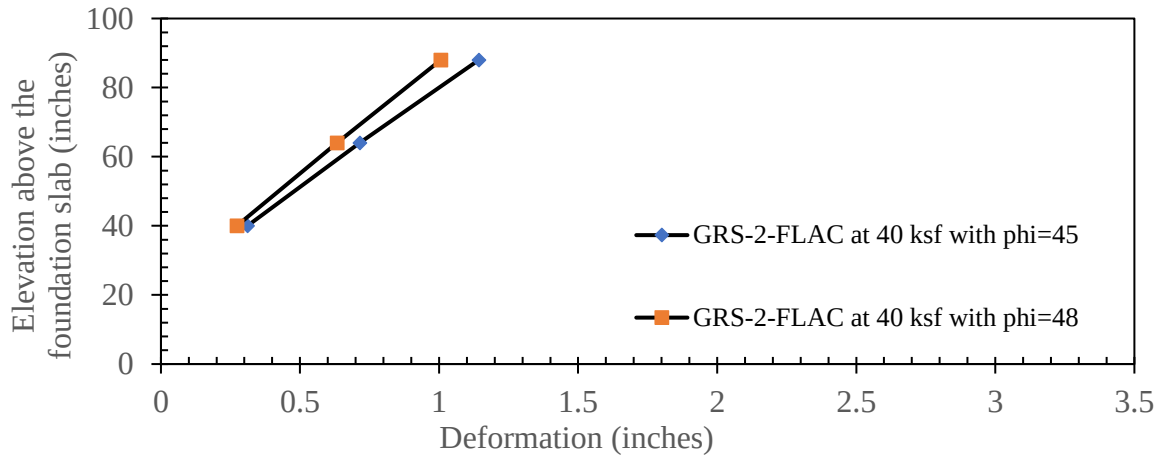

b)

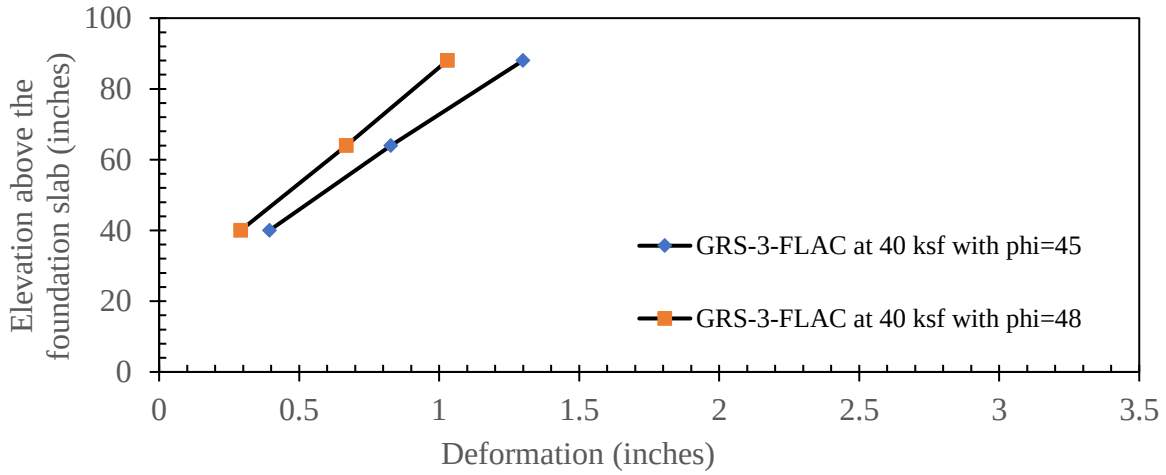

c)

Figure 141. Facing deformation comparison by using FLAC v.7.0 with different friction angles at 40 ksf surcharge level of a) GRS Abutment Model #1, b) GRS Abutment Model #2, c) GRS Abutment Model #3

The comparison of facing deformations of GRS Abutment Models #1-#3 by using Numerical Modeling (FLAC v.7.0) with different backfill elastic properties ($K=153\times10^6$ Pa, $G=139\times10^6$ Pa and $K=104\times10^6$ Pa, $G=60\times10^6$ Pa) were performed at 4, 10 and 40 ksf surcharge load levels (**Figures 142 through 144**, respectively).

Predicted results in **Figures 142 through 144** show that if the backfill elastic properties (i.e. $K=104\times10^6$ Pa, $G=60\times10^6$ Pa) get lower than calibrated value ($K=153\times10^6$ Pa, $G=139\times10^6$ Pa), the facing deformations increases. All GRS abutment models have similar facing deformation trends. Numerical Modeling was able to be performed for GRS Abutment Models #1-#3 up to 40 ksf surcharge load level.

GRS Abutment Model #2 has the best facing deformation performance for all backfill elastic properties that were used in Numerical Modeling based on the maximum facing deformation values at each surcharge load levels. On the other hand, GRS Abutment Model #3 has better facing deformation performance than GRS Abutment Model #1.

When the predicted results in **Figures 142 through 144** were compared to the predicted results in **Figures 139 through 141**, the effect of the backfill friction angle on the facing deformation performance is much more critical than the effect of the backfill elastic properties. Predicted results in **Figures 142 through 144** were very close to each other even with using 32% lower K and 57% lower G value than the calibrated K and G values. At higher surcharge load levels like 40 ksf, the difference gets higher at GRS Abutment Model #3 (i.e. reinforcement spacing was 12-inch). This may be due to having higher reinforcement spacing than GRS Abutment Models #1 and #2.

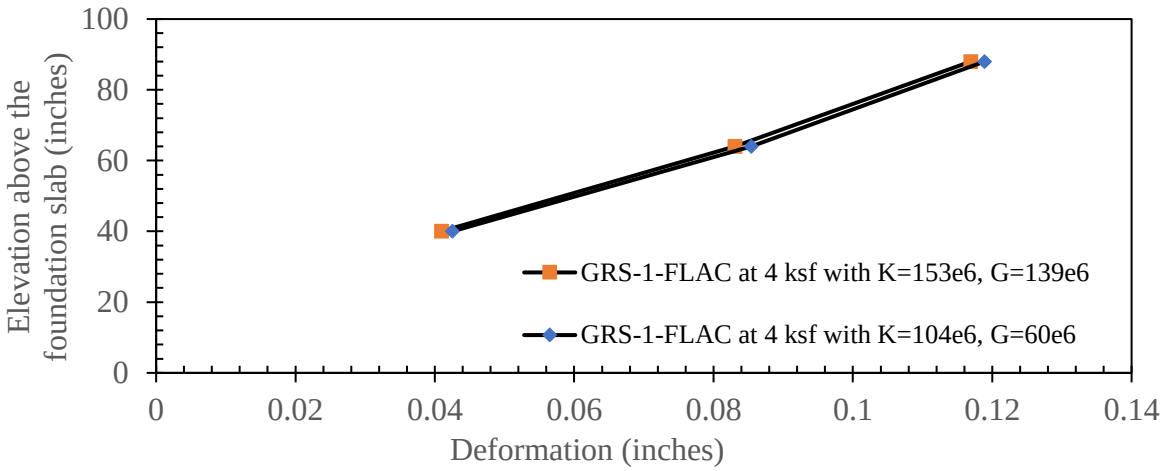

a)

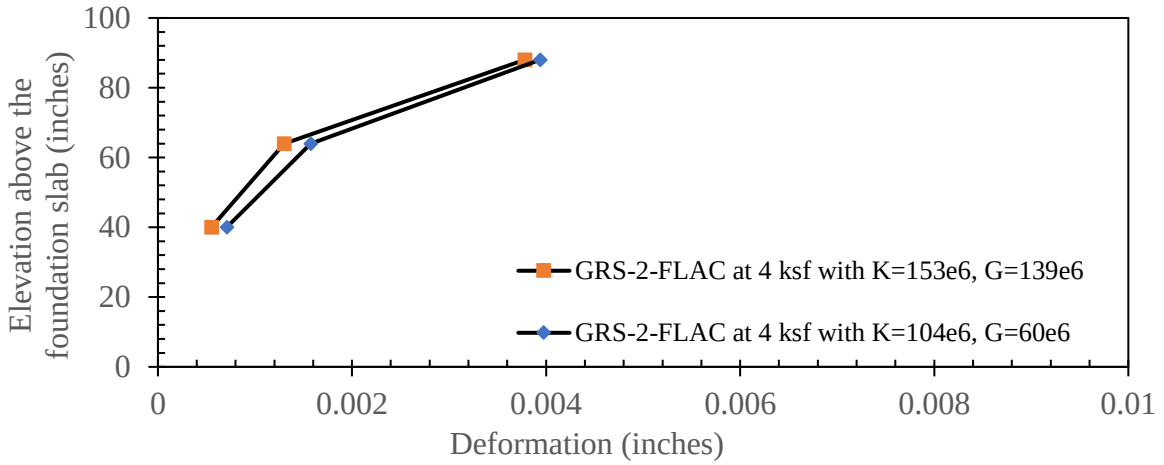

b)

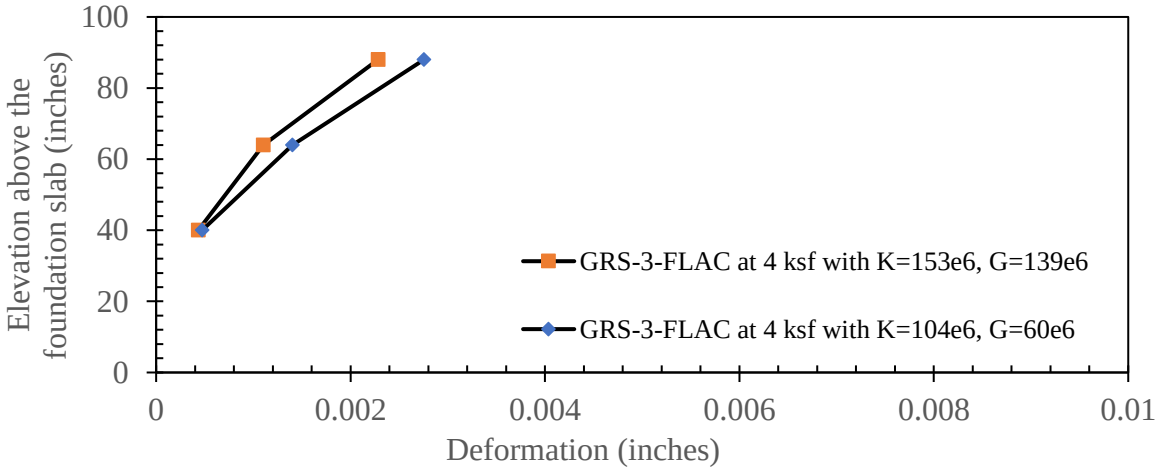

c)

Figure 142. Facing deformation comparison by using FLAC v.7.0 with different backfill elastic properties at 4 ksf surcharge level of a) GRS Abutment Model #1, b) GRS Abutment Model #2, c) GRS Abutment Model #3

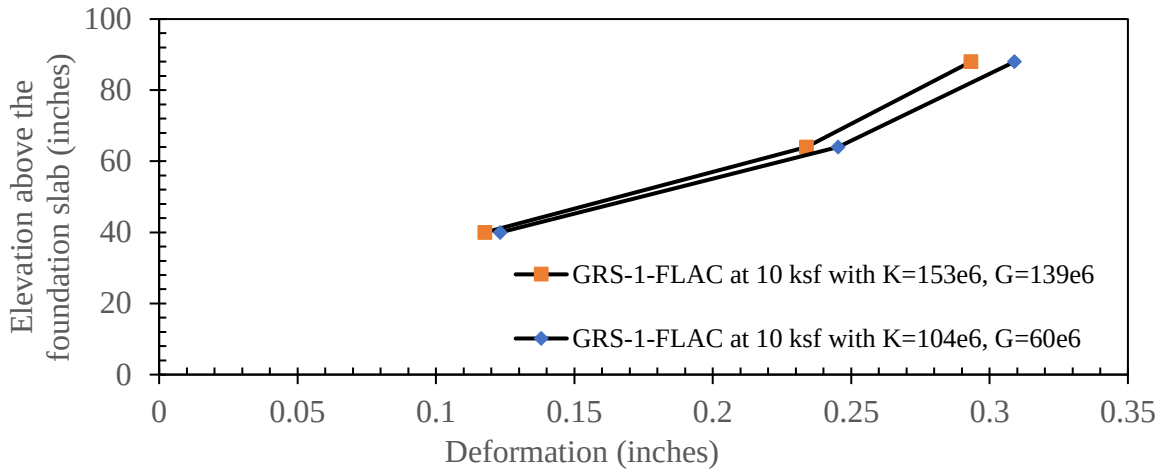

a)

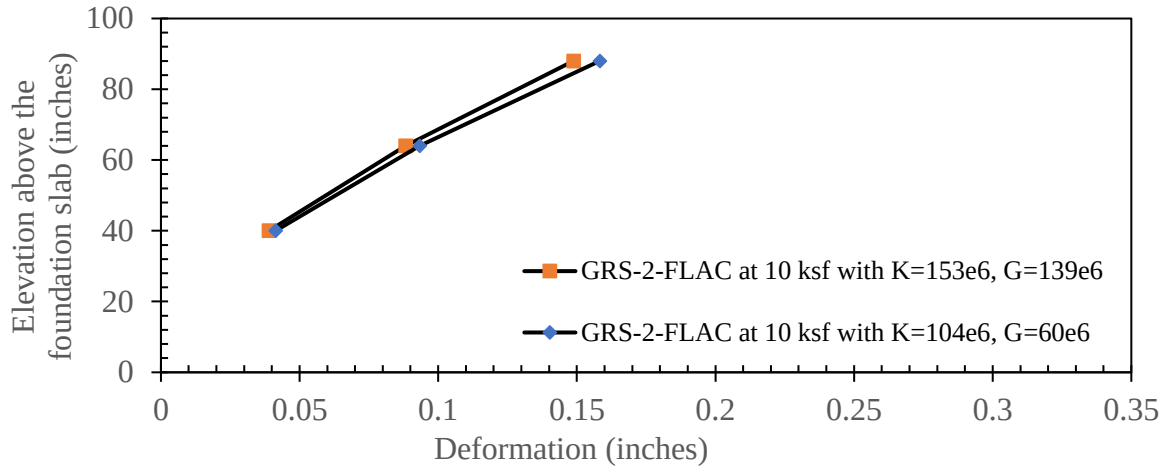

b)

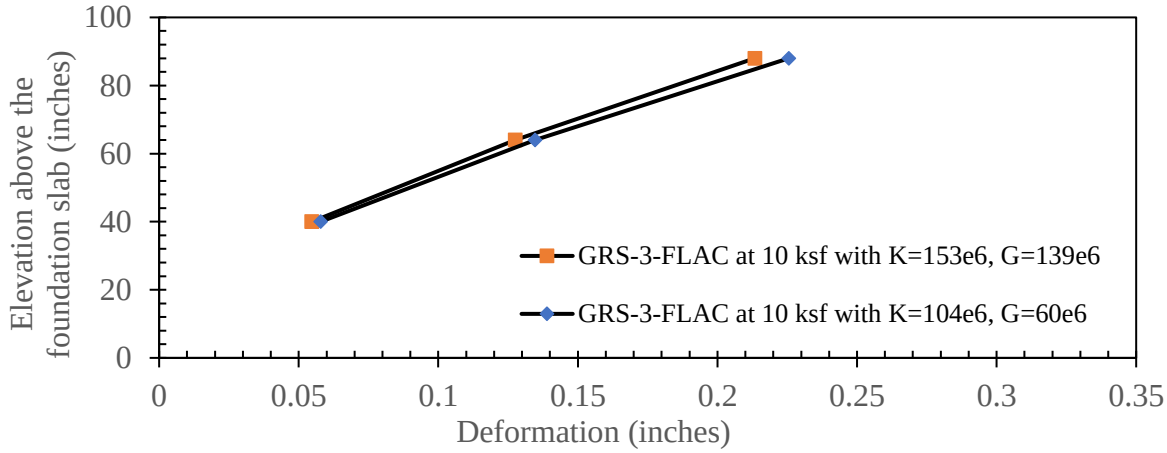

c)

Figure 143. Facing deformation comparison by using FLAC v.7.0 with different backfill elastic properties at 10 ksf surcharge level of a) GRS Abutment Model #1, b) GRS Abutment Model #2, c) GRS Abutment Model #3

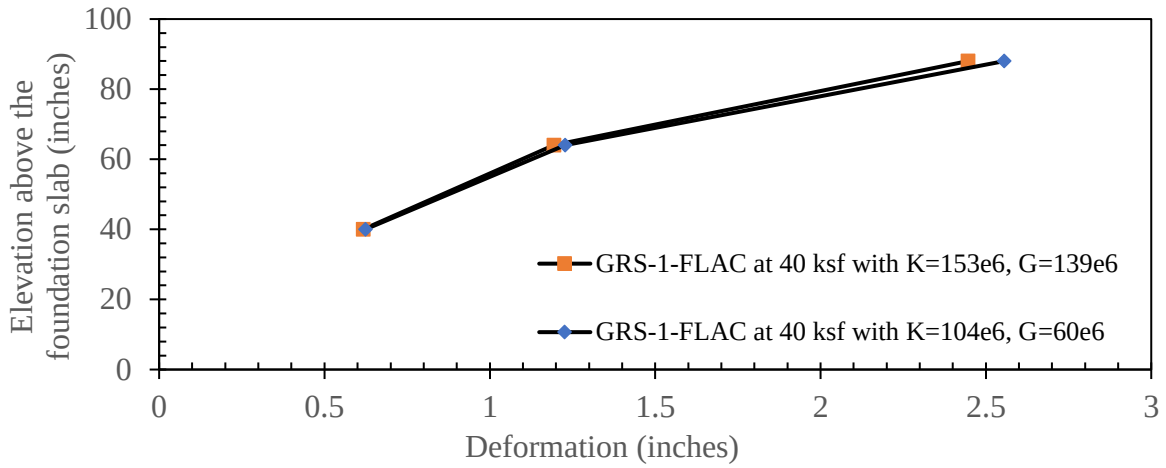

a)

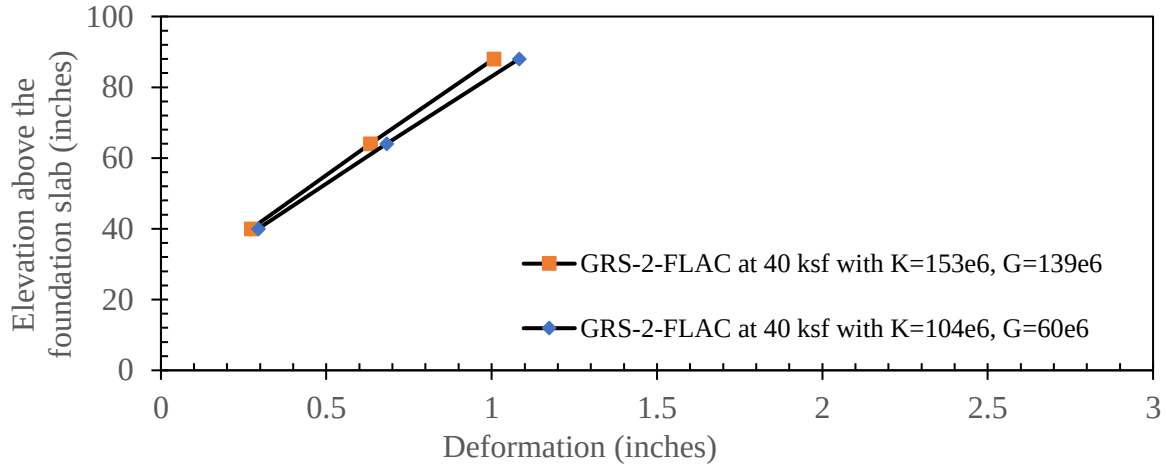

b)

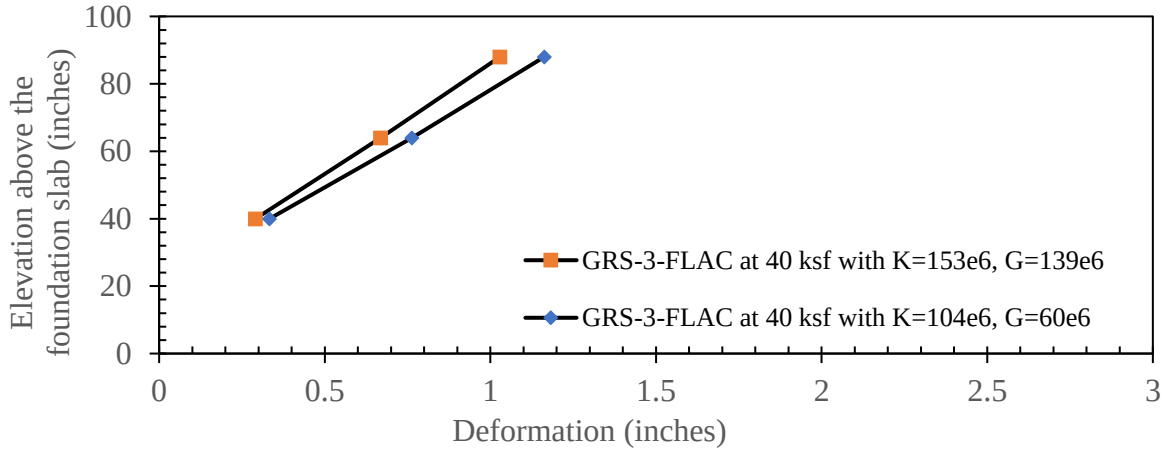

c)

Figure 144. Facing deformation comparison by using FLAC v.7.0 with different backfill elastic properties at 40 ksf surcharge level of a) GRS Abutment Model #1, b) GRS Abutment Model #2, c) GRS Abutment Model #3

The comparison of facing deformations of GRS Abutment Models #1-#3 by Numerical Modeling (FLAC v.7.0) using different reinforcement strength values (2.4 k/ft, 4.8 k/ft and 9.6 k/ft) at 4, 10 and 40 ksf surcharge load levels (**Figures 145 through 147**, respectively). Numerical Modeling was able to be performed for GRS Abutment Models #1-#3 up to 40 ksf surcharge load level.

Predicted results in **Figures 145 through 147** show that if the reinforcement strength value (i.e. 2.4 k/ft) gets lower than calibrated value (i.e. 4.8 k/ft), the lateral movement of the facing increases. All GRS abutment models have similar facing deformation trends. On the other hand, if the reinforcement strength values (i.e. 9.6 k/ft) gets higher than calibrated value, the positive effect on the facing deformation performance is minimal. Similar observation was indicated in Section 9.5. The facing deformation results also confirm that, selecting an optimum geotextile reinforcement value is important to build economical GRS bridge abutments.

GRS Abutment Model #2 has the best facing deformation performance for all reinforcement strength values that were used in Numerical Modeling based on the maximum lateral movement values at each surcharge load levels. On the other hand, GRS Abutment Model #3 has better facing deformation performance than GRS Abutment Model #1.

When the predicted results in **Figures 139 through 147** were compared altogether, overall picture shows that the effect of the backfill friction angle on the facing deformation performance is much more critical than the effect of the backfill elastic properties and reinforcement strength parameters.

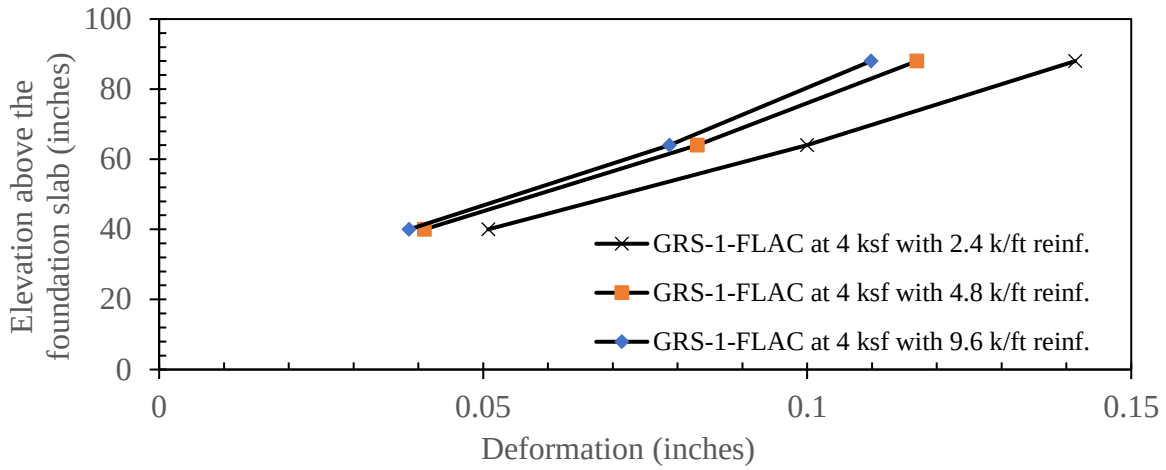

a)

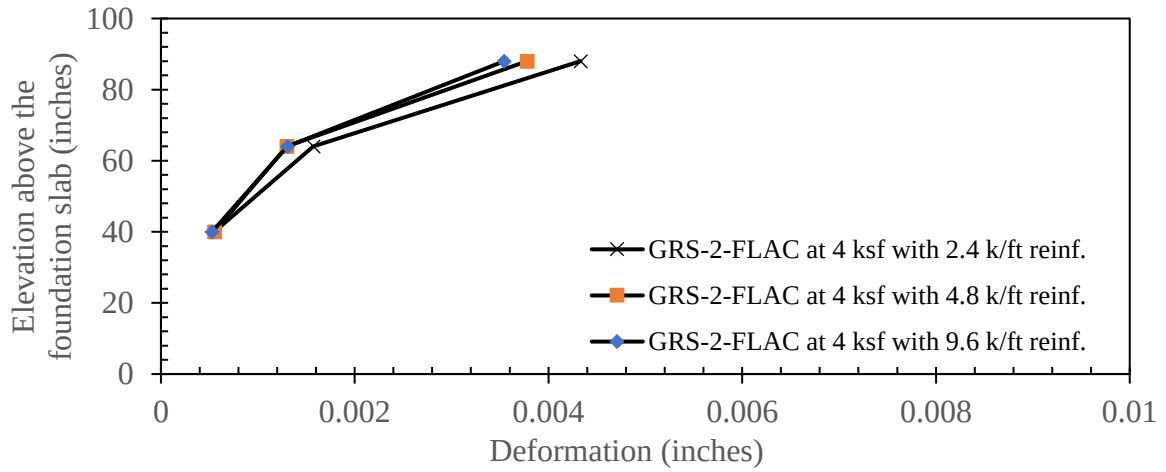

b)

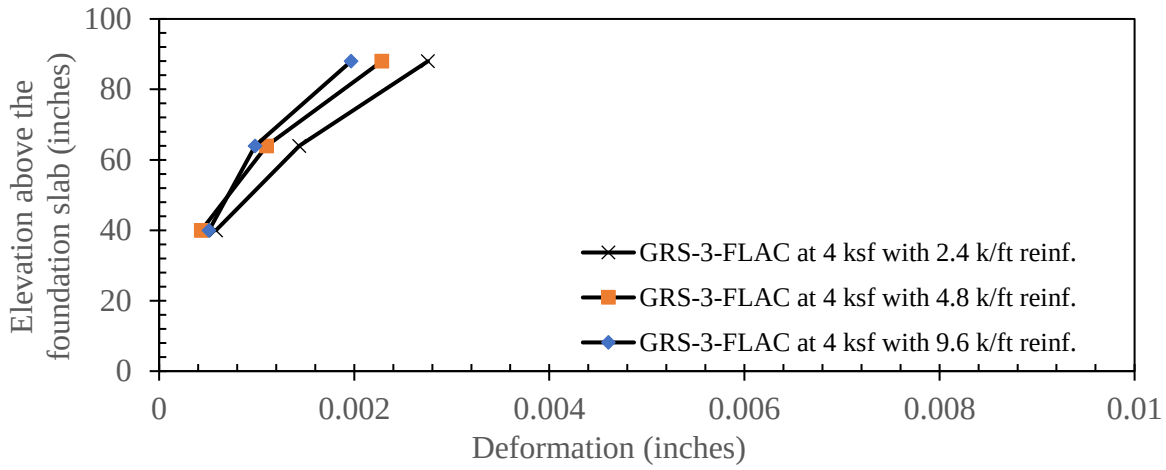

c)

Figure 145. Facing deformation comparison by using FLAC v.7.0 with different reinforcement strengths at 4 ksf surcharge level of a) GRS Abutment Model #1, b) GRS Abutment Model #2, c) GRS Abutment Model #3

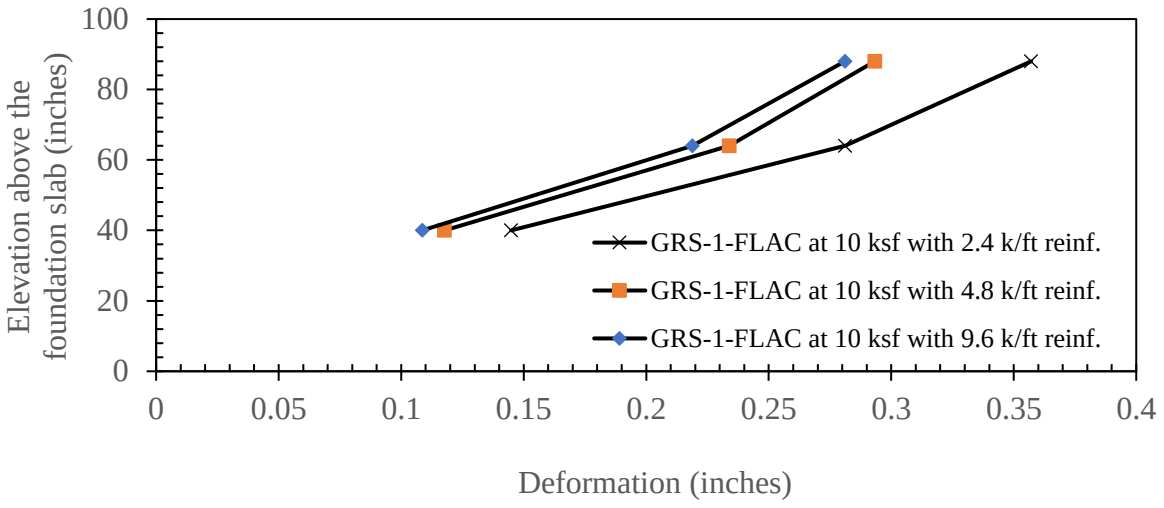

a)

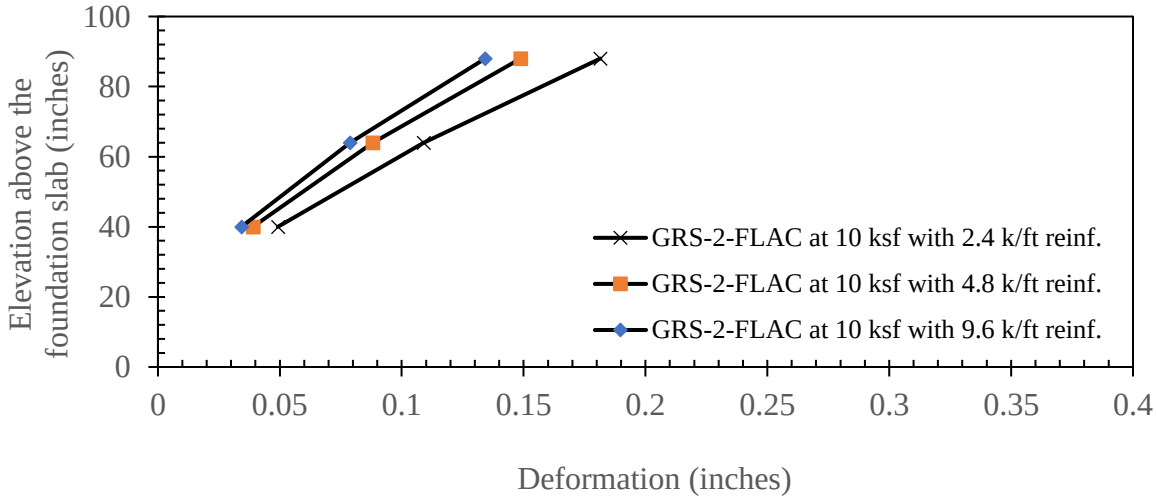

b)

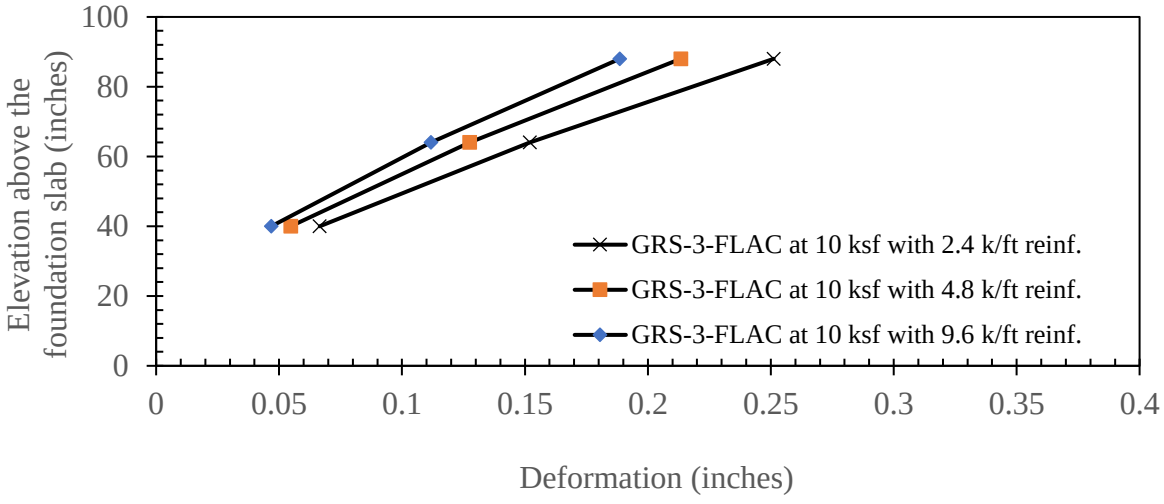

c)

Figure 146. Facing deformation comparison by using FLAC v.7.0 with different reinforcement strengths at 10 ksf surcharge level of a) GRS Abutment Model #1, b) GRS Abutment Model #2, c) GRS Abutment Model #3

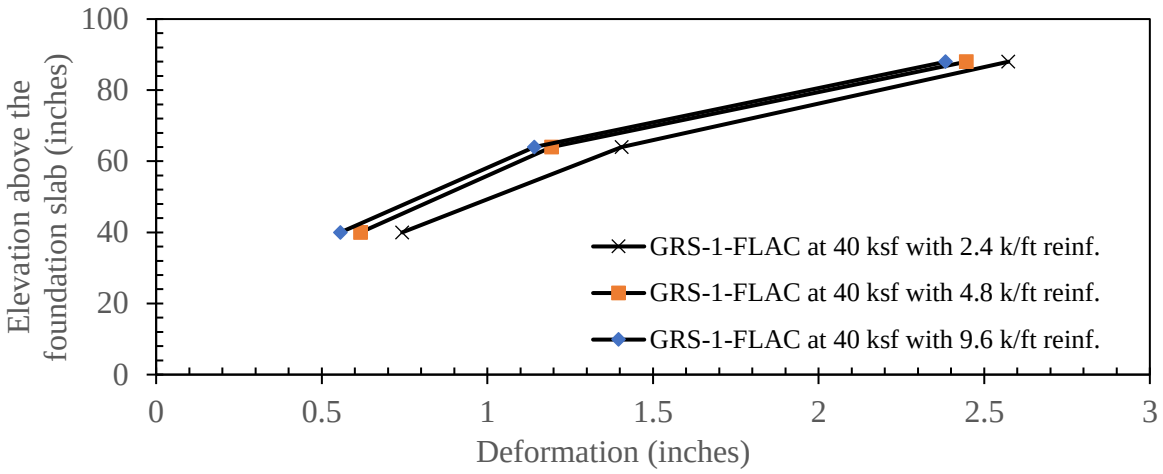

a)

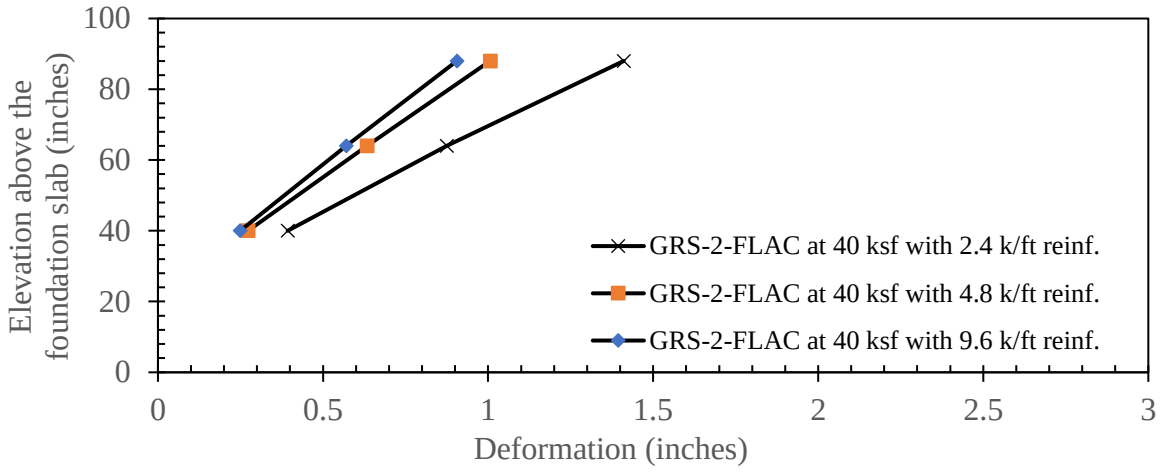

b)

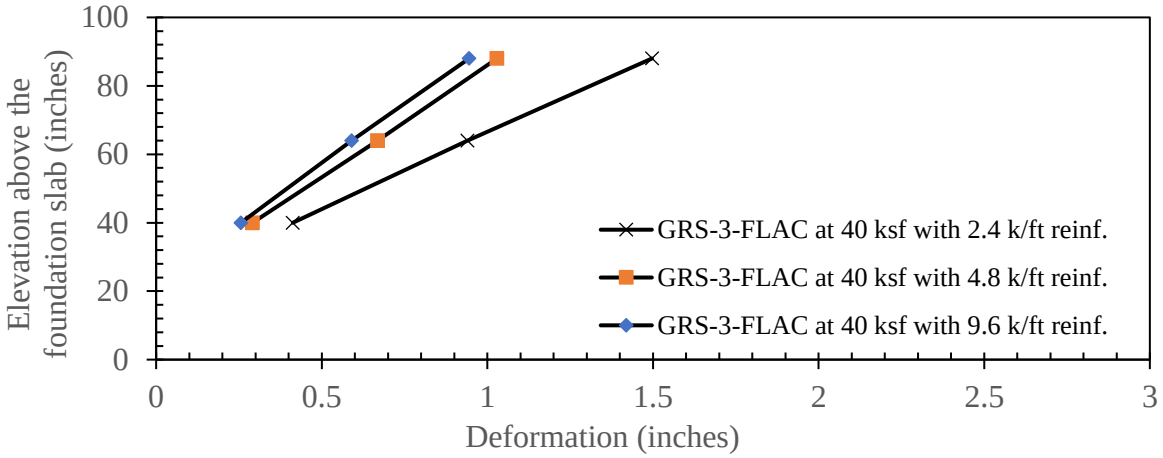

c)

Figure 147. Facing deformation comparison by using FLAC v.7.0 with different reinforcement strengths at 40 ksf surcharge level of a) GRS Abutment Model #1, b) GRS Abutment Model #2, c) GRS Abutment Model #3

Chapter 10. Concluding Remarks

10.1. Summary and Conclusions

Safer, faster, and more economical bridge abutment designs can easily be achieved by using GRS-IBS. These advantages can be improved by using large concrete block. These blocks are 2 ft. high × 2 ft. deep × 4 ft. wide in size and have longitudinal tongue-and-groove keys, which provide added stability when they need to be stacked up to heights higher than 8 ft.

The results from this study show time and cost savings of using the large concrete blocks, with comparing CMU block facing option. Using large concrete block as facing can reduce the construction time more than 50% compared with CMU.

Additionally, the compaction at closer locations to the facing blocks is much easier and safer when large concrete blocks are used. Maximum compaction can be achieved at the back of the facing without requiring any extra precautions. They provide better confinement for the backfill due to their significant weight and negligible movement during the construction process. Therefore, using large concrete block can help accelerate the construction speed by replacing several CMU blocks for each large concrete block, and by allowing reduced compaction time for a similar structural performance.

Instrumentation data collected during the full-scale testing of CMU and large concrete block facing GRS Abutment Models was successfully showed that using large concrete block as facing improves the load-settlement and facing deformation performance significantly. It should be also noted that current FHWA guidelines recommend lateral deformation limit under maximum service

load as 1%, and vertical settlement as 0.5% of total facing height. This research clearly showed that recommended vertical settlement limit governs the performance of GRS abutments under bridge service loads.

The parametric studies performed by Numerical Modeling show that if the backfill friction angle and elastic properties as well as reinforcement strength values get lower, then the vertical settlement increases. This is also true if the backfill friction angle and elastic properties as well as reinforcement strength get lower, then the facing deformations increase.

The effect of the backfill friction angle on the load-settlement and facing deformation performance is much more critical than the effect of the backfill elastic properties and reinforcement strength parameters. On the other hand, if the reinforcement strength gets higher, then the positive effect on the load-settlement and facing deformation performance is minimal.

Large concrete block facing option has better load-settlement and facing deformation performance than CMU facing option based on the full-scale testing and numerical modeling results. The research showed that the reinforcement spacing of GRS bridge abutment with large concrete facing can be increased to achieve the same performance with standard CMU facing for extra cost savings.

Successful construction and load testing of two large concrete block model GRS abutments have demonstrated that the drawings used for the construction of the full-scale test models could be used as reference for the construction of similar large concrete block GRS bridges on different local and county roads. A proposed cross-section for GRS abutments with large concrete block facing, together with construction notes based on FHWA guidelines is given in **Figure 148**.

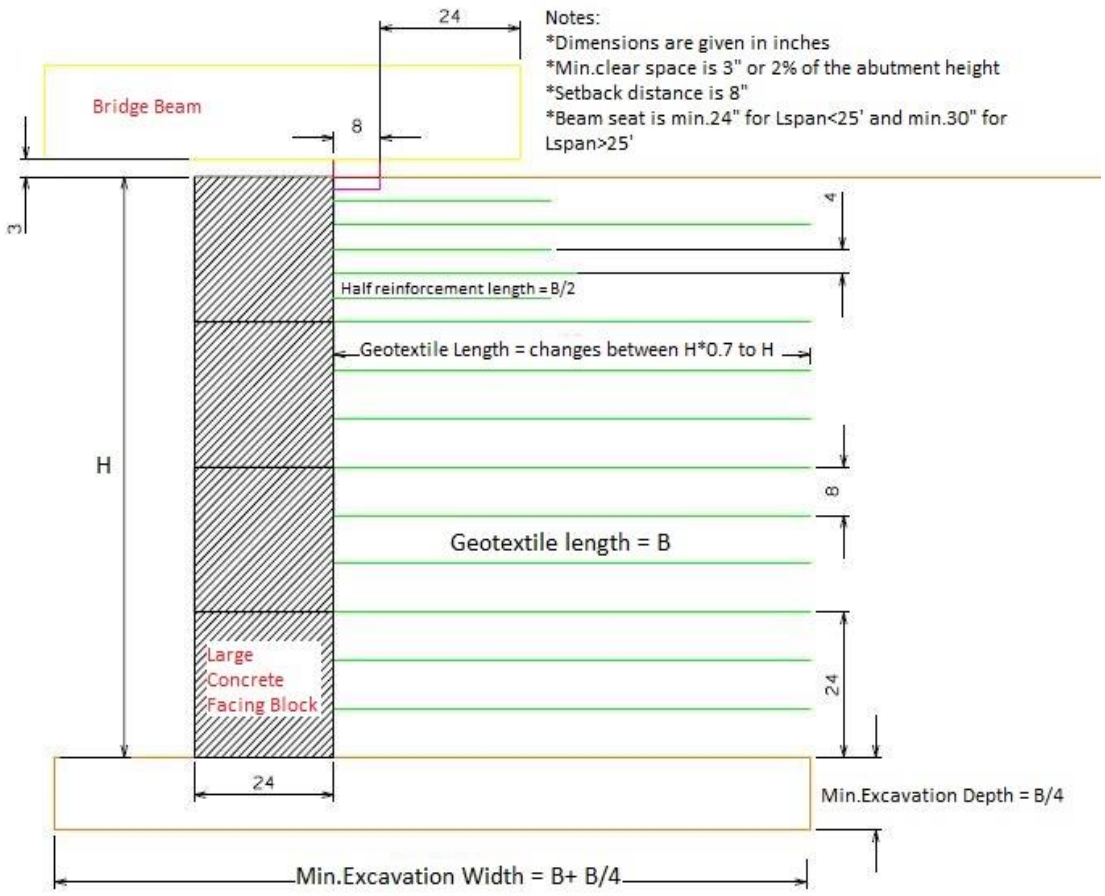

Figure 148. Typical cross-section of a GRS abutment with large concrete block facing

10.2. Limitations

Wire Potentiometer (WP) and Earth Pressure Cell (EPC) readings were recorded all throughout the construction of GRS Abutment Models #1-#3 as planned before the construction of the models. Unfortunately, the results were not good enough to prepare outputs to show in this dissertation after analyzing the data recorded during the construction. Cutting the power connection after finishing the daily construction activity was one of the reasons. Recording activity was stopped and started again after each daily model construction. Combining and resetting the non-continuous data did not give meaningful results.

A set of five EPCs were recorded during the surcharge load testing of the GRS abutment models. Excessive amount of surcharge load causes to move EPCs and their connection cables during the test. For example, recorded data stopped unexpectedly at high surcharge load levels at especially EPCs underneath the CMU or large concrete block. Some valuable data was collected at EPC-4 level. Low pressure levels were recorded at EPC-5 that is located far away horizontally from the loading beam.

Initial CMU blocks levels that were used in GRS Abutment Model #1 was moved due to compaction effort by Jumping-Jack compactor. The compaction was stopped at almost 1.5 ft. away from the back of the CMU facing blocks at each level. Although, the compaction was successfully performed even the closest locations at the back of the large concrete blocks at GRS Abutment Models #2 and #3.

The outdoor testing station at University of Oklahoma (Norman) Fears Lab was affected due to rain, storm, cold or high temperatures. It was a big challenge to protect the instruments that was installed during the construction. Using tarp and plastic covers helped to solve this problem. The construction was stopped several times due to severe weather conditions.

10.3. Recommendations for Future Research

The influence of GRS backfill unit weight on the GRS abutment performance needs to be investigated in a future study. The Jumping-Jack can be used in different number of passes on each lift during the construction of a GRS bridge abutment, resulting in potentially different GRS backfill properties (including unit weight and shear strength), which could influence the performance (e.g. settlement) of the bridge abutment due to traffic load. Therefore, it is important

to determine the influences that compaction energy have on the unit weight and shear strength properties of the GRS backfill. However, such information is currently not available. Therefore, a future research should be performed to help engineers understand and quantify the influence that the backfill compaction effort in the field could have on the predicted load-bearing capacity and performance of GRS abutments. The design and instrumentation of future research GRS abutment model should be identical to those for GRS Abutment Model #1 with CMU facing, except that the new GRS abutment model should be constructed with an increased amount of GRS backfill compaction relative to that in GRS Abutment Model #1 for a direct and valid comparison (i.e. Total of three passes of Jumping-Jack compactor on each 12 inch-lift over the entire area of the abutment vs. one pass that was done in GRS Abutment Model #1).

A replica of GRS Abutment Model #1 without the instrumentation inside or outside the model should also be built as a follow-up future research for comparing the labor requirement results with GRS Abutment Model #1. This will be a good comparison opportunity to check if the current research labor requirement data collection is good enough to reflect the real construction of a GRS abutment model without the interruption of instrument installation process.

A large concrete block facing GRS-IBS project has been constructed in Caddo County, Oklahoma. This GRS bridge abutment bridge is the first of its kind in Oklahoma. The height of the bridge abutments in this field project is also comparable with the full-scale GRS abutment models that were built and tested in the University of Oklahoma Fears Lab outdoor test facility. Performance data should be collected on bridge abutment movements of this newly constructed large concrete block facing GRS bridge and recently constructed bridges with using CMU facing blocks. This will give engineers an opportunity to compare field performances of these two different type GRS bridge abutments.

REFERENCES

Adams M., Nicks J., Stabile T., Wu J., Schlatter W., and Hartmann J. 2011. "Geosynthetic Reinforced Soil Integrated Bridge System Synthesis Report." *Report No. FHWA-HRT-11-027,* Federal Highway Administration, McLean, VA.

Adams M., Nicks J., Stabile T., Wu J., Schlatter W., and Hartmann J. 2012. "Geosynthetic Reinforced Soil Integrated Bridge System Interim Implementation Guide." *Report No. FHWA-HRT-11-026,* Federal Highway Administration, Washington, DC.

Adams M. and Nicks J. 2018. "Design and Construction Guidelines for Geosynthetic Reinforced Soil Abutments and Integrated Bridge Systems." *FHWA Publication No: FHWA-HRT-17-080 HRDI-40/06-18(200)E,* Federal Highway Administration, Washington, DC.

Ahmadi H. and Hajialilue-Bonab M. 2012. "Experimental and analytical investigations on bearing capacity of strip footing in reinforced sand backfills and flexible retaining wall." *Acta Geotech.* 7 (4).

Ahmadi H. and Bezuijen A. 2018. "Full-scale mechanically stabilized earth (MSE) walls under strip footing load." *Geotextiles and Geomembranes,* Vol. 46.

Ardah A. 2018. "Field instrumentations and numerical analysis of Geosynthetic Reinforced Soil – Integrated Bridge System (GRS-IBS)" *Doctoral Dissertation,* The Department of Civil and Environmental Engineering, LSU, Baton Rouge, LA.

ASTM C136-14 2014. "Standard Test Method for Sieve Analysis of Fine and Coarse Aggregates." *ASTM International,* West Conshohocken, PA.

ASTM D698-12 2012. “Standard Test Methods for Laboratory Compaction Characteristics of Soil Using Standard Effort (12 400 ft-lbf/ft^3 (600 kN-m/m3)).” *ASTM International,* West Conshohocken, PA.

ASTM D1557-12 2012. “Standard Test Methods for Laboratory Compaction Characteristics of Soil Using Modified Effort (56,000 ft-lbf/ft^3 (2700 kN-m/m3)).” *ASTM International,* West Conshohocken, PA.

Bathurst R.J. and Hatami K. 2006. “Physical to computational modeling of reinforced soil walls under static loading.” Keynote Paper, *International Conference on Physical Modeling in Geotechnics, ICPMG 2006*, Hong Kong, China, August 2006.

Bathurst R.J., Vlachopoulos N., Walters D.L., Burgess P.G. and Allen T.M. 2006. “The influence of facing rigidity on the performance of two geosynthetic reinforced soil retaining walls.” *Canadian Geotechnical Journal*, Vol. 43, No. 12.

Boeckmann A., Lindsey E., and Bowders J. 2017. “Advancing Implementation of Geosynthetic Reinforced Soil-Integrated Bridge Systems (GRS-IBS).” *Missouri Department of Transportation Midwest Transportation Center,* U.S. Department of Transportation Office of the Assistant Secretary for Research and Technology.

Bourgeois E., Soyez L., and Le Kouby A. 2011. “Experimental and numerical study of the behavior of a reinforced-earth wall subjected to a local load.” *Computers and Geotechnics*, Vol. 38.

Budge. A. S., Dasenbrock D. D., Mattison D. J., Bryan G. K., Grosser A. T., Adams M., Nicks J. 2014. “Instrumentation and Early Performance of Large Grade GRS-IBS Wall.” *Geo-Congress 2014 Technical Papers.*

Cuelho E., Ganeshan S. 2004. “Developing test protocols to determine geosynthetic material properties that better represent traffic loading conditions.” *Western Transportation Institute College of Engineering,* Montana State University - Bozeman, Final Report.

Daniyarov A., Zelenko B., and Derian A. 2017. “Deployment of the Geosynthetic Reinforced Soil Integrated Bridge System From 2011 to 2017.” *FHWA Publication No: FHWA-HIF-17-043,* Federal Highway Administration, Washington, DC.

Hatami K., Witthoeft A.F. and Jenkins L.M. 2008. “Influence of inadequate compaction near the facing on the construction response of wrapped-face MSE walls.” *Transportation Research Record,* 2045.

Hatami K., Ngo T., Pena L. 2015. “Feasibility Study of GRS Systems for Bridge Abutments in Oklahoma”, *Annual Project Status Report ~FFY 2015, ODOT SP&R Item No. 2262*, ODOT, OKC, OK.

Hatami K. 2016. “Personal communications with Shannon Sheffert, PE.” *Local Government Division, Oklahoma Department of Transportation (ODOT),* Oklahoma City, OK.

Hatami K. 2017. “Personal communications with Tom Simpson, PE.” *Bureau of Indian Affairs,* Anadarko Office, OK.

Hatami K., Pena L., Ngo T. and Miller G.A. 2016. “Feasibility Study of GRS-IBS for Bridge Abutments in Oklahoma.” *Final Report No. FHWA-OK-16-07, ODOT SP&R ITEM NUMBER 2262*, ODOT, Oklahoma City, OK, December 2016.

Hatami K., Doger R., Boutin J., 2020. “Feasibility Study of GRS Systems for Bridge Abutments in Oklahoma: Influence of Facing and Aggregate Fill on Performance.” *Final Report No.*

FHWA-OK-19-09, ODOT SP&R ITEM NUMBER 2262, ODOT, Oklahoma City, OK, January 2020.

International Code Council. 2000. "International building code." *Falls Church, VA :International Code Council*.

Itasca Consulting Group, Inc. 2011. "FLAC v.7.0, Fast Lagrangian Analysis of Continua." MN, USA, *https://www.itascacg.com/software/flac/updates/flac-700-32-bit*.

Kakrasul J., Han J., and Rahmaninezhad M. 2018. "Laboratory evaluation of deformations of geosynthetic-reinforced retaining walls subjected to footing loading." *Proceedings of the 11th International Conference on Geosynthetics*, 16-21 September 2018, Seoul, Korea.

Lawrence J. B. 2014. "Structural Health Monitoring of the First Geosynthetic Reinforced Soil – Integrated Bridge System in Hawaii." *Master's Thesis. Hamilton Library*, University of Hawaii at Manoa.

Montana Department of Transportation Research Programs, 2018. "Geosynthetic Reinforced Soil - Integrated Bridge System (GRS-IBS)." *Project number: STPP NHTSA 3-3(23)65, FHWA Project no. MT-12-04*, November 2018. Federal Highway Administration, Washington, DC.

NAVFAC 1986. "Soil Mechanics, Design Manual 7.01." *Naval Facilities Engineering Command*, Alexandria, VA.

NCMA 2010. "Design Manual for Segmental Retaining Walls, 3rd Ed." *TR 127B, National Concrete Masonry Association*, Herndon, VA.

Ngo T. 2016. "Feasibility study of geosynthetic reinforced soil integrated bridge systems (GRS-IBS) in Oklahoma." *M.Sc. Thesis*, CEES, OU, Norman, OK.

Nicks J.E., Adams M.T., Ooi P.S.K., Stabile T. 2013. “Geosynthetic Reinforced Soil Performance Testing—Axial Load Deformation Relationships.” *FHWA Publication No: FHWA-HRT-13-066 HRDI-40/08-13(WEB)E,* Federal Highway Administration, Washington, DC.

Nicks *et al.* 2014. “Large-Scale Direct Shear Testing of Common-Open Aggregates.” *Proceedings of Geo-Congress 2014*, GSP 234, ASCE.

Nicks J.E., Esmaili D.A., and Adams M.T. 2016. “Deformations of geosynthetic reinforced soil under bridge service loads.” *Geotextiles and Geomembranes*, Vol. 44.

Nicks J.E., Adams M.T. 2019. “Lateral Earth Pressure Distribution with Depth for GRS Mini-Abutments.” *Geosynthetics Conference 2019, Houston, Proceedings*.

Nicks J.E. 2019. “Geosynthetic Reinforced Soil–Integrated Bridge System—Bid Price Analysis and Cost Comparisons with Alternative Foundation Systems.” *FHWA Publication No: FHWA-HRT-19-024 HRDI-40/02-19(WEB)E,* Federal Highway Administration, Washington, DC.

Obrzud R. and Truty A. 2012. “The Hardening Soil Model - A Practical Guidebook Z Soil.” *PC 100701 report*, revised 31.01.2012, Lausanne, Switzerland: Zace Services Ltd.

Pena L. 2017. “Performance monitoring and analysis of geosynthetic reinforced soil-integrated bridge systems (GRS-IBS) in Oklahoma.” *M.Sc. Thesis*, CEES, OU, Norman, OK.

Saghebfar M., Abu-Farsakh M., Ardah A., Chen Q., Fernandez B.A. 2017. “Performance Monitoring of Geosynthetic Reinforced Soil Integrated Bridge System (GRS-IBS) in Louisiana.” *Geotextiles and Geomembranes*, January 2017.

Saghebfar M., Abu-Farsakh M., Ardah A., Chen Q., Fernandez B.A. 2017. “Full-Scale Testing of Geosynthetic-Reinforced, Soil-Integrated Bridge System.” *Transportation Research Record: Journal of the Transportation Research Board*, No. 2656, 2017.

Vennapusa P., White D.J., Klaiber F.W., Wang S., and Gieselman H. 2012. “Geosynthetic Reinforced Soil for Low-Volume Bridge Abutments.” *InTrans Project Reports*. 5, The Iowa Highway Research Board (IHRB Project TR-621), Ames, IA, USA.

Wu *et al.* 2006. “Design and Construction Guidelines for Geosynthetic-Reinforced Soil Bridge Abutments with a Flexible Facing.” *NCHRP Report 556*, Transportation Research Board, Washington, DC, USA.

Wu J. T. H., and T. Q. Pham. 2013. “Load-carrying capacity and required reinforcement strength of closely spaced soil-geosynthetic composites.” *J. Geotech. Geoenviron. Eng.* 139 (9).

Xiao C., Han J., and Zhang Z. 2016. “Experimental study on performance of geosynthetic-reinforced soil model walls on rigid foundations subjected to static footing loading.” *Geotextiles and Geomembranes,* Vol. 44.

Xie Y., Leschchinsky B., and Han J. 2019. “Evaluation of Bearing Capacity on Geosynthetic-Reinforced Soil Structures Considering Multiple Failure Mechanisms.” *American Society of Civil Engineers, J. Geotech. Geoenviron. Eng.* 145(9): 04019040-1-13.

Xu C., Mei X., and Han J. 2019. “Model Tests Investigating the Behavior of Geosynthetic-Reinforced Soil (GRS) Abutments Subjected to Static Footing Load.” *Geosynthetics Conference 2019, Houston, Proceedings*.

Zheng Y., Sander AC., Rong W. *et al.* 2018. “Shaking Table Test of a Half-Scale Geosynthetic-Reinforced Soil Bridge Abutment.” *Geotechnical Testing Journal*, Vol: 41(1).

Zhu T. 2016. “Some Useful Numbers on the Engineering Properties of Materials (Geologic and Otherwise).” GEOL 615, The University of Texas at Austin, Austin, Texas, USA, *https://www. https://www.jsg.utexas.edu/tyzhu/files/Some-Useful-Numbers.pdf.*